THE ERUPTION OF KIMBERLITE: INSIGHTS FROM THE VICTOR NORTH KIMBERLITE PIPES, NORTHERN ONTARIO, CANADA

by

Bram Ivo van Straaten

M.Sc., Utrecht University, 2003

A THESIS SUBMITTED IN PARTIAL FULFILMENT OF
THE REQUIREMENTS FOR THE DEGREE OF

DOCTOR OF PHILOSOPHY

in

The Faculty of Graduate Studies

(Geological Sciences)

THE UNIVERSITY OF BRITISH COLUMBIA
(Vancouver)

October 2010

ABSTRACT

This dissertation describes the volcanic facies, petrology and economic aspects of the diamondiferous Victor North kimberlite complex (Northern Ontario, Canada) using detailed drill core logging, petrographic observations, electron microprobe analysis, and physical volcanological calculations. This research project is aimed at improving our understanding of kimberlite emplacement models, as fragmentation and eruption mechanisms for these deposits are controversial.

The results of this study show that the youngest kimberlite pipe (Victor Northwest) is filled by two similar eruption cycles. Each cycle starts with explosive crater-excavation forming predominantly pyroclastic deposits, followed by crater-filling with dark and competent rocks, and ends with volcanic quiescence resulting in formation of pipe wall collapse breccias and minor resedimented volcaniclastic kimberlite. Textural observations and eruption duration calculations suggest that the second crater-excavating eruption is phreatomagmatic in nature. This is based on the presence of fine-grained, well-mixed country rock fragment-rich, broken olivine-rich pyroclastic deposits containing small variably vesicular irregularly shaped juvenile pyroclasts as well as clastic pyroclasts. The crater-excavation stage is followed by formation of spatter-fed dark and competent clastogenic rocks. Evidence for a clastogenic origin includes the deposit morphology, presence of remnant pyroclasts, angular broken olivines, as well as the gradational nature of contacts with the enveloping pyroclastic units. Estimated eruption durations for each cycle range from days to months.

The cross-cutting kimberlite pipe (Victor Main) comprises two macroscopically similar country rock fragment-poor pyroclastic kimberlites that have contrasting macro diamond sample grades. This study explains the variation in diamond grade within Victor Main by differential sampling of mantle material (incl. diamond) by two different magma batches that formed the high- and low-grade domains. Victor Main lacks textures indicative of phreatomagmatism, and the relatively long calculated phreatomagmatic eruption duration suggests that magmatic eruptions are most likely responsible for the formation of these deposits.

This study concludes that, despite the generally more extreme range of physical properties of kimberlite melt, kimberlites erupt in a similar fashion as common basaltic-rhyolitic volcanoes and display a similarly diverse range of fragmentation processes and deposition styles. The geological and emplacement models presented here have broad economic implications for kimberlite exploration and mining.

TABLE OF CONTENTS

LIST OF TABLES

LIST OF FIGURES

ACKNOWLEDGEMENTS

Completing this dissertation, and the incredible professional and personal life experiences that came with it, would not have been possible without the support and encouragement of a large number of people.

First off, thanks to my supervisors. I feel fortunate to have been able to work with four people with such a variety of expertise, backgrounds and interests, and hope this is reflected in the breadth of my dissertation. Maya, thanks for always being available for discussions and providing direction. I think the most important lesson you've taught me is that "scientific research is never finished". Hard to accept sometimes if you're a bit of a perfectionist like I am. Kelly, thanks for providing important directions for my research and always stressing the need to quantify your observations. I will not forget the valuable knowledge you have shared. Barbara, I don't think I've come across something related to the petrology or economic aspects of kimberlites that you don't know about. Apart from sharing your exhaustive know-how, I'm also grateful for the many insights into how to successfully present my ideas, whether for writing papers, or poster and oral presentations. Kimberley, thanks for introducing me to the ins-and-outs of the Victor kimberlite during core logging, sharing your contagious enthusiasm for kimberlite geology, and your help in organizing the logistics of my trips to Ontario.

Financial and logistical support for this project came from De Beers Canada Inc. I would like to thank the company's management for the incredible opportunity to allow access to drill core, samples and in-house data, as well as their permission to publish this research. This Ph.D. project would not have been possible without the extensive logistical

assistance of De Beers' employees in Sudbury and Toronto; in this regard, I would especially like to thank Stephan Kurszlaukis, Brad Wood, Cliff Revering, Don Boucher, Claude Bouffard, Dwayne Thomson, and Grant Wu. A visit to the Victor mine in October 2009 made my Ph.D. project complete; Stephan, Brad and the rest of the staff at the mine, I truly appreciate being able to see what is happening at the mine and be able to share and discuss my research.

Additional funding for this project came from a Natural Sciences and Engineering Research Council of Canada – Collaborative Research and Development (NSERC-CRD) grant to M.G. Kopylova and J.K. Russell. In addition, I am grateful for funding from a University Graduate Fellowship award, Thomas and Marguerite MacKay Memorial scholarship and travel grants from the 9th International Kimberlite Conference, International Union of Geodesy and Geophysics, the Earth and Ocean Science Department (UBC) and the Faculty of Graduate Studies (UBC).

Several researchers at the Department of Earth and Ocean Sciences at UBC and elsewhere have contributed to my research. Thanks to Dick Tosdal, Craig Hart, Lee Groat, Bern Klein, Greg Dipple, James Vercammen and Al Lewis for their presence and suggestions at my supervisory committee meetings and defence. Special thanks to Volker Lorenz for his comments as external examiner. The help of Mati Raudsepp and Elisabetta Pani with the SEM and EMP analyses is also greatly appreciated. Thanks to Ryan Turna, Alison Jolley and Karly Oliver for helping out with data analysis for my thesis as laboratory assistants. I'd like to thank D. Canil, T. McCandless, P. Hayman, A. Pittari and an anonymous reviewer for constructive criticism on the papers that constitute Chapters 2, 3 and 4 of my thesis. Thanks to Frank Brunton at the Ontario Geological

Survey in Sudbury for spending a couple of days looking at sedimentary drill core with me. Special thanks to Stephen Moss for the many discussions on kimberlites and related topics. Thanks also to Ray Cas and his crew for the great introduction into volcanology during a field trip and workshop in Australia in 2005. Lastly, I'd like to thank the many people at UBC and in the kimberlite community for discussion, including, but not limited to, Allison Rust, Tom Nowicki, Casey Hetman, Lucy Porritt, Pat Hayman, Tom McCandless, Volker Lorenz, Richie Brown, Roger Mitchell, Matthew Field.

Last but not least does not do justice to the people in this last paragraph. I think saying *"I wouldn't have to be able to do this without you"* would better summarize everyone this last section. First, thanks to my parents (Mom, Dad, Jan, Kestarina) and sister for their support and, despite the distance, for being there. Always. I hope you recognise something from yourself in this thesis, whether it is in the curiosity in trying to understand the nature around us, a certain hand-drawn illustration, some calculations, the writing or otherwise. A big thank you to all the amazing friends and roommates that I've spent most of the last five years with at our West Point Grey home, affectionately known as 'the orphanage'. Thomas Fritz, thanks for being a good friend during both the good and bad times that inevitably come up while working on one project for five years. Our regular writing sessions at the coffee shop the last couple of months have made the thesis writing progress that much faster. Thomas Brunner, thanks for all the amazing outdoor adventures, they have a special place in my heart! Lara, thanks for all the good memories from '06-'08! Shawn, Ayesha, thanks for the good times during the last two years; I won't forget those house parties! Stefan, Emily, you guys are just awesome! I cannot begin to thank all the people that I've met at or through the department; thanks for all the

good times in the pub, field, office and elsewhere. You know who you are. Thanks to all the friends that I've shared so many outdoor trips with, either through the VOC or otherwise. They've kept me sane through the years, and provided me with much-needed distraction from study. Thanks also to my friends back home. Some have spread their wings and moved to other places, others are still at home; wherever you are, I love seeing you guys whenever I get the chance!

CO-AUTHORSHIP STATEMENT

This dissertation comprises four manuscript-style chapters (Chapters 2-5) intended for publication in peer-reviewed international scientific journals. I am the first author for all the manuscripts, and have contributed 90-95% of the research. My supervisors Dr. M.G. Kopylova (UBC), Prof. J.K. Russell (UBC), Dr. B.H. Scott Smith (Scott-Smith Petrology Inc., North Vancouver; UBC) and Ms. K.J. Webb (formerly at De Beers Canada Inc., Toronto; currently at Mineral Services Canada Inc., North Vancouver) identified the initial project, sponsors and funding. With advice from my supervisors, I planned the research direction, dissertation outline, and identified the core issues to be addressed. Further details on each individual chapter are provided below.

Chapter 2 has been published in the **Journal of Volcanology and Geothermal Research** (van Straaten et al., 2008) and is co-authored by M.G. Kopylova, J.K. Russell, K.J. Webb and B.H. Scott Smith. I made all geological observations, collected all the samples, performed all scanning electron microscope and electron microprobe analyses and wrote the manuscript. My co-authors assisted in structuring the manuscript, and contributed multiple stages of editorial comments.

Chapter 3 has been published in **Lithos** (van Straaten et al., 2009), and is co-authored by M.G. Kopylova, J.K. Russell, K.J. Webb and B.H. Scott Smith. I was responsible for all core logging, petrographic observations on samples, compiling all the data into a consistent three-dimensional volcanic facies model and writing the manuscript. All co-authors contributed in structuring the manuscript and assisted during multiple stages of editorial comments.

Chapter 4 has been accepted for publication in the **Bulletin of Volcanology** (van Straaten et al., 2010), and is co-authored by M.G. Kopylova, J.K. Russell and B.H. Scott Smith. I conducted all the core logging, carried out all petrographic observations, wrote the manuscript and prepared all the figures. Counting of angular olivines was mostly accomplished by a research assistant, Karly Oliver. The manuscript scope and structure has benefitted greatly from involvement of all co-authors. All co-authors contributed multiple stages of editorial comments.

Chapter 5 will be submitted for publication, and is co-authored by M.G. Kopylova, J.K. Russell and B.H. Scott Smith. I collected all the geological data, wrote the manuscript, performed all calculations and drafted all figures and tables. Counting of angular olivines was mostly accomplished by a research assistant, Karly Oliver. All co-authors assisted in structuring the manuscript and contributed during multiple stages of editorial comments.

1 INTRODUCTION

Kimberlite is a rare rock type that is only found within the oldest parts of continents, where the surrounding rocks are generally more than 1.7 billion years old. Kimberlite occurs as meter thick tabular bodies or larger inverted cone shaped bodies that can be ~100-1500 m in maximum dimension. The molten rock (magma) that creates these kimberlite occurrences originates from very deep (below ~220 km) within the earth. During rapid ascent towards the surface these magmas invariably entrain fragments of solid rock and crystals; in rare instances this solid fraction can include small proportions of diamond. Our detailed knowledge of kimberlite comes mainly from the study of deposits that contain sufficient quantities of diamond to sustain mining. The diamond content within kimberlite rock types that are actively mined is very low compared to any other commercial mining operation, and ranges from ~0.001 to 10 carats per tonne of rock (i.e. 5 parts per billion to 50 parts per million by weight). The largest diamondiferous kimberlite deposits occur in inverted cone shaped bodies (pipes). The pipes and their deposits are the result of volcanic eruptions of kimberlite magmas that occurred sporadically throughout the earth's history (from roughly 2500 to 45 million years ago, possibly extending to the present time). The pipes we currently find at or near the earth's surface are the 'roots' or lower parts of the original volcanoes after millions of years of erosion.

This dissertation focuses on the Victor kimberlite occurrence in Northern Ontario (Canada), which is currently being mined for diamonds by De Beers Canada Inc. The study is aimed at reconstructing the volcanic eruption history of these kimberlite pipes by

looking at the properties and distribution of kimberlite rock types. In addition, the influence of processes deep within the earth and volcanic eruption processes on diamond mining are explored.

1.1 Literature review

1.1.1 Origin, composition and volatile content of kimberlite magma

Kimberlite magma is formed within the sub-cratonic asthenosphere, either by low (<1 %, Dalton and Presnall, 1998; Le Roex et al., 2003; Gudfinnsson and Presnall, 2005; Brey et al., 2008) or extensive (~10-50 %, Mitchell, 2004) degrees of partial melting. During rapid ascent towards the Earth's surface, the magma commonly incorporates abundant mantle xenocrysts, lesser mantle xenoliths and possible trace amounts of diamond. The total transit time of the magma from source to surface is estimated as hours to days (Canil and Fedortchouk, 1999; Kelley and Wartho, 2000; Sparks et al., 2006), and given the appropriate conditions, dissolution can significantly reduce the amount of diamond in the melt (Kozai and Arima, 2005; Fedortchouk et al., 2005; 2007; 2010).

The absence of modern kimberlite deposits, the lack of observed quenched kimberlite glass, and the hybrid (xenocryst-rich) nature of these rocks complicates the reconstruction of the primitive melt composition. However, several studies show that kimberlite melt has a very low silica content and is highly depolymerised (Price et al., 2000; Le Roux et al., 2003; Harris et al., 2004; Becker and Le Roux, 2006; Kopylova et al., 2007; Nielsen and Sand, 2008; Sparks et al., 2009), indicating a very low melt viscosity. In addition, the estimated melt compositions indicate the presence of abundant CO_2 and H_2O (7-20 wt.% combined, see references above; Sparks et al., 2006; Kavanagh and Sparks, 2009).

The high volatile content of the melt is generally translated in a high potential for massive exsolution of these volatiles upon magma ascent, decompression and eruption (e.g. Dawson and Hawthorne, 1970; Sparks et al., 2006). However, the potassic, alkaline and ultrabasic melt composition will generally result in a higher solubility of CO_3^{2-} in the melt (Brooker et al., 2001; Brooker, 2006; Sparks et al., 2009). In addition, the high carbonate content will also increase the solubility of OH^- into the melt phase (Keppler, 2003; Fedortchouk et al., 2007). Experimental constraints relevant to kimberlite melt compositions are lacking, but observations on rare modern volcanoes that erupt low viscosity, carbonate-rich, magmas are available. Observations on the Oldoinyo Lengai volcano show a range in activity from effusion of very low viscosity natrocarbonatite lava to more explosive eruptions of more silica-rich magmas (Dawson et al, 1990; 1994; Norton and Pinkerton, 1997). Hence I suggest that, despite the high abundance of potential volatile compounds (CO_3^{2-}, OH^-) in kimberlite melt, a range of effusive to explosive eruption styles should be expected.

1.1.2 Mineralogy and classification of kimberlite

Coherent kimberlite generally contains around 50 vol.% crystals (Mitchell, 1986), predominantly olivine macrocrysts (anhedral, commonly 0.5-10 mm in size, mantle derived grains) and olivine phenocrysts (euhedral and <0.5 mm in size). Other, less abundant, mantle-derived grains include garnet, Mg-ilmenite, Cr-diopside and phlogopite. The fine-grained matrix in coherent kimberlites generally comprises monticellite, phlogopite, perovskite, spinel, apatite, carbonates and/or serpentine (Shee, 1984; Mitchell, 1986; 1995; 1997; Woolley et al., 1996; Armstrong et al., 2004; Caro et al., 2004; Fedortchouk and Canil, 2004; Roeder and Schultze, 2008). Due to the

consistent contamination by mantle xenocrysts, kimberlite is defined by the above petrography and mineral assemblage, rather than petrochemistry (Woolley et al., 1996).

1.1.3 Kimberlite pipe types and emplacement models

Kimberlite is generally found in meter scale dykes and sills, as well as pipe shaped bodies that can range up to 100-1500 m in maximum dimension. Whereas dykes and sills are formed by passive intrusion of magma, kimberlite pipes are formed by explosive volcanic eruptions. In contrast to more common basaltic to rhyolitic volcanic systems, no kimberlite eruptions have ever been observed. The most recent deposits, apart from a possible Quaternary kimberlitic occurrence at Igwisi Hills (Tanzania; Reid et al., 1975; Dawson, 1994), are Middle to Late Eocene in age (Creaser et al., 2004; Heaman et al., 2004; Batumike et al., 2008). Worldwide, kimberlite pipes are the most important source for diamond, and mining predominantly focuses on these primary diamond deposits. Only a small fraction of kimberlite deposits are economically viable to mine. However, most of our knowledge about kimberlites comes from these rare economically diamondiferous kimberlite deposits.

Kimberlite deposits have traditionally been described as steep sided, carrot-shaped pipes, subdivided in a lower root zone, central diatreme zone and an upper crater zone based mainly on observations from Southern Africa (Clement, 1982; Clement and Skinner, 1985; Mitchell, 1986; Clement and Reid, 1989; Fig. 1.1). These so-called Southern African type kimberlite pipes will be described first. The discovery of many new kimberlite pipes in Canada and elsewhere in the last two decades has led to descriptions of numerous kimberlite pipes with a different pipe shape and infill; the latter kimberlite pipe types will be described in a subsequent section.

Southern African type pipes (Clement and Skinner, 1985; Hetman et al., 2004; Skinner and Marsh, 2004; Hetman, 2008) are generally hosted in competent country rock and have steep sided (~82º dipping) pipe walls. These pipes generally comprise a lower hypabyssal kimberlite (HK) root zone that gradually transitions into a tuffisitic kimberlite (TK) diatreme zone and an upper volcaniclastic kimberlite (VK) crater. Tuffisitic kimberlite is a fragmental rock that is typically poorly sorted, matrix supported, uniform, massive, macrocrystic and country rock fragment-rich (~50 vol.%) (Hetman, 2008). These rocks generally contain pelletal lapilli (thin melt selvages on olivine crystals), altered olivine macrocrysts and phenocrysts set within an altered, serpentine ± diopside matrix.

1.1.3.1 Southern African type pipes – magmatic emplacement models

There is considerable debate whether kimberlite deposits are products of magmatic or phreatomagmatic fragmentation. Magmatic fragmentation is driven by exsolution and expansion of large amounts of volatiles near the earth's surface and has been proposed for the majority of the kimberlite pipes (e.g. Clement, 1982; Mitchell, 1986; Clement and Reid, 1989; Field and Scott Smith, 1999; Sparks et al., 2006; Porritt et al., 2008; Porritt and Cas, 2009). Most of the recent work has focussed on Southern African type pipes, and a summary of relevant recent eruption models is presented below.

In the magmatic eruption scenario, the rising column of kimberlite magma and gas is hydraulically fracturing its way towards the surface. When the fractures are close enough to the surface that the gas overpressure overcomes the tensile strength of the overlying rock, the magma will breach the surface. The sudden decompression of the magma-gas system will trigger a high-energy explosion that will excavate a rough vent, and violently

eject a volume of country rock equivalent to the size of the initial vent (Cas et al., 2008b). Based on the dominantly massive and unfractured country rock adjacent to the pipe, Cas et al. (2008b) propose that after the initial vent opening, there was a sustained period of gas jet driven erosion and smoothing of the vent walls. This likely happened during the waxing stage of the eruption (i.e. when the eruption column is still building). Deposition could only have occurred during the waning stage of the eruption, and results in a column collapse pyroclastic deposit (Cas et al., 2008b; Porritt et al., 2008; Porritt and Cas, 2009; Fig. 1.2). Sparks et al. (2006) and Gernon et al. (2008) propose comparable eruption models. However, they suggest that at the end of the magmatic eruption the declining exit velocities and/or widening of the pipe cause ejecta to become trapped inside the pipe and deposit. In their model, the well-mixed and massive nature of the pipe-infill is caused by fluidization (i.e. gas flow through a bed of particles providing enough drag to support the buoyant weight of the bed; Walters et al., 2006; Sparks et al, 2006; Gernon et al., 2009a). However, the authors do not suggest a plausible source for the large quantities of gas needed to fluidize and mix the voluminous intra-pipe deposits (Cas, pers. comm., 2008). Another magmatic eruption model by Wilson and Head (2007) proposes that Southern African type pipes could have formed in as little as one hour, however this interpretation is controversial (see discussion and reply by Sparks et al., 2007; Wilson and Head; 2007). In addition, Wilson and Head (2007) do not provide equations that can be used to reproduce the calculations used for their interpretations.

1.1.3.2 Southern African type pipes – phreatomagmatic emplacement models

Phreatomagmatic deposits result from the explosive interaction of magma and water, and have been proposed to occur at a number of kimberlite bodies (Scott Smith et al., 1998;

Field and Scott Smith, 1999; Graham et al., 1999; Boyer, 2005; Pittari et al., 2008; Lefebvre and Kurszlaukis, 2008; Porritt and Cas, 2009). Other authors including Lorenz (1986), Lorenz et al. (1999), Lorenz and Kurszlaukis (2007) and Kurszlaukis and Lorenz (2008) propose that all pipes or diatremes are formed by phreatomagmatism. In their phreatomagmatic model of pipe formation, Kurszlaukis and Lorenz (2008) explain the formation of Southern African type kimberlite pipes by many single thermohydraulic (i.e. phreatomagmatic) explosions. The initial explosions are thought to occur close to the surface, and continued thermohydraulic explosions cause progressive deepening and widening of the pipe (Fig. 1.3). The thermohydraulic explosions fragment both the magma and the surrounding country rocks. Violent explosions in small pipes may clear the overlying diatreme for a short period of time, however diatreme-clearing events in larger pipes are difficult or impossible to maintain. Explosions in the root zone are also thought to cause homogenization of the lower diatreme tephra by collapse, inflation and deflation. This process could account for the massive, structureless, country rock fragment-rich, and well-mixed nature of tuffisitic kimberlite in large Southern African type kimberlite pipes (Kurszlaukis and Lorenz, 2008). In areas with low permeability crystalline basement, they propose that faults or other structural weaknesses cause focussing of fluid flow and consequent magma-water interaction. According to these authors, the magmatic equivalent of a hydrovolcanic kimberlite diatreme would be a kimberlite scoria cone with associated lava flows, without formation of a subsurface pipe (thus having a very low preservation potential; Lorenz 1986; Kurszlaukis and Lorenz, 2008).

1.1.3.3 Other pipe types and deposits – emplacement models

A large part of kimberlite research has focussed on Southern African type kimberlite pipes, but the dramatic increase in kimberlite emplacement studies in the last 7-20 years has led to the recognition of a large number of different pipes. Following the discovery of many new kimberlite pipes in Canada during the nineties, Field and Scott Smith (1999) made a first summary of these different kimberlite occurrences. Three pipe types or classes were distinguished (Field and Scott Smith, 1999; see also Skinner and Marsh, 2004). One of these is the so-called 'Southern African type' or 'class 1' pipe that is similar to the archetypical kimberlite pipe described above (Fig. 1.1). The two newly recognized pipes are the 'Fort-a-la-Corne type' or 'class 2' champagne glass shaped craters with a predominant volcaniclastic or pyroclastic kimberlite infill, and the 'Lac de Gras type' or 'class 3' steep sided pipes with a predominant volcaniclastic and resedimented volcaniclastic kimberlite infill (Fig. 1.4). The variety in pipe shapes and infill has predominantly been ascribed to differences in host rock competency (Field and Scott Smith, 1999; Scott Smith, 2008) and/or volatile content of the magma (Skinner and Marsh, 2004).

Since 2003, significant advances were made towards the understanding of the volcanology of kimberlite deposits (e.g. Berryman et al., 2004; Nowicki et al., 2004; Kjarsgaard et al., 2006; Porritt et al., 2006; Sparks et al., 2006; Brown et al., 2008; Cas et al., 2008a, b; Lefebvre and Kurszlaukis, 2008; Moss et al., 2008; Nowicki et al., 2008; Pittari et al., 2008; Porritt et al., 2008; Brown et al., 2009; Crawford et al., 2009; Gernon et al., 2009b; Moss, 2009; Porritt and Cas, 2009). These studies describe an extremely wide variety of pipe shapes and intra-pipe volcanic kimberite deposits, suggesting a large

variety of volcanic processes that can excavate a pipe, and a multitude of volcanic and sedimentary processes that can fill a pipe.

The intra-pipe location of kimberlite deposits contrasts markedly with other basaltic-rhyolitic volcanic systems where everything we know is derived from extra-crater deposits, and we know little to none about the intra-conduit deposits. Until recently, no well-described occurrences of extra-crater kimberlite deposits had been recognized. However, recent studies have indicated the possibility of such occurrences, which appear to be limited to areas of contemporaneous kimberlite volcanism and sedimentation (Boyer, 2005; Zonneveld et al., 2004; Kjarsgaard et al., 2006; Lefebvre and Kurszlaukis, 2008; Pittari et al., 2008; Harvey et al., 2009) and pyroclastic flows trapped in neighbouring kimberlite pipes (Moss et al., 2008; Porritt, 2008; Gernon et al., 2009b).

Pipe-filling coherent kimberlite deposits can be subdivided in two types. The first type occurs in the root zone of Southern African type kimberlite pipes, and has been described by Hetman et al. (2004), Skinner and Marsh (2004), Hetman (2008), Kurszlaukis and Lorenz (2008), Masun and Scott Smith (2008), Fitzgerald et al. (2009) and Seghedi et al. (2009). These rock types have generally been described as intrusive (hypabyssal) rocks, despite their gradational contacts to the overlying fragmental (tuffisitic) kimberlite facies. The second type comprises pipe-filling coherent kimberlite occurrences at a variety of other locations. Rare occurrences have been described by Kong et al. (1999), Nowicki et al. (2004), Webb et al. (2004), Brown et al. (2008), Nowicki et al. (2008), Brown et al. (2009) and Crawford et al. (2009). These coherent rock types have been explained by a variety of processes ranging from representing a frozen degassing front from TK to HK,

late intrusions of magma in the root zone of a pipe, welding, possible coalescence and/or effusion of lava.

1.2 Victor kimberlite

In this dissertation I study the Victor North kimberlite complex, located in the James Bay Lowlands, Northern Ontario, Canada (Fig. 1.5). The Victor complex is currently being mined for diamonds by De Beers Canada Inc. Victor is the largest kimberlite in the Middle-Late Jurassic Attawapiskat kimberlite province (Kong et al., 1999; Heaman and Kjarsgaard, 2000), and comprises three pipes, Victor South, Victor Main and Victor Northwest (Fig. 1.5). The kimberlite bodies have been described previously by Kong et al. (1999), Fowler et al. (2001) and Webb et al. (2004). The Victor kimberlite pipes crosscut an Ordovician to Silurian sedimentary succession, unconformably overlying Precambrian granitoid basement. The unconformity occurs at approximately 272 m below the present surface. Since emplacement the extra-crater material, as well as the top ~50-600 m (Kong et al., 1999; Brunton, pers. comm. 2006) of the kimberlite pipe, has been removed by erosion. Roughly 10-30 m of unconsolidated Quaternary overburden is currently present on top of the kimberlites.

Previous research by Webb et al. (2004) shows that the Victor Northwest pipe comprises dark and competent rocks that resemble fresh hypabyssal kimberlite but have unusual textures and are closely associated with pyroclastic kimberlite, volcaniclastic kimberlite and country rock breccia facies. In contrast to Victor Northwest, the neighbouring Victor Main pipe is filled with relatively homogeneous country fragment-poor pyroclastic kimberlite. Webb et al. (2004) shows that the latter pipe consists of two macroscopically similar, but petrographically distinct, pyroclastic kimberlites that have contrasting macro

diamond sample grades. In general, the pipe shape and infill of Victor North contrasts with the typical Southern African type kimberlite pipes (Webb et al., 2004).

1.3 Gaps in knowledge

Based on the previous sections, there are the following gaps in our knowledge with respect to kimberlite geology:

- Most kimberlite emplacement models are based on large-volume, steep-sided Southern African type kimberlite pipes, generally filled with massive, country rock fragment-rich, volcaniclastic kimberlite
- There is little consensus regarding the eruption and fragmentation mechanisms that created kimberlite deposit. This is illustrated by the variety of eruption mechanisms that have been proposed for Southern African type pipes, which range from *(i.)* unique volcanic processes with aspects that have not been documented elsewhere (e.g. Clement, 1982; Skinner and Marsh, 2004; Hetman et al., 2004) to *(ii.)* explosive magmatic eruptions (Sparks et al., 2006; Cas et al., 2008b) or *(iii.)* phreatomagmatic eruptions (Lorenz, 1986; Kurszlaukis and Lorenz, 2008)
- The general lack of physical volcanological studies on kimberlite pipes

From the summary in Section 1.2 it is clear that the Victor North kimberlite complex is an ideal location to study these and other aspects of kimberlite geology, based on the following reasons:

- The presence of a large variety of kimberlite facies that are substantially different from those normally encountered in Southern African type pipes. These rock types

have generally not been studied in detail, and could shed light on the origin and eruption styles of kimberlite deposits

- The presence of pipe-filling possibly coherent kimberlite. There has been no adequate volcanological description of pipe-filling coherent kimberlite facies, nor a detailed analysis of their emplacement mechanisms
- Victor North represents a unique opportunity to describe an economically diamondiferous kimberlite occurrence, and will allow a detailed study of the possible influences of mantle sampling, mantle transport and volcanic emplacement processes on the economic potential of diamond deposits

1.4 Thesis theme and objectives

This Ph.D. thesis is aimed at:

1. Reconstructing the three-dimensional architecture of the volcanic facies within the Victor Northwest kimberlite pipe.
2. Constraining the dynamics and emplacement mechanisms of the Victor Northwest and Main kimberlite volcanoes.
3. Improving our understanding of the deep mantle, magma transport and surface emplacement processes controlling diamond distribution in kimberlite deposits.

Each subsequent chapter of this thesis comprises a research manuscript prepared for publication in peer-reviewed international scientific journals. Two of the chapters have already been published (Chapters 2, 3), one chapter has been submitted for publication (Chapter 4), while the last chapter will be submitted shortly (Chapter 5).

1.4.1 Organization of dissertation

Chapter 2 discusses the geology of the Victor Main kimberlite pipe (referred to as Victor North Pyroclastic Kimberlite, or VNPK, in Chapter 2). The Victor Main pipe comprises one of the main diamond resources in the Victor mine plan. However, this pipe also contains some low-grade domains that appear to be non-economic. This chapter summarises the petrological and mineral chemical criteria that can be used to differentiate the high- and low-grade domains. In addition, the study shows that the variation in diamond grade is most likely caused by differential sampling of mantle material (incl. diamond) by two different magma batches that formed the high- and low-grade domains.

In **Chapter 3**, detailed drill core analyses and petrographic studies are used to reconstruct the intra-crater stratigraphy of the VNW kimberlite. This allows for a detailed reconstruction of the emplacement history of the pipe. In this chapter I show that the VNW pipe was formed by two separate eruption cycles. During the first eruption cycle, the main VNW crater is excavated and partly filled. The second eruption cycle excavates a smaller nested crater within the existing lithified pipe fill. Both eruption cycles can be subdivided into three comparable eruptive stages that produce a similar set of deposits. In both cycles these three stages comprise *(a)* a highly explosive eruption involving crater excavation and deposition of pyroclastic kimberlite, followed by *(b)* lower energy eruptions producing dark and competent kimberlite lithologies and *(c)* final volcanic quiescence resulting in major pipe wall collapse and minor resedimentation by water.

Chapter 4 focuses on the dark and competent unit formed during the second eruption cycle at VNW (cycle 2, stage b). Using a comprehensive volcanological and petrographic analysis of all available drill cores I show that this unit has a fresh well-crystallised

coherent groundmass and is extrusive and fragmental in origin. A spatter-fed clastogenic origin is based on the presence of remnant pyroclasts, angular broken olivines, deposit morphology, as well as gradational contacts to enveloping pyroclastic units. This chapter, and a growing number of publications, suggest that crater-filling clastogenic kimberlite in intra-crater settings may be more common than geologists previously thought. The emplacement history and volcanology of these pipes need to be reconsidered based on the emerging importance of this particular kimberlite facies.

In **Chapter 5** I provide new petrological descriptions on all units within the Victor North kimberlite complex, specifically focusing on textures indicative of eruption and fragmentation mechanisms. There is considerable debate within the scientific community whether kimberlite eruptions are caused by magmatic fragmentation and/or magma-water interaction; this chapter is aimed at addressing this topic by a combination of detailed textural observations and a unique set of eruption dynamics calculations. The textural observations and eruption duration calculations suggest that the crater-excavating eruptions at VNW are either completely phreatomagmatic in nature (cycle 2a), or formed by a combination of magmatic eruptions with possible phreatomagmatism at the end when the magma flux declined (cycle 1a). For both cycles, the phreatomagmatic stage is followed by magmatic lava fountaining eruptions (cycles 1b, 2b). Estimated eruption durations for each cycle ranges from days to months. In contrast, at VM the lack of textural indicators for phreatomagmatism, and the relatively long phreatomagmatic eruption durations of one to several years, suggest that magmatic eruptions are most likely responsible for the formation of these deposits.

Chapter 6 provides a summary of the most important implications of this research. In particular, I focus on the implications for mining and exploration, kimberlite emplacement models, and general volcanology. Directions for further research are provided at the end of this chapter.

1.4.2 Organization of appendices

Detailed datasets produced during this research are presented in accompanying electronic appendices. These include a graphic summary of all drill core logs intersecting VNW (Electronic appendix A), a tabulated summary of all drill core logs (Electronic appendix B), geographic coordinates and down hole surveys of all drill cores (Electronic appendix C), sample lists (Electronic appendix D), detailed graphic logs for Victor Northwest (Electronic appendix E) and Victor Main (Electronic appendix F), electron microprobe data on oxides, carbonates, phlogopites and apatites in Victor Main used in Chapter 2 (Electronic appendix G), data collected on olivine alteration for Chapter 4 (Electronic appendix H), angular broken olivine content for Chapters 4 and 5 (Electronic appendix I), maximum clast sizes for Chapter 5 (Electronic appendix J), pipe and unit volumes for Chapter 5 (Electronic appendix K), eruption duration calculations used in Chapter 5 (Electronic appendix L), image analysis methodologies and results (Electronic appendix M), and data on mantle indicator mineral abundance in VNW and VM (Electronic appendix N).

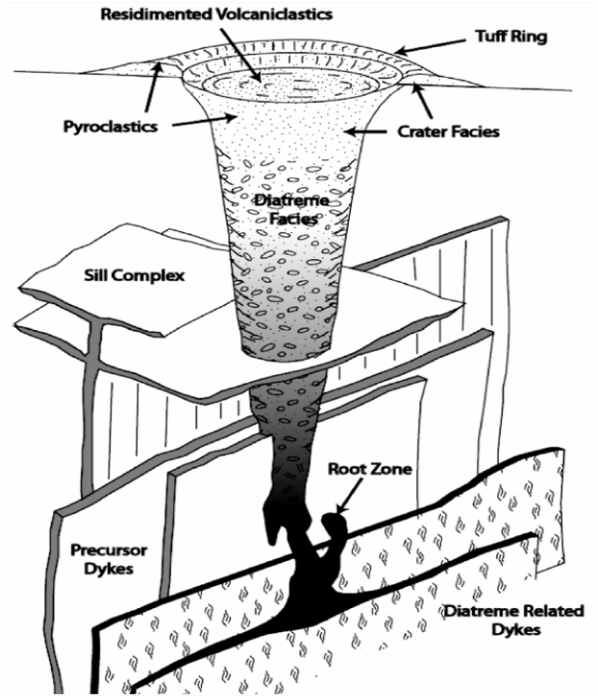

Figure 1.1 Schematic illustration of an archetypical Southern African style kimberlite pipe from 2-3 km depth to surface. Modified after Hawthorne (1973), Mitchell (1986) and Porritt (2008)

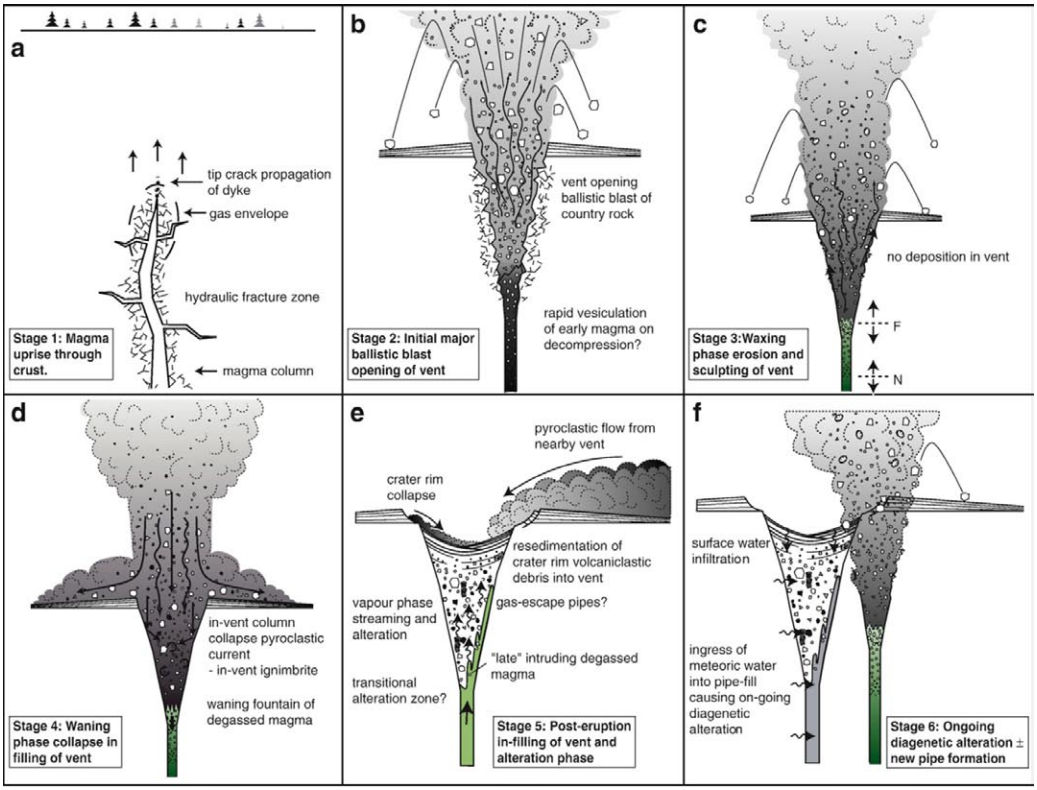

Figure 1.2 Magmatic emplacement model by Cas et al. (2008a) for Southern African style kimberlite pipes. The figure shows the dyke propagation (A), initial pipe opening (B), waxing (C) and waning stage (D) stages of the eruption, and possible subsequent events (E-F). Modified from Cas et al. (2008a)

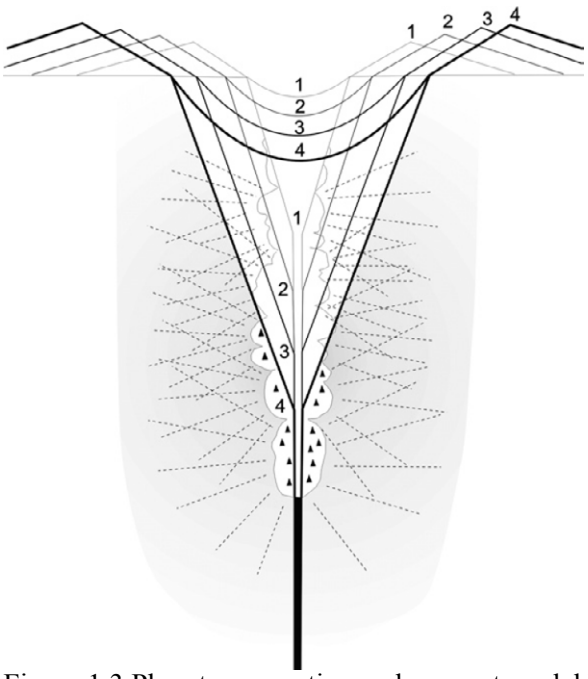

Figure 1.3 Phreatomagmatic emplacement model by Lorenz and Kurszlaukis (2007). The figure shows the evolution of a downward penetrating root zone with repeated collapse of the overlying diatreme and surrounding rocks, indicating also the downward cutting on the feeder dyke. Modified after Lorenz and Kurszlaukis (2007)

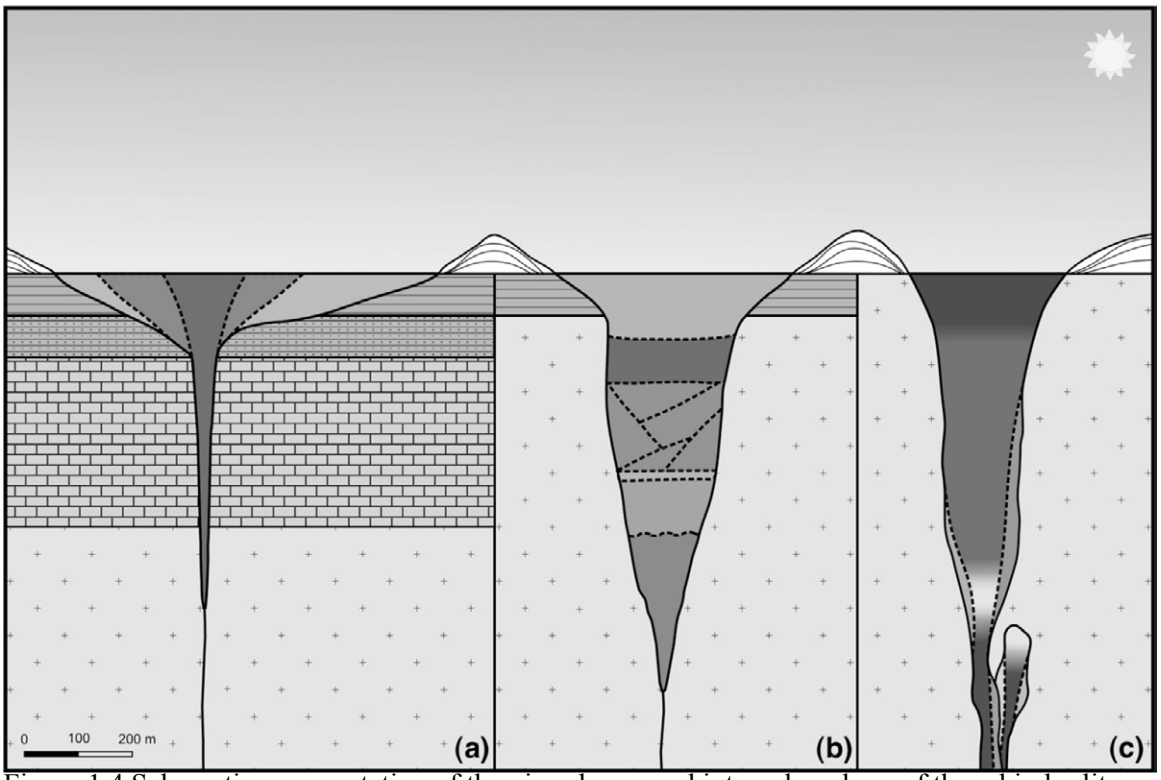

Figure 1.4 Schematic representation of the pipe shapes and internal geology of three kimberlite pipe types of Field and Scott Smith (1999) and Scott Smith (2008). Fort-a-la-Corne type craters (A), Lac de Gras type pipes (B) and Southern African type pipes (C). See text for discussion. Modified after Scott Smith (2008)

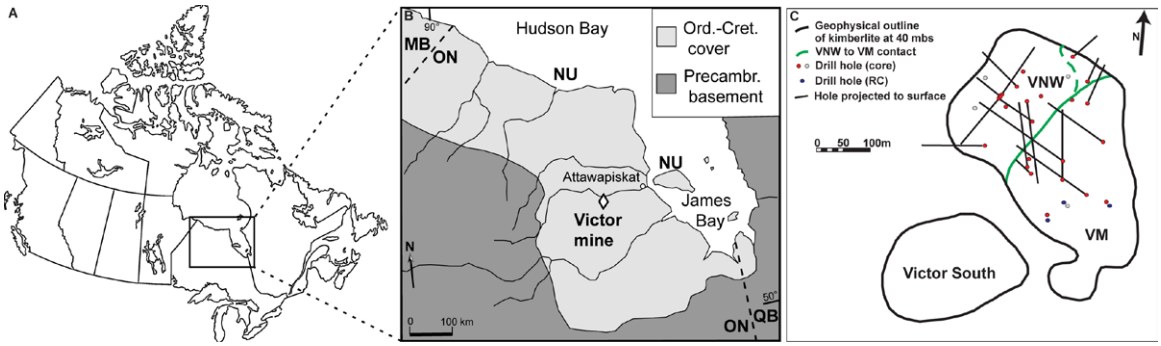

Figure 1.5 (A) map showing the location of the Victor kimberlite in Canada, (B) the regional geological setting of the kimberlite pipe (modified from Webb et al., 2004), and (C) the Victor kimberlite complex with three adjacent and cross-cutting pipes (see Fig. 3.1 and Electronic appendix C for drill core UTMs)

1.5 References

Armstrong, J.P., Wilson, M., Barnett, R.L., Nowicki, T. and Kjarsgaard, B.A., 2004. Mineralogy of primary carbonate-bearing hypabyssal kimberlite, Lac de Gras, Slave Province, Northwest Territories, Canada. Lithos, 76(1-4): 415-433.

Batumike, J.M. et al., 2008. LAM-ICPMS U-Pb dating of kimberlitic perovskite: Eocene-Oligocene kimberlites from the Kundelungu Plateau, D.R. Congo. Earth and Planetary Science Letters, 267(3-4): 609-619.

Becker, M. and Roex, A.P.L., 2006. Geochemistry of South African on- and off-craton, group I and group II kimberlites: petrogenesis and source region evolution. Journal of Petrology, 47(4): 673-703.

Berryman, A.K., Scott-Smith, B.H. and Jellicoe, B.C., 2004. Geology and diamond distribution of the 140/141 kimberlite, Fort a la Corne, central Saskatchewan, Canada. Lithos, 76(1-4): 99-114.

Boyer, L.P., 2005. Kimberlite volcanic facies and eruption in the Buffalo Head Hills, Alberta (Canada), University of British Columbia, Vancouver, B.C., Canada.

Brey, G.P., Bulatov, V.K., Girnis, A.V. and Lahaye, Y., 2008. Experimental melting of carbonated peridotite at 6-10 GPa. Journal of Petrology, 49(4): 797-821.

Brooker, R., 2006. The role of experiments and theory in understanding volatile control on the kimberlite eruption mechanisms, Kimberlite Emplacement Workshop, Saskatoon, Canada.

Brooker, R.A., Kohn, S.C., Holloway, J.R. and McMillan, P.F., 2001. Structural controls on the solubility of CO2 in silicate melts: Part I: bulk solubility data. Chemical Geology, 174(1-3): 225-239.

Brown, R., Tait, M., Field, M. and Sparks, R., 2009. Geology of a complex kimberlite pipe (K2 pipe, Venetia Mine, South Africa): insights into conduit processes during explosive ultrabasic eruptions. Bulletin of Volcanology, 71(1): 95-112.

Brown, R.J., Buse, B., Sparks, R.S.J. and Field, M., 2008. On the Welding of Pyroclasts from Very Low-Viscosity Magmas: Examples from Kimberlite Volcanoes. The Journal of Geology, 116(4): 354-374.

Canil, D. and Fedortchouk, Y., 1999. Garnet dissolution and the emplacement of kimberlites. Earth and Planetary Science Letters, 167(3-4): 227-237.

Caro, G., Kopylova, M.G. and Creaser, R.A., 2004. The hypabyssal 5034 kimberlite of the Gahcho Kue cluster, southeastern Slave craton, Northwest territories, Canada: a granite-contaminated group-I kimberlite1. The Canadian Mineralogist, 42: 183-207.

Cas, R., Porritt, L., Pittari, A. and Hayman, P., 2008. A new approach to kimberlite facies terminology using a revised general approach to the nomenclature of all volcanic rocks and deposits: Descriptive to genetic. Journal of Volcanology and Geothermal Research, 174(1-3): 226-240.

Cas, R.A.F., Hayman, P., Pittari, A. and Porritt, L., 2008. Some major problems with existing models and terminology associated with kimberlite pipes from a volcanological perspective, and some suggestions. Journal of Volcanology and Geothermal Research, 174(1-3): 209-225.

Clement, C.R., 1982. A comparative study of some major kimberlite pipes in the North Cape and Orange Free State. Unpublished Ph.D. thesis, University of Cape Town, Cape Town.

Clement, C.R. and Reid, A.M., 1989. The origin of kimberlite pipes: an interpretation based on a synthesis of geological features displayed by southern African occurrences. In: J. Ross and e. al. (Editors), Kimberlites and related rocks, Volume 1, Proceedings of the Fourth International Kimberlite Conference. Geological Society of Australia Special Publication 14, Perth, pp. 632-646.

Clement, C.R. and Skinner, E.M.W., 1985. A textural-genetic classification of kimberlites. Transactions of the Geological Society of South Africa, 88: 403-409.

Crawford, B., Hetman, C., Nowicki, T., Baumgartner, M. and Harrison, S., 2009. The geology and emplacement history of the Pigeon kimberlite, EKATI Diamond Mine, Northwest Territories, Canada. Lithos, 112(Supplement 1): 501-512.

Creaser, R.A., Grutter, H., Carlson, J. and Crawford, B., 2004. Macrocrystal phlogopite Rb-Sr dates for the Ekati property kimberlites, Slave Province, Canada: evidence for multiple intrusive episodes in the Paleocene and Eocene. Lithos, 76(1-4): 399-414.

Dalton, J.A. and Presnall, D.C., 1998. The continuum of primary carbonatitic-kimberlitic melt compositions in equilibrium with lherzolite: Data from the system CaO-MgO-Al2O3-SiO2-CO2 at 6 GPa. Journal of Petrology, 39(11-12): 1953-1964.

Dawson, J.B., 1994. Quarternary kimberlitic volcanism on the Tanzania Craton. Contributions to mineralogy and petrology, 116: 473-485.

Dawson, J.B. and Hawthorne, J.B., 1970. Intrusion features of some hypabyssal South African kimberlites. Bulletin Volcanologique, 34(3): 740-757.

Dawson, J.B., Pinkerton, H., Norton, G.E. and Pyle, D.M., 1990. Physicochemical properties of alkali carbonatite lavas:Data from the 1988 eruption of Oldoinyo Lengai, Tanzania. Geology, 18(3): 260-263.

Dawson, J.B., Pinkerton, H., Pyle, D.M. and Nyamweru, C., 1994. June 1993 eruption of Oldoinyo Lengai, Tanzania: Exceptionally viscous and large carbonatite lava flows and evidence for coexisting silicate and carbonate magmas. Geology, 22(9): 799-802.

Fedortchouk, Y. and Canil, D., 2004. Intensive Variables in Kimberlite Magmas, Lac de Gras, Canada and Implications for Diamond Survival. J. Petrology, 45(9): 1725-1745.

Fedortchouk, Y., Canil, D. and Carlson, J.A., 2005. Dissolution forms in Lac de Gras diamonds and their relationship to the temperature and redox state of kimberlite magma. Contributions to Mineralogy and Petrology, 150(1): 54-69.

Fedortchouk, Y., Canil, D. and Semenets, E., 2007. Mechanisms of diamond oxidation and their bearing on the fluid composition in kimberlite magmas. American Mineralogist, 92(7): 1200-1212.

Fedortchouk, Y., Matveev, S. and Carlson, J.A., 2010. H2O and CO2 in kimberlitic fluid as recorded by diamonds and olivines in several Ekati Diamond Mine kimberlites, Northwest Territories, Canada. Earth and Planetary Science Letters, 289(3-4): 549-559.

Field, M. and Scott-Smith, B.H., 1999. Contrasting geology and near-surface emplacement of kimberlite pipes in Southern Africa and Canada, Proceedings of the 7th International Kimberlite Conference, Cape Town.

Fitzgerald, C.E., Hetman, C.M., Lepine, I., Skelton, D.S. and McCandless, T.E., 2009. The internal geology and emplacement history of the Renard 2 kimberlite, Superior Province, Quebec, Canada. Lithos, 112(Supplement 1): 513-528.

Fowler, J.A., Grutter, H.S., Kong, J.M. and Wood, B.D., 2001. Diamond Exploration in Northern Ontario with Reference to the Victor Kimberlite, Near Attawapiskat. Exploration and Mining Geology, 10(1-2): 67-75.

Gernon, T.M. et al., 2009. Pyroclastic flow deposits from a kimberlite eruption: The Orapa South Crater, Botswana. Lithos, 112(Supplement 1): 566-578.

Gernon, T.M., Gilbertson, M.A., Sparks, R.S.J. and Field, M., 2008. Gas-fluidisation in an experimental tapered bed: Insights into processes in diverging volcanic conduits. Journal of Volcanology and Geothermal Research, 174(1-3): 49-56.

Gernon, T.M., Gilbertson, M.A., Sparks, R.S.J. and Field, M., 2009. The role of gas-fluidisation in the formation of massive volcaniclastic kimberlite. Lithos, 112(Supplement 1): 439-451.

Graham, I. et al., 1999. Exploration history and geology of the Diavik Kimberlites, Lac de Gras, Northwest Territories, Canada, Proceedings of the 7th International Kimberlite Conference, Cape Town, pp. 262-279.

Gudfinnsson, G.H. and Presnall, D.C., 2005. Continuous Gradations among Primary Carbonatitic, Kimberlitic, Melilititic, Basaltic, Picritic, and Komatiitic Melts in Equilibrium with Garnet Lherzolite at 3-8 GPa. Journal of Petrology, 46(8): 1645-1659.

Harris, M., le Roex, A. and Class, C., 2004. Geochemistry of the Uintjiesberg kimberlite, South Africa: petrogenesis of an off-craton, group I, kimberlite. Lithos, 74(3-4): 149-165.

Harvey, S. et al., 2009. Geology and evaluation strategy of the Star and Orion South kimberlites, Fort a la Corne, Canada. Lithos, 112(Supplement 1): 47-60.

Hawthorne, J.B., 1973. Model of a kimberlite pipe. Physics and chemistry of the earth, 9: 1-15.

Heaman, L.M. and Kjarsgaard, B.A., 2000. Timing of eastern North American kimberlite magmatism: continental extension of the Great Meteor hotspot track? Earth and Planetary Science Letters, 178(3-4): 253-268.

Heaman, L.M., Kjarsgaard, B.A. and Creaser, R.A., 2004. The temporal evolution of North American kimberlites. Lithos, 76: 377-397.

Hetman, C.M., 2008. Tuffisitic Kimberlite (TK): A Canadian perspective on a distinctive textural variety of kimberlite. Journal of Volcanology and Geothermal Research, 174(1-3): 57-67.

Hetman, C.M., Scott-Smith, B.H., Paul, J.L. and Winter, F., 2004. Geology of the Gahcho Kue kimberlite pipes, NWT, Canada: root to diatreme magmatic transition zones. Lithos, 76: 51-74.

Kavanagh, J.L. and Sparks, R.S.J., 2009. Temperature changes in ascending kimberlite magma. Earth and Planetary Science Letters, 286(3-4): 404-413.

Kelley, S.P. and Wartho, J.A., 2000. Rapid Kimberlite Ascent and the Significance of Ar-Ar Ages in Xenolith Phlogopites. Science, 289(5479): 609-611.

Keppler, H., 2003. Water solubility in carbonatite melts. American Mineralogist, 88(11-12): 1822-1824.

Kjarsgaard, B.A. et al., 2006. Volcanic stratigraphy, eruptive sequences and emplacement of the 140/141 kimberlite, Fort a la Corne field, Saskatchewan, Kimberlite Emplacement Workshop, Saskatoon.

Kong, J.M., Boucher, D.R. and Scott-Smith, B.H., 1999. Exploration and Geology of the Attawapiskat Kimberlites, James Bay Lowland, Northern Ontario, Canada. Proceedings of the 7th International Kimberlite Conference, The J.B. Dawson volume, Cape Town, 452-467 pp.

Kopylova, M.G., Matveev, S. and Raudsepp, M., 2007. Searching for parental kimberlite melt. Geochimica Et Cosmochimica Acta, 71(14): 3616-3629.

Kozai, Y. and Arima, M., 2005. Experimental study on diamond dissolution in kimberlite and lamproitic melts at 1300-1420°C and 1 GPa with controlled oxygen partial pressure. American Mineralogist, 90(11-12): 1759-1766.

Kurszlaukis, S. and Lorenz, V., 2008. Formation of "Tuffisitic Kimberlites" by phreatomagmatic processes. Journal of Volcanology and Geothermal Research, 174(1-3): 68-80.

Le Roex, A.P., Bell, D.R. and Davis, P., 2003. Petrogenesis of Group I Kimberlites from Kimberley, South Africa: Evidence from Bulk-rock Geochemistry. J. Petrology, 44(12): 2261-2286.

Lefebvre, N. and Kurszlaukis, S., 2008. Contrasting eruption styles of the 147 Kimberlite, Fort a la Corne, Saskatchewan, Canada. Journal of Volcanology and Geothermal Research, 174(1-3): 171-185.

Lorenz, V., 1986. On the growth of maars and diatremes and its relevance to the formation of tuff rings. Bulletin of Volcanology, 48(5): 265-274.

Lorenz, V. and Kurszlaukis, S., 2007. Root zone processes in the phreatomagmatic pipe emplacement model and consequences for the evolution of maar-diatreme volcanoes. Journal of Volcanology and Geothermal Research, 159(1-3): 4-32.

Lorenz, V., Zimanowski, B., Buttner, R. and Kurszlaukis, S., 1999. Formation of kimberlite diatremes by explosive interaction of kimberlite magma with groundwater: field and experimental aspects, Proceedings of the 7th International Kimberlite Conference, Cape Town, pp. 522-528.

Masun, K.M. and Scott Smith, B.H., 2008. The Pimenta Bueno kimberlite field, RondÙnia, Brazil: Tuffisitic kimberlite and transitional textures. Journal of Volcanology and Geothermal Research, 174(1-3): 81-89.

Mitchell, R.H., 1986. Kimberlites: Mineralogy, Geochemistry and Petrology. Plenum Press, New York, 442 pp.

Mitchell, R.H., 1995. Kimberlites, Orangeites, and related rocks. Plenum Press, New York, 410 pp.

Mitchell, R.H., 1997. Kimberlites, orangeites, lamproites, melilitites and minettes: a petrographic atlas. Almaz Press, Thunder Bay, Canada, 243 pp.

Mitchell, R.H., 2004. Experimental studies At 5-12 GPa of the Ondermatjie hypabyssal kimberlite. Lithos, 76(1-4): 551-564.

Moss, S., Russell, J.K. and Andrews, G.D.M., 2008. Progressive infilling of a kimberlite pipe at Diavik, Northwest Territories, Canada: Insights from volcanic facies architecture, textures, and granulometry. Journal of Volcanology and Geothermal Research, 174(1-3): 103-116.

Moss, S., Russell, J.K., Brett, R.C. and Andrews, G.D.M., 2009. Spatial and temporal evolution of kimberlite magma at A154N, Diavik, Northwest Territories, Canada. Lithos, 112: 541-552.

Nielsen, T.F.D. and Sand, K.K., 2008. The Majuagaa kimberlite dike, Maniitsoq region, West Greenland: constraints on an Mg-rich silicocarbonatitic melt composition from groundmass mineralogy and bulk compositions. Canadian Mineralogist, 46(4): 1043-1061.

Norton, G. and Pinkerton, H., 1997. Rheological properties of natrocarbonatite lavas from Oldoinyo Lengai, Tanzania. European Journal of Mineralogy, 9(2): 351-364.

Nowicki, T. et al., 2004. The geology of kimberlite pipes of the Ekati property, Northwest Territories, Canada. Lithos, 76: 1-27.

Nowicki, T., Porritt, L., Crawford, B. and Kjarsgaard, B., 2008. Geochemical trends in kimberlites of the Ekati property, Northwest Territories, Canada: Insights on volcanic and resedimentation processes. Journal of Volcanology and Geothermal Research, 174(1-3): 117-127.

Pittari, A. et al., 2008. Eruption processes and facies architecture of the Orion Central kimberlite volcanic complex, Fort a la Corne, Saskatchewan; kimberlite mass flow deposits in a sedimentary basin. Journal of Volcanology and Geothermal Research, 174(1-3): 152-170.

Porritt, L., 2008. The volcanology and sedimentology of the Ekati kimberlites, NWT, Canada, with consideration of the implications for diamond grade. Unpublished Ph.D. thesis, Monash University, Clayton, Australia.

Porritt, L.A. and Cas, R.A.F., 2009. Reconstruction of a kimberlite eruption, using an integrated volcanological, geochemical and numerical approach: A case study of the Fox Kimberlite, NWT, Canada. Journal of Volcanology and Geothermal Research, 179(3-4): 241-264.

Porritt, L.A., Cas, R.A.F. and Crawford, B.B., 2006. The origin and implications of the TK-like infill of the Fox kimberlite, Ekati Diamond Mine, NWT, Canada, Kimberlite Emplacement Workshop, Saskatoon, Canada.

Porritt, L.A., Cas, R.A.F. and Crawford, B.B., 2008. In-vent column collapse as an alternative model for massive volcaniclastic kimberlite emplacement: An example from the Fox kimberlite, Ekati Diamond Mine, NWT, Canada. Journal of Volcanology and Geothermal Research, 174(1-3): 90-102.

Price, S.E., Russell, J.K. and Kopylova, M.G., 2000. Primitive magma from the Jericho pipe, N.W.T. Canada: constraints on primary kimberlite melt chemistry. Journal of Petrology, 41(6): 789-808.

Reid, A.M., Donaldson, C.H., Dawson, J.B., Brown, R.W. and Ridley, W.I., 1975. The Igwisi Hills extrusive "kimberlites". Physics and Chemistry of The Earth, 9: 199-218.

Roeder, P.L. and Schulze, D.J., 2008. Crystallization of Groundmass Spinel in Kimberlite. J. Petrology, 49(8): 1473-1495.

Scott Smith, B.H., 2008. Canadian kimberlites: Geological characteristics relevant to emplacement. Journal of Volcanology and Geothermal Research, 174(1-3): 9-19.

Scott Smith, B.H., Orr, R.G., Robertshaw, P. and Avery, R.W., 1998. Geology of the Fort a la Corne Kimberlites, Saskatchewan, Seventh International Kimberlite Conference, Cape Town, South Africa, pp. 772-774.

Seghedi, I., Maicher, D. and Kurszlaukis, S., 2009. Volcanology of Tuzo pipe (Gahcho Kuè cluster) - Root-diatreme processes re-interpreted. Lithos, 112(Supplement 1): 553-565.

Shee, S.R., 1984. The oxide minerals of the Wesselton Mine kimberlite, Kimberley, South Africa. In: J. Kornprobst (Editor), Third international kimberlite conference. Elsevier, Clermont Ferrand, pp. 59-73.

Skinner, E.M.W. and Marsh, J.S., 2004. Distinct kimberlite pipe classes with contrasting eruption processes. Lithos, 76: 183-200.

Sparks, R.S.J. et al., 2006. Dynamical constraints on kimberlite volcanism. Journal of Volcanology and Geothermal Research, 155(1-2): 18-48.

Sparks, R.S.J. et al., 2009. The nature of erupting kimberlite melts. Lithos, 112(Supplement 1): 429-438.

Sparks, R.S.J., Brown, R.J., Field, M. and Gilbertson, M., 2007. Kimberlite ascent and eruption. Nature, 450(7172): E21-E21.

Walters, A.L. et al., 2006. The role of fluidisation in the formation of volcaniclastic kimberlite: Grain size observations and experimental investigation. Journal of Volcanology and Geothermal Research, 155(1-2): 119-137.

Webb, K.J., Scott-Smith, B.H., Paul, J.L. and Hetman, C.M., 2004. Geology of the Victor Kimberlite, Attawapiskat, Northern Ontario, Canada: cross-cutting and nested craters. Lithos, 76(1-4): 29-50.

Wilson, L. and Head III, J.W., 2007. An integrated model of kimberlite ascent and eruption. Nature, 447(7140): 53-57.

Wilson, L. and Head, J.W., 2007. Kimberlite ascent and eruption - Reply. Nature, 450(7172): E22-E22.

Woolley, A.R. et al., 1996. Classification of lamprophyres, lamproites, kimberlites, and the kalsilitic, melilitic and leucitic rocks. The Canadian Mineralogist, 34: 175-186.

Zonneveld, J.-P. et al., 2004. Sedimentologic and stratigraphic constraints on emplacement of the Star Kimberlite, east-central Saskatchewan. Lithos, 76: 115-138.

2 DISCRIMINATION OF DIAMOND RESOURCE AND NON-RESOURCE DOMAINS IN THE VICTOR NORTH PYROCLASTIC KIMBERLITE PIPE[1]

2.1 Introduction

Kimberlite magma originates as a sub-cratonic, asthenosphere-derived melt. During its ascent towards the surface, the magma commonly incorporates abundant mantle xenocrysts, lesser mantle xenoliths and possible trace amounts of diamond. In order to improve our understanding of kimberlite formation, it is important to study the processes that produce kimberlite rocks, including melt generation, magma ascent, emplacement and eruption. This study of the Victor kimberlite focuses on understanding the deeper mantle processes involved in melt generation, sampling of xenocrysts (± diamond), and the evolution of magma during transport. Here, we show that deep mantle processes have a direct influence on the petrological and economic characteristics of diamondiferous kimberlite deposits.

The Victor kimberlite is located in the James Bay Lowlands, Northern Ontario, Canada and is scheduled for open pit mining by De Beers Canada in 2008. Victor is the largest kimberlite in the Middle-Late Jurassic Attawapiskat kimberlite province (Kong et al., 1999), and forms a complex of several pipes. The steep-sided (~70°) pipes occur in an Ordovician to Silurian sedimentary succession, unconformably overlying Precambrian

[1] A version of this chapter has been published. van Straaten, B.I., Kopylova, M.G., Russell, J.K., Webb, K.J. and Scott Smith, B.H. (2008). Discrimination of diamond resource and non-resource domains in the Victor North pyroclastic kimberlite, Canada. Journal of Volcanology and Geothermal Research, 174(1-3): 128-138.

granitoid basement. About 10-30 m of unconsolidated Quaternary overburden is currently present on top of the kimberlite.

The primary focus of this paper is the Victor North pyroclastic kimberlite (VNPK) pipe (Webb et al., 2004). The VNPK pipe comprises one of the main resources in the mine plan, but also includes some low-grade domains that, at the present time, appear to be a non-resource (Fig. 2.1). *Mineral resource* is used here to refer to "a concentration or occurrence of material of intrinsic economic interest in or on the Earth's crust in such form and quantity that there are reasonable prospects for eventual economic extraction". *Grade* refers to "the relative quantity or the percentage of ore-mineral content in an orebody" (Glossary of Geology, 2005). One of the ongoing issues in terms of understanding the geology, delineating the ore and controlling grade, is distinguishing between the resource and non-resource domains of the VNPK pipe. The main rock type in the VNPK pipe is a massive, moderately sorted, loosely packed, crystal lapilli-tuff. The rock is dominated by *discrete* or *free olivine crystals* (crystals without selvages of crystallised melt) and minor *juvenile pyroclasts* (crystals rimmed by selvages of crystallised melt). The kimberlite contains the two different generations of olivine characteristic of most kimberlites: *olivine macrocrysts* (anhedral, commonly 0.5-10 mm in size, mantle derived grains) and primary *olivine phenocrysts* (euhedral and <0.5 mm in size).

A close correlation between kimberlite petrography and macrodiamond content in the VNPK pipe was established by Webb et al. (2004). The macrodiamond content distribution (Fig. 2.1) in the VNPK pipe is consistent with an emplacement model of nested craters resulting from two discrete eruptions (Webb et al., 2004). First, a magma

with a low diamond content and high abundance of olivine phenocrysts (~28%) erupted explosively, producing juvenile pyroclasts with a high olivine phenocryst abundance (Figs. 2.1, 2.2A). A second explosive eruption of kimberlite magma, having a high diamond content and lower abundance of olivine phenocrysts (~8%), from the same pipe formed a nested crater. The juvenile pyroclasts of this second kimberlite pulse have a distinctly lower proportion of olivine phenocrysts (Figs. 2.1, 2.2B). Intermediate diamond contents are found at the interface between the high- and low-grade deposits. The mixed interface is also characterised by the presence of both (e.g. olivine phenocryst-rich vs. olivine phenocryst-poor) juvenile pyroclast types (Fig. 2.1). An average sample grade of 23 carats per hundred tonnes has been established for the Victor kimberlite. With an approximate value of 419 US$/ct, Victor represents one of the highest value/carat primary diamond deposits in the world (grade and value figures courtesy of De Beers Canada Inc., 2007).

Prior to this study, the high- and low-grade kimberlite deposits were differentiated texturally in thin section using an optical microscope (Webb et al., 2004). This study finds that electron microprobe analyses of groundmass minerals can distinguish the low- and high-grade kimberlite units. In addition, it contributes to an improved understanding of the petrology of the Victor North kimberlite pipe, as well as the genesis and early evolution of the kimberlite magma that formed the Victor diamond deposit.

2.2 Analytical methods

Detailed core logging and sampling of two representative vertical drill cores (V-00-117c, V-00-125c, see Fig. 2.1 for location) in the VNPK pipe were undertaken. The selected drill cores both intersect all three of the contrasting grade zones, from bottom to top: low,

moderate and high. The diamond grades in these two drill holes are inferred from bulk sampling of two reverse circulation large diameter (61 cm) drill holes (each located ~10 m from the respective core holes) and detailed petrography on juvenile pyroclasts in samples from the aforementioned core holes (Webb et al., 2004; this study).

Representative polished core samples and thin sections of drill core V-00-117c and V-00-125c were studied petrographically. The goal of this study was to search for differences between the high- and low-grade kimberlite units in addition to those identified by Webb et al. (2004). The petrographic work focused on juvenile pyroclasts, comprising olivine grains rimmed by selvages of crystallised melt, which are viewed here as representative of the kimberlite magmas.

Detailed optical transmitted and reflective light microscope, scanning electron microscope (SEM) and electron microprobe (EMP) analyses were performed at the Department of Earth and Ocean Sciences, UBC. The SEM and EMP analyses were performed on four samples from drill core V-00-117c, two from the high-grade unit and two from the low-grade unit. A total number of 25 juvenile pyroclasts were analysed. Based on the presence of two petrographically distinct kimberlite units which are internally massive and show minor internal variation in componentry and petrography (Webb et al., 2004; this study), it is suggested that these samples form a representative subset for further analytical work. All groundmass minerals were studied under the SEM (Philips XL30) to determine the presence and nature of zoning. Subsequent quantitative EMP analyses (Tables 2.1, 2.2) were performed using the fully automated CAMECA SX-50 instrument, operating in the wavelength-dispersion mode. Data reduction was done using the 'PAP' $\phi(\rho Z)$ method (Pouchou and Pichoir, 1985). All oxides (spinel-group

minerals, ilmenite and rutile) were analysed with an excitation voltage of 15 kV, beam current of 20 nA, beam diameter of 2 µm, peak counting time of 20 seconds (s) and background counting time of 10 s. Analyses of vanadium were corrected for titanium interference. The proportion of ferric (Fe^{3+}) vs. ferrous (Fe^{2+}) iron was calculated using stoichiometric and charge balance equations (Droop, 1987). Micas were analysed at 15 kV, 10 nA, with a beam diameter of 5-10 µm, peak counting time of 20 s (40 s for F, Cl) and background counting time of 10 s (20 s for F, Cl). Carbonates were analysed at an accelerating voltage of 15 kV, beam current of 10 nA, with a beam diameter of 5-9 µm, a uniform peak counting time of 20 s and background counting time of 10 s. Apatite was analysed at an accelerating voltage of 15 kV, beam current of 10 nA, with a beam diameter of 2-5 µm, and peak counting time of 10 s (14 s for La, Ce; 20 s for Cl; 50 s for F) and background counting time of 5 s (7 s for La, Ce; 10 s for Cl, 25 s for F). Loss of fluorine in apatite due to electron beam induced diffusion was tested in four larger (≥30 µm) crystals, using methodology outlined in Stormer et al. (1993) and Coulson et al. (2001). Five analyses were conducted at the same point within each of these crystals. The initial value for fluorine was obtained by linear extrapolation back to the initial concentration. In these four cases the first measurement overestimated the fluorine concentration by only 1-11%. This overestimation has not been corrected for in other apatite analyses.

2.3 Petrography and mineralogy

2.3.1 Macroscopic features

The kimberlite intersected in drill core is generally massive and shows only slight variations in grain size. Less common are 1-2 m thick, graded beds of kimberlite lapilli-

tuff. The kimberlite has low concentrations of country rock lithic clasts (average ~7 vol.%). The only macroscopic observation that might serve to distinguish the high- and low-grade zones is a ~10 m thick interval with abundant country rock lithic clasts (~17 vol.%) that occurs on the outer margin of the high-grade zone. Otherwise, there are only minor macroscopic differences between the high- and low-grade kimberlite units, which attests to the indistinct gradational nature of this grade boundary. These features include (Webb et al., 2004; this study): (i.) slightly higher abundance of country rock basement clasts (granitic and dolerite), (ii.) greater degree of alteration of olivines, and (iii.) more abundant Cr-diopside macrocrysts in the low-grade unit. None of these features allows for a confident macroscopic division between the high- and low-grade kimberlite units.

2.3.2 Microscopic features

The juvenile pyroclasts in the high- and low-grade kimberlite units are remarkably similar in terms of their primary mineralogy. The only reliable microscale discriminator between these units is the abundance of olivine phenocrysts (Fig. 2.1). The low-grade kimberlite unit contains juvenile pyroclasts with a higher olivine phenocryst abundance (~28 vol.% vs. ~8 vol.% in the high-grade kimberlite unit; Webb et al., 2004). The groundmass of juvenile pyroclasts of both kimberlite units comprises, in order of abundance, euhedral calcite or dolomite laths, euhedral-subhedral spinel, minor small euhedral apatite and other less common opaque minerals (ilmenite, rutile; Figs. 2.2, 2.3). In addition, rare laths of phlogopite were observed. Groundmass phases are set in a cryptocrystalline matrix of dolomite ± serpentine (base). The juvenile pyroclasts are non-vesicular to poorly vesicular (typical abundance 0 to 4 vol.%) and have vesicle diameters of 50-150 μm.

2.3.3 Groundmass mineral composition

Olivine phenocrysts from the low-grade kimberlite unit are all altered and, thus, their original compositions cannot be measured. The chromites, however, are very resistant to alteration, and are pervasive in both the high- and low-grade kimberlite units. The chromite occurs as cores within grains of groundmass spinel (Fig. 2.3). The spinel is usually euhedral-subhedral, 20-50 μm in diameter and strongly zoned from chromite core to magnetite rim (Fig. 2.4A, Table 2.1). The chromite cores in the VNPK are themselves zoned and this zoning trend is observed in almost all larger (≥20 μm) cores. They are zoned from an early Al-rich chromite centre to an Al-poor and Cr-rich chromite edge (Figs. 2.3, 2.4B, Table 2.1). The shape of the chromite centre is commonly anhedral (n=11/15), whereas the edge of the chromite usually has a more euhedral-subhedral outline.

There are clear differences between the spinels occurring in the high- and low-grade kimberlite units. The first difference is the development of magnetite rims (Fig. 2.3A-C). The low-grade kimberlite unit spinel grains (n=10) commonly have an obvious atoll-textured rim (80-90% of spinel grains, Fig. 2.3A). In addition, the magnetite in the atoll-rim is never in contact with the chromite core (100% of spinel grains, Fig. 2.3A). The high-grade kimberlite unit spinel grains (n=17) typically have no atoll-textured rim (71% of spinel grains, Fig. 2.3B, C). The magnetite rim is usually in contact with the chromite core (59% of spinel grains, Fig. 2.3C). An additional 23% of the spinel grains have a magnetite rim in contact with the chromite core on one side of the crystal, but no magnetite rim in contact with the chromite core on the other side (Fig. 2.3B). The remaining 18% of the high-grade unit spinel grains have no magnetite rim at all. The

major difference between spinels from the high- and low-grade kimberlite is the distinct contrast in the chromite core compositions (Fig. 2.4B). Both the centres and the edges of the chromite cores of spinel crystals in the low-grade kimberlite unit have lower Mg-numbers ($Mg/Mg+Fe^t$) at a similar Cr-number (Cr/Cr+Al), relative to those in the high-grade unit. A slight difference in Ti-content of the chromite cores is also observed between the high- and low-grade units in the VNPK, although not as distinct as the difference in Cr# (Fig. 2.4B). The low-grade unit chromites generally have a higher Ti-content then those in the high-grade unit at similar Mg#.

Minor opaque phases in the groundmass include ilmenite and rutile. The range (average ± 1 SD) in mole fractions for the ilmenite analyses (n=33) are 0.57-0.65 geikielite ($MgTiO_3$), 0.29-0.37 ilmenite ($Fe^{2+}TiO_3$), 0.04-0.06 haematite ($Fe^{3+}{}_2O_3$), and <0.01 pyrophanite ($MnTiO_3$); see Table 2.1. The groundmass ilmenites plot in the same field as groundmass ilmenites and ilmenite inclusions in olivine from the Wesselton kimberlite (Shee, 1984; Fig. 2.5A). Rutile analyses (Table 2.1; n = 22) yield an average X^{Ti} (Ti p.f.u./ all cations) of 0.88 ± 0.04 (1 SD). Analyses with X^{Ti} below 0.82 were excluded. Oxide intergrowths (Fig. 2.3C, D) are commonly observed in the juvenile pyroclast groundmass. Touching Al-poor chromites and Mg-rich ilmenite and rutile, as well as chromites being partly surrounded by ilmenite and rutile indicate that ilmenite and rutile crystallised during or after crystallisation of the Al-poor chromite. The mineral composition of the groundmass ilmenites shows a similar difference between the high- and low-grade kimberlite units as the chromites (Fig. 2.5B): the low-grade kimberlite unit ilmenites have a slightly lower Mg# than their high-grade counterparts. The difference in Mg# is less pronounced than that for the chromite centres.

Euhedral calcite or dolomite laths are common and occur within a cryptocrystalline base of dolomite and minor serpentine (Fig. 2.3E, F). The carbonate phases are stoichiometrically close to pure end-member compositions of calcite and dolomite (Table 2.2). In addition, all calcite laths have a moderate Sr content (Fig. 2.6A) with respect to calcite replacing olivine and calcite veins. There is a difference in composition of the groundmass dolomite laths between the high- and low-grade kimberlite units. The low-grade kimberlite unit dolomite laths have slightly lower Mg# (higher Fe content, see Fig. 2.6B), similar to observations of oxide groundmass minerals.

Groundmass apatites are fluorine-bearing hydroxylapatites (Table 2.2), whereas the (OH, F, Cl) cation site in phlogopite is dominated by hydroxide with trace amounts of fluorine and chlorine (Table 2.2).

2.4 Discussion

2.4.1 Early crystallisation sequence

The first minerals to crystallise from kimberlite magma are commonly olivine phenocrysts and chromites (e.g. Mitchell, 1986; Fedortchouk and Canil, 2004). Within the VNPK pipe, chromite in the groundmass of juvenile pyroclasts is found as cores within multiphase spinel crystals. The rim enveloping the chromite core is commonly composed of magnetite. The mineral zoning pattern from chromite to magnetite, and the presence of abundant atoll-textures on these spinels is typical of Group I kimberlites (Mitchell, 1986; Fig. 2.4A). The magnetite rims are commonly interpreted as products of late-stage crystallisation (Mitchell, 1986). Similar zoning trends and texturally comparable vermiform rims are found in chromites in basalts (Roeder et al., 2001; 2006).

We have compared the chemical composition of the earlier formed chromite cores of groundmass spinel crystals in the VNPK with chromites from other kimberlites, including euhedral chromite inclusions in olivine phenocrysts and euhedral chromites in the groundmass (data from Shee, 1984; Fedortchouk and Canil, 2004). The chemical composition of the VNPK groundmass chromites is comparable to euhedral chromites included in olivines from the Lac de Gras kimberlites (Fedortchouk and Canil, 2004; similar range in Cr#, slightly lower Mg#), and very similar to both a euhedral chromite inclusion in olivine and groundmass chromites from the Wesselton kimberlite (Shee, 1984; Fig. 2.4B). During contemporaneous olivine and chromite crystallisation, some chromites are included in olivine phenocrysts during its growth, while others remain in the groundmass. The comparison of chromite compositions in kimberlite (Fig. 2.4B) suggests that the groundmass chromite grains in the VNPK crystallised at the same time as olivine and have not reequilibrated with the evolving melt. The chromite cores of groundmass spinel crystals in the VNPK show an atypical Cr-Al trend of Al-depletion from the centres towards the edges of the cores (Figs. 2.3A-C, 2.4B). This trend could be explained by co-crystallisation of olivine and chromite (e.g. Cr-Al trend; Barnes and Roeder, 2001).

Common oxide intergrowths (Fig. 2.3C, D) give important information about the timing of crystallisation of the various oxide mineral phases. Touching Al-poor chromites and Mg-rich ilmenite and rutile, as well as chromites being partly surrounded by ilmenite and rutile, indicate that the latter two phases crystallised during or after crystallisation of the Al-poor chromite. A comparison of groundmass ilmenite compositions in the VNPK with groundmass ilmenite and ilmenite included in olivine phenocrysts in other kimberlites

(Shee, 1984; Fedortchouk and Canil, 2004) was made. More than two thirds of the groundmass ilmenite analyses from the VNPK plot in the field for ilmenite inclusions in olivine phenocrysts (Fig. 2.5A) established by Shee (1984) for the Wesselton kimberlite. In addition, almost all of the analyses plot on the low MgO-side of the groundmass ilmenite field. Based on this comparison, it is suggested that all ilmenites with ≤ 18.0 wt.% MgO are the result of early crystallisation together with olivine, irrespective of their position in the groundmass or as inclusion in olivine.

2.4.2 Geothermometry and oxygen barometry

Co-crystallised spinel – olivine and rutile – ilmenite were used to estimate the temperature and/or oxygen fugacity (fO_2) of the magma at the time of crystallisation. The oxygen fugacity, or the oxidation state, of kimberlite magma is an important parameter that controls diamond resorption (Fedortchouk et al., 2005; Kozai and Arima, 2005).

The following geothermometers and oxygen barometers were used:

4. Spinel – olivine geothermometer and oxygen barometer (Ballhaus et al., 1991): Based on groundmass chromite compositions from VNPK and a range in worldwide olivine phenocryst composition. Unknown variables: P, X^{Fo} (forsterite) in olivine.
5. Rutile – ilmenite oxygen barometer (Zhao et al., 1999): Based on intergrown groundmass rutile and ilmenite in VNPK. Unknown variables: P, T.

2.4.2.1 Spinel – olivine

Groundmass chromite compositions in this study suggest crystallisation together with olivine phenocrysts (see section 2.4.1). As no olivine phenocrysts were analysed in this study, a range in composition from worldwide kimberlite occurrences was used (Fo_{87}-

Fo_{93}; Mitchell, 1995). The spinel – olivine Fe/Mg exchange geothermometer (Ballhaus et al., 1991) and oxygen barometer based on the olivine – orthopyroxene – spinel equilibrium (Ballhaus et al., 1991) were used. The geothermometer and oxygen barometer have been applied successfully to numerous mantle rocks and mantle-derived melts. The oxygen barometer requires the presence of orthopyroxene, and for orthopyroxene-undersaturated rocks such as kimberlites the barometer gives maximum oxygen fugacity values (Ballhaus et al., 1991). A correction can be made if the silica activity of the rock is known. However, due to the absence of suitable silica-bearing mineral phases in the groundmass that could limit the silica activity below the forsterite – enstatite buffer (Ballhaus et al., 1991; Barker, 2001; Fedortchouk and Canil, 2004), a correction was not made.

The temperature and oxygen fugacity were calculated using 46 analyses of chromites (23 from the high-grade kimberlite unit, 23 from low-grade), assuming a pressure of 10 kbar (1 GPa). Pressure has a fairly small effect on temperature and oxygen fugacity calculations (up to 1.5% decrease in temperature, up to 0.02 log unit decrease in fO_2^{NNO} from 10 kbar to 1 bar). The dominant influence on T and fO_2 is the olivine composition (X^{Fo}), and the average result (n=46) varies from 919 °C, 2.0 log units above NNO for Fo_{93} to 1209 °C, 0.8 log unit above NNO for Fo_{87}, both at 10 kbar (Fig. 2.7A; where NNO is the nickel – nickel oxide buffer, after Ballhaus et al., 1991). This range in temperature correlates well with estimates from chromite inclusions in olivine by Fedortchouk and Canil (2004) using the same methodology. Results from the latter study are: temperatures of 1030-1170 °C ± 50 °C (mean 1080 °C), and oxygen fugacity values of 0.4-0.9 log unit above NNO (when uncorrected for silica activity). The oxygen

fugacity results from this study show only slight differences between the high- and low-grade kimberlite units (low-grade kimberlite unit is up to 0.3 log unit more oxidised).

2.4.2.2 Rutile – ilmenite

Rutile – ilmenite intergrowths (Fig. 2.3D) are common in the groundmass of juvenile pyroclasts of both kimberlite units, and allow for estimation of the oxygen fugacity of the magma. The oxygen barometer of Zhao et al. (1999) was applied to touching mineral pairs and analyses with good totals (Tables 2.2, 2.3). The barometer has been used successfully for rutile-ilmenite assemblages in mantle xenoliths incorporated in kimberlite (Zhao et al., 1999) and for rutile and ilmenite inclusions in olivine phenocrysts in kimberlites (Fedortchouk and Canil, 2004). The oxygen barometer (Zhao et al., 1999, Eq. 4) depends on the temperature, pressure, and the activities of $FeTiO_2$ in ilmenite, Fe_2O_3 in ilmenite and TiO_2 in rutile. The oxygen barometer of Zhao et al. (1999) uses the solid solution models by Ghiorso (1990) and Ghiorso and Sack (1991) to calculate the activities for the ilmenite end members (an online version for calculating the activities of rhombohedral oxides is available at http://melts.ofm-research.org/CalcForms/index.html). In the oxygen barometer calculations, the activity of TiO_2 in rutile is equal to X^{Ti}. The rutile – ilmenite oxygen barometer is calibrated on ilmenites with a range in X^{ilm} of 0.42-0.67, significantly more iron-rich than ilmenites in kimberlites (our study, average X^{ilm} = 0.29-0.37; Fedortchouk and Canil (2004), X^{ilm} ranges from 0.34-0.36). Despite the difference in composition, a comparison of the rutile – ilmenite (Zhao et al., 1999) and the olivine – spinel oxygen barometer (Ballhaus et al., 1991) by Fedorchouk and Canil (2004) yielded similar results, when the latter results are uncorrected for silica activity.

The ilmenites used in the oxygen fugacity calculations have an average MgO content of 17.6 wt.% (range: 15.3-19.8; n=17), and 11 out of these 17 ilmenites have MgO ≤ 18.0 wt.%, suggesting co-crystallisation with olivine (see section 2.4.1). Based on this data it is proposed that all rutile – ilmenite intergrowths crystallised during or slightly after olivine crystallisation. The redox state calculations in this study were conducted for spinel-olivine crystallisation temperatures, as estimated for the Lac de Gras kimberlites, Canada (1080 °C at 10 kbar, Fedortchouk and Canil, 2004). These conditions are comparable to the range in temperatures derived from olivine – spinel geothermometry for the VNPK rocks (919-1209 °C, see section 2.4.2.1). To check the sensitivity of the oxygen barometer to pressure and temperature, oxygen fugacities were also calculated at intermediate pressure – temperature conditions (~800 °C, 1 kbar), and low pressure – temperature conditions prevalent during groundmass crystallisation at the surface (~600 °C, 1 bar; Kopylova et al., 2007).

Similar oxygen fugacities were obtained for the high- and low-grade kimberlite units (Fig. 2.7B), irrespective of P, T conditions (Table 2.3). At 1080 °C and 10 kbar the results are about 3.2-3.8 log units above the diamond/graphite – CO_2 (D/GCO) buffer of Frost and Wood (1997), and 0.9-0.3 log unit below the nickel – nickel oxide (NNO) buffer of Ballhaus et al. (1991). These results are ~1.3 log units lower (i.e. less oxidised) than estimates by Fedortchouk and Canil (2004) for Lac de Gras kimberlites, when compared to the oxygen fugacities not corrected for silica activity (Fig. 2.7A). Similar oxygen fugacities in both the high- and low-grade kimberlite units suggest that diamond resorption was not responsible for the observed grade difference. In addition, the oxygen fugacity at the time of rutile and ilmenite crystallisation could, in principle, allow

diamond resorption. In light of the above, it is interesting to look at experimental data of diamond dissolution. Experiments by Kozai and Arima (2005) suggest that the diamond oxidation rate decreases with increasing carbonate concentration in the melt. However, recent studies by Fedortchouk et al. (2007) imply that diamond oxidation requires the presence of a free fluid phase. The latter authors suggest that the decreasing oxidation rate at increasing carbonate concentration in the melt obtained in the Kozai and Arima (2005) study is caused by an increase of water solubility in the more carbonate-rich melt. This would decrease the amount of fluid in the system, and decrease the diamond oxidation rate. Thus, the carbonate-rich (possibly fluid phase-poor) kimberlite magma at Victor (see section 2.4.3) might have prevented much of the diamond dissolution in both the high- and low-grade kimberlite magmas.

2.4.3 Nature of carbonates

Late stage groundmass crystallisation included precipitation of various carbonate phases, and most likely, apatite. The calcite laths contain moderate amounts of Sr (Fig. 2.6A) relative to the concentrations found in the secondary calcite that forms veins or replaces olivine. The concentration of Sr found in calcite laths is consistent with magmatic crystallisation (e.g. Mitchell, 1986; Armstrong et al., 2004). The preservation of variable Mg#'s of groundmass dolomite laths between the two kimberlite units (Fig. 2.6B) presents additional evidence that these carbonates are primary. There is no compositional evidence (e.g. moderate Sr content) that the dolomite base is a result of direct crystallisation from the magma. However, in all cases where olivine is fresh it is considered unlikely that the dolomite has been altered while adjacent carbonate laths and olivine have been preserved. The abundant carbonate in the juvenile pyroclasts at Victor

indicates that the late-stage melt was dominantly carbonatitic in composition. The fact that co-crystallisation of carbonate and apatite is commonly observed in carbonatites (Le Bas, 1981; Deans and Roberts, 1984; Stoppa et al., 2000; Rosatelli et al., 2003) provides further evidence for a primary origin of these carbonates.

2.4.4 Magma genesis, evolution and entrainment of diamonds

There are two important observations that constrain the origins of the high- and low-grade kimberlite units in the VNPK pipe. The first is related to the chemistry of various groundmass minerals in the juvenile pyroclasts. Despite the fact that not all mineral phases in the high- vs. low-grade kimberlite units show statistically different populations, there is a consistent shift of all minerals in the high-grade kimberlite unit towards more Mg-rich compositions (Figs. 2.4, 2.5, 2.6). A difference in Mg# of chromite between different phases of kimberlite and different kimberlite localities is very common (e.g. Shee, 1984; Mitchell, 1986; Fedortchouk and Canil, 2004; see Fig. 2.4B). Therefore, it seems likely that the high- and low-grade kimberlite units in the VNPK are derived from two distinct kimberlite magma pulses with a different genesis and/or evolution. These results are in good agreement with the study by Webb et al. (2004), which showed that the high- and low-grade kimberlite units are derived from separate magma pulses, based on different olivine phenocryst abundances in the high- and low-grade kimberlite juvenile pyroclasts (Figs. 2.1, 2.2).

The second observation relates to the diamond content and oxygen fugacity estimates for the high- and low-grade kimberlite units. Similar oxygen fugacity estimates for the high- (Δ log fO_2^{NNO} -0.6 ± 0.4 (2 SD) for Rt-Ilm at 1080 °C, 10 kbar) and low-grade kimberlite magma pulse (Δ log fO_2^{NNO} -0.6 ± 0.5) were obtained. This negates the possibility that a

difference in oxygen fugacity between the two magmas caused preferential resorption of diamond in the earlier, diamond-poor, kimberlite. Thus, it is most likely that the difference in diamond content between the two magmas is caused by differential mantle sampling. The later kimberlite magma, forming the present-day high-grade deposit, picked up more diamonds during its rise through the mantle.

Based on the above considerations, we are proposing four processes that could explain the consistent difference in Mg# between the various mineral phases that crystallised in the high- vs. low-grade kimberlite magma pulses: (i.) Slight differences in composition of the mantle protoliths where the kimberlite melts are formed, resulting in a different bulk chemistry of the two kimberlite magmas. (ii.) A difference in the source degree of melting, also resulting in a different bulk chemistry of the magmas. (iii.) Variable amount of olivine phenocryst crystallisation in the magmas during ascent. Olivine crystallisation will deplete the remaining magma in Mg relative to Fe (decrease in Mg#), resulting in less Mg-rich oxides being formed by subsequent crystallisation. This scenario accords well with the different olivine phenocryst abundances in the high- and low-grade juvenile pyroclasts. I.e. more olivine phenocryst crystallisation in the low-grade kimberlite magma would result in relatively lower Mg# for the melt and subsequently crystallising oxide minerals. (iv.) The temperatures of crystallisation (e.g. Ballhaus et al., 1991), whereby a higher crystallisation temperature causes a higher Mg# in chromite.

2.5 Conclusions

1. Our results show that the groundmass chromites, ilmenites and dolomite laths from the low-grade kimberlite unit all have lower Mg-numbers than groundmass minerals

in the high-grade kimberlite unit. Also, the low-grade kimberlite unit is characterised by a higher abundance of olivine phenocrysts.

2. This study confirms the conclusion by Webb et al. (2004) that the high- and low-grade kimberlite units in the VNPK pipe formed from two distinct magma pulses. In addition, it shows that these magmas had a different origin in the asthenosphere and/or experienced different crystallisation histories causing a consistent shift in Mg-numbers of most mineral phases.
3. The similar oxygen fugacity values for the two magma pulses indicate that differential diamond dissolution cannot be responsible for the grade difference between the high- and low-grade kimberlite units. Thus, the two magmas entrained contrasting amounts of diamond during their ascent towards the surface.
4. This validates the geological and emplacement models, which in turn predict the diamond distribution within the pipe (Fig. 2.1).

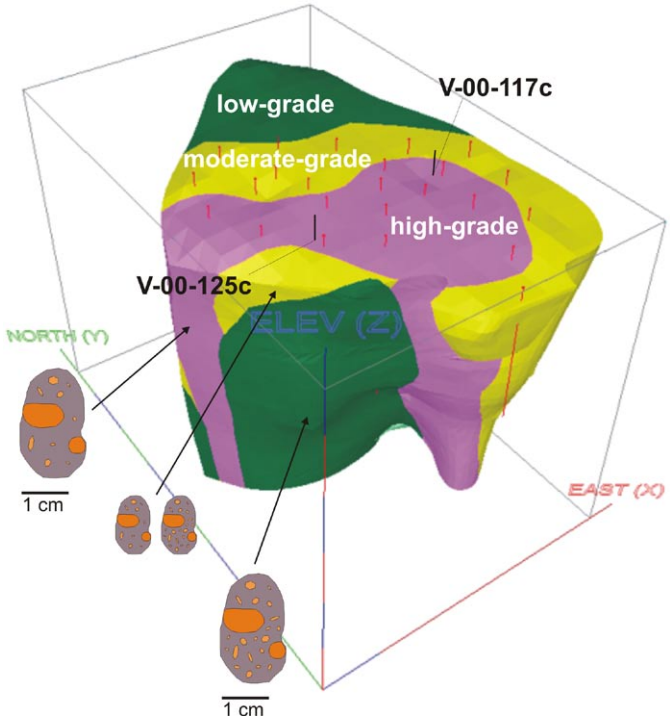

Figure 2.1 Macrodiamond content distribution (2001-2002 bulk sample programme) defining high-, moderate- and low-grade zones of the Victor North pyroclastic kimberlite pipe. Characteristic juvenile pyroclasts for each grade zone are shown schematically. Note the higher abundance of olivine phenocrysts in the low-grade juvenile pyroclasts and mixed pyroclasts (i.e. derived from both high- and low-grade kimberlite magma pulses) in the moderate-grade zone. Vertical axis is 300m long. Vertical lines indicate the location of large diameter bulk sampling drill holes. The location of drill cores V-00-117c and V-00-125c is also shown. Figure modified from Webb et al. (2004).

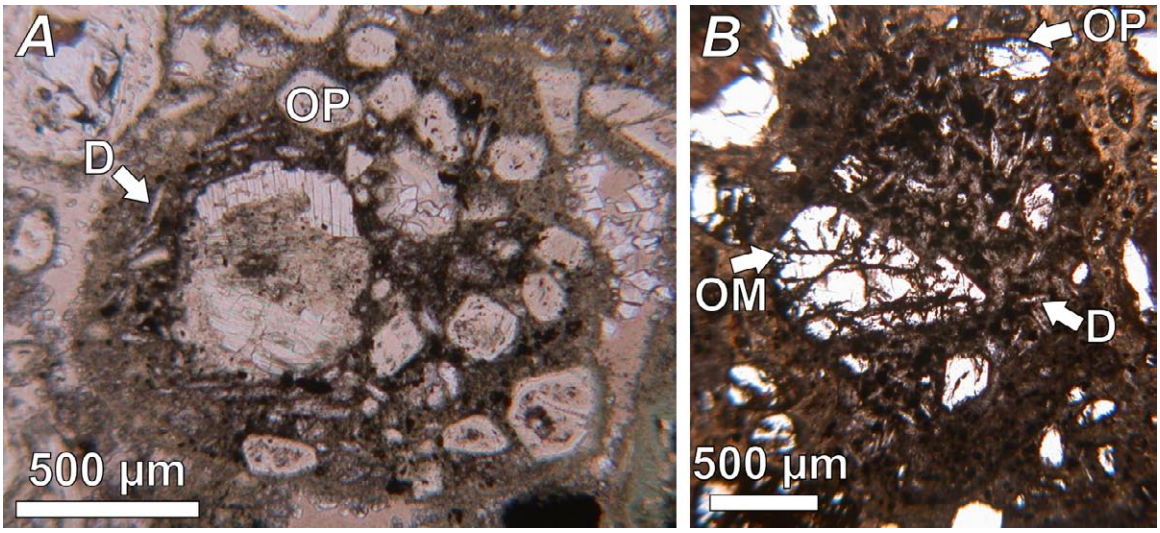

Figure 2.2 Photomicrographs of juvenile pyroclasts
Photomicrographs of characteristic juvenile pyroclasts in the low-grade (A) and high-grade (B) kimberlite units. Low-grade juvenile pyroclasts have a higher abundance of olivine phenocrysts. *OM*: olivine macrocryst, *OP*: olivine phenocryst (altered in low-grade juvenile pyroclast), *D*: dolomite lath.

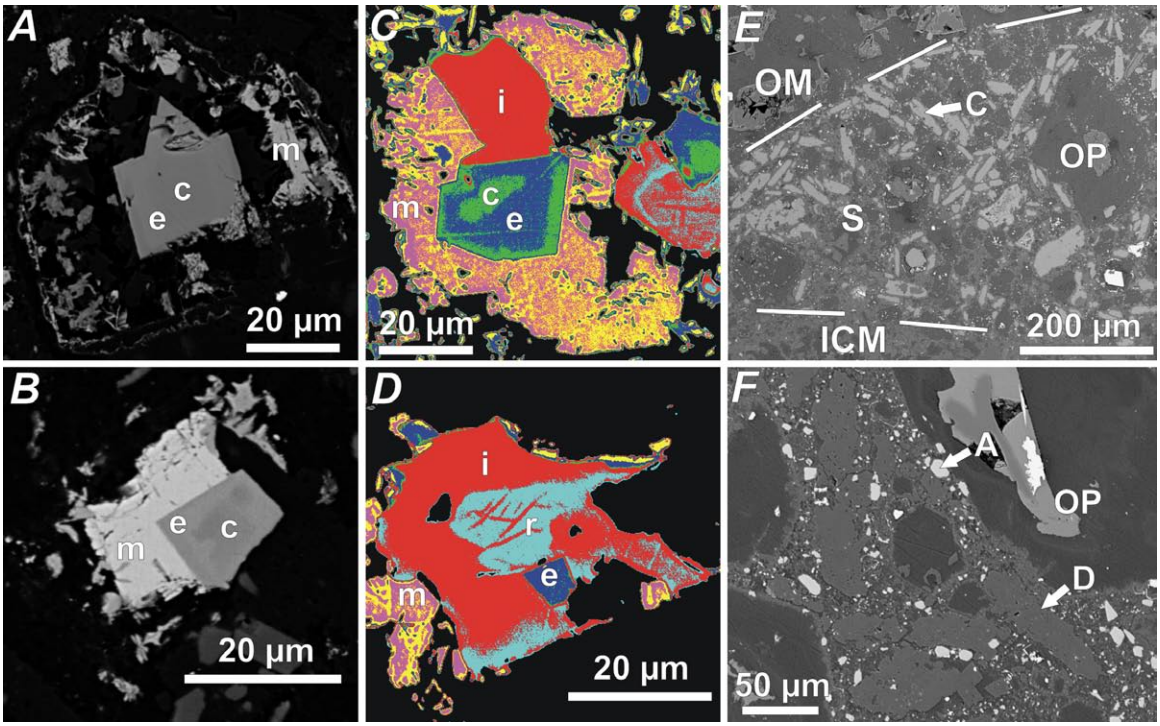

Figure 2.3 Backscatter electron (BSE) images of groundmass phases within juvenile pyroclasts. (A) Typical low-grade kimberlite unit spinel with zoned chromite core (*c*: Al-rich centre, *e*: Al-poor edge) and magnetite (*m*) atoll-rim. (B-C) Typical high-grade kimberlite unit spinels with zoned chromite core and enveloping magnetite rim. Note irregular shape of chromite centre (*c*). (C-D) False colour BSE images of chromite, ilmenite (*i*) and rutile (*r*) intergrowths. Note that only the Al-poor chromite edge (*e*) is in direct contact with ilmenite. (E) Juvenile pyroclast selvage (*S*) around altered olivine macrocryst (*OM*) with abundant calcite laths (*C*) and one altered olivine phenocryst (*OP*). *ICM*: inter-clast matrix. (F) Dolomite laths (*D*) and apatite crystal (*A*) in the groundmass of a juvenile pyroclast.

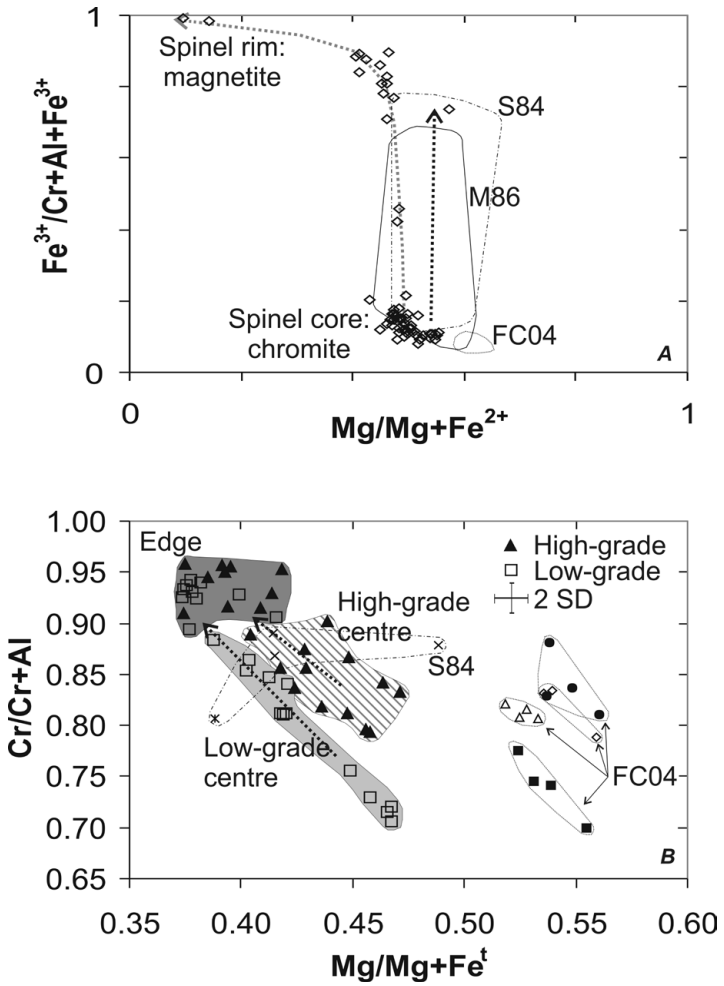

Figure 2.4 Groundmass spinel compositions. (A) Chromite to magnetite zoning trend in spinels from the VNPK kimberlite, shown in a $Mg/Mg+Fe^{2+}$ vs. $Fe^{3+}/Cr+Al+Fe^{3+}$ plot. All chromites in (B) plot in the lower part of the graph. Typical zoning trends in kimberlites are shown by the black arrow, and the fields marked M86 (data from Mitchell, 1986) and S84 (Shee, 1984). The small field marked FC04 (Fedortchouk and Canil, 2004) represents chromite inclusions in olivine phenocrysts from the Lac de Gras area. (B) $Mg/Mg+Fe^{t}$ vs. Cr/Cr+Al plot with Cr-Al zoning trend from chromite centres to edges of the cores. Fields marked FC04 represent chromite inclusions in olivine phenocrysts from the Torrie (lower left), Leslie, Grizzly and Aaron (upper right) kimberlites in the Lac de Gras area. Field marked S84 represents groundmass chromites (crosses) and a chromite included in olivine (star), each representing a different unit in the Wesselton kimberlite. Error bar indicates 2 SD analytical precision of EMP analysis.

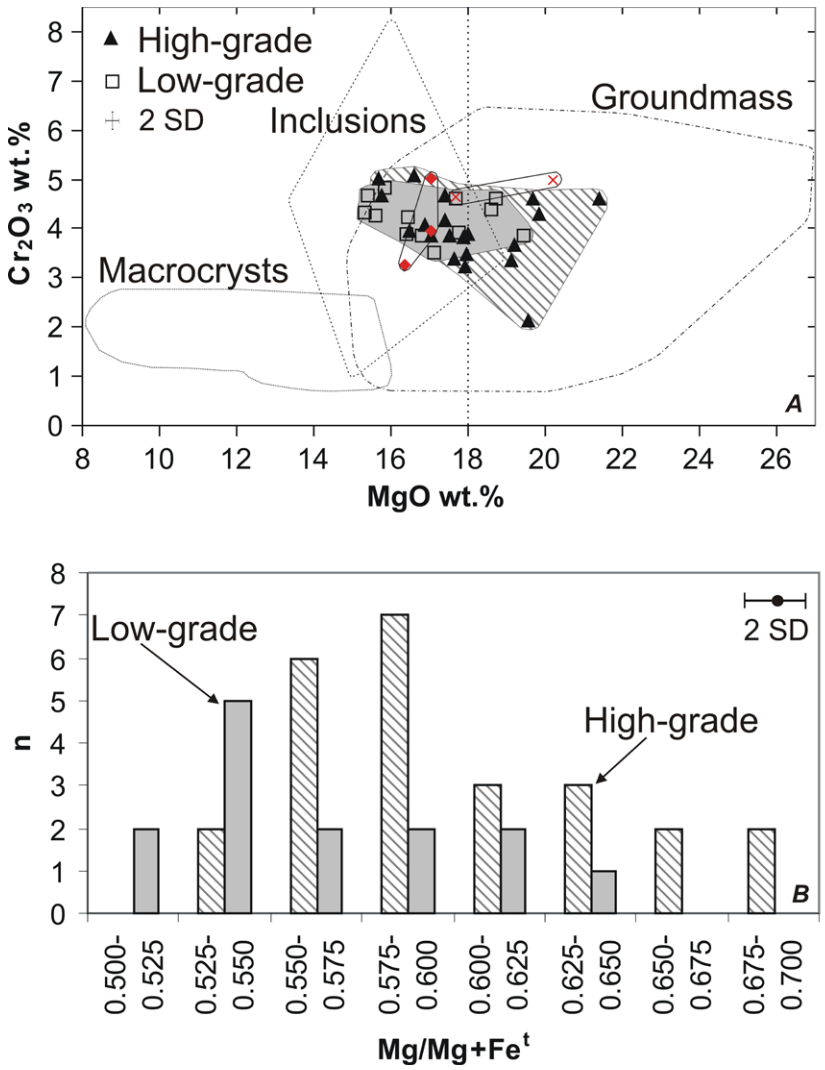

Figure 2.5 Groundmass ilmenite compositions. (A) Cr_2O_3 vs. MgO wt.% plot comparing VNPK groundmass ilmenites with macrocryst, inclusion (in olivine phenocryst) and groundmass fields established by Shee (1984) for the Wesselton kimberlite. Ilmenite inclusions in olivine phenocrysts (diamonds) and ilmenite in the groundmass (crosses) from the Lac de Gras kimberlites (Fedortchouk and Canil, 2004) are shown for reference. The 18.0 wt.% MgO line represents the suggested upper limit for ilmenites crystallising together with olivine. (B) Mg-number histogram of groundmass ilmenite. 2 SD indicates precision.

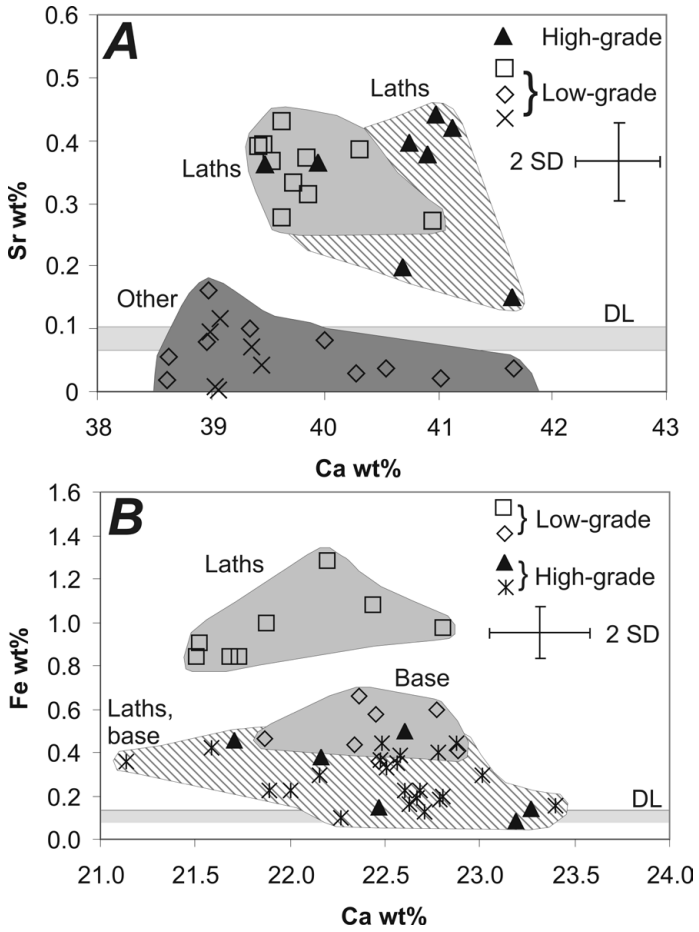

Figure 2.6 Groundmass carbonate compositions. (A) Sr (wt.%) vs. Ca (wt.%) plot for groundmass calcite laths (upper fields) and calcite in veins and olivine replacements (lower field). (B) Fe (wt.%) vs. Ca (wt.%) plot for groundmass dolomite that occurs in laths and in the interstitial base. DL: upper and lower detection limit; error bar indicates 2 SD precision.

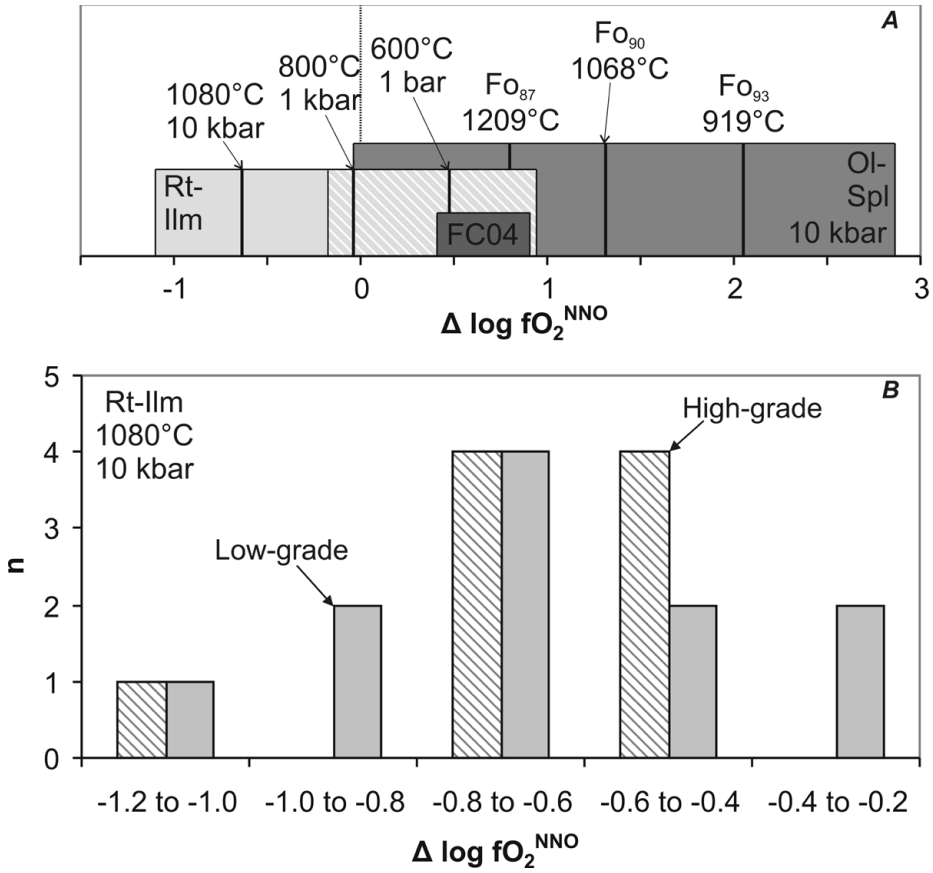

Figure 2.7 Oxygen fugacity estimates for the VNPK. (A) Range in oxygen fugacity values relative to the NNO buffer at different pressures and temperatures (rutile – ilmenite; Zhao et al., 1999) and variable olivine phenocryst compositions (olivine – spinel; Ballhaus et al., 1991; at 10 kbar). Average values at different T, P, X conditions (heavy black lines) ± 2 SD are shown. Field of FC04 (Fedortchouk and Canil, 2004) shows the range in oxygen fugacity results for chromite, ilmenite and rutile inclusions in olivine for the Lac de Gras kimberlites (1080 ºC, 10 kbar; not corrected for silica activity). (B) Oxygen fugacity values relative to the NNO buffer (1080 ºC, 10 kbar) for the high- and low-grade kimberlite units, based on groundmass rutile – ilmenite intergrowths and the oxygen barometer of Zhao et al. (1999).

Table 2.1 Representative electron microprobe (EMP) analysis of groundmass spinel, ilmenite and rutile in high- and low-grade kimberlite unit juvenile pyroclasts

Depth [a]	125.69	125.69	070.25	125.69	211.24	156.90	125.69	125.69	156.90	156.90	125.69	156.90
Grade	High	High	High	High	Low	Low	High	High	Low	Low	High	Low
Mineral [b]	Chr 'edge'	Chr centre	Mag-Usp	Mag	Chr edge	Chr centre	Ilm	Ilm (+Rt)	Ilm	Ilm (+Rt)	Rt (+Ilm)	Rt (+Ilm)
MgO	10.28	11.69	11.26	2.56	10.24	10.87	19.55	18.01	17.11	16.80	1.63	3.22
Al_2O_3	1.97	7.34	4.22	0.21	2.57	7.43	n.d.	n.d.	n.d.	n.d.	n.d.	n.d.
SiO_2	n.d.	0.06	n.d.	0.44	n.d.	0.07	0.11	0.04	0.07	n.d.	0.05	0.07
CaO	0.14	0.11	0.30	0.36	0.30	0.31	0.25	0.14	0.20	0.28	0.19	0.40
TiO_2	5.29	2.24	12.07	0.54	5.59	4.18	55.22	55.09	53.90	54.96	91.39	86.20
V_2O_5	n.d.	0.17	n.d.	n.d.	n.d.	0.07	n.d.	n.d.	n.d.	n.d.	n.d.	n.d.
Cr_2O_3	50.69	54.45	0.79	0.71	47.27	47.57	2.14	3.88	3.53	3.87	3.22	3.76
MnO	n.d.	n.d.	0.39	0.29	0.26	0.27	0.40	0.31	0.41	0.36	n.d.	0.27
Fe_2O_3 [c]	9.78	6.60	45.32	67.44	11.32	8.55	8.07	5.42	6.50	5.64		
FeO	20.45	17.44	24.55	27.45	20.42	19.23	14.27	16.92	17.35	18.82	1.43	4.65
NiO	0.21	n.d.	0.24	n.d.	0.13	0.17	n.d.	n.d.	0.10	n.d.	n.d.	n.d.
Nb_2O_5	n.d.	n.d.	n.d.	n.d.	n.d.	n.d.	0.13	n.d.	n.d.	n.d.	1.61	1.35
Ta_2O_5	n.d.	n.d.	n.d.	n.d.	n.d.	n.d.	n.d.	n.d.	n.d.	n.d.	0.08	n.d.
Total wt%	98.81	100.10	99.14	100.00	98.10	98.72	100.14	99.81	99.17	100.73	99.60	99.92
$Mg/Mg+Fe^t$	0.385	0.471	0.235	0.049	0.374	0.419	0.618	0.596	0.568	0.556		
Cr/Cr+Al	0.945	0.833	0.111	0.692	0.925	0.811						

n.d.: not detected (below minimum detection limit)

[a] All samples are from V-00-117c, number represent depth/sample number in meters

[b] Mineral abbreviations after Kretz (1983), (+..) denotes intergrowth with mineral in brackets

[c] Ferric (Fe^{3+}) vs. ferrous (Fe^{2+}) iron calculated using stoichiometric and charge balance equations (Droop, 1987).

Table 2.2 Representative electron microprobe (EMP) analysis of groundmass carbonate, apatite and phlogopite in high- and low-grade kimberlite unit juvenile pyroclasts

Depth [a]	125.69	156.90	156.90	156.90	070.25	211.24	125.69	156.90	125.69	125.69	156.90	125.69
Grade	High	Low	Low	Low	High	Low	High	Low	High	High	Low	High
Mineral [b]	Cal - lath	Cal - lath	Cal - repl.ol.	Cal - vein	Dol - lath	Dol - lath	Dol - base	Dol - base	Ap	Ap [c]	Ap	Phl - g.m.
Na_2O	-	-	-	-	-	-	-	-	0.23	0.15	0.62	0.20
MgO	0.13	0.84	1.89	1.48	20.30	20.33	20.66	20.66	0.55	0.35	0.73	25.71
Al_2O_3	-	-	-	-	-	-	-	-	-	-	-	11.21
SiO_2	-	-	-	-	-	-	-	-	-	-	-	42.51
P_2O_5	-	-	-	-	-	-	-	-	40.49	41.28	39.97	-
K_2O	-	-	-	-	-	-	-	-	-	-	-	8.89
CaO	56.91	55.31	54.05	54.66	32.56	30.60	31.87	31.25	54.66	54.85	54.59	0.40
TiO_2	-	-	-	-	-	-	-	-	-	-	-	0.66
Cr_2O_3	-	-	-	-	-	-	-	-	-	-	-	0.30
MnO	n.d.	0.02	n.d.	n.d.	0.32	0.28	0.33	0.21	n.d.	n.d.	n.d.	n.d.
FeO	0.16	0.15	0.23	0.09	0.18	1.28	0.51	0.56	0.22	0.19	0.20	3.91
SrO	0.23	0.44	n.d.	n.d.	0.29	0.57	0.14	0.12	0.27	n.d.	0.14	-
BaO	n.d.	n.d.	n.d.	n.d.	n.d.	n.d.	n.d.	n.d.	-	-	-	n.d.
La_2O_3	-	-	-	-	-	-	-	-	n.d.	n.d.	n.d.	-
Ce_2O_3	-	-	-	-	-	-	-	-	n.d.	n.d.	n.d.	-
F	-	-	-	-	-	-	-	-	1.14	1.09	1.12	0.10
Cl	-	-	-	-	-	-	-	-	0.14	0.11	0.26	0.14
H_2O [d]									1.20	1.23	1.19	4.12
O=F									-0.48	-0.46	-0.47	-0.04
O=Cl									-0.03	-0.02	-0.06	-0.03
CO_2 [e]	45.01	44.61	44.65	44.57	48.15	47.42	48.15	47.61				
Total wt.%	102.44	101.37	100.82	100.80	101.80	100.48	101.66	100.41	98.39	98.77	98.29	98.08

n.d.: not detected (below minimum detection limit); "-": not analysed

[a] All samples are from V-00-117c, number represents depth/sample number in meters

[b] Mineral abbreviations after Kretz (1983). Repl.ol: replacing olivine, g.m.: groundmass

[c] Fluorine calculated by linear extrapolation from five successive measurements on same spot (for methodology, see Stormer et al., 1993; Coulson et al., 2001)

[d] H_2O in apatite and phlogopite determined by stoichiometry, assuming 1 (OH,F,Cl) for apatite and 2 (OH,F,Cl) for phlogopite

[e] CO_2 in carbonate calculated by stoichiometry.

Table 2.3 Oxygen fugacity results from high- and low-grade kimberlite units, based on rutile-ilmenite intergrowths in juvenile pyroclast ground-mass

	Rutile		Ilmenite [a]						At 1080 °C, 10 kbar						At 600 °C, 1 bar				
									Activities[b]		log fO_2	ΔlogfO_2	ΔlogfO_2		Activities[b]		log fO_2	ΔlogfO_2	ΔlogfO_2
	EMP # [c]	X^{Ti}	EMP # [c]	X^{Ilm}	X^{Gei}	X^{Prn}	X^{Hem}	Fe^{3+}/Fe^{t}	Fe_2O_3	$FeTiO_3$	[kbar]	[d] NNO [e]	D/GCO [e]		Fe_2O_3	$FeTiO_3$	[kbar]	[d] NNO [e]	D/GCO [e]
High-grade	1-12569-20	0.937	1-12569-21	0.327	0.620	0.006	0.047	0.223	0.014	0.441	-8.26	-0.43	3.73		0.056	0.468	-17.49	0.68	2.43
	1-12569-1	0.905	1-12569-3	0.279	0.673	0.007	0.041	0.227	0.011	0.389	-8.32	-0.48	3.67		0.045	0.408	-17.50	0.67	2.43
	3-07025-23	0.916	3-07025-	0.334	0.611	0.013	0.041	0.197	0.011	0.451	-8.55	-0.72	3.44		0.044	0.481	-17.78	0.39	2.14
	3-07025-18	0.914	3-07025-20	0.334	0.616	0.006	0.044	0.208	0.012	0.450	-8.44	-0.60	3.55		0.050	0.478	-17.67	0.50	2.26
	3-07025-17	0.920	,,	0.334	0.616	0.006	0.044	0.208	0.012	0.450	-8.43	-0.59	3.56		0.050	0.478	-17.66	0.51	2.27
	3-07025-6	0.833	3-07025-7	0.284	0.659	0.009	0.048	0.251	0.014	0.393	-8.24	-0.40	3.75		0.058	0.413	-17.45	0.72	2.48
	3-12569-3	0.912	3-12569-5	0.280	0.676	0.007	0.037	0.208	0.009	0.392	-8.47	-0.64	3.52		0.038	0.411	-17.65	0.53	2.28
	3-12569-4	0.876	,,	0.280	0.676	0.007	0.037	0.208	0.009	0.392	-8.54	-0.71	3.45		0.038	0.411	-17.72	0.45	2.21
	3-12569-13	0.848	3-12569-14	0.399	0.555	0.006	0.040	0.166	0.010	0.518	-8.97	-1.14	3.02		0.042	0.554	-18.21	-0.04	1.71
Low-grade	3-15690-5	0.838	1-15690-7	0.305	0.642	0.008	0.044	0.225	0.012	0.418	-8.47	-0.63	3.53		0.050	0.442	-17.68	0.49	2.25
	1-15690-8	0.828	,,	0.305	0.642	0.008	0.044	0.225	0.012	0.418	-8.49	-0.65	3.51		0.050	0.442	-17.70	0.47	2.23
	,,	0.828	1-15690-9	0.338	0.613	0.008	0.040	0.191	0.011	0.456	-8.78	-0.95	3.21		0.043	0.486	-18.01	0.17	1.92
	1-21124-3	0.861	1-21124-4	0.377	0.559	0.007	0.057	0.231	0.019	0.487	-8.31	-0.47	3.68		0.073	0.521	-17.58	0.59	2.34
	,,	0.861	1-21124-5	0.361	0.572	0.007	0.060	0.251	0.021	0.470	-8.17	-0.33	3.82		0.080	0.502	-17.44	0.73	2.48
	3-15690-7	0.824	1-15690-12	0.277	0.662	0.008	0.053	0.277	0.017	0.383	-8.07	-0.24	3.92		0.068	0.402	-17.28	0.89	2.65
	,,	0.824	1-15690-13	0.305	0.639	0.008	0.048	0.239	0.014	0.416	-8.36	-0.52	3.63		0.058	0.440	-17.58	0.59	2.35
	3-15690-9	0.820	3-15690-10	0.397	0.545	0.008	0.050	0.201	0.015	0.510	-8.67	-0.83	3.32		0.059	0.546	-17.93	0.24	1.99
	,,	0.820	3-15690-11	0.364	0.580	0.007	0.049	0.212	0.015	0.478	-8.58	-0.74	3.41		0.058	0.511	-17.83	0.34	2.09
	3-15690-13	0.832	3-15690-14	0.406	0.545	0.006	0.043	0.176	0.012	0.523	-8.91	-1.08	3.08		0.047	0.560	-18.16	0.01	1.76
	,,	0.832	3-15690-15	0.385	0.553	0.007	0.055	0.221	0.018	0.496	-8.45	-0.62	3.54		0.069	0.530	-17.72	0.45	2.20

[a] Mineral abbreviations after Kretz (1983). Gei: geikielite, Prn: pyrophanite

[b] Calculated using Ghiorso (1990) and Ghiorso and Sack (1991). An online version for calculating the activities of rhombohedral oxides is available at http://melts.ofm-research.org/CalcForms/index.html

[c] All samples are from V-00-117c, first digit represents EMP day #, next five digits represent depth/sample number (12569 is 125.69m), last digits are EMP spot #

[d] Calculated using oxygen barometer by Zhao et al. (1999)

[e] Buffer equations after Ballhaus et al. (1991) for NNO; Frost and Wood (1997) for D/GCO

2.6 References

Armstrong, J.P., Wilson, M., Barnett, R.L., Nowicki, T. and Kjarsgaard, B.A., 2004. Mineralogy of primary carbonate-bearing hypabyssal kimberlite, Lac de Gras, Slave Province, Northwest Territories, Canada. Lithos, 76(1-4): 415-433.

Ballhaus, C., Berry, R. and Green, D., 1991. High pressure experimental calibration of the olivine-orthopyroxene-spinel oxygen geobarometer: implications for the oxidation state of the upper mantle. Contributions to Mineralogy and Petrology, 107(1): 27-40. Two errata: Contributions to Mineralogy and Petrology, 108(3): 384; Contributions to Mineralogy and Petrology, 118(1): 109.

Barker, D.S., 2001. Calculated silica activities in carbonatite liquids. Contributions to Mineralogy and Petrology, 141(6): 704-409.

Barnes, S.J. and Roeder, P.L., 2001. The range of spinel composition in terrestrial mafic and ultramafic rocks. Journal of Petrology, 42(12): 2279-2302.

Coulson, I.M., Dipple, G.M. and Raudsepp, M., 2001. Evolution of HF and HCl activity in magmatic volatiles of the gold-mineralized Emerald Lake pluton, Yukon Territory, Canada. Mineralium Deposita, 36: 594-606.

Deans, T. and Roberts, B., 1984. Carbonatite tuffs and lava clasts of the Tinderet foothills, western Kenya; a study of calcified natrocarbonatites. Journal of the Geological Society of London, 141(3): 563-580.

Droop, G.T.R., 1987. A general equation for estimating Fe^{3+} concentrations in ferromagnesian silicates and oxides from microprobe analysis, using stoichiometric criteria. Mineralogical Magazine, 51: 431-435.

Fedortchouk, Y. and Canil, D., 2004. Intensive variables in kimberlite magmas, Lac de Gras, Canada and implications for diamond survival. Journal of Petrology, 45(9): 1725-1745.

Fedortchouk, Y., Canil, D. and Carlson, J.A., 2005. Dissolution forms in Lac de Gras diamonds and their relationship to the temperature and redox state of kimberlite magma. Contributions to Mineralogy and Petrology, 150(1): 54-69.

Fedortchouk, Y., Canil, D. and Semenets, E., 2007. Mechanisms of diamond oxidation and their bearing on the fluid composition in kimberlite magmas. American Mineralogist, 92(7): 1200-1212.

Frost, D.J. and Wood, B.J., 1997. Experimental measurements of the fugacity of $C0_2$ and graphite/diamond stability from 35 to 77 kbar at 925 to 1650 °C. Geochimica et Cosmochimica Acta, 61(8): 1565-1574.

Ghiorso, M.S., 1990. Thermodynamic Properties of hematite ilmenite geikielite solid-solutions. Contributions to Mineralogy and Petrology, 104(6): 645-667.

Ghiorso, M.S. and Sack, R.O., 1991. Fe-Ti oxide geothermometry - thermodynamic formulation and the estimation of intensive variables in silicic magmas. Contributions to Mineralogy and Petrology, 108(4): 485-510.

Glossary of Geology, 2005. Neuendorf, K.K.E., Mehl J.P.Jr., and Jackson, J.A. (eds.), American Geological Institute, 779 pp.

Kong, J.M., Boucher, D.R. and Scott Smith, B.H., 1999. Exploration and geology of the Attawapiskat kimberlites, James Bay Lowland, Northern Ontario, Canada. Proceedings of the 7th International Kimberlite Conference, The J.B. Dawson volume, Cape Town, 452-467.

Kopylova, M.G., Matveev, S. and Raudsepp, M., 2007. Searching for parental kimberlite melt. Geochimica et Cosmochimica Acta, 71(14): 3616-3629.

Kozai, Y. and Arima, M., 2005. Experimental study on diamond dissolution in kimberlite and lamproitic melts at 1300-1420 °C and 1 GPa with controlled oxygen partial pressure. American Mineralogist, 90(11-12): 1759-1766.

Kretz, R., 1983. Symbols for rock-forming minerals. American Mineralogist, 68: 227-279.

Le Bas, M.J., 1981. Carbonatite magmas. Mineralogical Magazine, 44: 133-140.

Mitchell, R.H., 1986. Kimberlites: mineralogy, geochemistry and petrology. Plenum Press, New York, 442 pp.

Mitchell, R.H., 1995. Kimberlites, orangeites, and related rocks. Plenum Press, New York, 410 pp.

Pouchou, J.L. and Pichoir, F., 1985. PAP $\phi(\rho Z)$ procedure for improved quantitative microanalysis. Microbeam analysis: 104-106.

Roeder, P., Gofton, E. and Thornber, C., 2006. Cotectic proportions of olivine and spinel in olivine-tholeiitic basalt and evaluation of pre-eruptive processes. Journal of Petrology, 47(5): 883-900.

Roeder, P.L., Poustovetov, A. and Oskarsson, N., 2001. Growth forms and composition of chromian spinel in morb magma: diffusion-controlled crystallization of chromian spinel. Canadian Mineralogist, 39(2): 397-416.

Rosatelli, G., Wall, F. and Le Bas, M.J., 2003. Potassic glass and calcite carbonatite in lapilli from extrusive carbonatites at Rangwa Caldera Complex, Kenya. Mineralogical Magazine, 67(5): 931-955.

Shee, S.R. (1984). The oxide minerals of the Wesselton mine kimberlite, Kimberley, South Africa. Proceedings of the 3rd International Kimberlite Conference, Volume I: kimberlites and related rocks, Elsevier, Development in Petrology Series, 59-73.

Stoppa, F., Woolley, A.R., Lloyd, F.E. and Eby, N., 2000. Carbonatite lapilli-bearing tuff and a dolomite carbonatite bomb from Murumuli crater, Katwe volcanic field, Uganda. Mineralogical Magazine, 64(4): 641-650.

Stormer, J.C., Pierson, M.L. and Tacker, R.C., 1993. Variation of F and Cl X-ray intensity due to anisotropic diffusion in apatite during electron microprobe analysis. American Mineralogist, 78(5-6): 641-648.

Webb, K.J., Scott Smith, B.H., Paul, J.L. and Hetman, C.M., 2004. Geology of the Victor kimberlite, Attawapiskat, Northern Ontario, Canada: cross-cutting and nested craters. Lithos, 76(1-4): 29-50.

Zhao, D.G., Essene, E.J. and Zhang, Y.X., 1999. An oxygen barometer for rutile-ilmenite assemblages: oxidation state of metasomatic agents in the mantle. Earth and Planetary Science Letters, 166(3-4): 127-137.

3 STRATIGRAPHY OF THE INTRA-CRATER VOLCANICLASTIC DEPOSITS OF THE VICTOR NORTHWEST KIMBERLITE PIPE[2]

3.1 Introduction and regional geology

Kimberlites generally occur as pipe-shaped deposits that are formed by explosive volcanic eruptions of crystal-rich, low viscosity, low volume and intra-cratonic magmas. Worldwide, these kimberlite pipes are the most important source for diamond, however their emplacement mechanisms are as yet not fully understood. The key in unravelling the emplacement history of these volcanic pipes is establishing the detailed volcanic facies architecture of the deposit. This type of research can provide valuable tools to guide diamond exploration and define ore units; in addition, it also sheds light onto intra-crater and intra-conduit volcanic processes, a topic that is not well understood in present-day volcanology. Here we present a detailed reconstruction of the complex intra-crater volcanic stratigraphy of a kimberlite pipe. This study provides unique insights into the emplacement of this particular kimberlite pipe and has important general implications for the volcanic processes involved in kimberlite formation.

The Victor kimberlite complex is located in the James Bay Lowlands, Northern Ontario, Canada and is currently being mined for diamonds by De Beers Canada Inc. Victor is the largest kimberlite in the Middle-Late Jurassic Attawapiskat kimberlite province (Kong et

[2] A version of this chapter has been published. van Straaten, B.I., Kopylova, M.G., Russell, J.K., Webb, K.J. and Scott Smith, B.H. (2009). Stratigraphy of the intra-crater volcaniclastic deposits of the Victor Northwest kimberlite, northern Ontario, Canada. Lithos, 112(Supplement 1): 488-500.

al., 1999), and comprises three pipes, Victor South, Victor Main and Victor Northwest (Fig. 3.1A). The kimberlite bodies have been described previously by Kong et al. (1999), Webb et al. (2004) and in chapter 2.

The Victor kimberlite pipes crosscut an Ordovician to Silurian sedimentary succession, unconformably overlying Precambrian granitoid basement. The unconformity occurs at approximately 272 m below the present surface. Roughly 10-30 m of unconsolidated Quaternary overburden is currently present on top of the kimberlites. The amount of erosion since kimberlite emplacement is difficult to constrain, and current estimates range from ~50 m to 600 m of post-emplacement erosion (Kong et al., 1999; F. Brunton, pers. comm. 2006).

In this paper we present the results of detailed studies of drill core, polished drill core samples and thin sections of the Victor Northwest kimberlite pipe. The results allow for the first comprehensive reconstruction of the complex volcanic facies architecture within the Victor Northwest pipe, and provide significant advances into the understanding of the emplacement and eruption history of the pipe. It is interpreted that this kimberlite pipe was formed by a sequence of variably explosive eruptions, ranging from highly explosive events to lower energy eruptions and major pipe wall collapse at the end of the eruption.

3.2 Terminology

In this study, we use the following terms. *Volcaniclastic kimberlite* (VK) refers to all rocks or unconsolidated deposits that consist of volcanic fragments, irrespective of the mode of fragmentation or final deposition (Cas et al., 2008). Hence, these deposits encompass both primary pyroclastic (*pyroclastic kimberlite, PK*) and *resedimented volcaniclastic kimberlite (RVK)* deposits. After careful study, some of the volcaniclastic

kimberlite units are interpreted to be pyroclastic kimberlite (PK). For units with an unclear origin, the term volcaniclastic kimberlite is retained.

The most complicated aspect of the volcanic stratigraphy in VNW is the interpretation of coherent-looking kimberlite. In general, a coherent rock refers to intrusive dykes or sills, or extrusive lavas. In this study, we called a rock *coherent* only when these rocks show a well crystallised groundmass of evenly distributed oxides, carbonate ± phlogopite laths and possible monticellite pseudomorphed by serpentine (e.g. hypabyssal kimberlite or HK, Field and Scott Smith, 1999). In other cases where kimberlite was not unequivocally proven to be coherent in nature, the rocks are named using the descriptive terms dark and competent kimberlite (DCK). It should be noted that many densely welded or completely coalesced pyroclastic rocks in basaltic to rhyolitic volcanic settings can appear coherent (or lava-like, see Ekren et al., 1984; Branney and Kokelaar, 1992; Le Pennec and Fernandez, 1992; Andrews et al., 2008) and on the hand sample and microscopic scale these rocks can be indistinguishable from lavas. These types of pyroclastic rocks generally give little to no clues to their original fragmental derivation, hence distinguishing volcaniclastic from coherent rocks in these settings can be difficult.

We distinguished the following pyroclast types: (1) *juvenile pyroclasts*, which form two subtypes: (1a) *cored juvenile pyroclasts* comprise a crystal or lithic clast core surrounded by a selvage of crystallised kimberlite melt, (1b) *uncored juvenile pyroclast*, composed of crystallised kimberlite melt without such a core; (2) *discrete olivines* are crystals without a melt selvage; and (3) *clastic pyroclasts* include both *accretionary lapilli* (comprising only ash-sized material) and *ash-armoured clasts* (comprising ash-sized material around a larger central core; Schumacher and Schmincke, 1991). The crystallized kimberlite

within juvenile pyroclasts features a well crystallised groundmass with a network of carbonate ± phlogopite laths and evenly distributed groundmass oxides usually set in a cryptocrystalline carbonate matrix. On the other hand, clastic pyroclasts contain selvages made up of generally fine grained clastic components, i.e. small (broken) olivines, etc. The percentage of broken olivine in the matrix is generally estimated by counting twenty or more olivines of different sizes in a thin section. In addition, the term *macrocryst* is used here to refer to large (>0.5 mm) anhedral crystals interpreted to be mantle-derived xenocrysts, whereas *phenocryst* refers to smaller (typically <0.5 mm) euhedral-subhedral crystals that likely crystallised from the kimberlite magma (Mitchell, 1986).

3.3 Methods

The external shape and internal geology of the Victor Northwest (VNW) kimberlite pipe have been reconstructed using a total of 22 drill cores (Figs. 3.1, 3.2), with a total cumulative length of ~4.2 km. All drill cores intersecting VNW were drilled in between 1998 and 2003 by De Beers Canada Inc. Initial drill core logging for advanced exploration, evaluation and geotechnical purposes was carried out by De Beers and associated personnel, and has been presented in Webb et al. (2004). For this study, we re-examined 20 drill cores to determine the volcanic stratigraphy of the VNW pipe; these drill core investigations included detailed logging as well as petrographic examination of about two hundred representative polished core samples and thin sections. The average collar elevation of drill holes in VNW is 83.3 m above sea level. This is considered to be the average present surface elevation, and all depths are given relative to this level (e.g. 100 mbs is 100 meters below the present surface).

3.4 Results

3.4.1 Pipe morphology

The contact between the Victor Northwest kimberlite and the host country rock has been intersected in only five drill cores (Fig. 3.1B). Of these five drill cores, only one drill core intersects the kimberlite to country rock contact above ~100 mbs. The four other drill cores intersect the contact between ~200 and 300 mbs. As a result, the confidence in the external pipe shape is low at shallow levels and moderate at deeper levels. Geophysical surveys have been used to aid the reconstruction of the pipe shape, but interpretations are complicated by the probable presence of a pipe-marginal country rock breccia unit at shallow levels (unit CRB-L_2, see Fig. 3.2 and section 3.4.2.2) that has a similar geophysical response to the surrounding in situ country rock. The only vertical drill core that intersects the lower pipe wall contact (V-00-124c) shows a ~70° dipping, knife-sharp pipe wall contact with the granitoid basement. The other drill cores show a sharp or probably sharp contact as well.

Geophysical surveys indicate that the minimum pipe dimensions at ~40 mbs (completely below the unconsolidated overburden) are about 280 m in a SW-NE direction and 160 m NW-SE (Fig. 3.1). Core drilling shows that the kimberlite extends to a minimum depth of 370 mbs. Based on depth contour spacing (Fig. 3.1B), the dip of the pipe walls appears to vary from 45° to 75°, which fits with limited direct measurements of the pipe wall angle in preserved sharp contacts in vertical drill core. An average pipe wall dip of roughly 70° has been inferred based on analogy with the adjacent, and much better delineated, Victor Main kimberlite pipe (Webb et al., 2004).

The southeastern side of the VNW pipe is in contact with the Victor Main (VM) pipe (Fig. 3.1). The following observations unequivocally show that VNW is an early-formed pipe cross-cut by the later VM pipe: (1) the reconstructed steeply SE-dipping contact as well as the contrasting magnetic signature between VNW and VM pipes define an outward curving pipe contact that matches the general morphology of the VM pipe (Fig. 3.1A), (2) volcanic units within VNW (section 3.4.2) appear to be cross-cut by the VNW to VM contact, (3) the presence of steeply-dipping, contact-parallel bedding on the VM side of the sharp contact, (4) clasts (olivine crystals, country rock fragments) cut by the VNW to VM contact on the VNW side of the contact, (5) the presence of a fracture within VNW close to the VNW to VM contact that is filled with volcaniclastic material derived from VM, and (6) the presence of cognate lithic clasts of VNW kimberlite within the VM pipe.

It is inferred that a shallow (max. depth ~100 mbs) extension of the VM crater cross-cuts the top of the easternmost portion of the VNW pipe. This inferred shallower crater could not be identified using geophysical methods, likely because of a lack of geophysical contrast with respect to the surrounding VNW kimberlite. Drill core studies indicate that the rocks within this probable shallow crater are very altered, but appear to have a similar pyroclastic texture, and a similarly abundant mantle xenocryst suite (especially garnet, ilmenite and Cr-diopside) as the VM kimberlite. This shallow extension of VM is in contact with a WNW striking depression within the bedrock (up to ~200 m deep, ~1 km wide and ~2 km long) that is filled with unconsolidated sediments of an unconstrained age (Armstrong and Gao, 2002; Hydrological Consultants Inc., 2004; F. Brunton, pers. comm. 2006; Fig. 3.1A). The depression is in direct contact with the northeastern side of

the Victor kimberlite pipes, and likely explains the intense alteration and lack of a distinct geophysical signature of the shallow extension of the VM crater.

The approximate centre of the VNW pipe based on the external pipe shape is indicated in Fig. 3.1B. Assuming that the VNW pipe was approximately circular in plan view prior to eruption of VM, the minimum pipe diameter at 40 mbs was about 280 m, and a considerable part of the VNW pipe has been removed by the formation of the VM pipe.

3.4.2 Internal geology

3.4.2.1 General lithologies

The rocks within the VNW pipe have distinctly different components (e.g. juvenile clasts, country rock fragments) and textures, and are subdivided into four broad lithologies and one lithological association shown in Figures 3.2 and 3.3. The lithologies are listed below in order of decreasing apparent volume within the pipe.

Dark and competent kimberlite (DCK, blue in Figs. 3.2, 3.3) is generally country rock fragment (CRF) poor, massive, featureless and matrix-supported in nature (Fig. 3.4A, B, C). This lithology commonly exhibits a subhorizontal preferred orientation of elongate olivine grains and/or CRFs (Fig. 3.4B, C). The DCK often contains intervals of coherent kimberlite where the groundmass comprises a uniform distribution of carbonate and phlogopite laths, evenly distributed spinel and perovskite crystals and possible monticellite set in a microcrystalline carbonate groundmass (Fig. 3.4D). Other DCK intervals contain clastic textures such as patchy grain size variations (Fig. 3.4C), horizons that are variably rich in CRFs and faint pyroclast outlines (Fig. 3.4E). Gradational contacts between DCK with clastic textures and coherent kimberlite are present.

Sedimentary country rock breccia (CRB, green in Figs. 3.2, 3.3) comprises 10 cm to m-scale sedimentary country rock fragments (Fig. 3.5) of limestones (reacts to dilute HCl), dolostones (does not react to dilute HCl), mudstones and/or siltstones. The monolithic to heterolithic breccia generally contains little or no kimberlite matrix (> 75% CRFs).

Volcaniclastic kimberlite (VK, red in Figs. 3.2, 3.3) is generally variably country rock fragment-rich, massive (Fig. 3.6A) to layered (Fig. 3.6B, C), clast-supported (Fig. 3.6D) to matrix-supported (Fig. 3.6A) and juvenile pyroclast and/or clastic pyroclast-bearing. All units termed volcaniclastic kimberlite in the VNW pipe represents primary pyroclastic material that has possibly been reworked or redeposited without addition of non-kimberlitic detrital material, and without direct obvious evidence for such reworking or redeposition (e.g. sorting and bedding that is atypical of primary pyroclastic deposits). Certain VK units contain abundant broken olivines (Fig. 3.6E) and one unit contains angular cognate lithic clasts (Fig. 3.6F).

Resedimented volcaniclastic kimberlite (RVK, vertically striped red and white in Fig. 3.2) varies considerably from CRF-rich (Fig. 3.7A) to CRF-poor (Fig. 3.7B) and massive (Fig. 3.7A) to layered (Fig. 3.7B) in nature. All resedimented volcaniclastic kimberlite in the VNW pipe shows clear evidence for reworking or redeposition and/or addition of non-kimberlitic detrital material.

Bedded kimberlite (BK, horizontally striped red, blue and/or green in Fig. 3.2); this lithological association contains two or three of the above lithologies, usually alternating on the metre scale (Fig. 3.3).

3.4.2.2 Stratigraphy

Each of the four lithologies and one lithological association (section 3.4.2.1) occurs in several locations within the VNW pipe, with a total of 2 to 4 units per lithology/lithological association. Each unit has characteristic textures that distinguish it from broadly similar lithological units; in addition, each unit has a distinct stratigraphic position within the pipe (Table 3.1). For ease of reference, the stratigraphy of the pipe has been split into two parts, the lower stratigraphy (L) and the upper stratigraphy (U; see Table 3.1). The lower and upper stratigraphy correspond to two separate eruption cycles, as will be discussed in section 3.6. Within the upper and lower stratigraphy, lithologically similar units are numbered from lower to upper stratigraphic levels. The combined volcanic stratigraphy of the VNW pipe, the location, thickness, shape, depth interval, data density (number of drill cores that intersects a unit) of each individual unit as well as the contact relationships between adjacent units are listed in Table 3.1.

The dark and competent kimberlite occurs in four units. The combined units DCK-L_1 and DCK-L_2 occupy almost the entire lower part of the pipe down to at least 369 mbs, whereas the combined units DCK-U_1 and DCK-U_2 are present in the central part of the upper stratigraphy and are 45 to over 110 m thick. Each individual unit slightly varies in texture and in componentry (Table 3.2). Country rock breccia occurs in three individual units (Table 3.3), two units in the upper part of the lower stratigraphy (CRB-L_1, CRB-L_2) and one unit in the upper part of the upper stratigraphy (CRB-U). Both CRB-L_1 and CRB-U are heterolithic sedimentary country rock breccias that are laterally continuous and vary in thickness from 10 to 65 m. CRB-L_2 is a ~23 m thick pipe-marginal monolithic sedimentary country rock breccia that is generally present between all units of

the upper stratigraphy and the pipe wall. Volcaniclastic kimberlite is found in three units in the upper stratigraphy of the pipe (Table 3.4). The lower unit (VK-U_1) contains abundant broken olivines, small clastic and juvenile pyroclasts, whereas the higher units (VK-U_2, VK-U_3) do not contain significant broken olivines and lack clastic pyroclasts. The two higher volcaniclastic units are very dissimilar; VK-U_2 is CRF-poor, whereas VK-U_3 is variably CRF-rich (Table 3.4). Well-sorted resedimented volcaniclastic kimberlite occurs in the top of both the lower and upper stratigraphy (Table 3.5). These two units are distinctly different; unit RVK-L contains abundant CRFs, whereas unit RVK-U contains only minor CRFs, and abundant exotic (quartz, mud) material (Fig. 3.8). Two units of bedded kimberlite occur in the lower stratigraphy (Table 3.5). The lower unit (BK-L_1) comprises volcaniclastic and dark and competent kimberlite that is found alternating at the metre scale (Fig. 3.3). The upper unit (BK-L_2) comprises country rock breccia, dark and competent kimberlite and/or volcaniclastic kimberlite that are found alternating at the metre scale as well (Fig. 3.3). The two bedded units are easily distinguished; BK-L_1 contains abundant broken olivines as well as clastic pyroclasts (Fig. 3.9A, B), both of which are absent in BK-L_2.

3.5 Facies interpretation

3.5.1 Lower stratigraphy

The lower stratigraphy comprises units BK-L_1, DCK-L_1, DCK-L_2, BK-L_2, CRB-L_1, CRB-L_2 and RVK-L (Figs. 3.2, 3.3, Table 3.1). BK-L_1 is found at the pipe wall (Figs. 3.2, 3.3), and we interpret it to be the first unit to form after the pipe excavation. This unit is bedded, contains both VK and DCK, is variably country rock fragment-rich, broken olivine-rich, contains clastic (ash-armoured) pyroclasts (Fig. 3.9A, B) and the matrix is

inferred to be ash-rich. Based on the presence of broken olivines at all scales as well as other observations, it is clear that in addition to the volcaniclastic intervals, the dark and dense kimberlite is also clastic in origin. We infer that this unit is a primary pyroclastic deposit based on the following observations: (1) the presence of fragile clastic pyroclasts, (2) the absence of significant sorting and bedding that is typical of reworked deposits, and (3) the absence of detrital non-volcanic material. The characteristics of this unit suggest that the pipe excavation was highly explosive, causing pervasive shattering of olivine crystals and the production of abundant kimberlite ash. In addition, the explosive eruptions that formed unit BK-L_1 were likely accompanied by ongoing pipe wall erosion that supplied the moderately abundant country rock fragments within this unit. The lack of basement clasts (granitoid, dolerite) in the lowermost intra-crater deposits suggests that an earlier (phase of the) eruption excavated and expelled most of the country rock material that originally occupied the crater.

Units DCK-L_1 and DCK-L_2 form the volumetrically dominant part of the lower stratigraphy in the pipe. The country rock fragment content is much lower compared to the underlying unit BK-L_1, and notably, the abundance of broken olivines decreases away and upward from the pipe wall contact (Table 3.2). This most likely indicates a gradual decrease in the fragmentation intensity. In addition, the decrease in country rock fragment abundance (Fig. 3.3) indicates that the pipe enlargement came to an end. Both features are suggestive of a transition to much lower energy eruptions by the time the uppermost part this unit was formed. The dark and competent kimberlite that makes up this unit (Fig. 3.4A) generally shows textures suggestive of a clastic origin, such as broken olivines, faint subhorizontal fabric, patchy grain size variations, clast-supported areas and

faint pyroclast outlines. The dark and competent kimberlite is enveloped by solely extrusive units, and gradational contacts with the surrounding pyroclastic units are present. The upper and central parts of this unit contain numerous intervals of coherent kimberlite with gradational contacts to the dense and dark kimberlite with abundant clastic features. Based on the deposit geometry, the lack of sharp contacts and the abundant clastic textures within this unit the dark and competent kimberlite cannot be an intrusion into either consolidated or unconsolidated pyroclastic deposits. Based on these observations it is evident that this entire unit is extrusive in origin.

The next unit in the stratigraphic sequence is a sedimentary country rock breccia (CRB-L_1) formed by pipe wall collapse. When present, the underlying BK-L_2 (a country rock fragment-rich kimberlite) is most likely representative of the transition from low energy eruptions (unit DCK-L) to volcanic quiescence and the onset of pipe wall collapse (unit CRB-L_1). A mostly monolithic country rock breccia (CRB-L_2) is present at the pipe margins, and is inferred to have formed at the same time as CRB-L_1. A small volume, bedded, well-sorted and closely packed resedimented volcaniclastic unit (RVK-L, Fig. 3.7A) is generally present within close proximity to the sedimentary country rock breccia (CRB-L_1), suggesting the presence of water in the open crater.

3.5.2 Upper Stratigraphy

The upper stratigraphy comprises the units VK-U_1, DCK-U_1, DCK-U_2, VK-U_2, VK-U_3, RVK-U and CRB-U. The lowermost unit in this stratigraphic package, VK-U_1, is composed of bedded and sedimentary country rock fragment-rich volcaniclastic kimberlite. Based on similar evidence as presented for unit BK-L_1 (see section 3.5.1), we conclude that this unit was formed by pyroclastic processes. High fragmentation

intensities are inferred from the presence of abundant broken olivines (Fig. 3.6E), kimberlite ash and small angular country rock fragments (Fig. 3.6A).

The two dark and competent units (DCK-U_1, DCK-U_2) have low country rock fragment-abundance, contain mostly intact olivine, and lack accretionary lapilli and variably vesicular pyroclasts. The dominant part of the dark and competent units are clastic in origin, as shown by the presence of a fabric, patchy grain size variations, clast-supported areas (Fig. 3.4C), and faint pyroclast outlines (Fig. 3.4E). In many ways, units DCK-U_1 and DCK-U_2 are similar to the upper parts of DCK-L_1 and -L_2, and were likely formed by relatively low energy eruptions producing dark, competent and extrusive rocks. Hence, the transition from VK-U_1 to DCK-L_1 and DCK-L_2 is characterised by a marked decrease in explosivity.

Unit VK-U_2 (country rock fragment-poor volcaniclastic kimberlite, Fig. 3.6B, D) most likely represents the pyroclastic equivalents of the enveloping and underlying dark and competent units (DCK-U_1, DCK-U_2).

Overlying both units DCK-U_2 and VK-U_2 are variably country rock fragment-rich volcaniclastic deposits (VK-U_3, Fig. 3.6C) that contain some country rock breccia intervals. This unit likely represents a gradual transition to the end of the eruption and the onset of pipe wall collapse. These volcaniclastic deposits might, in part, originate from the collapse of tephra-ring deposits into the pipe.

Unit RVK-U includes mud to sandstone intervals containing both kimberlitic and exotic (quartz grit, mud) material. This small volume unit comprises fining upward and cross-bedded sequences (Figs. 3.7B, 3.8) implying resedimentation by water. The presence of exotic material suggests that a stream might have cut through the tephra ring to supply

foreign debris and water. This presents supporting evidence for the fact that some or all of unit VK-U_3 could be tephra ring material that collapsed back into the vent during the onset of tephra ring erosion and pipe wall instability.

Unit CRB-U represents the true end of the eruption at VNW, and the continuation and climax of pipe wall collapse. It comprises a thick package of heterolithic sedimentary country rock breccia (Fig. 3.5) that blankets all previous deposits.

3.6 Discussion and conclusions

There is a striking similarity between the order of kimberlite units that comprise the lower and the upper stratigraphy of the pipe (Fig. 3.3, Table 3.1). Both stratigraphic sequences start with an early volcaniclastic kimberlite containing abundant broken olivines, followed by dark and competent kimberlite, and capped by country rock breccia deposits. We interpret that the Victor NW kimberlite pipe was formed by two similar eruptive cycles that are described below. Cycle 1 comprises all six units in the lower stratigraphy, whereas cycle 2 includes all seven units in the upper stratigraphy (Table 3.1).

Cycle 1 starts with initial crater excavation that formed a large, inverted-cone-shaped pipe within the pre-existing country rock (Fig. 3.1B). The lack of country rock breccias at the lower pipe wall contact, and the relatively low abundance of country rock fragments in the lower pipe fill, indicates that significant pipe wall erosion and ejection of country rock material took place before deposition of unit BK-L_1. The early and middle part of this cycle records a transition from highly explosive activity (unit BK-L_1) to lower energy eruptions (central and upper parts of units DCK-L_1 and DCK-L_2), whereas the latest part

of this cycle involved pipe wall collapse and the formation of country rock breccias (CRB-L_1, CRB-L_2).

We suggest that cycle 2 starts with the excavation of a cross-cutting nested crater. This assertion is based on the funnel-shaped geometry of the basal contact of VK-U_1 (Fig. 3.1C) and the presence of cognate lithic clasts (Fig. 3.6F) in the base of this unit. The excavation of the nested crater within the earlier lithified lower stratigraphy of the pipe likely occurred prior to and/or during formation of VK-U_1. The nested crater is situated on top of the initial pipe centre (Fig. 3.1B, C), suggesting that the subsequent eruptions exploited the same vent as during cycle 1. The presence of angular cognate lithic clasts indicates that the time gap between cycle 1 and 2 was long enough to allow for lithification of at least some of the underlying deposits. The pipe shape and spatial distribution of unit VK-U_1 (Fig. 3.2) suggests limited pipe enlargement during the early stages of the second eruption cycle. Hence, the sedimentary country rock fragments in VK-U_1 are most likely not derived from the erosion of in situ sedimentary stratigraphy on the upper pipe wall, but more likely, from recycling of the earlier formed underlying and adjacent country rock breccias (units CRB-L_1, CRB-L_2).

Based on the data and interpretations presented here, it is evident that the VNW pipe was formed by two separate but comparable eruption cycles, each of which involved (1) an early highly explosive crater excavation and deposition of pyroclastic kimberlite containing abundant broken olivine, (2) a subsequent episode of lower energy eruptions that formed dark and competent kimberlite deposits containing minor to no broken olivine, and (3) cessation of the eruption, resulting in redeposition of minor volcaniclastic

kimberlite by water, and major pipe wall collapse resulting in voluminous sedimentary country rock breccia deposits.

In summary, the Victor Northwest kimberlite pipe fill provides an example of the possible degree of complexity and small-scale variability within intra-crater volcanic deposits.

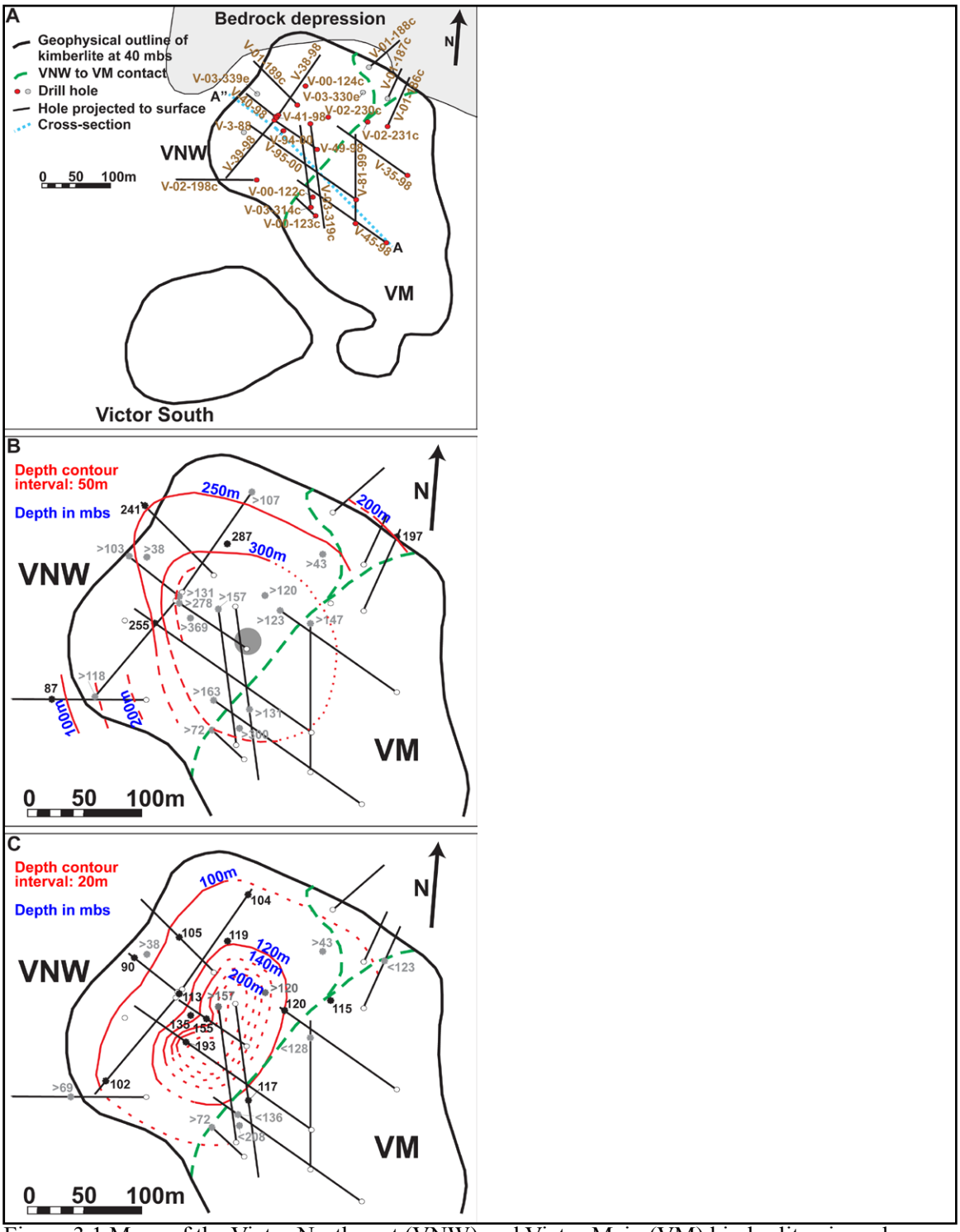

Figure 3.1 Maps of the Victor Northwest (VNW) and Victor Main (VM) kimberlite pipes showing: (A) modelled geophysical pipe outlines, bedrock depression filled with unconsolidated material, locations of drill cores and cross-section. (B) Depth contours of the external pipe shape and the reconstructed pipe centre (grey circle). (C) Contours of the base of kimberlite unit VK-U_1. Black dots indicate depth of contact intersects (in metres below the surface, mbs); grey dots indicate that the contact was not intersected and is likely present below (>) or above (<) the indicated depth.

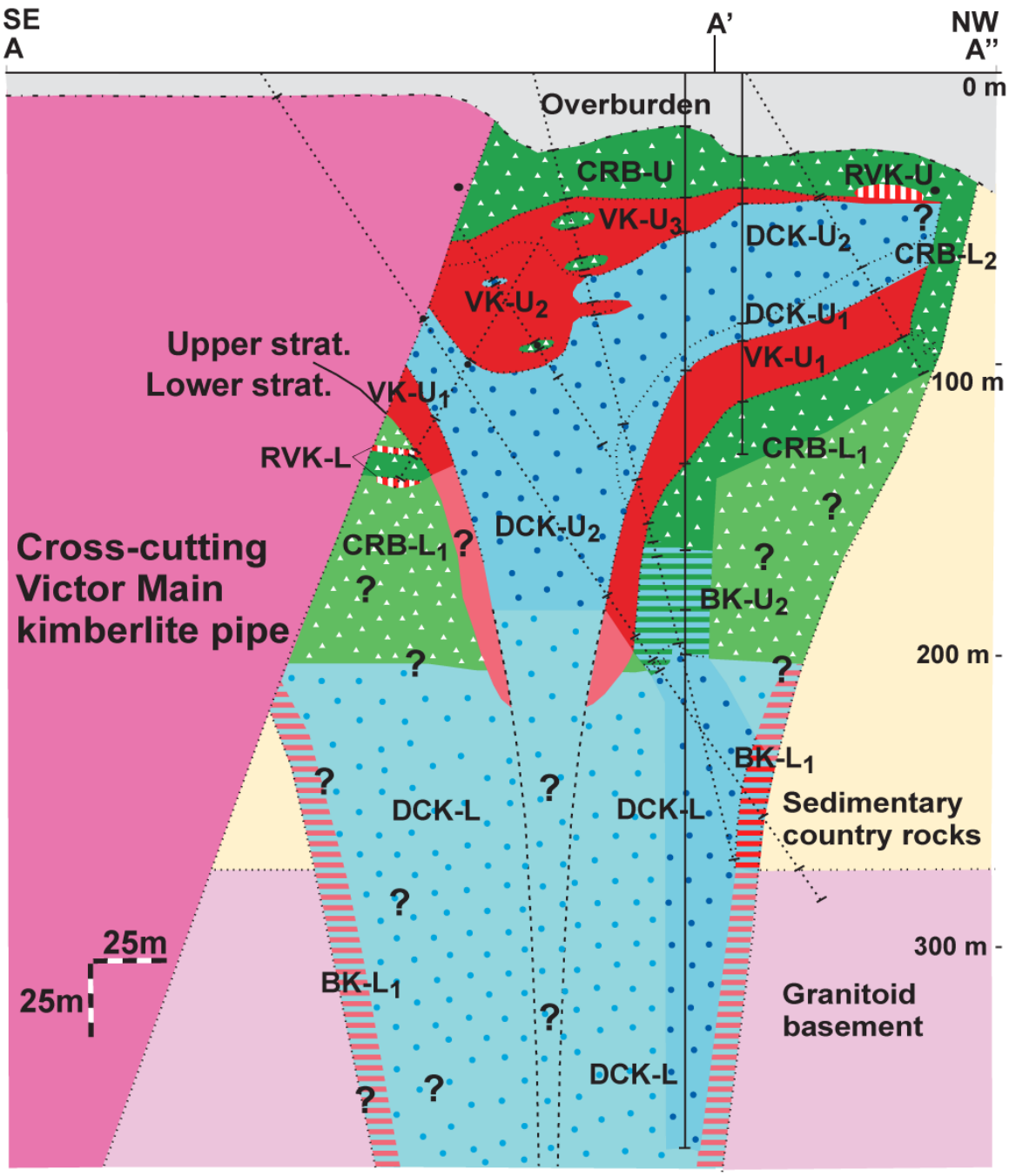

Figure 3.2 Cross-section through the VNW pipe showing all units in the lower (*L*) and upper (*U*) stratigraphy. Blues indicate dark and competent lithologies, green denotes sedimentary country rock breccia bodies, reds are volcaniclastic kimberlite, vertically striped reds are resedimented volcaniclastic kimberlite and horizontally striped green/red/blue domains are bedded kimberlite units. Extrapolated areas are lighter coloured. Location of cross-section is shown in Figure 3.1.

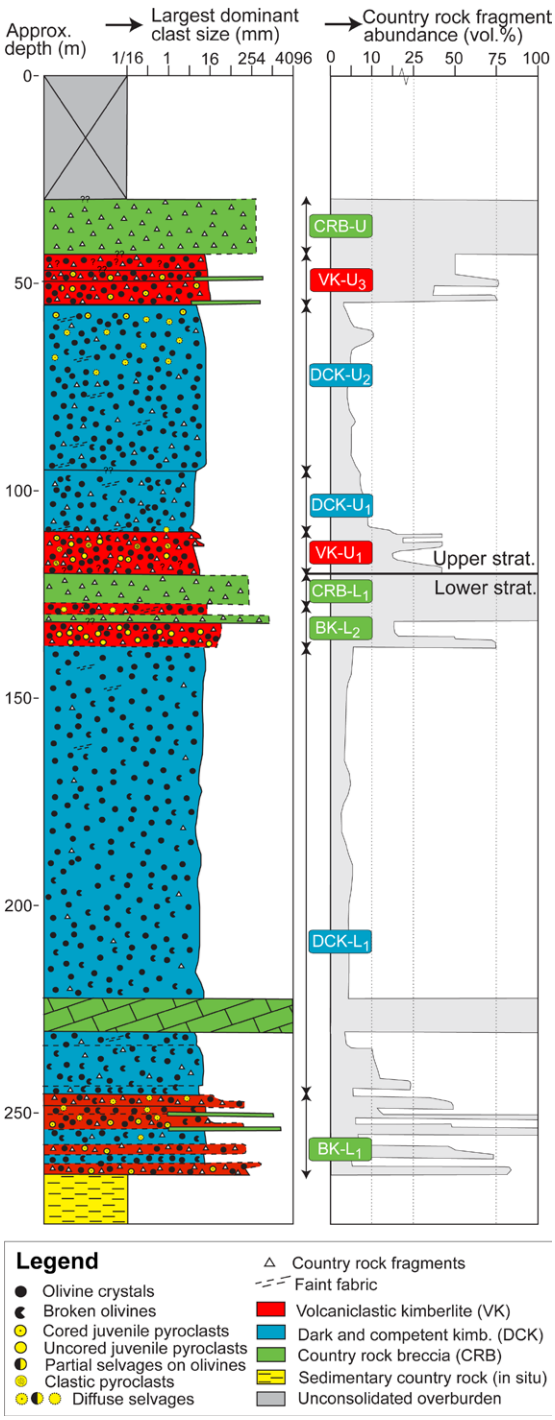

Figure 3.3 Graphic log summarising the stratigraphic sequence in the VNW pipe (upper 55 m taken from drill core V-03-319c, rest from V-01-189c). Each unit is labelled with a unique abbreviation. Note that the sequence comprises a lower (*L*) and upper (*U*) stratigraphy. BK stands for bedded kimberlite, see legend for explanation of other abbreviations.

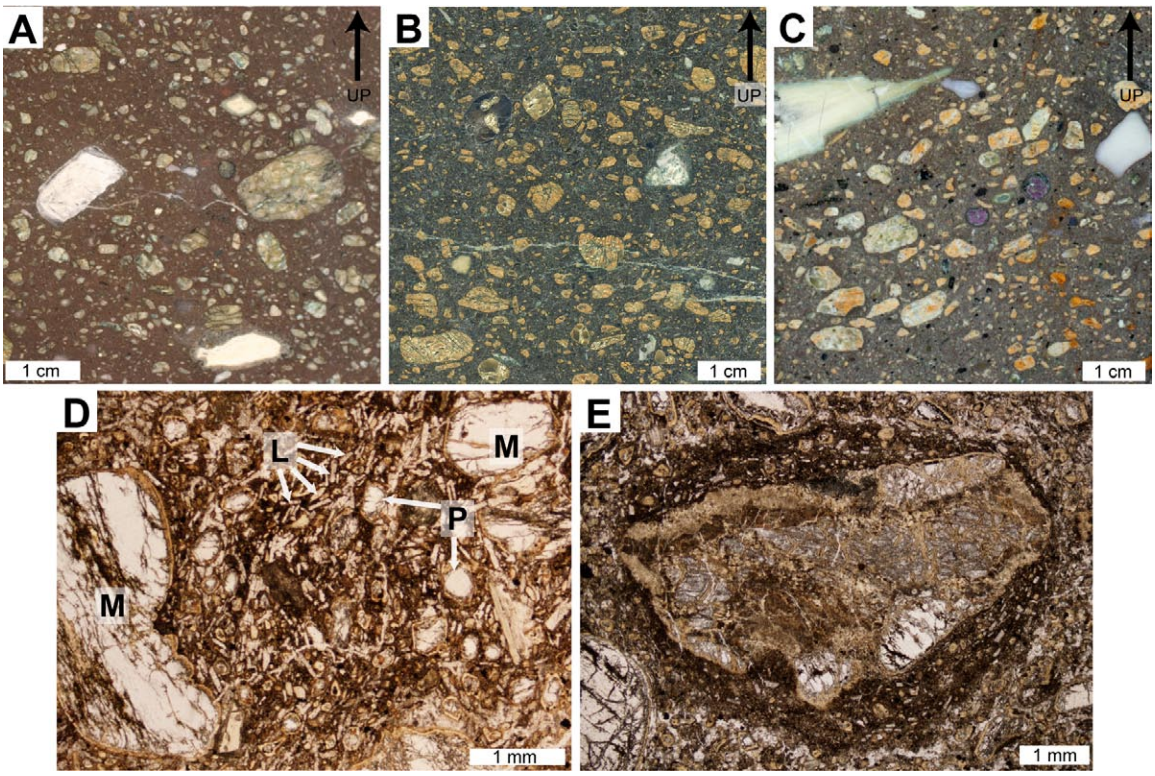

Figure 3.4 Typical textures for dark and competent units. (A) Polished core sample of DCK-L_1. (B) Polished core sample showing dark, competent and massive appearance with slight fabric in DCK-U_2. (C) Polished core sample of DCK-U_2 with more pronounced fabric and diffuse grain size variations. (D) Photomicrograph of coherent kimberlite showing a well crystallised groundmass with carbonate laths (*L*), groundmass oxides and evenly distributed olivine phenocrysts (*P*), and olivine macrocrysts (*M*) in DCK-U_2. (E) Photomicrograph of diffuse pyroclast outline surrounding olivine in DCK-U_2.

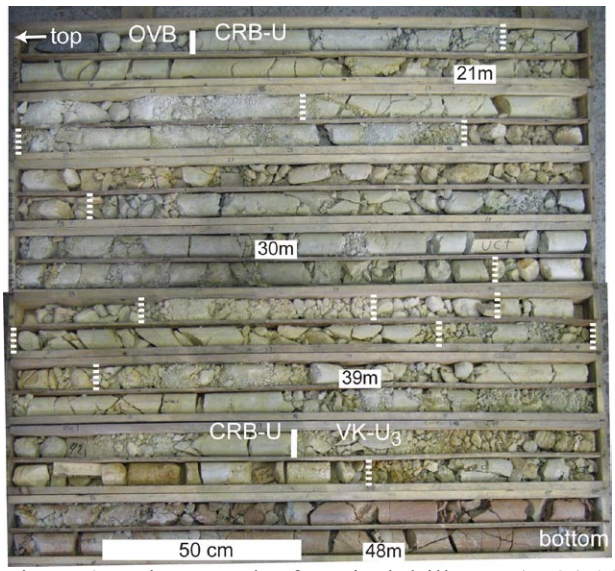

Figure 3.5 Photograph of vertical drill core (V-94-00) showing various blocks of country rock material in CRB-U, depth in metres below the surface.

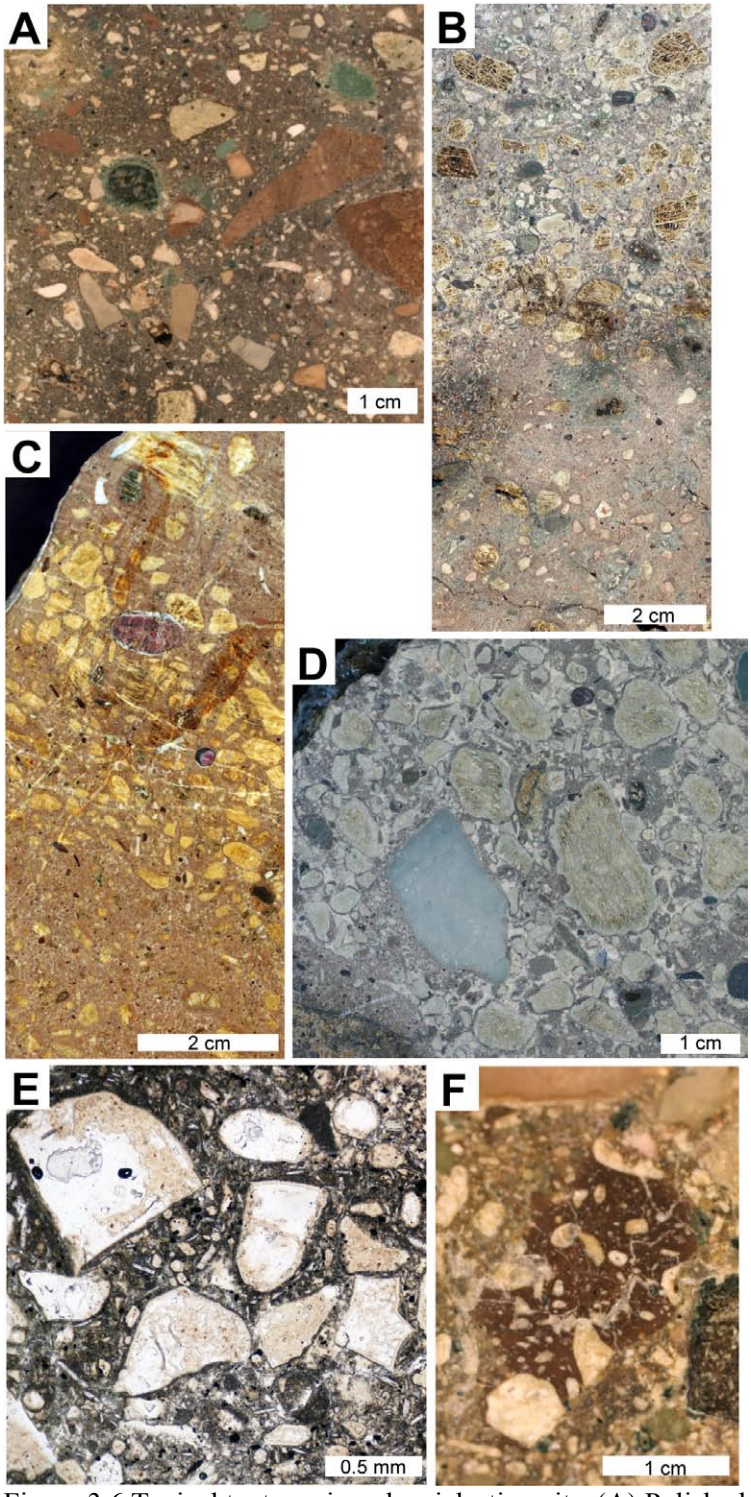

Figure 3.6 Typical textures in volcaniclastic units. (A) Polished core sample in VK-U_1, note abundant small angular country rock fragments. (B) Polished core sample showing top of fining upward sequence including top contact and start of new bed in VK-U_2. (C) Polished core sample of bedding in VK-U_3. (D) Polished core sample showing clast-supported VK-U_2. (E) Photomicrograph of broken olivines in VK-U_1. (F) Core sample of VK-U_1 showing an angular and broken cognate lithic clast.

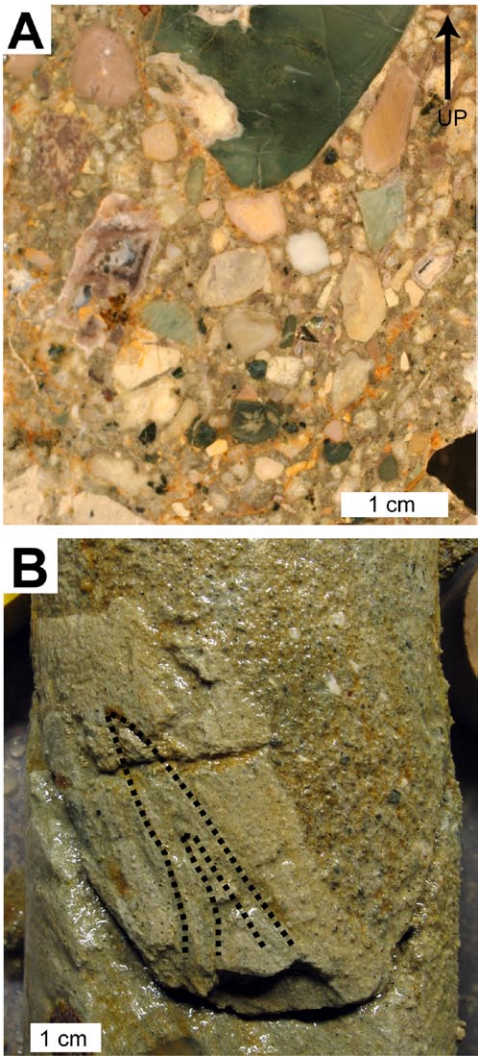

Figure 3.7 Resedimented volcaniclastic kimberlite. (A) Polished core sample of well-sorted CRF-rich RVK-L. (B) Core sample with soft-sediment deformation feature in RVK-U.

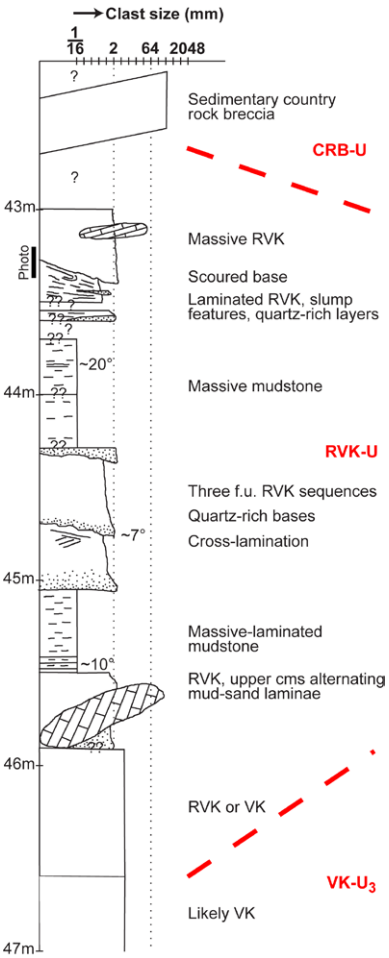

Figure 3.8 Detailed graphic log of resedimented volcaniclastic kimberlite (RVK-U) in drill core V-01-189c (70 ° dipping hole), down hole depth indicated. Location of Figure 3.7B indicated. F.u. = fining upward

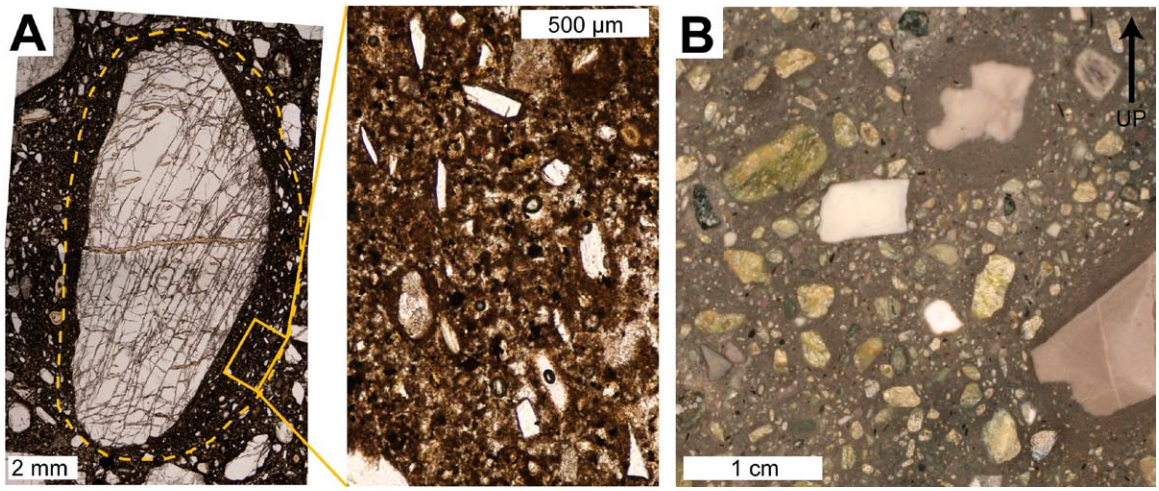

Figure 3.9 Textures in bedded kimberlite. (A) Photomicrographs of ash armoured olivine macrocryst in unit BK-L_1, note small fresh olivine shards that are present within the clastic selvage. (B) Polished core sample with ash armoured country rock fragments in BK-L_1.

Table 3.1 Volcanic stratigraphy (top to bottom) of the Victor NW pipe, focussing on the vertical thickness, morphology, contact relationships and number of drill cores that intersect each unit

Unit	Thickness (m)	No. of drill cores	Location, morphology	Lower contact
CRB−U	11-35	13	Laterally continuous, caps all previous units	Grades into VK−U_3 below
RVK−U	~3	1	Probably limited in extent	Unclear
VK−U_3	5-27	12	Laterally continuous	Likely gradational
VK−U_2	35-40	2 (3?)	Only present in the reconstructed centre of the pipe, with an estimated lateral distribution of ~50 m	Gradational contacts with DCK−U_2
DCK−U_2	35 to ≥100 near centre of pipe	17	Volumetrically dominant part of the upper stratigraphy	Gradational contacts with DCK−U_1
DCK−U_1	0-12	14	10 out of 14 drill cores that intersect both DCK−U_2 and VK−U_1/CRB−L_2 contain this unit	Mostly gradational contacts with VK−U_1
VK−U_1	16-32	13	A thin unit that is present on top of a funnel-shaped depression within the lower stratigraphy of the VNW pipe (Fig. 1C)	Sharp contact with RVK−L (when present), gradually increasing CRF-abundance towards contact with CRB−L_1 and CRB−L_2
RVK−L	~5	4	Generally overlies CRB−L_1, but in one drill core RVK occurs below or within CRB−L_1 and in another drill core RVK appears to be present within the overlying VK−U_1	Unclear
CRB−L_2	23 *	1	Pipe marginal unit, only one drill core intersects the central to upper pipe contact	Gradually transitions into in situ fractured country rock
CRB−L_1	10-65	15	Present above 160 mbs, over the entire width of the pipe (except the centre)	Likely gradational, generally shows gradually decreasing CRF-abundance into BK−L_2 and DCK−L
BK−L_2	0-24	6	Only 3 out of 6 drill cores that intersect both CRB−L_1 and DCK−L contain this unit	Likely gradational, generally shows a decrease in CRF abundance from CRB−L_1 to the top of DCK−L
DCK−L_1 + DCK−L_2	≥200 (occupying entire lower pipe)	7	Fills entire lower part of the pipe from at least 369 mbs (deepest intersection of kimberlite in VNW) to about 160 mbs. Apparent significant volume of unit is not well constrained due to limited drill core data. Split up into outer NW to NE part of pipe (DCK−L_1) and deeper levels in centre of pipe (DCK−L_2)	Gradational lower contact, suggesting the units are genetically and temporally related
BK−L_1	7-18 *	3 (4?)	Pipe marginal unit, only recorded in the outer N−NE portion of the pipe	Generally sharp lower contact with in situ country rock

* Thickness measured perpendicular to pipe wall

Table 3.2 Descriptions of individual dark and competent kimberlite (DCK) units within the Victor NW pipe (+ Present, Occasionally present, – Not present)

Unit	Appearance	CRF		Textures						Olivine				Pyroclasts			
		CRF (vol.%)	General description	Massive, no fabric	Massive, fabric	Layered	Clast-supported	Matrix-supported	General description	Broken	Fresh	Altered	General description	Faint	Juvenile	Clastic	General description
DCK−L_1		3-8, rarely 25-30, some CRB intervals	Dominant CRF type is a bleached white limestone, the CRFs are frequently smooth and irregular in shape. Contains a 3−10 m intersection of white limestone. Around these country rock blocks, the proportion of CRF is generally somewhat higher	-	+	-	-	+	Fabric in vertical drill cores is mostly subhorizontal. Includes some intervals of coherent kimberlite near the top of this unit with gradational contacts to surrounding DCK. Minor patchy clast distributions and horizons that are variably rich in CRFs	+/-	+	+/-	Broken olivine abundance generally decreases upwards and inwards, from about 60% broken grains near the contact with unit BK−L_1 to about 20% broken grains near the top of this unit	+	-	+/-	Diffuse selvages on olivine macrocrysts tend to be absent in this domain, except between, or immediately surrounding, large limestone blocks in one of these drill cores
DCK−L_2	Similar characteristics to DCK−L_1, except for features described here. Some intervals show similarities with unit BK−L_1	5-20, some CRF-rich intervals	Intervals with higher CRF abundances (25-60, rarely 100 vol.%) are present	-	+	-	+/-	+	Variably matrix- to clast-supported	+/-	+	+/-	Drill core V−94−00 generally contains broken olivines, whereas V−00−122c contains minor to no broken olivine	+	?	?	Diffuse selvages on olivine are generally present in V−94−00 (below 242 mbs) as well as in V−00−122c. In the latter drill core the nature of the selvages (clastic vs. coherent) is not clear
DCK−U_1	Same as unit DCK−U_2, except for features described here	~10	CRF abundance increases towards lower contact	-	+	+/-	+/-	+	More common occurence of patchy grain size variations and clast-supported textures than DCK−U_2	+/-	+/-	+/-	Finer grain size (largest dominant olivines are 1−5 mm in DCK−U_1 vs. 2−10 mm in DCK−U_2)	+	-	-	
DCK−U_2		2-10	CRF abundance increases towards the upper contact	-	+	-	-	+	Bedding is rare to absent. The matrix in this facies is variable. Includes some intervals of coherent kimberlite (Fig. 4D) with gradational contacts. A coherent and possibly vesicular interval was intersected in one drill core (V−02−198c)	-	+	+/-	Broken olivines are present but not common	+	-	-	Faint thin selvages around olivine macrocrysts occur in distinct intervals (~1−5 m thick) in the upper parts of this unit and are thought to represent juvenile pyroclasts (Fig. 4E). These selvages typically contain slightly finer-grained carbonate laths, and less and smaller olivine phenocrysts compared to the surrounding matrix

Table 3.3 Descriptions of individual country rock breccia (CRB) units within the Victor NW pipe (+ Present, Occasionally present, – Not present)

Unit	Appearance	CRF		Textures						Olivine				Pyroclasts			
		CRF (vol.%)	General description	Massive, no fabric	Massive, fabric	Layered	Clast-supported	Matrix-supported	General description	Broken	Fresh	Altered	General description	Faint	Juvenile	Clastic	General description
CRB−L_1	Core loss is typically high	75-100	Heterolithic breccia composed of 10 cm to 1 m sized sedimentary country rock clasts, comprising a mixture of various limestones, dolostones, mudstones and siltstones	+	-	-	+	-		-	-	-		-	-	-	
CRB−L_2	Core loss is typically high	100	Monolithic sedimentary country rock breccia, composed mainly of limestone	+	-	-	+	-		-	-	-		-	-	-	
CRB−U	Core loss is typically high. Poorly consolidated mud is occasionally found as the interstitial medium in between the country rock clasts, and may be of similar external origin as the mudstone intervals in unit RVK−U	100	Heterolithic breccia comprising various types of 10 cm to 1 m sized sedimentary country rock clasts (Fig. 5; siltstones, limestones, dolostones and mudstones) with minor to no interclast kimberlite. Bedding angles in CRF are extremely variable	+	-	-	+	-		-	-	-		-	-	-	

Table 3.4 Descriptions of individual volcaniclastic kimberlite (VK) units within the Victor NW pipe (+ Present, Occasionally present, – Not present)

Unit	Appearance	CRF		Textures						Olivine				Pyroclasts			
		CRF (vol.%)	General description	Massive, no fabric	Massive, fabric	Layered	Clast-supported	Matrix-supported	General description	Broken	Fresh	Altered	General description	Faint	Juvenile	Clastic	General description
$VK{-}U_1$		15-40	CRFs are common and include abundant small (<1−2 cm, Fig. 6A) CRFs as well as variable amounts of larger CRFs	+/-	-	+	+	+	Mainly massive intervals and rarer graded (2−9 m thick) beds. Detailed study of samples on a macro- and microscale shows that the matrix-supported intervals contain abundant ash-sized components such as small olivines, individual groundmass oxide minerals and juvenile pyroclasts. Angular cognate lithic clasts are present in the base of this unit (Fig. 6F)	+	-	+	Olivines are pseudomorphed by carbonate and/or serpentine	-	+	+/-	Juvenile pyroclasts in this unit range from 50 µm juvenile ash particles to 3 mm uncored juvenile lapilli. The edges of these juvenile pyroclasts are generally difficult to discern, but where visible they feature more irregular shapes. The juvenile pyroclasts are non-vesicular to moderately vesicular (up to 20% vesicles). Clastic pyroclasts are present, these include mostly rim-type accretionary pyroclasts (sensu Schumacher and Schmincke, 1991) having ash-sized components within the core and fine ash-sized components within the rim, as well as rare country rock fragments armoured with fine ash
$VK{-}U_2$	One drill core contains a 2 m thick interval of DCK with gradational contacts to the surrounding rocks	~6	CRF-poor	+	-	+/-	+	+/-	Massive to variably bedded kimberlite, includes 1−4 m scale graded beds (Fig. 6B), some of which are fining upward	-	-	+		-	+	-	Contains variable, but generally higher, proportions of discrete olivines to juvenile pyroclasts
$VK{-}U_3$		~10-40, locally up to 100	Country rock breccia intervals (4−5 m thick) occur locally within this unit	+/-	-	+	+	+/-	Graded beds (1−6 m thick) are common (Fig. 6C)	-	-	+	Olivines are pseudomorphed by carbonate and/or serpentine	-	+	-	Contains discrete olivines and minor round-ovoid shaped juvenile pyroclasts

Table 3.5 Descriptions of individual resedimented volcaniclastic kimberlite (RVK) and bedded kimberlite (BK) units within the Victor NW pipe (+ Present, Occasionally present, – Not present)

Unit	Appearance	CRF		Textures						Olivine				Pyroclasts			
		CRF (vol.%)	General description	Massive, no fabric	Massive, fabric	Layered	Clast-supported	Matrix-supported	General description	Broken	Fresh	Altered	General description	Faint	Juvenile	Clastic	General description
RVK−L		~25-50		-	+/-	+	+	-	Bedded, relatively well-sorted, closely-packed (Fig. 7A)	-	-	+		-	+/-	-	
RVK−U		~8		+/-	-	+	+	-	Small-scale soft-sediment deformation features (Fig. 7B), cross-bedding, fining upward sequences with coarser quartz-rich lag deposits and massive to laminated mudstone intervals (Fig. 8). The RVK is generally very well sorted and contains both volcanic (kimberlitic) and exotic (quartz, mud) material	-	-	+		-	-	-	
BK−L_1	*VK*	~45	Typically only comprises sedimentary CRFs	+	-	+/-	-	+	Alternating VK and DCK likely represent metre-scale layering. A number of gradational contacts between the volcaniclastic and dark, dense and competent rock types within this unit are present	-	-	+		-	+	+/-	
	DCK	~10		-	+	-	-	+	Generally massive, featureless, matrix-supported. Olivines are set in a matrix of fairly evenly distributed minerals (spinel, perovskite and phlogopite). Patchy grain size variation (slight cm-scale variations in packing) is often observed	+	+	+/-	Contains abundant broken olivine crystals (roughly ranging in size from 5 mm to 50 μm). Generally comprises fresh olivines	+	-	+/-	Contains diffuse fine grained selvages on olivine macrocrysts and country rock fragments (Fig. 9A, B). The diffuse fine grained selvages are commonly found around larger (olivine) cores, and rarely contain crystals greater than 0.2−0.5 mm in size. Tiny broken olivine fragments are often observed as constituents within these selvages (Fig. 9A), indicating that the selvages are clastic in origin
BK−L_2	*Light-coloured VK*	~25-30		+	-	-	+	+/-	Alternating VK, DCK and CRB likely represent layering	-	-	+		-	+	-	
	DCK	~10		-	+	-	-	+	Similar to upper and central part of unit DCK−L	-	+	+/-	Minor to no broken olivines	-	-	-	
	CRB	~100		+	-	-	+	-		-	-	-		-	-	-	

3.7 References

Andrews, G.D.M., Branney, M.J., Bonnichsen, B., McCurry, M., 2008. Rhyolitic ignimbrites in the Rogerson Graben, southern Snake River Plain volcanic province: volcanic stratigraphy, eruption history and basin evolution. Bulletin of Volcanology 70 (3), 269-291.

Armstrong, D., Gao, G., 2002. Drift deposits in drill holes V-01-190c and V-01-191c, at Victor kimberlite pipe, Northern Ontario. Ontario Geological Survey, Sedimentary Geoscience Section, Preliminary report to De Beers Canada Inc., 8 pp. plus figures.

Branney, M.J., Kokelaar, P., 1992. A reappraisal of ignimbrite emplacement: progressive aggradation and changes from particulate to non-particulate flow during emplacement of high-grade ignimbrite. Bulletin of Volcanology 54 (6), 504-520.

Brunton, F., 2006. Geologist at the Ontario Geological Survey, Sudbury, Canada. Personal communication.

Cas, R., Porritt, L., Pittari, A., Hayman, P., 2008. A new approach to kimberlite facies terminology using a revised general approach to the nomenclature of all volcanic rocks and deposits: Descriptive to genetic. Journal of Volcanology and Geothermal Research 174 (1-3), 226-240.

Ekren, E.B., McIntyre, D.H., Bennett, E.H., 1984. High-temperature, large-volume, lavalike ash-flow tuffs without calderas in southwestern Idaho. Geological Survey Professional Paper 1272, 1-76.

Field, M., Scott Smith, B.H., 1999. Contrasting geology and near-surface emplacement of kimberlite pipes in Southern Africa and Canada, Proceedings of the 7th International Kimberlite Conference. J.B. Dawson volume, 214-237.

Hydrological Consultants Inc., 2004. Dewatering of the Victor diamond project. Report to De Beers Canada Inc., available on http://www.debeerscanada.com, 71 pp. plus figures.

Le Pennec, J.-L., Fernandez, A., 1992. Fragmental lava versus welded ignimbrite on Mount Etna: arguments inferred from crystal preferred orientation. Journal of Volcanology and Geothermal Research 51 (4), 323-337.

Mitchell, R.H., 1986. Kimberlites: mineralogy, geochemistry and petrology. Plenum Press, New York, 442 pp.

Kong, J.M., Boucher, D.R., Scott Smith, B.H., 1999. Exploration and geology of the Attawapiskat kimberlites, James Bay Lowland, Northern Ontario, Canada. Proceedings of the 7th International Kimberlite Conference, Cape Town, J.B. Dawson volume, 452-467.

Schumacher, R., Schmincke, H.-U., 1991. Internal structure and occurrence of accretionary lapilli - a case study at Laacher See volcano. Bulletin of Volcanology 53 (8), 612-634.

Webb, K.J., Scott Smith, B.H., Paul, J.L., Hetman, C.M., 2004. Geology of the Victor Kimberlite, Attawapiskat, Northern Ontario, Canada: cross-cutting and nested craters. Lithos 76 (1-4), 29-50.

4 A RARE OCCURRENCE OF A CRATER-FILLING CLASTOGENIC EXTRUSIVE COHERENT KIMBERLITE AT VICTOR NORTHWEST[3]

4.1 Introduction

Coherent kimberlite commonly occurs as intrusive sheets, dykes, and is also found to fill or partly fill pipes and diatreme root zones (e.g. Field and Scott Smith, 1999; Skinner and Marsh, 2004). For the most part, these coherent deposits have a well-crystallised igneous groundmass and have been interpreted as being intrusive coherent (or hypabyssal) in origin. This paper reports a rare occurrence of extrusive coherent kimberlite in a pipe-filling geometry at Victor Northwest (Northern Ontario, Canada).

Coherent extrusive rocks can form by a variety of processes. Most commonly they result from simple effusion of lava onto the earth's surface. Coherent extrusive rocks may also result from explosive volcanism. For example, many lavas are clastogenic in that they result from accumulation and coalescence of pyroclasts produced from lava fountaining events (Sumner, 1998; Sumner et al. 2005). In addition, welded fall-out deposits can form in vent-proximal environments given high enough eruption temperatures and accumulation rates (Walker, 1984; Carey et al., 2008). More explosive eruptions can also produce pyroclastic flows that are remade coherent or lava-like (Ekren et al., 1984; Branney and Kokelaar, 1992) by dense welding, generally aided by the overburden pressure of the overlying rocks. In all cases coalescence, agglutination or welding can

[3] A version of this chapter has been accepted for publication. van Straaten, B.I., Kopylova, M.G., Russell, J.K. and Scott Smith, B.H. (2010). A rare occurrence of a crater-filling clastogenic extrusive coherent kimberlite, Victor Northwest (Ontario, Canada). Bulletin of Volcanology.

produce rocks that are coherent and may be indistinguishable from lavas on the hand sample and microscopic scale (Sumner and Branney, 2002, and references therein). These lava-like pyroclastic deposits are generally believed to have formed by syn-depositional coalescence of mostly molten magma droplets. From these examples it is clear that there is a complete continuum between effusive lava flows, lava fountain-fed clastogenic lavas and lava-like welded deposits.

In this paper we identify *coherent kimberlite* as those rocks having an igneous, well-crystallised groundmass. In addition, we use *reconstituted coherent rock* as an umbrella term to describe magmas or lavas that have undergone pyroclastic fragmentation but were remade coherent by syn- to immediately post-depositional processes ranging from *welding* (sticking together at point contacts and compaction of particles under the influence of the overburden pressure in a still-hot deposit; terminology after Sumner et al., 2005), *agglutination* (the flattening, sticking together and gradual cooling of hot, fluid pyroclasts as they impact on an accumulation surface; Sumner et al., 2005) and *coalescence* (a process where fluidal droplets form a homogeneous liquid in which the remnant particle outlines are obliterated; Sumner et al., 2005). In contrast, the term *clastogenic extrusive coherent rock* only applies to deposits that were formed by coalescence, and are generally formed in lava fountaining environments (definition following Wolf and Sumner, 2000). The range of processes that can create reconstituted coherent rocks can be seen as a continuum from welding to agglutination and coalescence, where the latter is favoured by a decrease in viscosity, load and an increase in temperature.

In this study we use a comprehensive volcanological and petrographic analysis of all available drill cores and describe one extensive dark and competent kimberlite unit in Victor Northwest, show that it is coherent and demonstrate that it has an extrusive origin. We consider the potential of alteration, which is commonly quoted as an important process masking original textures in kimberlites (e.g. Stripp et al., 2006; Hayman et al., 2009). In addition, we discuss which processes among effusive activity, lava fountaining and welding may have been involved in the emplacement of the Victor Northwest extrusive coherent kimberlite. Finally, we show that the deposit has a fragmental origin, and represents a clastogenic extrusive coherent deposit most likely formed by explosive lava fountaining.

4.2 Geology of the Victor kimberlite

The Victor kimberlite complex is located in Northern Ontario, Canada and is part of the Middle-Late Jurassic Attawapiskat kimberlite province (Kong et al., 1999). De Beers Canada Inc is currently mining the Victor kimberlite pipes for diamonds. The Victor diamond deposit comprises several cross-cutting and adjacent steep-sided kimberlite pipes (Webb et al., 2004; chapters 2 and 3), emplaced within a ~275 m thick Ordovician to Silurian sedimentary sequence which overlies Precambrian granitoid basement (Fig. 4.1). We studied the internal geology, petrography and volcanic stratigraphy of the earliest pipe in the Victor complex, the Victor Northwest pipe, using detailed megascopic, macroscopic and microscopic investigations of drill cores, polished drill core samples and thin sections, respectively. The results are summarised in Figures 4.1-4.4 and representative samples are illustrated in Figures 4.5, 4.7 and 4.8. The Victor Northwest pipe is crosscut by the later Victor Main pipe (Fig. 4.1; chapter 3).

The internal geology of the Victor Northwest (VNW) kimberlite pipe is complex, and comprises numerous small-volume stratigraphic units (Fig. 4.1). The stratigraphic units can be subdivided in two sequences, upper (U) and lower (L), each of which can be shown to correspond to a separate eruptive cycle (Fig. 4.1; chapter 3). Each eruptive cycle comprises an early explosive phase that produces pyroclastic deposits containing abundant angular broken olivine grains. In this context it is important to note that sub-round olivine grains are the dominant crystal component in pre-eruption kimberlite magmas. The early pyroclastic deposits are overlain by dark and competent kimberlite (DCK), which is massive, featureless, and characterized by mostly unbroken olivines. The last deposits of each eruptive cycle comprise (resedimented) volcaniclastic kimberlite and a thick blanket of sedimentary country rock breccias. Each eruptive cycle is believed to represent an early explosive eruption followed by less explosive eruptive activity, with subsequent post-eruption pipe-wall collapse and production of country rock breccias (chapter 3). The dark competent kimberlite within the upper eruptive cycle (DCK-U) is the focus of this paper (Fig. 4.1).

4.3 Geology of the DCK-U

The upper dark and competent kimberlite in the Victor Northwest pipe (DCK-U in Fig. 4.1 and chapter 3) was investigated using detailed megascopic, macroscopic and microscopic observations on drill cores, polished drill core samples and thin sections, respectively. For this study we logged all 16 drill cores in which this rock type was found; intersections of this rock type totalled 805 m (Figs. 4.2, 4.3). The macroscopic and microscopic examinations were undertaken on polished slabs and thin sections prepared from 77 representative core samples (see Fig. 4.3 for sample locations). The results of

this study are summarised in Figures 4.1-4.4 and the representative samples are illustrated in Figures 4.5, 4.7 and 4.8.

4.3.1 Megascopic features

The three dimensional distribution of the different rock types within the upper sequence of the VNW pipe (Fig. 4.1) was reconstructed by extrapolating the data between the drill holes shown in Figure 4.3. Figure 4.2 maps the location of all drill cores, and the reconstructed contours for the base of the DCK-U. The data presented in Figures 4.1-4.3 clearly shows the pipe-wide extent of the DCK-U, the funnel shaped geometry and the fact that this unit is the volumetrically dominant unit in the upper stratigraphy of the Victor Northwest pipe-fill. The average vertical thickness of the unit varies from 45 m to over 95 m near the reconstructed pipe centre.

The DCK-U is underlain by pyroclastic kimberlite (VK-U_1) and overlain by pyroclastic, volcaniclastic, resedimented volcaniclastic kimberlite and sedimentary country rock breccias (VK-U_2, VK-U_3, RVK-U and CRB-U; see Fig. 4.1, 4.3). These units are discussed in more detail in section 4.4.

4.3.2 Macroscopic and microscopic features

Detailed petrographic observations on drill core and representative samples show that this rock type is dark, dense, competent, and generally matrix-supported, massive and featureless in nature. The unit can be divided into two subunits, an upper and lower subunit (DCK-U_2 and DCK-U_1, respectively). DCK-U_2 is the volumetrically dominant subunit, and comprises an estimated 80% of the total volume of the DCK-U. The two subunits are described separately below.

4.3.2.1 DCK-U_2

The DCK-U_2, the dominant DCK-U, is a fairly homogenous unit, as shown by the similarity of five representative core samples from different parts of the VNW pipe (Fig. 4.5). The rocks contain abundant 0.5-10 mm sub-round mostly unbroken olivine macrocysts (Figs. 4.4C, 4.5) and minor macrocrystic phlogopite. Other mantle-derived macrocrysts (mantle indicator minerals, MIMs) are rare; an average of about 3 MIMs per 40 cm^2 of core surface are present (Fig. 4.6). These macrocrysts are dominated by ilmenite, garnet (purple coloured garnets dominate) and minor Cr-diopside (dominantly present as intergrowths with larger olivine macrocrysts). The DCK-U_2 typically has low abundances of country rock fragments, with about 1-2 vol.% basement clasts (granitoid and dolerite) and 1-8 vol.% sedimentary clasts (white-grey limestone and green mud/siltstone). The sedimentary country rock fragment abundance is highest towards the upper and lower contacts (Fig. 4.4A). In addition, the limestone clasts often have irregular/fluidal shapes.

The area between the macrocrysts in the dark and competent rocks generally comprises the following euhedral minerals: olivine phenocrysts set in a groundmass of evenly distributed oxides (spinel), perovskite, carbonate laths, phlogopite laths, and interstitial serpentine altered 10-20 μm six-sided minerals after monticellite (Fig. 4.7). In addition to the various euhedral minerals listed above, volumetrically minor (< 5%) interstitial carbonate and/or serpentine of uncertain origin is present throughout the groundmass. The latter occur as interstitial micro- to cryptocrystalline carbonate ± serpentine, as well as minor distinct 0.5-1 mm sized pool or segregation-shaped carbonate ± serpentine areas. The olivine macrocrysts are generally partly fresh, which contrasts distinctly with

the complete replacement of olivine by carbonate ± serpentine in the overlying and underlying volcaniclastic kimberlite units (Fig. 4.4B). Some of the groundmass carbonate laths have been pseudomorphed by a later carbonate, as laths occurring in clusters extinguish together (Fig. 4.7G, H). In most cases it is clear that the groundmass has been produced by crystallisation from a melt, and that the rock is coherent in nature (Figs. 4.3, 4.7B-H). However, in certain samples (~20% of DCK-U_2) the nature of the groundmass is less discernible (Figs. 4.3, 4.7A). In these locations the rocks lack clearly visible groundmass carbonate laths, and generally contain more abundant (5-15%) interstitial carbonate ± serpentine. Despite the above observations, these rocks still have a similar appearance and texture as the main DCK-U_2, both at the macroscopic and microscopic scale. Based on the textural similarity, it is interpreted that these rocks are coherent.

About 35-40% of the DCK-U_2 contains macroscopically distinguishable selvages around olivine macrocrysts. The selvages are generally present within the upper N-NE parts and in the central to lower parts of the central areas of the DCK-U_2 unit (Fig. 4.3). These features can best be described as 100 μm to 1 mm thick symmetrical or asymmetrical complete or partial selvages on olivine crystals (Fig. 4.8). The selvages are texturally different in appearance from the surrounding groundmass, as they contain notably finer grained olivine phenocrysts (maximum dimensions of up to 100-280 μm within the selvages vs. up to 1-2 mm outside the selvages) and carbonate laths (up to 100-260 vs. 240-360 μm within and outside the selvages, respectively). In certain cases the selvages are set in an unequivocally well-crystallised coherent groundmass (Figs. 4.3, 4.8B). The selvages are similar in texture to juvenile pyroclasts in the overlying pyroclastic and volcaniclastic units (VK-U_2, VK-U_3; see section 4.4, and chapter 3).

Other significant features within the DCK-U_2 include minor areas that show patchy grain size variations, as well as the presence of a generally subhorizontal preferred orientation of elongate grains (e.g. Fig. 4.5D). A vesicular coherent interval was intersected in one drill core (V-02-198; Fig. 4.3).

4.3.2.2 DCK-U_1

The DCK-U1 is present below DCK-U_2 in eleven out of fourteen drill holes that intersect the lower DCK-U contact (Fig. 4.3). If present, the unit generally has a vertical thickness of 5-30 m. In most cases the rocks are similar to DCK-U_2 in that they show a well-crystallized coherent (~70%) or probably coherent (~30%) groundmass (Fig. 4.3). The unit generally shows a larger range in angular broken olivine content than DCK-U_2 (Fig. 4.4C). DCK-U_1 includes three slightly different textural types: Type a, which generally contains slightly finer grained olivine macrocrysts compared to DCK-U_2. Type b, which also contains finer grained olivines (similar to type a,) but has more common patchy grain size variations. Type c generally has a more volcaniclastic appearance and shows abundant variation between clast-supported and matrix-supported domains (Fig. 4.9). The different types are shown with a different cross-hatching pattern in Figure 4.3. It is important to note that the DCK-U_1 type a to type c increasingly shows features that are different from DCK-U_2 and increasingly comparable to VK-U_1. The DCK-U_1 tends to be absent near the centre of the VNW pipe, and the texturally more distinct varieties (i.e. DCK-U_1 type b, c) are generally more common near the outer portions of the pipe (Fig. 4.3).

4.4 Geology of the units surrounding the DCK-U

In this section we will shortly summarise the pertinent geology of the units surrounding the DCK-U (see chapter 3 for additional details). The DCK-U is underlain by pyroclastic kimberlite (VK-U_1) and overlain by pyroclastic, volcaniclastic, resedimented volcaniclastic kimberlite and sedimentary country rock breccias (VK-U_2, VK-U_3, RVK-U and CRB-U; see Figs. 4.1, 4.3). The CRB-U comprises 10 cm to m-scale sedimentary country rock fragments of limestones, dolostones, mudstones and siltstones, and is interpreted to form by pipe wall collapse following the eruption (chapter 3). The RVK-U is only intersected in one drill core (V-01-189, Fig. 4.3) and comprises a thin intersection of well-sorted country rock fragment-poor massive to layered RVK containing abundant foreign (quartz, mud) material. This particular unit shows clear evidence for addition of non-kimberlitic detrital material and resedimentation by water (chapter 3). The three major volcaniclastic kimberlite units VK-U_1, VK-U_2 and VK-U_3 have been interpreted as pyroclastic, pyroclastic and volcaniclastic in origin, respectively (chapter 3). The pyroclastic nature of VK-U_1 and VK-U_2 is based on the presence of fragile clastic pyroclasts (VK-U_1 only), the absence of significant sorting and bedding that is typical of reworked deposits, and the absence of detrital non-volcanic material. In contrast, the volcaniclastic origin of VK-U_3 is suspected on the basis of the gradual transition to RVK-U and overlying pipe-wall collapse CRB-U (chapter 3). Discriminating features between rock types include changes in the country rock fragment abundance, the proportion of angular broken olivine grains, as well as olivine alteration, which are illustrated in Figure 4.4 for VK-U_1, DCK-U and VK-U_3. The relatively small-volume unit VK-U_2 is located in the pipe centre (Figs. 4.1, 4.3 chapter 3) and is characterised by low country rock

fragment abundances (~6 vol.%), altered olivines and mostly intact olivine macrocrysts. In addition to the features shown in Figure 4.4, the juvenile pyroclasts can also be used to differentiate units within VNW. The juvenile pyroclast shape, size and constituents within the pyroclasts show distinct textural patterns between the four units that contain pyroclasts (VK-U_1, DCK-U_2, VK-U_2 and VK-U_3). The VK-U_1 is most distinct from all other units, and shows predominantly small, generally uncored irregularly shaped variably vesicular juvenile pyroclasts and rarer rim-type accretionary pyroclasts (sensu Schumacher and Schmincke, 1991). In contrast, VK-U_2 shows mostly non-vesicular juvenile pyroclasts cored by olivine macrocrysts, as well as rare >5 cm uncored poorly vesicular juvenile pyroclasts. The pyroclasts in both DCK-U_2 and VK-U_3 are very similar to the dominant pyroclast type in VK-U_2, and mostly comprise juvenile pyroclasts cored by olivine macrocrysts (see Fig. 4.8 for DCK-U_2 pyroclasts).

Contact relationships between the DCK-U and the enveloping extrusive and fragmental deposits are characterized by an absence of sharp contacts (Fig. 4.3). Twenty-three out of twenty-five drill core intersections of the VK-U_3 to DCK-U_2, VK-U_2 to DCK-U_2 or DCK-U to VK-U_1 contact do not show sharp contacts. Generally, the contacts between the DCK-U and the enveloping extrusive and fragmental deposits are characterized by a gradational change in componentry over tens of metres including country rock fragment type and abundance, abundance and type of pyroclasts and broken olivine content (Figs. 4.3, 4.4). These contact relationships contrast markedly with other contacts at Victor that show knife-sharp erosional contacts with abrupt changes in componentry within 1-10 mm (e.g. VM to VNW contact, see Fig. 4.3 and chapter 3). Features such as the olivine alteration change within 3-10 m (Fig. 4.4B). In addition, in certain cases the

groundmass/matrix texture as observed in thin section can change from clearly coherent over a few metres from the contact to clearly volcaniclastic (fragmental) on the other side of the contact (Fig. 4.3).

Despite the abundant textural differences between the different kimberlite lithologies in the upper stratigraphy of the VNW pipe, there are a number of striking similarities between the VK-U_3, VK-U_2, DCK-U_2, DCK-U_1 and VK-U_1 units. One of the similarities is the mantle indicator mineral (MIM) content shown in Fig. 4.6. The absolute abundance, relative proportions of MIMs, grain sizes and textural occurrence are very similar between units. Changes in absolute abundance can easily be explained by the higher abundance of country rock fragments in the samples of volcaniclastic kimberlite with respect to the mostly country rock fragment-poor DCK-U_2 and DCK-U_1. In addition, changes in the total macrocryst (mantle-derived coarse crystal) content can easily change the absolute abundance of MIMs by magmatic (filter pressing, flow) and volcanic (fragmentation, deposition) processes. Apart from similarities in mantle indicator minerals, the five above mentioned kimberlite units also have very similar mineralogical and petrological characteristics. The juvenile pyroclast groundmass in the volcaniclastic units, as well as the coherent groundmass in the dark and competent units is very similar in terms of mineralogy, textural relationship between minerals and individual mineral morphology; individual mineral modal abundance and individual mineral size are similar between the five units (cf. Fig. 4.7 and chapter 3). As presented in section 4.3, the DCK-U_2 unit comprises, apart from macrocrysts and olivine phenocrysts, a groundmass of (in order of modal abundance, see Fig. 4.7): carbonate laths, spinel, monticellite, perovskite,

minor phlogopite and micro- to cryptocrystalline carbonate ± serpentine. Petrological observations on the other four units show the same pattern.

4.5 Interpretation and discussion

4.5.1 VNW upper stratigraphy: single batch of magma

Based on observations detailed in section 4.4 we infer that the kimberlite units of the entire upper stratigraphy within the VNW pipe are derived from a single batch of magma. This interpretation is based on the similarities in observations on mantle indicator minerals (Fig. 4.6) as well as on groundmass mineralogy. This interpretation has important economic implications, as one batch of magma generally carries the same mantle-derived crystal cargo and contains one distinct macrodiamond population (e.g. Gurney and Kirkley, 1996; Scott Smith and Smith, 2009). In this case it is fair to assume that any differences in diamond grade and quality between the different kimberlite units in the upper stratigraphy of VNW will be caused by volcanic processes such as dilution by country rock fragments, sorting and crystal breakage, as well as chemical processes such as potential prolonged diamond resorption in slowly cooling coherent deposits.

4.5.2 DCK-U: textural-genetic interpretation

4.5.2.1 Single unit of well-crystallized coherent kimberlite

Alteration has been cited as an important process modifying the original igneous texture and mineralogy of kimberlite deposits (Sparks et al., 2006; Stripp et al., 2006; Cas et al., 2008a, b; Porritt, 2008; Hayman et al., 2009). Thus, we first consider whether the dark and competent kimberlite at Victor Northwest could represent a pyroclastic rock that has been consolidated by post-emplacement modification/alteration processes resulting in a

dark, competent, uniform rock that resembles coherent kimberlite. The following observations show that the DCK-U has undergone minor alteration and that the main textures of the DCK-U are not a result of alteration. Firstly, the entire unit contains partly or completely fresh olivine macrocrysts and/or phenocrysts, partly or completely fresh fine-grained minerals (Figs. 4.4B, 4.7, 4.8), and does not show the pervasive alteration that is characteristic of the Southern African-style (sensu Field and Scott Smith, 1999) kimberlite pipes quoted in recent papers on alteration (Stripp et al., 2006; Cas et al., 2008a, b; Porritt, 2008). Secondly, the fine-grained minerals in the DCK-U have euhedral shapes and textural inter-relationships with other minerals typical of igneous crystallization rather than alteration (Fig. 4.7). No colloform carbonate typical of late inter-clast void infilling in pyroclastic kimberlites (e.g. Mitchell, 1997, p.18) is present. Domains of carbonate ± serpentine presently occupy the area in between the fine-grained groundmass minerals, and there is some disagreement in the literature whether these domains are the result of crystallisation from late-stage magmatic fluids (e.g. Mitchell, 1984; Skinner and Marsh, 2004), alteration (Cas et al., 2008a) and/or represent remnant pore space in densely welded rocks (Brown et al., 2008). However, even if these domains are secondary, they generally comprise only a small volume (0-15%) of the rock, and therefore the groundmass is predominantly igneous in origin. Lastly, the nature and crystallisation sequence of the groundmass of the DCK-U kimberlite is typical of worldwide kimberlites (Shee, 1984; Mitchell, 1986; 1995; Armstrong et al., 2004; Caro et al., 2004; Fedortchouk and Canil, 2004; Roeder and Schulze, 2008; chapter 2), and comparable to experimental studies (Mitchell, 1986, p.343-354; Otto and Wyllie, 1993; Bellis and Canil, 2007; Canil and Bellis, 2008; Sparks et al., 2009).

From the above discussion, it can be concluded that the DCK-U does not represent an altered volcaniclastic rock, but instead represents a single funnel-shaped unit of well-crystallised coherent kimberlite created by magmatic crystallisation.

4.5.2.2 Extrusive coherent origin

The DCK-U unit of the Victor Northwest kimberlite displays many lines of evidence for an extrusive origin:

(1.) The funnel-shape morphology of the DCK-U deposit (Figs. 4.1-4.3).

(2.) The funnel shape of the basal contact of the DCK-U mirrors the lower contact of the underlying earlier pyroclastic kimberlite (VK-U_1; see Fig. 4.2 as well as Fig. 3.1C in chapter 3). The well-constrained and coincident location of the vents for each of the deposits (VK-U_1 and DCK-U) suggests that the magma from which these rock types formed exploited the same feeder system. The similarity in mantle-derived macrocrysts and groundmass mineralogy (sections 4.4, 4.5.1), combined with the textural difference between the VK-U_1 and DCK-U (Figs, 4.4, 4.6; chapter 3) shows that the two rock types were formed from the same batch of magma, but by distinctly different eruptive processes. This suggests that the DCK-U originated from the same central feeder as VK-U_1 and was deposited in a vacant crater, on top of extrusive primary pyroclastic deposits.

(3.) There is a lack of evidence for intrusion into consolidated deposits. The DCK-U unit is limited to within the nested crater discussed above, and does not extend into the country rock. There is also a lack of dykes, sills or apophyses in the surrounding in situ country rock.

(4.) There is a lack of evidence for intrusion into, and mixing with, unconsolidated deposits.

(5.) The DCK-U is enveloped by extrusive fragmental facies and lacks sharp contacts. Only 2 out of 25 drill cores show a sharp contact with enveloping volcaniclastic kimberlite units. Despite limitations of working with drill core, it appears that the contacts with the under- and overlying pyroclastic kimberlite are gradational over several meters (Fig. 4.4).

(6.) The presence of mixed country rock fragments derived from different stratigraphic levels of the sedimentary country rocks. The magma could likely not have accessed this variety of clasts if the DCK-U was intrusive into earlier kimberlite.

The above discussion shows that the DCK-U represents a single batch of coherent magma that was emplaced into an open nested crater where it underwent mostly en masse uniform rapid crystallisation. The mode of emplacement of the magma into the nested crater is discussed below.

4.5.3 Emplacement mechanisms of extrusive coherent DCK-U

4.5.3.1 Theoretical constraints

To consider the emplacement of the DCK-U which is massive, fresh, coherent, well-crystallized and extrusive in nature, we need to address theoretical constraints on the likelihood of kimberlite magma to erupt effusively and/or form reconstituted (i.e. clastogenic or welded) coherent deposits. This will help to formulate criteria for recognizing these rock types in the field and in thin sections.

4.5.3.1.1 Possibility of kimberlite lava formation

Possible kimberlite lava occurrences have been proposed in Angola (Skinner and Marsh, 2004; Eley et al., 2008), India (Mainkar et al., 2004) and Tanzania (Igwisi Hills: Reid et al., 1975; Dawson, 1994). The kimberlites in Angola and India, however, have not been well documented. The Igwisi Hills occurrence in Tanzania is currently the best candidate for a kimberlite lava, but has been argued by some to be a somewhat atypical kimberlite in that it is very calcite rich (comparable to the evolved kimberlite sills at Benfontein and Wesselton described by Dawson and Hawthorne, 1973 and Mitchell, 1984 respectively) and contains groundmass spinels that could be indicative of significant crustal contamination (Mitchell, 1986, p. 31; Mitchell, 2008).

The extreme rarity or absence of kimberlite lavas in the geological record could be explained by the susceptibility to erosion of the upper reaches of the kimberlite volcanic systems (e.g. Lorenz, 1986), combined with the absence of uneroded modern kimberlite volcanoes. The postulated extremely volatile-rich nature of kimberlite magma (e.g. Dawson and Hawthorne, 1970; Kopylova et al., 2007; Fedortchouk et al., 2010) does not mean that the magma cannot erupt effusively. No other magma type erupts only explosively, and comparable magma types such as carbonatites and lamproites can form intra-crater lava lakes (Krafft and Keller, 1989; Smith and Lorenz, 1989; Mitchell and Bergman, 1991, p.125-137) and/or extra-crater lava flows (Woolley and Church, 2005; Sedeghi et al., 2007). High concentrations of carbon dioxide in carbonatites and kimberlites are compensated by its higher solubility as CO_3^{2-} in the melt phase (Brooker et al., 2001). CO_3^{2-} in carbonatites is generally not easily exsolved into the vapour phase

during ascent and decompression, allowing for non-explosive eruptions to occur; a similar behaviour is expected for carbonate-rich kimberlites.

In summary, the above discussion suggests that effusive kimberlite lavas are expected to form, but have a very low preservation potential unless formed in a sufficiently deep intra-crater setting.

4.5.3.1.2 Coalescence, welding and hot pressing in kimberlite

The unique composition of kimberlite magmas affects volcanological processes, and particularly the way welding will proceed in this rock type. Kimberlite melt is characterized by low silica content and a high depolymerisation. Estimates on the ratio of non-bridging oxygens (NBO) over cations in the tetrahedral site (T) range from 2 to 6 for typical kimberlite melts (Russell et al., 2006; Kopylova et al., 2007). The currently best-available viscosity models for silicate melts (Giordano et al., 2008) are based on melts with NBO/T values of 0-1.8 and give viscosities down to 0.1-1.3 Pa·s. In contrast, physical property measurements on vesicle and crystal-poor carbonatite pahoehoe lava flows (Dawson et al., 1990; Norton and Pinkerton, 1997) give viscosities of 0.15-5 Pa·s. Both viscosity estimates indirectly suggest a very low viscosity for kimberlite melt, likely below 1-10 Pa·s. The presence of ~50 vol.% olivine crystals will increase the viscosity by at least one order of magnitude (Krieger & Dougherty, 1959; Mueller et al, in press). In addition, the commonly sub-spherical shape, vesicle-poor nature of kimberlite juvenile pyroclasts and common presence of abundant free crystals as kimberlite pyroclasts is also suggestive of very low melt viscosities.

One of the commonly quoted requirements for welding is the presence of hot (with temperatures above the glass transition temperature, T_g) glassy pyroclasts (Quane and

Russell, 2005 and references therein). Pyroclasts that crystallize rather than quench to a glass are unlikely to undergo conventional welding. Glassy pyroclasts produced by brittle fragmentation of the magma during eruption can relax, flow viscously and anneal over the longer timescales associated with cooling (e.g. Dingwell, 1996; Russell and Quane, 2005). In the case of kimberlites, it is unclear whether the melt will quench to a glass or crystallize during an eruption. Firstly, the gap between the liquidus and glass transition temperature for kimberlite magmas is very high (Russell et al., 2006), making it difficult to quench the melt to a glass. We assessed the liquidus temperature for kimberlite melts as ~1200 °C (Fedortchouk and Canil, 2004), and the glass transition temperatures as ~600 °C (see Russell et al., 2006; these calculations are based on the Giordano et al., 2008 model applied to several estimates of primitive kimberlite melt compositions). Secondly, degassing is unlikely to cause a significant increase in the glass transition temperature of kimberlite. This conclusion follows modeling of T_g's for water-bearing and water-free kimberlite melts using the Giordano et al. (2008) model (Russell et al., 2006), as well as recent studies on the effect of moderate amounts of CO_2 on the glass transition temperature (Morizet et al., 2007). The absence of a possible mechanism to lower the T_g during an eruption contrasts markedly with other more common silicate melts where degassing is one of the most common quenching mechanisms (Dingwell, 1996). Thirdly, as a result of the difficulty in forming glass in such low-viscosity melts, crystallization is likely to occur very fast in kimberlites (Brown et al., 2008). It is only in extremely small melt pyroclasts that we can envisage the cooling rate to be fast enough for glass to form. Fourthly, no kimberlite glass has ever been observed, however this

could also be related to the absence of recent kimberlite deposits combined with the poor preservation potential of these glasses (e.g. Marshall, 1961).

The above theoretical considerations imply that glass might not form during a typical kimberlite eruption. Instead, the pyroclasts would crystallize with cooling. The pyroclastic deposit could still form an annealed, dark, competent and massive rock via a process referred to as hot pressing in the ceramics industry (Vieira and Brook, 1984; Venkatachari and Ray 1986). This process has received only little attention in the geological literature (Russell and Quane, 2005), but may be analogous to welding in consolidating hot porous crystalline particles at relatively short timescales.

Both welded or hot pressed kimberlite deposits will look very different from common ignimbrites. Welding in kimberlites will not produce a well-developed fabric with elongated fiamme because kimberlite pyroclasts are commonly non-vesicular, crystal-rich and equant in shape. Compaction in kimberlites can proceed only via the reduction of inter-clast pore space and, hence, welding would not produce classic fiamme. Furthermore, the lack of porous pyroclasts severely limits the total amount of volumetric strain to less than ~36% which is a typical value for the inter-clast porosity for random jammed monodisperse spheres (e.g. Scott and Kilgour, 1969). For more common rhyolitic ignimbrites, the high porosity of the pyroclasts allows for values of total volumetric strain that are at least double (Quane et al., 2009). Both the lower volumetric strain and extremely equant grain shape population of kimberlites decreases the visibility of the compaction and pore space reduction that accompany welding or hot pressing.

In summary, fragmental coherent kimberlite deposits are likely to occur, and are most likely to form due to coalescence of (mostly) liquid pyroclasts. Despite the fact that glass

is unlikely to form during a typical kimberlite eruption, crystallized pyroclasts can still form a consolidated deposit by hot pressing. In the latter case the densification of these deposits containing non- to poorly vesicular equant pyroclasts will likely involve only moderate volumetric strain, hence classical welding textures such as fiamme or a strong fabric will not be present.

4.5.3.1.3 Possible occurrences of reconstituted coherent kimberlite

Despite the likelihood of coalescence, agglutination and welding to occur in low viscosity intra-crater kimberlite deposits, few descriptions of possible reconstituted coherent kimberlite occurrences have been made. Brown et al. (2008, 2009) suggest they have found welded kimberlite deposits in the K2 West pipe (Venetia, South Africa) and the B/K9 pipes (Damtshaa Mine, Botswana). The authors base their conclusion on variations in abundance of polymict country rock fragments, the occurrence of coherent kimberlite within layered sequences of volcaniclastic rocks, gradations to volcaniclastic kimberlites and microscale segregations thought to represent void space. In addition, some coherent rocks within the Ekati kimberlite pipes (NWT, Canada) have been suggested to have a welded or clastogenic origin based on geochemical analyses indicating loss of ash (Nowicki et al., 2008) as well as detailed geological observations on one of the pipes in the cluster (Crawford et al., 2009).

4.5.3.2 DCK: emplacement process

In this section we discuss whether the DCK has a purely effusive origin, or was fragmented and then reconstituted after deposition.

The DCK at Victor may have had a purely effusive lava origin, based on the fact that it displays a uniform well-crystallized coherent groundmass texture, and is fairly

homogeneous in overall nature. In this case the deposit would most likely have formed as a crater-filling lava lake, as there is no textural or mineralogical evidence for the presence of multiple batches of kimberlite magma or multiple lava flows.

However, arguments against a purely effusive origin of DCK-U are numerous, and the evidence listed below suggests that a model in which the deposit formed by reconstitution of hot, predominantly liquid, pyroclasts is more likely.

(1.) The kimberlite deposit lacks a sharp and flat top contact (Figs. 4.1, 4.3), which is a feature we would expect for a lava lake. Especially the presence of the central pyroclastic facies VK-U_2 that formed from the same magma batch is at odds with a lava lake origin. Given the above-vent location, primary pyroclastic origin and the presence of large (>5 cm) pyroclasts we infer that VK-U_2 represents the proximal pyroclastic equivalents of the underlying and surrounding DCK-U.

(2.) The selvages in the top and central deeper part of the DCK-U_2 are texturally similar to juvenile pyroclasts in the overlying VK-U_2 and VK-U_3 facies. The only other textures that have been described in coherent hypabyssal kimberlite and resemble the selvages are globular segregations. The latter textures are believed to form by separation of silicate-oxide melt droplets and volatile-rich residual melt (Clement, 1982; Mitchell 1986, p.68-71). However, globular segregations have only been described in an intrusive environment such as under overhanging pipe segments, blind intrusions, dykes or sills (Clement, 1982; Field and Scott Smith, 1999). The occurrence of such segregations near the top of a possible lava lake at Victor seems implausible as the volatile-rich phase would simply disappear into the atmosphere. In addition, the diffuse selvages at VNW contrast to globular segregations in being partly asymmetric (Fig. 4.8B, C) and having the

same mineralogy as the surrounding groundmass. Based on the dissimilarities to globular segregations, and similarities to juvenile pyroclasts in the overlying fragmental deposits (Fig. 4.6, section 4.4), these selvages are thought to have a pyroclastic origin.

(3.) The DCK-U contains more angular broken olivine than typical intrusive coherent dykes (Fig. 4.4C); this is especially true for the lower half of this unit. We interpret this as additional evidence for the fact that the magma has been fragmented.

(4.) The groundmass within the various stratigraphic levels of the DCK-U is fairly uniform both in mineralogy and grain size (Fig. 4.7), suggesting a very similar cooling history for the entire deposit. This is at odds with geological observations on lamproite (Smith and Lorenz, 1989; Mitchell and Bergman, 1991; p.125-137) and modern basaltic lava lakes (Helz et al., 1989), as well as simple conductive cooling models (e.g. Russell and Quane, 2005). Lava lakes generally show a quenched or finer grained top contact, as well as an increase in groundmass mineral grain size from the exterior to the interior of the deposit due to slower cooling of the interior. In addition, lava lakes often show evidence for crystal settling or chemical differentiation. Notably, all of these features are absent at Victor. A reconstituted coherent origin could explain the absence of all of these features, predominantly due to increased pre-deposition cooling compared to a purely effusive eruption.

(5.) The lack of sharp erosional contacts, gradual change in componentry over tens of meters from the underlying VK-U_1 to DCK-U and back to the overlying VK-U_2 and VK-U_3 (Figs. 4.4A, C, 4.6) suggests conformable or gradational contacts. In turn, this suggests a gradual change in eruption processes that generated pyroclastic non-

reconstituted (VK-U_1) to reconstituted coherent (DCK-U) back to pyroclastic non-reconstituted (VK-U_2, VK-U_3) deposits.

(6.) Finally, low viscosity melts are much more likely to undergo coalescence, agglutination or welding (Schmincke, 1974; Sumner, 1998; Sumner and Branney, 2002; Sumner et al., 2005; Sparks et al., 2006; Brown et al., 2008), hence increasing the likelihood of a fragmental origin.

Based on the mostly well-crystallised coherent nature of the groundmass within the DCK-U we interpret the deposit to have formed from predominantly coalescence of liquid pyroclasts. We would not expect a welded or hot pressed kimberlite deposit to show such a well-crystallised groundmass, but instead form a deposit with a more non-uniform matrix, as well as show remnant pore-space and a possible welding gradient due to vertical changes in the overburden pressure. Consequently, we think it is most likely that the deposit formed by explosive intra-crater lava fountaining. In this context it is interesting to note that typical maximum Hawaiian lava fountain heights are about 500m (Sparks et al., 1997, p. 256-277; Sumner, 1998; Wolff and Sumner, 2000), and as such, most of the lava fountain at VNW could have been contained within the crater, which has an estimated pre-erosional depth of 170-720 m (chapter 3). This would have significantly limited mixing with the atmosphere, reduced pyroclast cooling, and increased the likelihood of forming a clastogenic coherent kimberlite deposit.

Of additional interest is the presence of the generally finer grained DCK-U_1, which is absent near the reconstructed vent location. Perhaps the relatively thin and basal DCK-U_1 was formed from the outer and/or upper and generally finer grained portion of a waxing lava fountain (Wilson et al., 1987, p. 89). In this scenario, we could envisage that hot

molten clasts from the inner portion of the still waxing lava fountain subsequently covered the DCK-U_1.

4.6 Conclusions

We report a well-documented rare occurrence of a fresh clastogenic extrusive coherent kimberlite that formed due to intra-crater lava fountaining. The unit is dark, dense, competent, and generally matrix-supported, massive, featureless with a well-crystallized igneous groundmass. Despite the textural similarity to many intrusive hypabyssal kimberlites, these rocks are extrusive in origin, as suggested by the geometry of the unit and the nature of the contacts. A fragmental and clastogenic coherent extrusive origin is based on the presence of remnant pyroclasts, angular broken olivines, lack of evidence for an origin as a purely effusive lava lake or lava flows such as the lack of a sharp flat top, as well as gradational contacts to enveloping pyroclastic units. An absence of clear fragmental textures in reconstituted extrusive coherent kimberlite deposits such as stretched vesicular pyroclasts in basaltic clastogenic lavas or flattened pyroclasts (fiamme) and compaction fabrics in welded felsic ignimbrites makes recognition of these rock types an extremely difficult task. This study and a growing number of publications suggest that pipe-filling reconstituted extrusive coherent kimberlite in intra-crater settings may be more common than geologists previously thought. The emplacement history and volcanology of these pipes need to be reconsidered based on the emerging importance of this particular kimberlite facies.

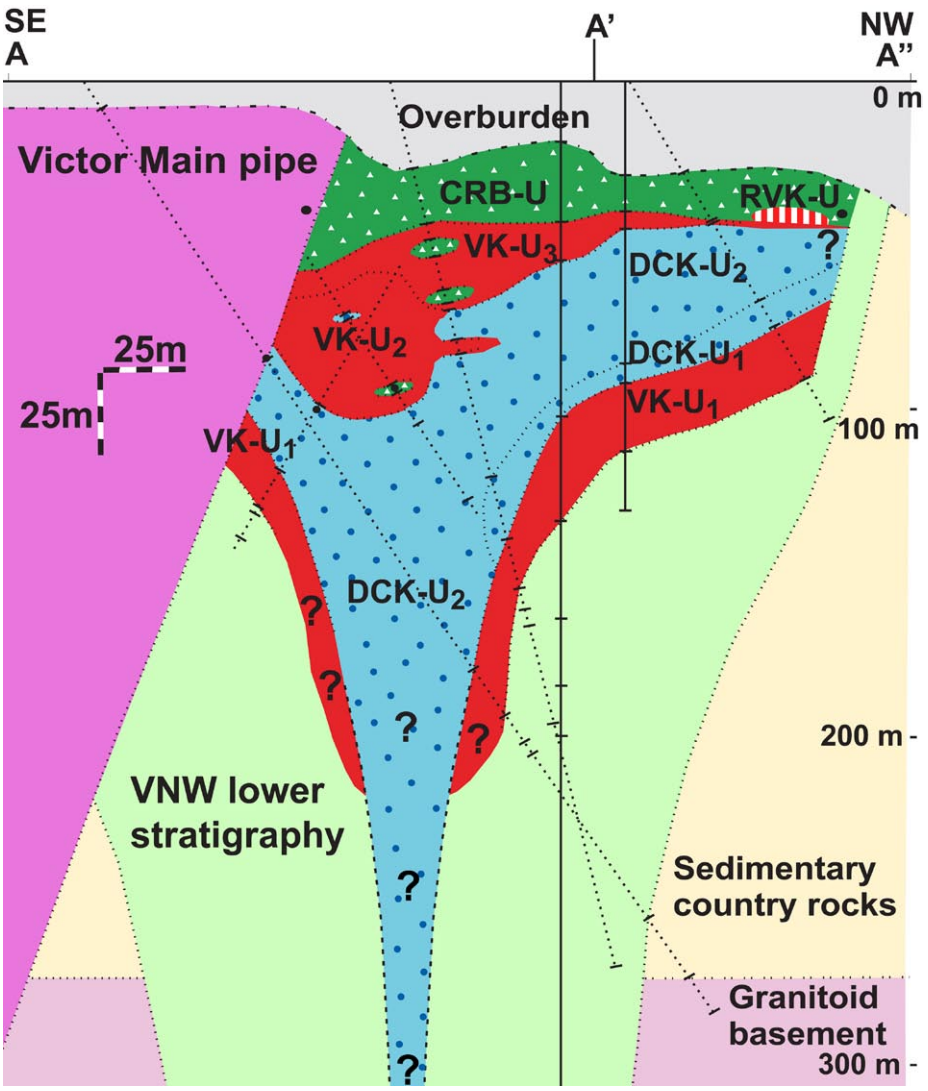

Figure 4.1 Cross-section through the Victor Northwest (VNW) pipe showing the detailed stratigraphy in the upper (*U*) part of the pipe. Location of cross-section is shown in Figure 4.2. Blue colours = dark and competent lithologies (*DCK*; note that this rock type has a funnel shape); green colours = sedimentary country rock breccias (*CRB*); red colours = volcaniclastic kimberlite (*VK*); red-white striped colours = resedimented volcaniclastic kimberlite (*RVK*). Numbers indicate sub-units of each rock type. Pale green indicates the combined lower (*L*) VNW kimberlite pipe stratigraphy. Magenta shows location of the later cross-cutting Victor Main (*VM*) pipe. Pale yellow and pink are country rocks. Depths are in metres below the surface. Lines are drill holes, tick marks on drill holes are rock type subdivisions based on logging (see Fig. 4.3 for details). After chapter 3 where further details are provided.

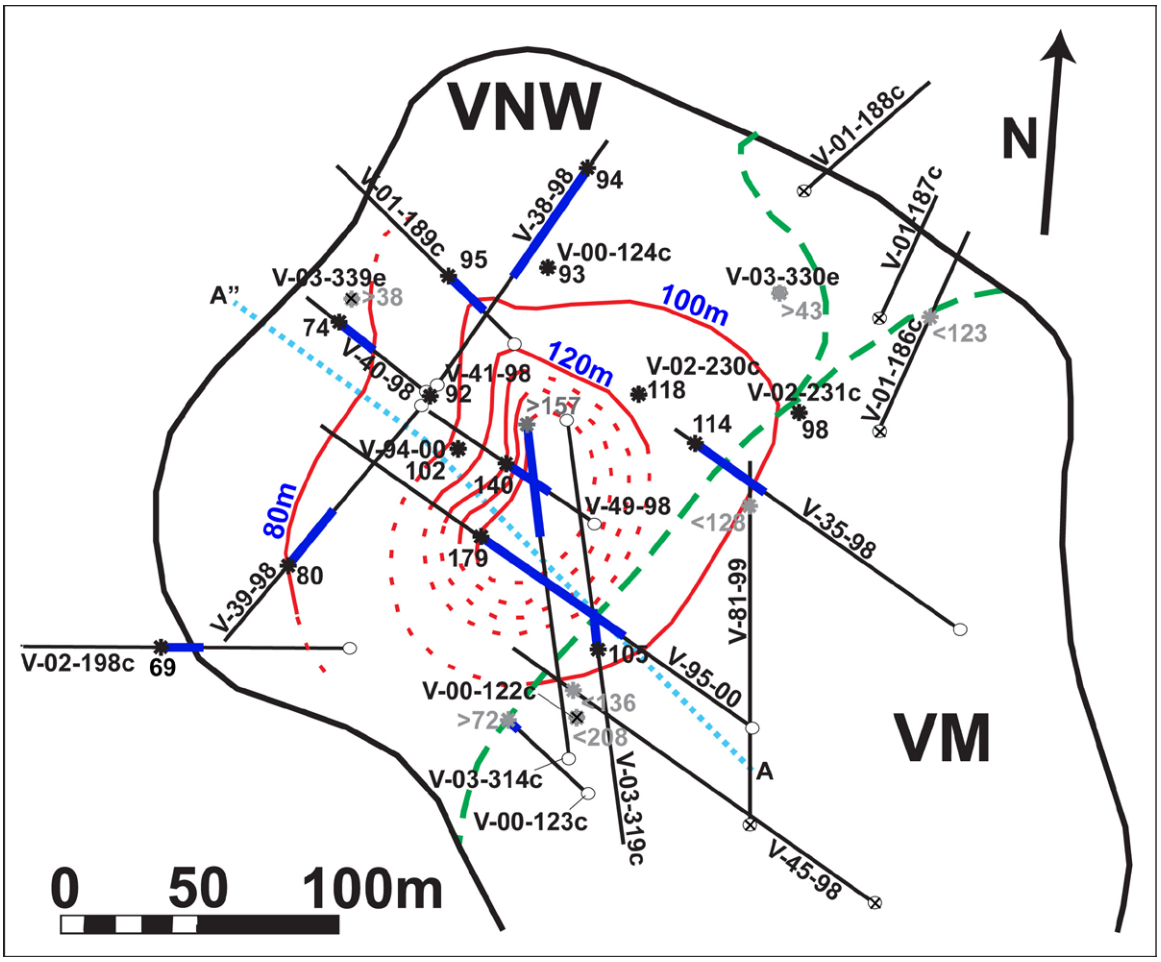

Figure 4.2 Plan view of the Victor Northwest (VNW) kimberlite pipe showing contours for the base of the VNW kimberlite unit DCK-U (contour interval 20 m, depth in metres below the surface). VM = later Victor Main pipe. Black solid line = outline of the VNW and VM kimberlite bodies, green dashed line = internal contact between the two pipes. Locations of 18 drill holes that intersect VNW are shown. Open circles = drill hole collar locations (x inside collar location circle indicates drill cores that do not intersect the upper stratigraphy of VNW); straight black lines = surface traces of angled drill holes. Lithologies in all drill holes are shown in Figure 4.3. The thickened blue parts of the drill holes indicate intersections of DCK-U in angled drill holes. Black star and number = depth of the basal contact of the DCK-U; grey star and number = contact not intersected but likely occurs below (>) or above (<) the indicated depth. Cross section A-A'-A" is shown in Figure 4.1.

Figure 4.3 Distribution of lithologies in all drill cores that intersect the Victor Northwest (VNW) upper stratigraphy, showing the dark and competent kimberlite (DCK-U) underlain by volcaniclastic kimberlite (VK-U_1) and overlain by volcaniclastic kimberlites (VK-U_2, VK-U_3), resedimented volcaniclastic kimberlite (RVK-L) and country rock breccia (CRB-U). Note the funnel shaped geometry of the DCK-U unit. See Figure 4.2 for drill hole locations. Mbs = metres below surface. Tick marks on side of drill holes are representative petrographic samples; open circled tick marks are shown in Figures 4.5 and 4.7, closed squares are illustrated in Figure 4.8, open square is shown in Figure 4.9.

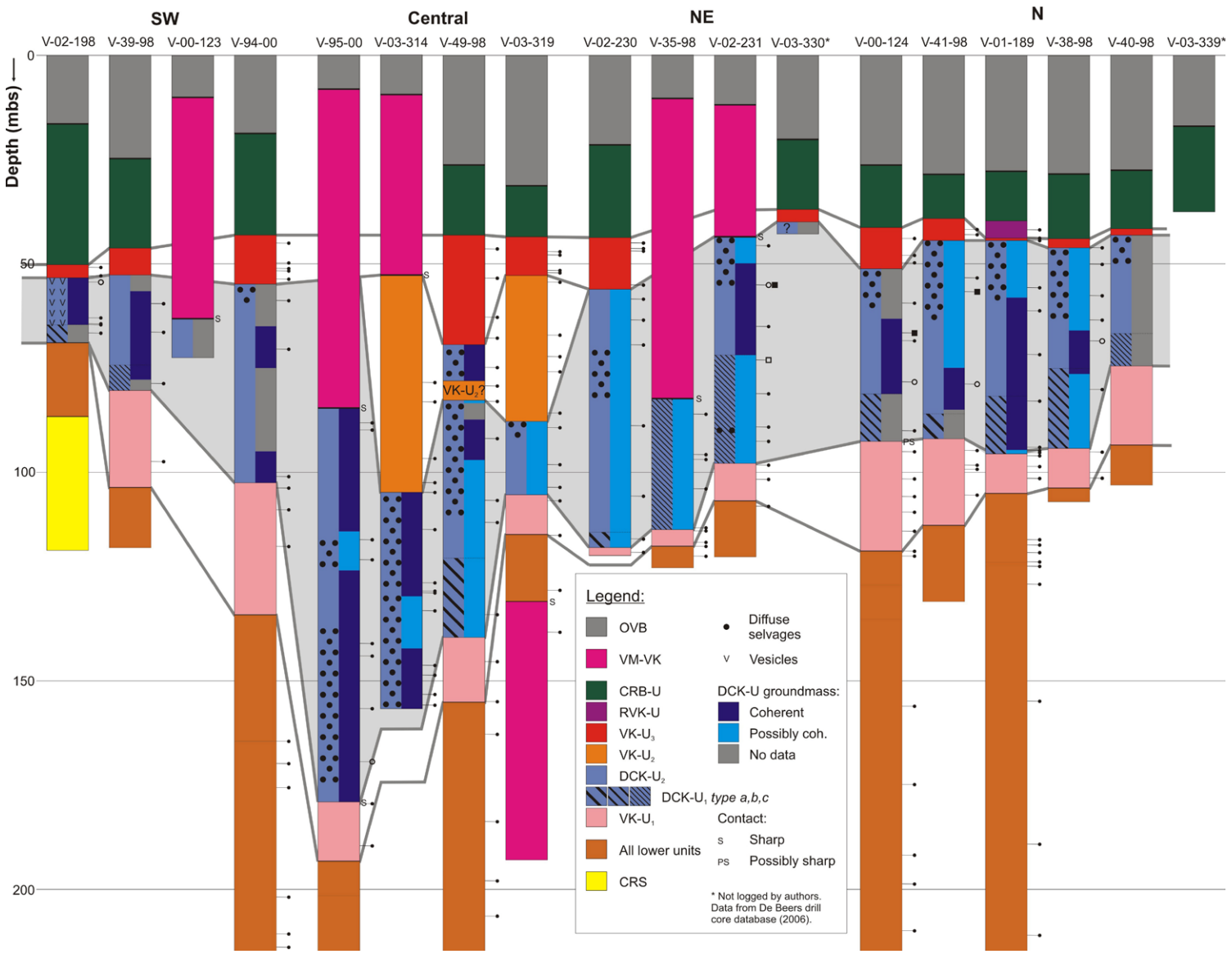
SW
Central
NE
N
V-02-198
V-39-98
V-00-123
V-94-00
V-95-00
V-03-314
V-49-98
V-03-319
V-02-230
V-35-98
V-02-231
V-03-330*
V-00-124
V-41-98
V-01-189
V-38-98
V-40-98
V-03-339*
Depth (mbs)
0
50
100
150
200
VK-U3?
Legend:
OVB
VM-VK
CRB-U
RVK-U
VK-U3
VK-U2
DCK-U2
DCK-U1 type a,b,c
VK-U1
All lower units
CRS
Diffuse selvages
Vesicles
DCK-U groundmass:
Coherent
Possibly coh.
No data
Contact:
S Sharp
PS Possibly sharp
* Not logged by authors. Data from De Beers drill core database (2006).

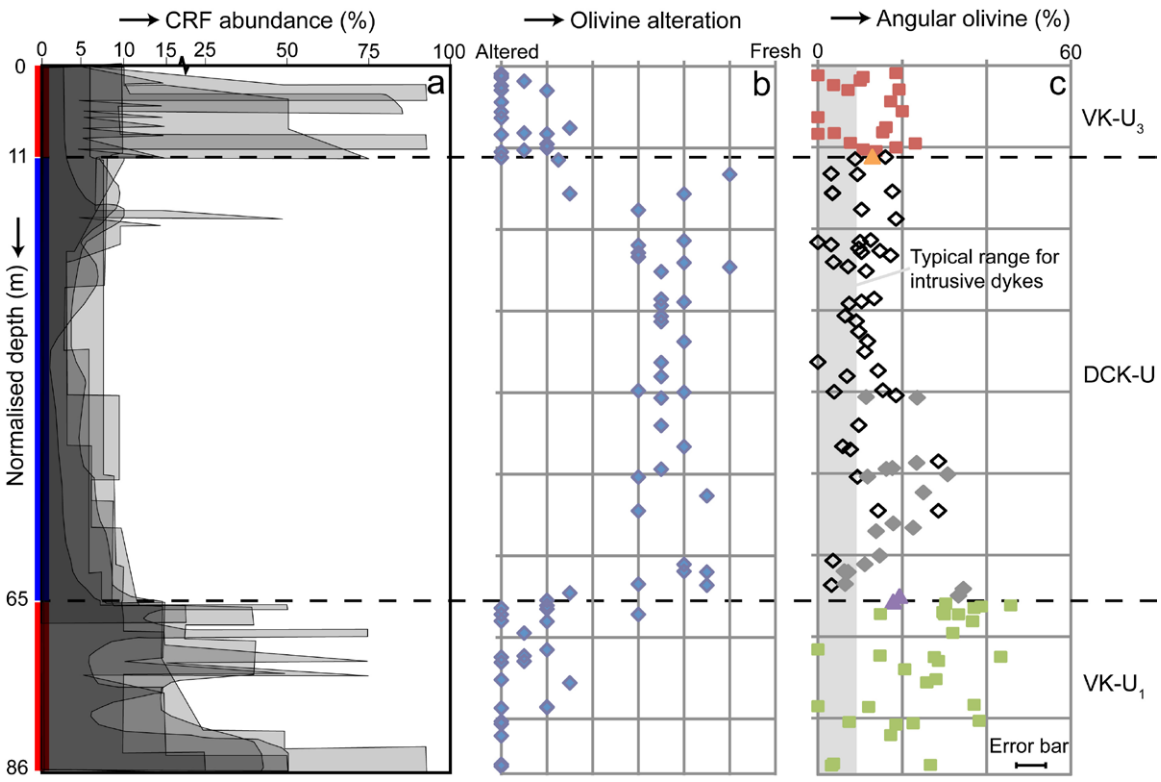

Figure 4.4 Graphs of petrographic properties plotted vs. depth, including (A) abundance of country rock fragments, (B) amount of fresh olivine and (C) proportion of olivine macrocrysts that have an angular shape. A total of six to thirteen drill holes are shown. Note that the depths from different drill holes are normalized to the average thickness of units VK-U_3 (11 m), DCK-U (54 m) and VK-U_1 (21 m). Dashed line = boundary between rock units. Country rock fragment abundance is based on a visual estimate in drill core, alteration is based on extent of alteration of olivine macrocrysts and phenocrysts observed in thin section, proportion of angular olivine was established by counting the number of olivines with one or more sharp angle (< 80°) out of at least 25 olivine macrocrysts in thin section and is interpreted to represent the proportion of angular broken grains. Triangles in (C) are samples on the contact between the DCK-U (diamonds) and VK (squares), filled diamonds indicate DCK-U_1 samples. Counting of two typical macrocrystic intrusive coherent dykes (Snap Lake and Diavik lower A154N pipe, NWT, Canada; see Field et al., 2009 and Moss, 2009 respectively, for location) yields angular olivine values from 0-9%.

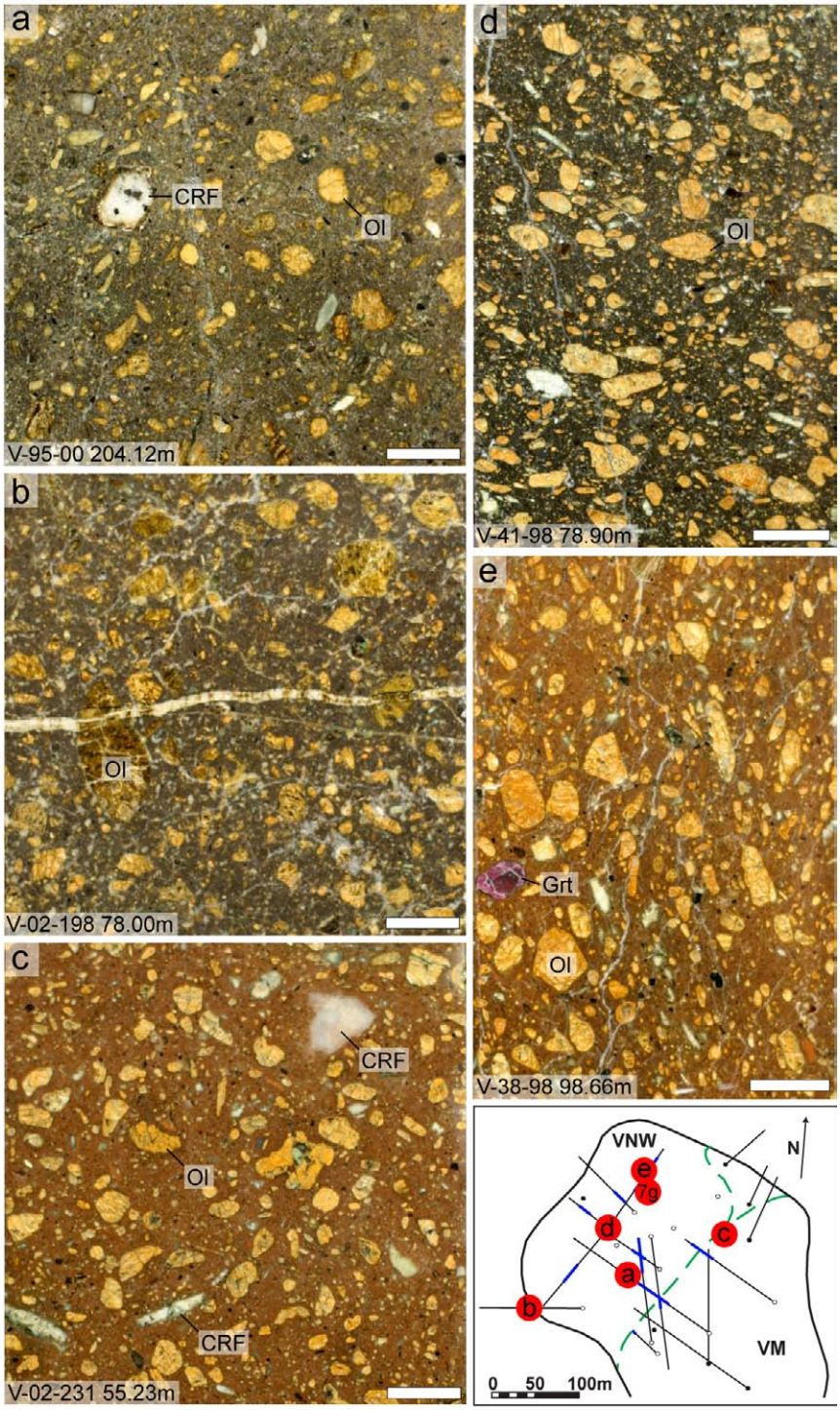

Figure 4.5 Macroscopic characteristics of DCK-U_2 illustrated using photographs of representative polished core samples from different parts of the pipe as shown in the plan view map inset (sample 7G shown in Fig. 4.7G) and from different depths (see tick marks with open circle in Fig. 4.3). DCK-U_2 contains abundant intact olivine macrocysts (*Ol*), minor country rock fragments (*CRF*, predominantly white limestone) and rare garnet macrocrysts (*Grt*). The macroscopic constituents are set in a dark coloured fine-grained groundmass as shown in Figure 4.7. Scale bar = 10 mm. Note pronounced fabric in samples (D) and (E).

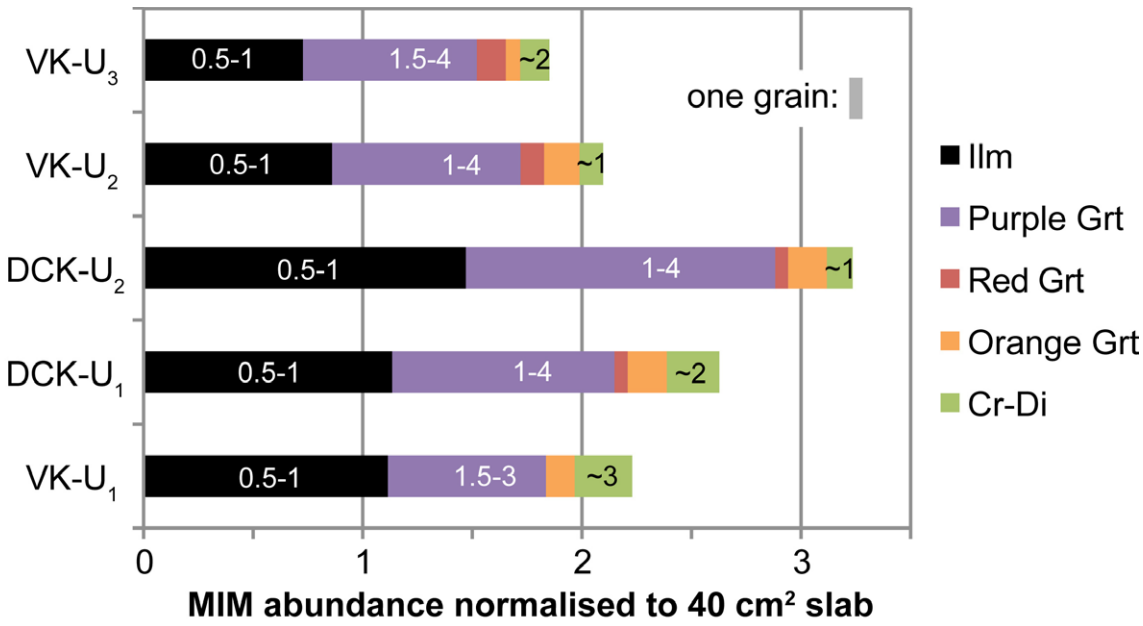

Figure 4.6 Mantle indicator mineral (MIM) abundance for all five kimberlite units within the upper stratigraphy of the VNW pipe. The graph shows the normalised abundance of ilmenite (*Ilm*), purple/pink peridotitic garnet (*Grt*), red garnet, orange/yellow eclogitic garnet, and Cr-diopside (*Cr-Di*) within a 40 cm^2 slab surface. Number in bar graph refers to the typical sizes (in mm) of the ilmenite, garnet and Cr-diopside grains. For each unit we counted grains in seven polished core samples with the aid of a binocular microscope. The total cumulative area counted for each unit was 600-750 cm^2. Only grains ≥ 0.5 mm were counted, and in all five units combined a total of 200 grains were identified (approximate width of one grain is show on top right of graph). The plots are not corrected for variable olivine macrocryst abundance due to (e.g.) sorting processes and/or variable CRF dilution. The latter complicating factor was avoided by preferentially choosing samples with low dilution (samples used had CRF abundances ~0-15%).

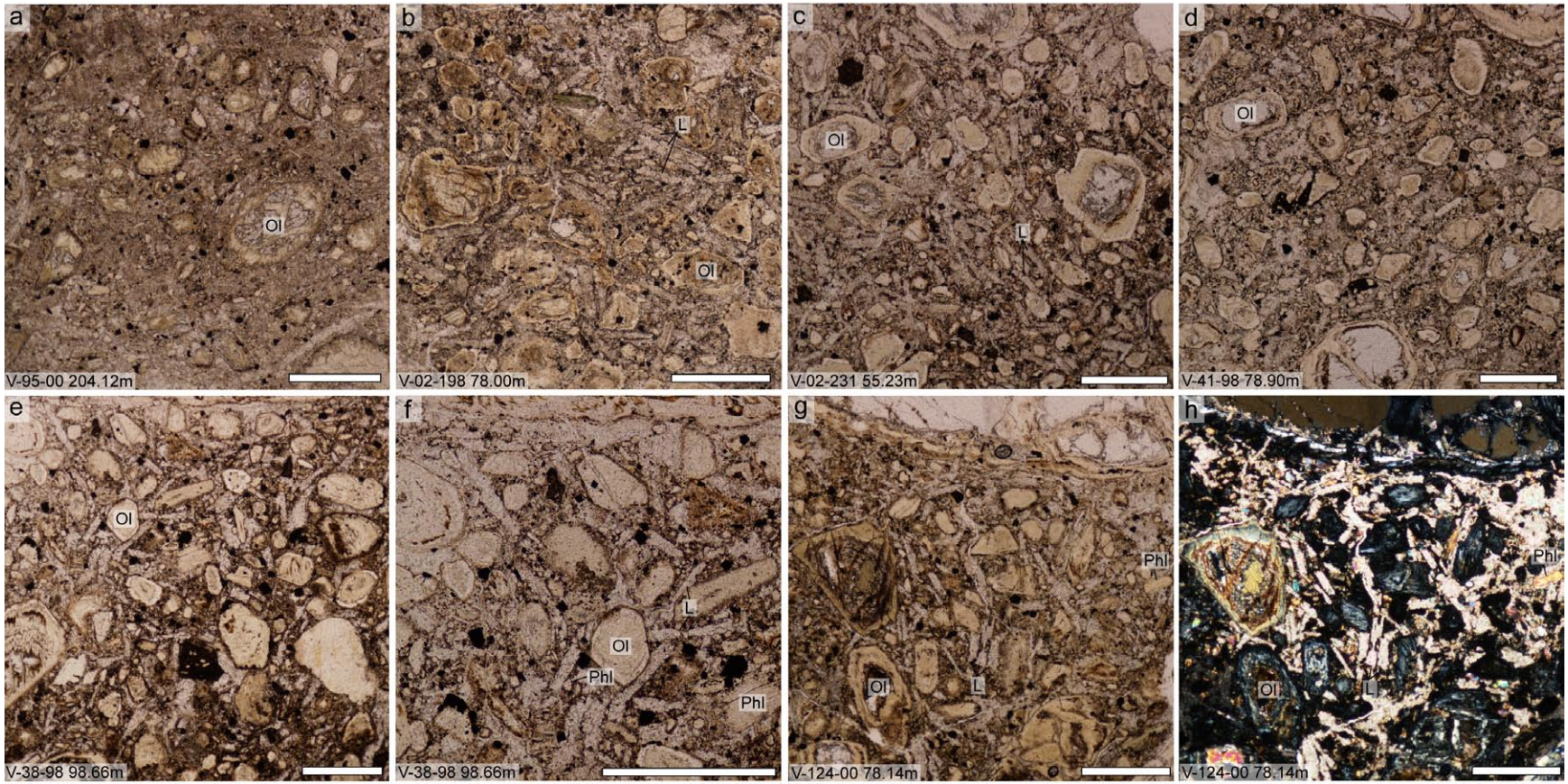

Figure 4.7 Microscopic characteristics of DCK-U_2 illustrated using photomicrographs of thin sections of the same representative samples shown in Figure 4.5. In between the macroscopic components shown in Figure 4.5, the DCK-U_2 contains abundant evenly distributed olivine phenocrysts (*Ol*) set in a fine-grained well-crystallized coherent groundmass (B-H) containing black oxides (spinel), perovskite, carbonate laths (*L*), phlogopite laths (*Phl*) and monticellite (F). Plane polarised light, except (H). The latter is shown in crossed polarised light to highlight the clustering of carbonate laths shown in (G). Scale bar = 500 μm.

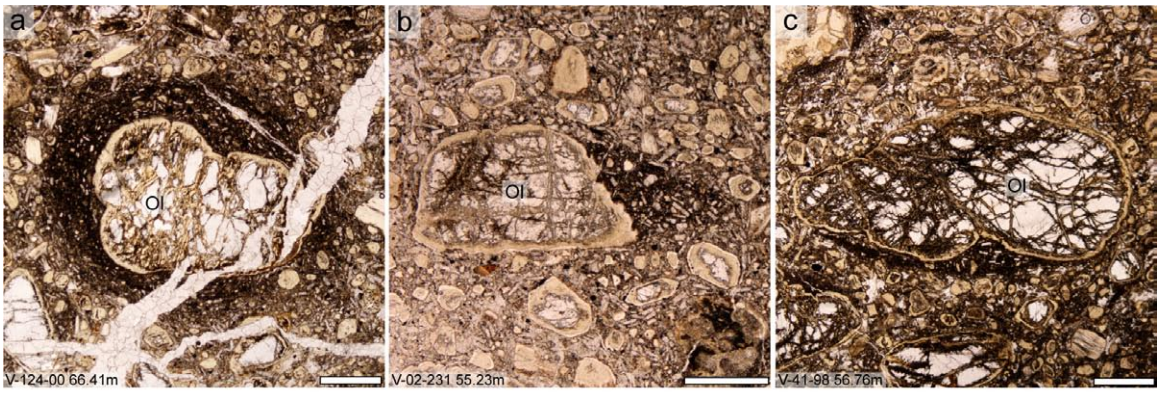

Figure 4.8 Photomicrographs of thin sections in DCK-U_2 that contain typical diffuse selvages. The selvages around olivine crystals range from symmetrical (A) to partial asymmetrical (B, C). The selvage in (A) is cross-cut by a late-stage carbonate vein. Note distinct finer grained nature of olivine phenocrysts and carbonate laths within the selvage relative to the surrounding groundmass. Also note coherent groundmass adjacent to selvage in (B). Sample locations shown by tick marks with square in Figure 4.3. Scale bar = 1 mm.

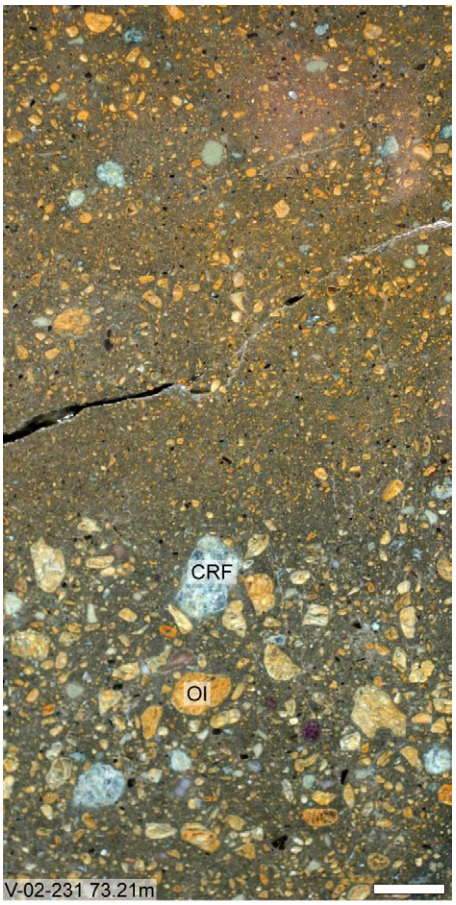

Figure 4.9 Photograph of typical type c DCK-U_1 polished core sample, showing different domains of coarse-grain-supported and fine-grain-matrix-supported kimberlite. Sample location shown by tick mark with open square in Figure 4.3. Scale bar = 1 cm.

4.7 References

Armstrong JP, Wilson M, Barnett RL, Nowicki T, Kjarsgaard BA (2004) Mineralogy of primary carbonate-bearing hypabyssal kimberlite, Lac de Gras, Slave Province, Northwest Territories, Canada. Lithos 76(1-4): 415-433

Bellis A, Canil D (2007) Ferric iron in $CaTiO_3$ perovskite as an oxygen barometer for kimberlitic magmas I: experimental calibration. Journal of Petrology 48(2): 219-230

Branney MJ, Kokelaar P (1992) A reappraisal of ignimbrite emplacement: progressive aggradation and changes from particulate to non-particulate flow during emplacement of high-grade ignimbrite. Bulletin of Volcanology 54(6): 504-520

Brooker RA, Kohn SC, Holloway JR, McMillan PF (2001) Structural controls on the solubility of CO_2 in silicate melts: Part I: bulk solubility data. Chemical Geology 174(1-3): 225-239

Brown R, Tait M, Field M, Sparks R (2009) Geology of a complex kimberlite pipe (K2 pipe, Venetia Mine, South Africa): insights into conduit processes during explosive ultrabasic eruptions. Bulletin of Volcanology 71(1): 95-112

Brown RJ, Buse B, Sparks RSJ, Field M (2008) On the welding of pyroclasts from very low-viscosity magmas: Examples from kimberlite volcanoes. The Journal of Geology 116(4): 354-374

Canil D, Bellis AJ (2008) Phase equilibria in a volatile-free kimberlite at 0.1MPa and the search for primary kimberlite magma. Lithos 105(1-2):111-117

Carey RJ, Houghton BF, Thordarson T (2008) Contrasting styles of welding observed in the proximal Askja 1875 eruption deposits I: Regional welding. Journal of Volcanology and Geothermal Research 171(1-2): 1-19

Caro G, Kopylova MG, Creaser RA (2004) The hypabyssal 5034 kimberlite of the Gahcho Kue cluster, southeastern Slave craton, Northwest territories, Canada: a granite-contaminated group-I kimberlite1. The Canadian Mineralogist 42: 183-207

Cas R, Porritt L, Pittari A, Hayman P (2008) A new approach to kimberlite facies terminology using a revised general approach to the nomenclature of all volcanic rocks and deposits: Descriptive to genetic. Journal of Volcanology and Geothermal Research 174(1-3): 226-240

Cas RAF, Hayman P, Pittari A, Porritt L (2008) Some major problems with existing models and terminology associated with kimberlite pipes from a volcanological perspective, and some suggestions. Journal of Volcanology and Geothermal Research 174(1-3): 209-225

Clement CR (1982) A comparative study of some major kimberlite pipes in the North Cape and Orange Free State. Unpublished Ph.D. thesis. Department of Geology, University of Cape Town, Cape Town, South Africa

Crawford B, Hetman C, Nowicki T, Baumgartner M, Harrison S (2009) The geology and emplacement history of the Pigeon kimberlite, EKATI Diamond Mine, Northwest Territories, Canada. Lithos 112(Supplement 1): 501-512

Dawson JB (1994) Quarternary kimberlitic volcanism on the Tanzania Craton. Contributions to mineralogy and petrology 116: 473-485

Dawson JB, Hawthorne JB (1970) Intrusion features of some hypabyssal South African kimberlites. Bulletin Volcanologique 34(3): 740-757

Dawson JB, Hawthorne JB (1973) Magmatic sedimentation and carbonatitic differentiation in kimberlite sills at Benfontein, South Africa. Journal of the Geological Society 129(1): 61-85

Dawson JB, Pinkerton H, Norton GE, Pyle DM (1990) Physicochemical properties of alkali carbonatite lavas: Data from the 1988 eruption of Oldoinyo Lengai, Tanzania. Geology 18(3): 260-263

Dingwell DB (1996) Volcanic dilemma: flow or blow? Science 273(5278): 1054-1055

Ekren EB, McIntyre DH, Bennett EH (1984) High-temperature, large-volume, lavalike ash-flow tuffs without calderas in southwestern Idaho. Geological Survey Professional Paper 1272: 1-76

Eley R, Grütter H, Louw A, Tunguno C, Twidale J (2008) Exploration Geology of the Luxinga Kimberlite Cluster (Angola) with Evidence Supporting the Presence of Kimberlite Lava. Long abstract, 9th International Kimberlite Conference. Frankfurt, Germany http://www.cosis.net/abstracts/9IKC/00166/9IKC-A-00166-1.pdf

Fedortchouk Y, Canil D (2004) Intensive Variables in Kimberlite Magmas, Lac de Gras, Canada and Implications for Diamond Survival. Journal of Petrology 45(9): 1725-1745

Fedortchouk Y, Matveev S, Carlson JA (2010) H_2O and CO_2 in kimberlitic fluid as recorded by diamonds and olivines in several Ekati Diamond Mine kimberlites, Northwest Territories, Canada. Earth and Planetary Science Letters 289(3-4): 549-559

Field M, Gernon TM, Mock A, Walters A, Sparks RSJ, Jerram DA (2009) Variations of olivine abundance and grain size in the Snap Lake kimberlite intrusion, Northwest Territories, Canada: A possible proxy for diamonds. Lithos 112(Supplement 1): 23-35

Field M, Scott-Smith BH (1999) Contrasting geology and near-surface emplacement of kimberlite pipes in Southern Africa and Canada. In: Gurney JJ, et al. (eds) Proceedings of the 7th International Kimberlite Conference, The J.B. Dawson Volume, Cape Town, South Africa, p. 214-237

Giordano D, Russell JK, Dingwell DB (2008) Viscosity of magmatic liquids: A model. Earth and Planetary Science Letters 271(1-4): 123-134

Gurney JJ, Kirkley MB (1996) Kimberlite dyke mining in South Africa. Africa Geoscience Review 3(2): 191-201

Hayman PC, Cas RAF, Johnson M (2009) Characteristics and alteration origins of matrix minerals in volcaniclastic kimberlite of the Muskox pipe (Nunavut, Canada). Lithos 112(Supplement 1): 473-487

Helz RT, Kirschenbaum H, Marinenko JW (1989) Diapiric transfer of melt in Kilauea Iki lava lake, Hawaii: A quick, efficient process of igneous differentiation. Geological Society of America Bulletin 101(4): 578-594

Kong JM, Boucher DR, Scott-Smith BH (1999) Exploration and Geology of the Attawapiskat Kimberlites, James Bay Lowland, Northern Ontario, Canada. In: Gurney JJ, et al. (eds) Proceedings of the 7th International Kimberlite Conference, The J.B. Dawson Volume, Cape Town, South Africa,p. 452-467

Kopylova MG, Matveev S, Raudsepp M (2007) Searching for parental kimberlite melt. Geochimica Et Cosmochimica Acta 71(14): 3616-3629

Krafft M, Keller J (1989) Temperature Measurements in Carbonatite Lava Lakes and Flows from Oldoinyo Lengai, Tanzania. Science 245(4914): 168-170

Krieger IM, Dougherty TJ (1959) A Mechanism for Non-Newtonian Flow in Suspensions of Rigid Spheres. Transactions of The Society of Rheology 3(1): 137-152

Lorenz V (1986) On the growth of maars and diatremes and its relevance to the formation of tuff rings. Bulletin of Volcanology 48(5): 265-274

Mainkar D, Lehmann B, Haggerty SE (2004) The crater-facies kimberlite system of Tokapal, Bastar District, Chhattisgarh, India. Lithos 76: 201-217

Marshall RR (1961) Devitrification of Natural Glass. Geological Society of America Bulletin 72(10): 1493-1520

Mitchell RH (1984) Mineralogy and origin of carbonate-rich segregations in a composite kimberlite sill. Neues Jahrbuch Miner. Abh. 150(2): 185-197

Mitchell RH (1986) Kimberlites: Mineralogy, Geochemistry and Petrology. Plenum Press, New York, pp. 442

Mitchell RH (1997) Kimberlites, orangeites, lamproites, melilitites and minettes: a petrographic atlas. Almaz Press, Thunder Bay, Canada, pp. 243

Mitchell RH (2008) Petrology of hypabyssal kimberlites: Relevance to primary magma compositions. Journal of Volcanology and Geothermal Research 174(1-3): 1-8

Mitchell RH, Bergman SC (1991) Petrology of Lamproites. Plenum Press, New York, pp. 476

Morizet Y, Nichols ARL, Kohn SC, Brooker RA, Dingwell DB (2007) The influence of H_2O and CO_2 on the glass transition temperature: insights into the effects of volatiles on magma viscosity. European Journal of Mineralogy 19(5): 657-669

Moss SW (2009) Volcanology of the A154N kimberlite at Diavik: Implications for eruption dynamics. Unpublished Ph.D. thesis. University of British Columbia, Vancouver, B.C., Canada

Mueller S, Llewellin EW, Mader HM (in press) The rheology of suspensions of solid particles. Proceedings of the Royal Society A: Mathematical, Physical and Engineering Science, DOI: 10.1098/rspa.2009.0445

Norton G, Pinkerton H (1997) Rheological properties of natrocarbonatite lavas from Oldoinyo Lengai, Tanzania. European Journal of Mineralogy 9(2): 351-364

Nowicki T, Porritt L, Crawford B, Kjarsgaard B (2008) Geochemical trends in kimberlites of the Ekati property, Northwest Territories, Canada: Insights on volcanic and

resedimentation processes. Journal of Volcanology and Geothermal Research 174(1-3): 117-127

Otto JW, Wyllie PJ (1993) Relationships between silicate melts and carbonate-precipitating melts in CaO-MgO-SiO_2-CO_2-H_2O at 2 kbar. Mineralogy and Petrology 48(2): 343-365

Porritt L (2008) The volcanology and sedimentology of the Ekati kimberlites, NWT, Canada, with consideration of the implications for diamond grade. Unpublished Ph.D. thesis. Monash University, Clayton, Australia

Quane SL, Russell JK (2005) Ranking welding intensity in pyroclastic deposits. Bulletin of Volcanology 67(2): 129-143

Quane SL, Russell JK, Friedlander EA (2009) Time scales of compaction in volcanic systems. Geology 37(5): 471-474

Reid AM, Donaldson CH, Dawson JB, Brown RW, Ridley WI (1975) The Igwisi Hills extrusive "kimberlites". Physics and Chemistry of the Earth 9: 199-218

Roeder PL, Schulze DJ (2008) Crystallization of Groundmass Spinel in Kimberlite. Journal of Petrology 49(8): 1473-1495

Russell JK, Giordano D, Kopylova M, Moss S (2006) Transport properties of kimberlite melt. Long abstract, Kimberlite Emplacement Workshop. Saskatoon, Canada

Russell JK, Quane SL (2005) Rheology of welding: inversion of field constraints. Journal of Volcanology and Geothermal Research 142(1-2): 173-191

Schmincke H-U (1974) Volcanological aspects of peralkaline silicic welded ash-flow tuffs. Bulletin of Volcanology 38(2): 594-636

Schumacher R, Schmincke HU (1991) Internal structure and occurrence of accretionary lapilli - a case study at Laacher See volcano. Bulletin of Volcanology 53(8): 612-634

Scott GD, Kilgour DM (1969) The density of random close packing of spheres. Journal of Physics D: Applied Physics (6): 863

Scott Smith BH, Smith SCS (2009) The economic implications of kimberlite emplacement. Lithos 112(Supplement 1): 10-22

Seghedi I, Szakács A, Pacheco AH, Matesanz J-LB (2007) Miocene lamproite volcanoes in southeastern Spain – an association of phreatomagmatic and magmatic products. Journal of Volcanology and Geothermal Research 159(1-3): 210-224

Shee SR (1984) The oxide minerals of the Wesselton Mine kimberlite, Kimberley, South Africa. In: Kornprobst J (ed) Third international kimberlite conference. Elsevier, Clermont Ferrand, p. 59-73

Skinner EMW, Marsh JS (2004) Distinct kimberlite pipe classes with contrasting eruption processes. Lithos 76: 183-200

Smith CB, Lorenz V (1989) Volcanology of the Ellendale lamproite pipes, Western Australia. In: Ross J et al (ed) Proceedings of the 4th International Kimberlite Conference, Volume 1. Geological Society of Australia, Perth, p. 505-519

Sparks RSJ, Baker L, Brown RJ, Field M, Schumacher J, Stripp G, Walters A (2006) Dynamical constraints on kimberlite volcanism. Journal of Volcanology and Geothermal Research 155(1-2): 18-48

Sparks RSJ, Brooker RA, Field M, Kavanagh J, Schumacher JC, Walter MJ, White J (2009) The nature of erupting kimberlite melts. Lithos 112(Supplement 1): 429-438

Sparks RSJ, Bursik MI, Carey SN, Gilbert JS, Glaze LS, Sigurdsson H, Woods AW (1997) Volcanic plumes. John Wiley & Sons, pp. 574

Stripp GR, Field M, Schumacher JC, Sparks RSJ, Cressey G (2006) Post-emplacement serpentinization and related hydrothermal metamorphism in a kimberlite from Venetia, South Africa. Journal of Metamorphic Geology 24(6): 515-534

Sumner JM (1998) Formation of clastogenic lava flows during fissure eruption and scoria cone collapse: the 1986 eruption of Izu-Oshima Volcano, eastern Japan. Bulletin of Volcanology 60(3): 195-212

Sumner JM, Blake S, Matela RJ, Wolff JA (2005) Spatter. Journal of Volcanology and Geothermal Research 142: 49-65

Sumner JM, Branney MJ (2002) The emplacement history of a remarkable heterogeneous, chemically zoned, rheomorphic and locally lava-like ignimbrite: 'TL' on Gran Canaria. Journal of Volcanology and Geothermal Research 115(1-2): 109-138

Venkatachari KR, Raj R (1986) Shear deformation and densification of powder compacts. Journal of the American Ceramic Society 69(6): 499-506

Vieira JM, Brook RJ (1984) Kinetics of hot-pressing: The semilogarithmic law. Journal of the American Ceramic Society 67(4): 245-249

Walker GPL, Self S, Wilson L (1984) Tarawera 1886, New Zealand; a basaltic plinian fissure eruption. Journal of Volcanology and Geothermal Research 21(1-2): 61-78

Webb KJ, Scott-Smith BH, Paul JL, Hetman CM (2004) Geology of the Victor Kimberlite, Attawapiskat, Northern Ontario, Canada: cross-cutting and nested craters. Lithos 76(1-4): 29-50

Wilson L, Pinkerton H, Macdonald R (1987) Physical processes in volcanic eruptions. Annual Review of Earth and Planetary Sciences 15(1): 73-95

Wolff JA, Sumner JM (2000) Lava fountains and their products. In: Sigurdsson H (ed) Encyclopedia of Volcanoes. Academic Press, p. 321-329

Woolley AR, Church AA (2005) Extrusive carbonatites: A brief review. Lithos 85(1-4): 1-14

5 TRANSITIONS FROM PHREATOMAGMATIC TO MAGMATIC ERUPTIONS AT THE VICTOR NORTH PIPES: TEXTURAL AND QUANTITATIVE EVIDENCE[4]

5.1 Introduction

There is considerable debate whether explosive kimberlite eruptions are products of magmatic or phreatomagmatic processes. Magmatic fragmentation is driven by exsolution and expansion of large amounts of juvenile volatiles near the earth's surface and has been proposed for the majority of the kimberlite pipes (e.g. Clement, 1982; Mitchell, 1986; Field and Scott Smith, 1999; Sparks et al., 2006; Cas et al., 2008b; Porritt et al., 2008; Porritt and Cas, 2009). In contrast, phreatomagmatic deposits result from the explosive interaction of magma and external water and have been proposed at a number of kimberlite bodies (Field and Scott Smith, 1999; Lefebvre and Kurszlaukis, 2008; Pittari et al., 2008; Porritt and Cas, 2009). Other authors, including Lorenz (1986), Lorenz et al. (1999) and Kurszlaukis and Lorenz (2008), propose that pipe excavation and all volcaniclastic deposits within kimberlite pipes are the result of phreatomagmatism. In their phreatomagmatic model of pipe formation Kurszlaukis and Lorenz (2008) explain the formation of kimberlite pipes by many single phreatomagmatic explosions. The initial explosions are thought to occur close to the surface, and continued explosions cause progressive deepening and widening of the pipe.

---

[4] A version of this chapter will be submitted for publication. van Straaten, B.I., Kopylova, M.G., Russell, J.K. and Scott Smith, B.H. (2010). Transitions from phreatomagmatic to magmatic eruptions at the Victor North pipes (Canada): textural and quantitative evidence.

This paper describes the geology, emplacement style and history of the Victor North kimberlite complex in Northern Ontario, Canada. The pipes contain a large variety of pyroclastic rock types, ranging from massive country rock fragment (CRF) poor pyroclastic, to bedded variably CRF-rich pyroclastic, to coherent deposits (Chapters 2-4). The latter are unequivocally magmatic in origin (Chapter 4), and are interpreted to have formed by coalescence of hot pyroclasts. However, textures indicative of high fragmentation intensity are present in certain pyroclastic deposits (Chapter 3). Detailed volcanic facies analysis indicates that water was present within the crater subsequent to each eruption (Chapter 3), indicating that ample ground and/or surface water was available at the time of eruption. On this basis, some kimberlite deposits within the Victor pipes could be phreatomagmatic in origin. For example, Webb et al. (2004) suggested the possibility of phreatomagmatic crater excavation based on the presence of an artesian aquifer within the sandstone layer overlying the basement (unit B in Fig. 5.1).

In this paper we present detailed observations on the textural properties of all major units within Victor North. These properties are used to decipher the fragmentation mechanisms for the different deposits within Victor North. In addition to textural observations, we use maximum clast sizes and geohydrological data from the Victor diamond mine site to present the first quantitative estimates on kimberlite eruption durations for both magmatic and phreatomagmatic eruption scenarios. The data for each unit within Victor North is used to constrain whether the fragmentation and emplacement mechanisms were magmatic and/or phreatomagmatic in nature.

5.1.1 Review of magmatic vs. phreatomagmatic eruptions

In this section we summarize the geological evidence for magmatic vs. phreatomagmatic eruptions in normal basaltic-rhyolitic systems before proceeding to the more complex kimberlite systems below.

Most terrestrial volcanic eruptions are driven by magmatic fragmentation. These eruptions feature a variety of styles (e.g. hawaiian, strombolian, vulcanian to plinian) and produce a range of deposits (i.e. fall, flow and surge). In general, all pyroclastic deposits resulting from magmatic eruptions have the following characteristics: *(i.)* presence of highly vesicular glassy juvenile clasts with a low spread in vesicularity values, *(ii.)* production of fine ash-sized bubble wall glass shards which are especially prevalent at higher fragmentation values (e.g. for plinian eruptions) and for more viscous magmas, and *(iii.)* the possibility of coalescence, agglutination and/or welding of hot pyroclasts upon deposition (e.g. Walker, 1973; Cas and Wright, 1987; Quane and Russell, 2005). The most dominant pyroclastic deposits associated with magmatic activity are generally formed by air-fall (i.e. tephra fallout) and pyroclastic flows (e.g. Fisher and Schmincke, 1984; Cas and Wright, 1987). Volumetrically minor ground surge and ash-cloud surge deposits commonly envelop pyroclastic flow deposits. For magmatic air-fall deposits, high ash fractions caused by high fragmentation values are generally only found for more explosive vulcanian to plinian eruptions with higher eruption columns and wider dispersal patterns. Air-fall dispersal (D) versus fragmentation (F) plots are generally used to classify volcanic eruptions, where D is the area in km^2 enclosed by the thickness $T = 0.01 \cdot T_{max}$ isopach line, and F is the weight percent of tephra clasts < 1 mm along the dispersal axis where $T = 0.1 \cdot T_{max}$ (Walker, 1973; Cas and Wright, 1987).

Extra-crater phreatomagmatic deposits from basaltic-rhyolitic maar and tuff cone tephra rings have been studied extensively, and in these systems the following features are generally taken as evidence for magma-water interaction: *(i.)* presence of glassy pyroclasts with lower vesicularity compared to their magmatic counterparts, *(ii.)* variable vesicular pyroclasts, *(iii.)* generally fine grain size due to intense fragmentation, as shown by a high percentage of clasts < 1 mm in proximal air-fall deposits (high F value), *(iv.)* high abundance of blocky to irregular glass shards relative to bubble wall shards, *(v.)* deposits rich in country rock fragments that are typically very small, and *(vi.)* the possible presence of accretionary lapilli, ash plastering on inclined surfaces, soft-sediment deformation structures and other textures indicating the presence of liquid water during deposition (e.g. Walker, 1973; Wright et al., 1980; Sheridan and Wohletz, 1981; Fisher and Schmincke, 1984; Cas and Wright, 1987; Houghton and Wilson, 1989; Schumacher and Schmincke, 1991; Buettner et al., 1999). The most dominant pyroclastic deposits associated with phreatomagmatic activity are generally formed by pyroclastic surges (Wohletz and Sheridan, 1983), and only to a lesser extent by air-fall and pyroclastic flows. Archetypal phreatomagmatic base surge deposits are dilute (low particle concentration) pyroclastic flows resulting from direct blasts from the locus of phreatomagmatic explosions or from collapse of the eruption column (Cas and Wright, 1987). A characteristic feature of surge deposits is the high energy thinly bedded planar to low angle cross-bedded nature. Base surges are generally divided into dry (hot) and wet (cold) flows, depending on the presence of water as vapour or liquid, respectively (Sheridan and Wohletz, 1981). Phreatomagmatic air-fall deposits contain a high percentage of clasts < 1 mm in proximal air-fall deposits (high F value caused by intense

fragmentation), and show limited dispersal (D). Pyroclastic flows are only rarely associated with phreatomagmatic systems, but proximal high particle concentration lithic clast-rich flow deposits have been described and are generally associated with the initial vent-clearing phase (White, 1991; Brand et al., 2009). Due to the high fragmentation intensity, phreatomagmatic deposits are generally finer grained and poorer sorted than most other pyroclastic deposits. In addition, a significant proportion of the fine-grained fraction is retained within proximal pyroclastic deposits (e.g. Fisher and Schmincke, 1984; Cas and Wright, 1987).

5.2 Geological setting

The Victor kimberlite complex is located in the James Bay Lowlands (Northern Ontario, Canada), and is currently being mined for diamonds by De Beers Canada Inc. Victor is the largest kimberlite in the Middle-Late Jurassic Attawapiskat kimberlite province (Kong et al., 1999), and comprises two adjacent bodies: Victor North and Victor South. In this contribution we will focus on Victor North, which comprises two crosscutting pipes: Victor Northwest and Victor Main (Fig. 5.1; see also Webb et al., 2004; Chapters 2-4). The kimberlite pipes have been emplaced within an Ordovician to Silurian sedimentary sequence atop of Precambrian basement. The interface between the sedimentary country rock and basement rocks is found at 272 meters below the present surface (mbs). The kimberlites are overlain by approximately 8-30 m of unconsolidated Quaternary overburden.

We reconstructed the local country rock stratigraphy using three 280-310 m deep vertical drill cores in the vicinity of the Victor kimberlite (V-03-337c, V03-270ah, V-97-00; see

Electronic Appendix B). The country rock stratigraphy around the Victor pipe is fairly uniform laterally and comprises from bottom to top (Fig. 5.1):

(A.) Granitoid basement with the occasional dolerite dyke (intersected in one deep drill hole, V-00-117c). The granitoid is variably deformed, commonly compositionally banded, and can best be described as a quartz + plagioclase + K-feldspar + biotite ± amphibole ± rare garnet bearing gneiss (deepest drill hole indicates a minimum thickness of 33 m)

(B.) A fining upward sequence of grit- to sandstone to siltstone (~1.7 m thick)

(C.) Burrowed silt/mudstones and dolomitic mudstones/dolostones (12 m thick)

(D.) Grey evaporitic mudstone (13 m thick)

(E.) Clastic red beds surrounding a laminated-massive chalky mud/dolostone (30 m thick)

(F.) Dolostone to bioturbated limestone to dolostone; the limestone unit in the centre often contains shelly beds and corals (27 m thick)

(G.) Numerous complete-incomplete cycles from bioturbated limestone (with common vugs and gypsum casts) to cream coloured chalky laminated-massive non-bioturbated non-fossiliferous mud/dolostone to grey mudstone, siltstone and/or sandstone (59 m thick)

(H.) Burrowed to massive grey-yellow limestone (~100 m thick, depending on overburden thickness)

The hydrogeology at the Victor mine site has been studied in detail by Hydrological Consultants Inc. (HCI, 2004) to plan for open pit mine dewatering. The results from this

study are also shown in Figure 5.1. In this regard, it is also important to note that several faults of Silurian (or younger) age occur in the immediate area surrounding the Victor kimberlite (Suchy and Stearn, 1993; HCI, 2004). Two inferred steeply dipping faults that are cross-cut by the kimberlite bodies have been included in the hydrogeological model (HCI, 2004; see Fig. 5.1).

5.3 Victor North kimberlite geology

The detailed geology of the Victor North kimberlite pipes has been presented and discussed in Webb et al. (2004) and Chapters 2-4. Only observations relevant to the reconstruction of phreatomagmatic and magmatic eruption mechanisms are presented here.

The two Victor North kimberlite pipes have contrasting internal geology. The VNW pipe comprises a large variety of rock types, ranging from variably country rock fragment (CRF) rich pyroclastic kimberlite, CRF-poor pyroclastic kimberlite, coherent extrusive kimberlite to sedimentary country rock breccias (Chapters 3, 4). In contrast, the entire VM pipe is filled with a different relatively homogenous CRF-poor pyroclastic kimberlite (Chapter 2).

The stratigraphic units within the VNW pipe can be subdivided in two sequences, upper (U) and lower (L), each of which can be shown to correspond to a separate but similar eruptive cycle (Chapter 3). Each eruptive cycle comprises an early explosive phase that produces pyroclastic deposits containing abundant angular broken olivine grains. The olivine shapes and sizes in these deposits are very different from sub-round olivine grains that dominate the crystal component in pre-eruption kimberlite magmas. The early pyroclastic deposits are overlain by dark and competent kimberlite (DCK), which is

massive, featureless, and characterized by mostly unbroken (sub-round) olivine grains. Each eruptive cycle is capped by resedimented volcaniclastic kimberlite and a thick blanket of sedimentary country rock breccias. The two cycles show a consistent decrease in explosivity, and begin with high intensity explosive activity, followed by less explosive eruptive activity, and subsequent post-eruption pipe-wall collapse producing country rock breccias (Chapter 3). The less explosive activity in the upper stratigraphy comprises dark and competent rocks (DCK-U) that are described in detail in Chapter 4. These rocks represent extrusive coherent rocks interpreted to be clastogenic deposits formed by explosive intra-crater lava fountaining. The VM deposit comprises surprisingly homogeneous pyroclastic kimberlite, however, during bulk sampling the kimberlite was found to comprise distinctly different diamond grade domains (Webb et al., 2004; Chapter 2; Fig. 2.1). Interestingly, there appears to be a gradational contact between the high- and low-grade zones, and the two rock types cannot be confidently distinguished using mega- or macroscopic features. Subsequent detailed petrological observations on textural aspects of juvenile pyroclasts (Webb et al., 2004) and mineralogical composition of the minerals within the pyroclasts (Chapter 2) indicated that the VM pipe was filled by two separate magma batches with distinct mineralogical characteristics and contrasting diamond grade; it is shown that mixing between the late (centrally located) high-grade and early (now only located in the outer part of the pipe) partly unconsolidated low-grade phase produced the intermediate moderate-grade zone with gradational contacts.

5.4 Kimberlite textures indicative of fragmentation and emplacement mechanisms

This section includes textural observations from the Victor North kimberlite pipe relevant to the fragmentation and emplacement mechanisms. We focus on the abundance of angular broken olivines, which likely reflects the degree of fragmentation during eruption. We also track the shapes, sizes and types of pyroclasts, and describe the abundance of ash particles containing groundmass opaque minerals. In addition, we document the largest sizes of country rock fragments, as well as juvenile clasts and mantle xenoliths. All these observations are summarized below from the oldest to the youngest stratigraphic units.

The lower stratigraphy within VNW contains the BK-L_1 (first bedded kimberlite in the lower stratigraphy; see Chapter 3 for details) and DCK-L units. The BK-L_1 comprises both (usually alternating) volcaniclastic and dark and competent lithologies (Fig. 3.3, Table 3.5). Both intervals contain abundant broken olivines (Figs. 3.9, 5.2, 5.3A). Pyroclasts in the BK-L_1 are dominated by clastic pyroclasts (Figs. 3.9, 5.4); in rare instances juvenile pyroclasts might be present in the volcaniclastic kimberlite (VK) intervals. The clastic pyroclasts generally comprise 0.5-2 mm thick rims around 0.5-3 cm olivines or country rock fragments, and in fresh samples the rim can be shown to contain abundant splintery broken olivines (Fig. 3.9). In this study we only looked at DCK-L_1 (outer DCK-L), because of the lack of data on the central DCK-L_2 facies and difficulty correlating between the three drill cores that intersect DCK-L_2 (see Chapter 3); in general, the two units are fairly comparable. The DCK-L_1 shows an upward decreasing

abundance of angular broken olivine (Figs. 5.2, 5.3A), and generally does not contain diffuse selvages (Table 3.2).

The upper stratigraphy within VNW contains the VK-U_1, DCK-U, VK-U_2 and VK-U_3 units. The VK-U_1 comprises abundant broken olivines (Figs. 3.6, 5.2, 5.3A), abundant heterolithic small (< 1 cm) angular country rock fragments (Fig. 3.6) and small (50 μm to 5 mm) irregular shaped variably vesicular juvenile pyroclasts (Fig. 5.4; see also Webb et al., 2004, Fig. 5C). Uncored juvenile pyroclasts dominate over cored examples, and the vesicularity varies from 0-10 vol.%. In addition to juvenile pyroclasts, VK-U_1 also contains small (1-4 mm) clastic pyroclasts with a coarse to fine ash (< 100-200 μm) core and a 100-400 μm thick fine ash (< 25-50 μm) rim (Fig. 5.4C, rim type accretionary pyroclasts following the definition by Schumacher and Schmincke, 1991). The coherent DCK-U contains non-vesicular spherical cored partial diffuse fine-grained selvages in the upper outer portions, as well as the central and deeper levels of the deposit (Figs. 3.4, 4.3, 4.8, 5.4). The selvages are generally cored by olivine crystals, and are generally 1-8 mm in size. The unit contains minor angular broken olivines in the lower part, and negligible proportions of angular broken olivines in the upper part (Figs. 4.4, 5.2, 5.3A). The volumetrically small and centrally located VK-U_2 contains no significant angular broken olivines (Figs. 5.2, 5.3A) and the pyroclasts are generally 1-15 mm in size and spherical and cored in shape. Only the rare larger (> 5 cm) juvenile pyroclasts contain some vesicles (~0-5 vol.%). The overlying VK-U_3 doesn't contain significant angular broken olivine either (Figs. 4.4, 5.2, 5.3A) and comprises mainly 3-10 mm non-vesicular cored pyroclasts (Fig. 5.4).

The earliest low diamond grade (LG) phase within VM contains minor to no angular broken olivine (Figs. 5.2, 5.3A), and 0.2-15 mm spherical cored and lesser uncored non-vesicular to poorly vesicular (0-4 vol.%) juvenile pyroclasts (Fig. 5.4). The VM high diamond grade (HG) phase contains similarly low abundances of angular broken olivine (Figs. 5.2, 5.3A), and similarly sized spherical cored and lesser uncored non-vesicular juvenile pyroclasts (Fig. 5.4). Rare larger, cm-sized, juvenile pyroclasts in the high-grade unit are also non-vesicular.

In addition to the above characteristics, Figure 5.3B shows the maximum basement clasts, cognate lithic clasts, juvenile pyroclasts and/or mantle xenolith sizes, as well as typical ranges for the maximum sedimentary country rock fragments (mainly white-grey limestone and lesser green country rock sedimentary clasts) within each unit.

We also studied the abundance of fine-grained opaque minerals in all units (see Figs. 5.2, 5.4 as well as Figs. 2.2, 3.4, 3.6, 3.9, 4.8). The opaque minerals are spinel (~10 μm) in both VNW and VM, plus perovskite (~10–50 μm) in VNW. The results indicate abundant opaques in the coherent or clastogenic coherent lithologies (VM pyroclast, DCK-L, DCK-U), as well as in VK-U_1 and BK-L_1 (both DCK and VK lithologies). The other units (VK-U_2, VK-U_3, VM-LG, VM-HG) contain significantly less opaque minerals compared to the original erupting magma.

5.5 Eruption dynamics calculations

To calculate eruption durations, the total volume of each pipe and nested crater (Section 5.5.1), and in turn the total volume for each unit within the VNW and VM pipes were determined (Section 5.5.2). Using these volume estimates the total erupted tephra volumes were calculated (Section 5.5.3). Consequently, magmatic eruption durations

were calculated using the maximum clast size (Section 5.4, Fig. 5.3B) that appears to have been supported by the volcanic plume (Section 5.5.4). Estimates for phreatomagmatic eruption durations were derived using estimates on water flow into the planned open pit at the Victor diamond mine (Section 5.5.5).

5.5.1 Pipe and nested crater volume estimates

Victor North comprises two cross cutting pipes, VNW and VM, each with a later nested crater. Volumes for the total pipes and nested craters are determined in this section. For the calculation of pipe and nested crater volumes in each case a symmetrical pipe and nested crater shape around a vertical central axis was assumed. The total volume of each pipe and nested crater was calculated using several slices of a right circular cone. For VNW all available drill core data was used to reconstruct a model for the original pipe shape, i.e. before part of the pipe was removed by the later cross-cutting VM eruption, and before the northeast part of the pipe was eroded by the bedrock depression (see Fig. 3.1B in Chapter 3). The VNW pipe was extrapolated to depth using the estimated pipe wall angle in the basement. Changing the lower pipe wall angle does not have a big influence on the total pipe volume (2 vol.% of the total pipe is present below 350 mbs and is not intersected by drill cores). A better estimate on the pipe-marginal country rock breccia volume has been included, resulting in a somewhat larger VNW pipe than previously shown (Webb et al., 2004; Chapters 3-4). We have alluded to this possibility in Section 3.5.1 (Chapter 3), and attribute the difference to the presence of significant volumes of pipe-marginal country rock breccias at higher stratigraphic levels that do not stand out in the geophysical survey used to delineate the pipe. Limited study of open pit

exposures at the 16-33 mbs level in October 2009 confirm the fact that the VNW pipe is flaring considerably at shallow levels.

The upper stratigraphy within VNW is interpreted to represent a nested crater excavated into the previous infill of the VNW pipe (Chapter 3). The reconstructed volume for this nested crater (before part of the crater was removed by the later VM eruption) was calculated using data presented in Chapter 3 (Fig. 3.1C).

For the VM pipe an average 70° (Webb et al., 2004) dipping right circular cone with a 127.5 m radius at 40 mbs was used. The pipe is extrapolated to depth as well as to the present day surface at 8 mbs using the average pipe wall angle specified above. Approximately 5 vol.% of the pipe volume is not intersected by drill core (below 250 mbs). The VM high-grade (VM-HG) phase is also interpreted as a later nested crater emplaced into unconsolidated VM low-grade (VM-LG) tephra. The two phases are separated by a wide gradational contact composed of mixed tephra from both phases (Webb et al., 2004; Chapter 2). The volume of the VM-HG nested crater is not presented here, see Section 5.5.3 for details. The reconstructed symmetrical pipe and nested crater shapes for VNW and VM are shown in Figure 5.1. The resulting total pipe volumes (V_{pipe}) for VNW, the VNW nested crater and VM are $23.4 \cdot 10^6$, $9.5 \cdot 10^6$ and $7.8 \cdot 10^6$ m^3 respectively (see Table 5.1).

5.5.2 Intra-pipe unit volume estimates

In addition to the pipe volumes (V_{pipe}) discussed above, the total intra-pipe deposit volumes ($V_{dep\text{-}ic}$) for the following units within VNW were calculated: BK-L_1, DCK-L, CRB-L_1 (including BK-L_2 and RVK-L), CRB-L_2, VK-U_1, DCK-U, VK-U_2, VK-U_3, and

CRB-U (including RVK-U). The intra-crater deposit volumes are summarized in Table 5.1.

5.5.3 Total erupted tephra volume estimates

The upper portion of most kimberlite volcanic systems has been eroded during the millions of years of erosion since emplacement. Hence, for most kimberlites we can only reliably estimate the non-eroded intra-crater deposit volume ($V_{dep\text{-}ic}$). In addition to the non-eroded intra-crater deposit volume, the total tephra erupted by each kimberlite volcano (V_t) also comprises the eroded upper portion of the intra-crater ($V_{dep\text{-}ic\text{-}er}$) and the extra-crater deposit volume ($V_{dep\text{-}ex}$).

Eq. 5-1 $$V_t = V_{dep\text{-}ic} + V_{dep\text{-}ic\text{-}er} + V_{dep\text{-}ex}$$

Since the amount of erosion for Victor is not very well constrained (estimates vary from 50-600 m, see Chapter 3), we ignored the influence of $V_{dep\text{-}ex\text{-}er}$ in Equation 5-1 and only calculated the extra-crater deposit volume. As a result, the total erupted tephra volumes are minimum estimates.

For pipe- and nested crater-excavating eruptions we can constrain the extra-crater deposit volume ($V_{dep\text{-}ex}$) by considering the total excavated country rock (V_{exc}) by each eruption. The first deposits that are formed subsequent to pipe and nested crater excavation include BK-L_1 and VK-U_1 within VNW, and both the low- and high-grade deposits within VM. Only the eruptions associated with BK-L_1 and VM-LG excavate in situ country rock. In contrast, VK-U_1 erupted through poorly consolidated country rock breccias (CRB-U) and minor lithified dark and competent rocks (DCK-L; see Fig. 5.1). Since the eruption that forms VM-HG does not excavate or mix with country rock, the total tephra volume (V_t)

could not be estimated using methods outlined below. In addition, volume estimates for VM-HG were not available due to the confidential nature of this data. The combined volume of country rock fragments in the intra- and extra-crater deposit is equal to the total excavated country rock (V_{exc}) within each pipe/nested crater:

Eq. 5-2 $$V_{exc} = CRF_{ic} \cdot V_{dep\text{-}ic} + CRF_{ex} \cdot V_{dep\text{-}ex}$$

where CRF_{ic} and CRF_{ex} are the fractions of country rock fragments within the intra-crater deposit and extra-crater tephra ring, respectively.

The excavated (country) rock volume (V_{exc}) is mostly equal to the total pipe/nested crater volume (V_{pipe}), except for the VNW nested crater. The VNW nested crater was likely excavated within a partly filled pipe. Hence, the excavated rock volume (V_{exc}; Fig. 5.5, Table 5.1) associated with nested crater excavation at VNW is smaller than the total nested crater volume (V_{pipe}). We used a conservative estimate of a pipe filled to about 60 mbs, and only the excavated rock volume was used in magmatic eruption duration calculations (Section 5.5.4).

Solving Equation 5-2 for $V_{dep\text{-}ex}$, and combining it with Equation 5-1 (ignoring $V_{dep\text{-}ic\text{-}er}$) gives:

Eq. 5-3 $$V_t = V_{dep\text{-}ic} + \{V_{exc} - (CRF_{ic} \cdot V_{dep\text{-}ic})\} / CRF_{ex}$$

To solve this equation for the total tephra volume (V_t), we need to assume a value for the fraction of country rock fragments within the extra-crater deposit (CRF_{ex}). The reciprocal relationship between the total tephra volume and the assumed value of CRF_{ex} is shown for each crater-excavating phase in Figure 5.6. This plot illustrates the range from CRF_{ex}

= CRF_{ic} where all tephra has the same fraction of country rock fragments as the intra-crater deposits, to $CRF_{ex} = 1$ where no magma is involved in the crater excavation phase.

In this graph, the maximum total tephra volume is representative of eruptions where the magma to country rock fragment content does not change over time, i.e. progressive excavation of the pipe with a constant involvement of magma. In contrast, the minimum total tephra volume can only be produced by an initial eruption that does not involve any magma (e.g. phreatic or vent-clearing vulcanian eruptions that produce tephra comprised of only country rock fragments), followed by a sudden transitions to a pipe-filling eruption that produces tephra with relatively low country rock fragment content. From a geological perspective, the latter process is highly unlikely to occur. In addition, using the minimum tephra volume to calculate eruption durations will also lead to relatively low eruption durations. Hence, we have only used the maximum and average total tephra volumes (see Figure 5.6; Sections 5.5.4, 5.5.5).

After calculating the total tephra volume, we can easily calculate the total erupted magma (V_m; or tephra without CRF, see Eq. 5-4). The total erupted magma volumes are used in Section 5.5.5 for the magma – water interaction calculations.

Eq. 5-4 $$V_m = (1 - CRF_{ic}) \cdot V_{dep\text{-}ic} + (1 - CRF_{ex}) \cdot V_{dep\text{-}ex}$$

For DCK-L, DCK-U, VK-U_2 andVK-U_3 we simply assumed that the intra-pipe volume is about half of the total tephra volume. The resultant total deposit volumes, tephra volumes and magma volumes are shown in Table 5.1.

5.5.4 Magmatic eruption durations

Magmatic eruption durations were calculated using methods outlined in Wilson (1976; 1978) and Porritt and Cas (2009), and are based on the maximum observed clast sizes that are supported within a sub-plinian to plinian eruption column. For this we used the largest observed basement or juvenile clast in each unit (Figure 5.3); these clasts are without a doubt brought up by the eruption. In addition, we also used conservative estimates on the largest sedimentary country rock fragments that might have been supported by the eruption. We used a 20 cm value for the sedimentary country rock clast diameter, as some of the rarer >20 cm limestone clasts could be the result of incorporating pipe-wall material during the waning stage of the eruption (i.e. during column collapse). Using the above clast radii (R_c) we can calculate the gas flow rate (U_c):

Eq. 5-5 $$U_c = \{(8 \cdot R_c \cdot P_c \cdot g) / (3 \cdot P_g \cdot C_d)\}^{0.5}$$

with P_c = clast density, g = acceleration due to gravity (9.81 m/s^2), C_d = coefficient of drag ($C_d \approx 1$) and P_g = gas density within the eruption column. The tephra mass eruption rate (m_t) can be calculated using:

Eq. 5-6 $$m_t = (P_g \cdot U_c \cdot \pi \cdot x^2) / n$$

with P_g = gas density within the eruption column, n = gas fraction of exsolved gas in the erupting mixture (% value) and x = vent radius. The eruption duration (T_e) for each unit then follows from:

Eq. 5-7 $$T_e = M_t / m_t = (V_t \cdot P_t) / m_t$$

with M_t = total mass of the tephra deposit, V_t = tephra volume and P_t = tephra density (Eq. 5-5 to 5-7 after Wilson, 1976; Porritt and Cas, 2009).

A significant number of these variables are difficult to constrain for normal volcanic eruptions, let alone kimberlite eruptions. However, Porritt and Cas (2009) provide a good overview of this subject, and we have used the same values here. Porritt and Cas (2009) suggest gas density (P_g) values of 0.265 kg/m^3 (50% H_2O, 50% CO_2 gas mixture) to 0.38 kg/m^3 (100% CO_2) at eruption conditions (P_{atm} and T = 1150 °C), and melt gas fractions (n) of 7, 15 and 20 % based on literature estimates of primitive magma compositions. Based on density measurements on drill core V-94-00 (De Beers database) we use tephra densities (P_t) of 2200 kg/m^3 (all units except DCK) to 2450 kg/m^3 (DCK units only). Tephra densities during eruption were likely higher due to subsequent alteration of olivine (3300 kg/m^3) to serpentine (~2500 kg/m^3), i.e. the eruption durations presented here could be up to ~14% longer. Clast types sustained within the eruption column range from granite (P_c = 2750 kg/m^3), limestone (P_c = 2360 kg/m^3) to kimberlite lithic clasts and juvenile pyroclasts (both P_c = 2600 kg/m^3). The latter density is based on density measurements of the freshest coherent rocks within Victor Northwest (De Beers database). It should be noted that theoretically predicted kimberlite melt densities range from ~2600-3000 kg/m^3 at eruption conditions (Russell et al., 2008), and adding ~40% olivine crystals will increase the non-vesiculated magma density to 2900-3100 kg/m^3. Using these values for the kimberlite lithic clast and juvenile pyroclast densities will decrease the eruption duration values that are based on these clast types (see Table 5.2) by ~13%. The calculated magmatic eruption durations are shown in Table 5.2.

5.5.5 Phreatomagmatic eruption durations

In order to explore the likelihood of a phreatomagmatic origin for the two crater-excavating events in VNW (units BK-L_1 and VK-U_1) and at VM (low-grade

volcaniclastic units), we performed basic modelling of the magma-water interaction. For this exercise, we assumed that:

- During kimberlite emplacement the geohydrological situation was comparable to the present time. Both the presence of water in the crater after each eruptive cycle in VNW (see Chapter 3 and Section 5.3) and the presence of rare non-eroded remnants of deltaic Jurassic sediments in the James Bay region (Mistuskwia beds in the Moose River Basin; see Norris, 1993, p.683) indicate a non-arid climate, presence of surface water and a water table that intersected the upper crater. These conditions support the assumption of similarly charged aquifers within the country rock stratigraphy during kimberlite eruption.
- We use estimates of passive water flow rates ($71 \cdot 10^3$ m^3/day; HCI, 2004) for the open pit mine after 7 years of mining (includes the Victor Main and part of the Victor NW pipe) to provide flow rates into the individual kimberlite pipes at the time of emplacement. The morphology of the nested VNW crater (Figure 5.1) will likely allow less groundwater to flow into and interact with the erupting magma. However, given the presence of resedimented kimberlite that indicates the possibility of a crater lake at the time of the excavation of this nested crater, we used the same water flow rate.
- Water to magma mass ratios varied from 0.3 (most efficient magma-water interaction) to 0.15 (less efficient interaction; Sheridan and Wohletz, 1981)
- Total volumes of tephra (V_t) and magma (V_m) as discussed in Sections 5.5.1, 5.5.3 (Table 5.1). We ignored the influence of 50-600 m of erosion (Chapter 3) on the total

tephra and magma volumes, since adding more stratigraphy would also have increased the total amount of water flow into the pipe by an unknown amount.

From the above figures we can calculate the typical magma mass eruption rate that would be able to interact at the specified 0.3 – 0.15 magma to water mass ratios and with the estimated water flow rates. This yields magma mass eruption rates (m_m) of 2739 – 5478 kg/s; lower eruption rates will yield tuff cone type volcanism where the explosivity is significantly reduced due to the excess presence of water, whereas higher eruption rates will only allow for magmatic fragmentation. Phreatomagmatic eruption durations (T_e) can be calculated using the total magma volume (V_m), magma density (P_m = 2600 kg/m^3, see Section 5.5.4) and the magma mass eruption rate (m_m):

Eq. 5-8 $$T_e = (V_m \cdot P_m) / m_m$$

Magma mass eruption rates can be converted to tephra mass eruption rates (m_t) using Equation 5-9, to allow comparison to magmatic tephra mass eruption rates.

Eq. 5-9 $$m_t = P_t \cdot (V_m + V_{pipe}) / T_e$$

The model durations for phreatomagmatic eruptions are shown in Table 5.2. Less conservative estimates for the magma density (see Section 5.5.3) would result in a slight increase (~15%) in eruption durations. It should be noted that geohydrological studies for the mine site (HCI, 2004; Fig. 5.1) predict that a significant part of the water that will enter the open pit originates from hydraulically conductive fault zones within the sedimentary succession (see Section 5.2). This means that phreatomagmatic eruptions would probably have exploited the same hydraulically active fault zones.

5.6 Discussion

5.6.1 Theoretical constraints on eruption mechanisms

In the introduction (Section 5.1.1) we summarized the indicators for magmatic and phreatomagmatic eruption mechanisms in basaltic-rhyolitic volcanic deposits. Below we will discuss the characteristics of intra-crater kimberlite deposits, with specific focus on textures that are expected to form as a result of magmatic vs. phreatomagmatic eruptions.

The dominant clast types in pyroclastic kimberlite deposits are 'free' or 'discrete' crystals without a juvenile melt selvage, as well as juvenile pyroclasts that generally comprise a relatively thin juvenile melt rim around an olivine crystal core. The juvenile pyroclasts are generally fluidal in shape and commonly spherical and non-vesicular in nature (Field and Scott Smith, 1999; Webb, 2006; Porritt et al., 2008; Moss et al., 2009). Some authors interpret the juvenile pyroclast morphology as evidence for a phreatomagmatic origin of all kimberlite pipes (e.g. Lorenz et al, 1999). However, most authors (e.g. Sparks et al., 2006; Cas et al., 2008a, b) ascribe the morphology of the juvenile pyroclasts to the low viscosity of the melt (Chapter 4, Section 4.5.3.1 and references therein). The very fast relaxation timescale for low viscosity melts (Dingwell and Webb, 1989; Dingwell, 1996) will likely allow kimberlite melt to relax viscously before crystallisation or glass formation takes place. This readily explains the spherical nature of the pyroclasts. The dominance of surface tension effects in creating spherical pyroclast shapes has also been described in magmatic eruption products of other low viscosity magmas such as carbonatites (Keller, 1989) and, to a lesser extent, basalts (achneliths; Walker and Croasdale, 1971). Despite the fact that some intermediate to low viscosity magmas such as foiditic and olivine melilititic volcanic systems have been described to form highly

vesicular pyroclasts (scoria) during magmatic eruptions (Lorenz, 1986; Kurszlaukis et al., 1998), we think that for kimberlites the low melt viscosity and fast relaxation time scales will likely allow most gas bubbles to quickly disappear from the melt before solidification (Cas et al., 2008a). As discussed in Chapter 4 (Section 4.5.3.1), glass is unlikely to form in most kimberlite eruptions, hence the juvenile pyroclasts will crystallise upon cooling. The low melt viscosity, fast relaxation timescale, and efficient separation of gas and melt will likely prevent the brittle fragmentation of glassy melt and preclude formation of bubble wall shards that is common in basaltic, and especially rhyolitic, volcanic systems (e.g. Fisher and Schmincke, 1984); instead small spherical crystallised juvenile melt ash particles are expected to form. Observations on fine ash (< 63 μm) particles in kimberlite systems are hampered by the increased susceptibility to alteration for these high-surface-area-to-volume-ratio particles; however, rare observations of small spherical juvenile melt pyroclasts (Fig. 5.4H; Moss et al., 2008, Fig. 7) support the above hypothesis. In addition to the juvenile pyroclast morphology, the low viscosity of the magma will likely promote effective separation of crystals and melt during a magmatic eruption, given high enough gas flow rates during the eruption (Moss, 2009, p. 160-174).

There are several complicating factors when identifying possible phreatomagmatic kimberlite deposits. Most kimberlite deposits are found within pipes or craters. These intra-crater settings are different from the extra-crater settings commonly studied for normal basaltic-rhyolitic volcanic systems. Whereas extra-crater phreatomagmatic deposits dominantly comprise tractional base surge bed forms, these deposit types are only rarely found in intra-crater settings (Boxer et al., 1989; Smith and Lorenz, 1989;

White 1991). Hence, for intra-crater kimberlite systems we are generally left with looking at textural evidence for phreatomagmatic fragmentation, rather than interpreting relatively straightforward base surge phreatomagmatic deposits. Characteristic textures resulting from phreatomagmatic fragmentation in kimberlite deposits are expected to be comparable to basaltic-rhyolitic systems in that they are fine grained, poorly sorted, generally country rock fragment-rich, contain variably vesicular pyroclasts and may contain clastic pyroclasts or other indicators of free liquid water. However, some differences are expected, especially in the morphology and texture of the pyroclasts. These differences result from the very low melt viscosity, as well as the crystal-rich nature of kimberlite magma. As discussed above, in magmatically produced deposits these magma properties result in a lack of formation of vesicular glassy juvenile pyroclasts and bubble wall glass shards. We suggest that the much higher cooling rates due to magma-water interaction could rapidly quench juvenile pyroclasts before surface tension effects cause them to become spherical. In addition, fast quenching could prevent juvenile pyroclasts to loose most of their vesicles (Cas et al., 2008a). Despite faster cooling rates in phreatomagmatic eruptions, we have not observed any evidence for glass formation. Hence, ash-sized blocky/irregular shaped fragments are not expected to form.

5.6.2 Interpretations based on textural evidence

The first deposits that are formed subsequent to crater excavation include BK-L_1 and VK-U_1 within VNW, and both the low- and high-grade deposits within VM. Below we will discuss the contrasting textures between the crater excavating deposits in VNW versus the deposits in VM. Subsequently we will discuss the pipe-filling deposits within VNW (i.e. DCK-L, DCK-U, VK-U_2, VK-U_3 at VNW).

Within the VNW BK-L_1 unit we see pervasively shattered olivines, abundant small (< 1 cm) angular country rock fragments and the presence of ash-armoured crystals/lithic clasts. In addition, the deposit is generally country rock fragment rich, with m-scale bedding defined by varying abundances of country rock fragments. The deposition mechanism of BK-L_1 is somewhat unclear, as it is unlikely to have been deposited as primary pyroclastic material on the steep-sided (45-75°) pipe walls. Instead, depositional mechanisms involving collapse from the tephra ring are more likely. In the VNW VK-U_1 unit we see the same features as described above, but in addition variably vesicular uncored small irregular shaped pyroclasts as well as rim-type accretionary pyroclasts are present. The irregular shape and the variably vesicular nature of the juvenile pyroclasts in unit VK-U_1 could be explained by quenching of variably vesicular magma due to interaction with water (Section 5.6.1). Study of the matrix of both deposits indicates that very little to no fine-grained opaque minerals have been lost during the eruption. This contrasts markedly with petrological observations and geochemical analysis on numerous – presumed magmatically produced – pyroclastic kimberlite deposits that show a significant loss of melt during the eruption (Nowicki et al., 2008; Hayman et al., 2009; Porritt and Cas, 2009). The lack of sorting combined with the retention of ash-sized juvenile ('melt') material in these deposits could be a hallmark of phreatomagmatism in kimberlite deposits, as phreatomagmatic eruptions produce general finer grained and poorer sorted deposits (e.g. Fisher and Schmincke, 1984). In this context we suggest that any kimberlite deposit that contains abundant evidence for high fragmentation intensities (i.e. contains angular broken olivines, small angular country rock fragments, small

juvenile pyroclasts) combined with a lack of loss of melt (i.e. opaques) should be investigated to see whether it could have a phreatomagmatic origin.

At VM we generally do not see any of the above features. Relative to VK-U_1, much larger (mm to cm scale) spherical non- to poorly vesicular juvenile pyroclasts are present. Microscale petrological observations allowed for a comparison of the abundance of opaque minerals in the VM-LG and VM-HG matrix vs. the abundance within the groundmass of >7 cm juvenile pyroclasts within VM. This showed that the matrix within the VM pyroclastic deposits does not contain as much opaque minerals (i.e. fine-grained juvenile 'melt' material) compared to the original magma. Given the lack of indication for obliteration of these opaques by alteration (e.g. Porritt, 2008) this suggests that a significant portion of the fine ash fraction has been lost during eruption. In addition, the deposits are better sorted and finer grained compared to what we infer to be the original magma (Electronic appendix M).

We suggest that the remaining kimberlite deposits (DCK-L, DCK-U, VK-U_2, VK-U_3 at VNW) are formed by magmatic eruptions. The upper dark and competent kimberlite unit (DCK-U) is unequivocally formed by magmatic eruptions (Chapter 4), based on an origin as coalesced fire-fountain deposit. Coalesced (or reconstituted rocks, see Chapter 4) can only form during magmatic eruptions. We assume DCK-L has a comparable origin as DCK-U, based on similar textures and position within the pipe. The relatively high proportion of broken olivine in the lower DCK-L indicates that crystals are still actively breaking, while at the same time coalescence processes are taking place. We infer that the olivine crystals break as a result of tensile failure due to the shock waves accompanying high-energy phreatomagmatic eruptions (e.g. Wohletz, 1986) rather than by massive

decompression accompanying gas exsolution and subsequent hydrodynamic fragmentation due to magmatic eruptions. As such, the presence of broken olivine crystals in the lower parts of the DCK-L and DCK-U might indicate a phreatomagmatic component during the early stages of DCK formation. Such simultaneous phreatomagmatic and magmatic eruptions are not uncommon in basaltic systems (Kienle et al., 1980).

The remaining units in the upper stratigraphy of VNW (VK-U_2 and VK-U_3) are most likely formed by the same magmatic eruption that formed the DCK-U. Evidence for this includes the fact that the VK-U_2 is enveloped by the DCK-U, contains identical juvenile pyroclasts, has similarly low angular olivine abundance, and likely contains gradational contacts with DCK-U (Fig. 5.3, Chapter 4). Along the same lines of evidence, we suggest that VK-U_3 is formed by magmatic fragmentation; it has similar textural characteristics and likely gradational contacts to VK-U_2 and DCK-U. As discussed in Chapter 3, some or all of VK-U_3 could have been derived from redistribution of tephra ring material.

5.6.3 Eruption duration considerations

A comparison of magmatic vs. phreatomagmatic eruption durations for each kimberlite unit is shown in a plot of tephra mass flux (F_t) versus eruption duration (T_e) (Fig. 5.7). The total tephra flux (see Table 5.2) is simply the mass of tephra that passes through 1 m^2 of the vent area (A in Fig. 5.5) per second. Figure 5.7 illustrates the reciprocal relationship between the two parameters (following Eq. 5-5), where phreatomagmatism can only occur during low tephra mass fluxes (and long eruption durations) due to the limited availability of water. In contrast, magmatic eruptions tend to prevail during high

tephra mass fluxes (and short eruption durations), as there is simply too much magma to efficiently interact with the $71 \cdot 10^3$ m^3 water that is available per day (see Section 5.5.5).

A summary of all eruption durations are shown in Figure 5.8, and also shows the relative explosivity of each eruptive phase based on the broken olivine content (Chapters 3, 4; Section 5.3, Figure 5.3A) as well as the likelihood of phreatomagmatic vs. magmatic eruption based on textural observations.

Eruption duration estimates for other kimberlite systems are rare, but range from:

- Days to months for large Southern African-type kimberlite pipes based on magma ascent rates in dykes of 1-10 m/s and magma supply rates of 100-1000 m^3/s (Lorenz and Kurszlaukis, 2007).
- Hours to months for large Southern African-type kimberlite pipes based on magma ascent rates in dykes of 4-16 m/s and magma supply rates of $500\text{-}1 \cdot 10^5$ m^3/s (Sparks et al., 2006). The ascent rates are based on calculations on dyke propagation dynamics.
- Days to weeks based on 0.1-1 m granodiorite clast radii that were sustained by gas velocities in the eruption column of 140-520 m/s for the Fox kimberlite pipe (NWT, Canada; Porritt and Cas, 2009). Note that we used the same equations to calculate eruption durations in Section 5.5.
- One hour, based on typical Southern African-type kimberlite pipes and magma ascent velocities of at least 20 m/s in dykes, increasing to 300-1400 m/s following massive exsolution due to breaching of the surface (Wilson and Head, 2007).

Except for the extremely short (and controversial, see Sparks et al., 2007) eruption durations presented by Wilson and Head (2007) these literature estimates have a slightly higher, but overlapping, range compared to eruption duration estimates presented here. Calculations in Section 5.5 yield tephra eruption rates for magmatic eruptions of 5.5-230 m^3/s ($1.2 \cdot 10^4$ to $5.0 \cdot 10^5$ kg/s, see Table 5.2) and 75-153 m/s gas velocities in the eruption column. Using calculations by Wilson et al. (1978), these tephra eruption rates could yield column heights of < 2 to 7.5 km. The total tephra volumes (Table 5.1) and eruption column heights correspond to a maximum volcanic explosivity index (VEI, Newhall and Self, 1982) of 3.

The eruption products involved in the initial pipe excavating and the later excavation of the nested crater at VNW are indicative explosive eruptions with high fragmentation intensities. Evidence for this is found in the unusually high abundance of splintery broken olivines within these pyroclastic facies. Modelling of BK-L_1 as a product of phreatomagmatic eruptions leads to durations of 17 weeks to 1.3 year (Fig. 5.8, Table 5.2). This is significantly longer than suggested durations for VK-U_1. If the initial excavation of the VNW crater were driven by phreatomagmatism, this would have required progressive deepening of the pipe during a long eruptive phase with explosions forceful enough to clear most of the country rock material out of the vent. Another, equally valid, interpretation is that the initial crater excavation occurred in a much shorter time span (2-15 days), with dominantly explosive magmatic (gas driven) fragmentation, and magma flow rates that were too high to allow efficient magma-water interaction. Perhaps phreatomagmatism took place only during the waning stage of the eruption, when magma flow rates declined. This could still explain the presence of some of the

textures observed today in the BK-L_1 deposit, which is likely the product of the latest stages of eruption and crater excavation at VNW. Of additional interest in this regard is that the VNW crater extends to at least 90 m (likely ~295 m, see Fig. 5.1) below the basement – Palaeozoic country rock interface. At these levels hydraulic conductivities are low and predominantly confined to faults, dolerite dyke contacts and joint surfaces in the granitoid (Fig. 5.1), decreasing the likelihood of phreatomagmatic pipe excavation. In contrast to the relatively long phreatomagmatic eruption durations for BK-L_1, the modelling yields phreatomagmatic eruption durations of 6-20 weeks for VK-U_1 (Fig. 5.8, Table 5.2). The latter values are comparable to those found in modern maar volcanoes (Ukinrek 1977, Kienle et al., 1980; Self et al., 1980; see also general discussion in Cas and Wright, 1987, p. 382). Together with textural observations such as abundant broken olivines, the presence of clastic pyroclasts, and irregular variably vesicular pyroclasts (Sections 5.4, 5.6.1), this is suggestive of a phreatomagmatic origin.

The lower (and decreasing) abundance of angular olivines in the subsequent crater-filling extrusive coherent and pyroclastic kimberlite deposits (DCK-L, DCK-U, VK-U_2, VK-U_3; Fig. 5.3A) indicates a gradual decrease in eruption intensity. As detailed above (Section 5.6.1), we think these crater-filling deposits are formed by magmatic eruptions. Eruption duration calculations indicate that units DCK-U, VK-U_2 and VK-U_3 could have formed in as little as 3-17 days. Similarly low eruption durations of 1-4 days are inferred for the DCK-L. Despite the fact that the eruption dynamics calculations were developed for sustained sub-plinian and plinian eruption columns (Wilson et al., 1976), the resulting magma eruption rates (4.5-26 m^3/s for DCK-U, 31-181 m^3/s for DCK-L) and eruption durations (several days, Table 5.2) are comparable or lower than modern lava fountains

(Kilauea Iki 1959-1960, several lava fountaining episodes with maximum magma eruption rates of 100-400 m^3/s, Richter et al., 1970; Wilson and Head, 1981, Wilson et al., 1995; Askja 1961, 350 m^3/s, Wilson et al., 1995; Heimaey 1973, 100 m^3/s, Wilson et al., 1995; Sierra Negra 2005, 9 day eruption with an average 193 m^3/s magma eruption rate, Geist et al., 2008). Hence it is likely that the magmatic eruption durations presented here represent the maximum possible values.

For Victor Main, the modelling results show phreatomagmatic eruption durations ranging from 0.8 to 3.1 years for VM-LG (Fig. 5.8, Table 5.2). Given the lack of textures indicating phreatomagmatism, textural similarity to the magmatically produced VK-U_2 and VK-U_3, as well as the long phreatomagmatic eruption durations, current evidence points towards a magmatic origin for these deposits. The magmatic eruption durations range from 5 days to 4 weeks.

5.7 Summary and conclusions

5.7.1 Emplacement history: four eruption cycles

The emplacement of the Victor North kimberlite complex can be subdivided into four volcanic cycles based on the internal geology and the interpretation of the separate units. The first two volcanic cycles comprise three comparable eruptive stages. For each cycle and/or stage we calculated the eruption duration in case of phreatomagmatic or magmatic fragmentation (Fig. 5.8).

Cycle 1, stage a: Victor Northwest (VNW) pipe excavation, could be magmatic or phreatomagmatic. The explosive eruptions with high fragmentation intensity produced abundant broken olivines within this pyroclastic facies. During the last stages of pipe

excavation (with lower magma flux) possibly saw magma-water interaction, which could explain the abundant broken olivines and clastic pyroclasts within this pyroclastic facies.

Stage b: VNW lower crater filled with dark and competent rocks. Given the similarity to rock types formed during stage 2b, we infer this unit was formed by magmatic explosive eruptions with gradually decreasing fragmentation intensity, as recorded in decreasing abundance of broken olivines.

Stage c: The first eruption cycle at VNW ended and left a partially open hole. Major pipe wall collapse breccias formed, as well as resedimented kimberlite deposited in standing water.

Cycle 2, stage a: VNW nested crater excavation, likely phreatomagmatic, possibly interaction with a standing body of water. Textures within this pyroclastic unit indicate explosive eruptions with high fragmentation intensities.

Stage b: The upper VNW crater is filled with dark and competent kimberlite. Gradually decreasing fragmentation intensity as recorded in decreasing abundance of broken olivines. This deposit was formed by intra-crater lava fountaining that created clastogenic kimberlite (Chapter 4). Minor pyroclastic kimberlite was formed in the centre of the pipe.

Stage c: The second eruption cycle at VNW ended, and left a partially open hole. There is evidence for mass wasting of tephra ring material, deposition of resedimented volcaniclastic kimberlite formed in the presence of water, as well as the formation of voluminous sedimentary country rock pipe wall collapse breccias.

Cycle 3: The Victor Main (VM) crosscutting crater formed, either by magmatic or phreatomagmatic activity. Crater is filled with low diamond grade, relatively homogeneous country rock fragment-poor pyroclastic kimberlite.

Cycle 4: VM nested crater formed, eruption durations were not estimated. Grain-on-grain mixing on the interface suggests the previous deposit was not fully consolidated yet (Webb et al., 2004; Chapter 2). The central part of the crater is now filled with high diamond grade relatively homogeneous country rock fragment-poor pyroclastic kimberlite, with a moderate-grade mixing zone in between the high- and low-grade domains.

5.7.2 Emplacement history: implications for Victor North

The two cycles involved in formation of VNW (cycles 1 and 2) show a change in eruption from explosive phreatomagmatic crater-excavation to low energy magmatic lava fountaining that fills the excavated crater. Transitions from phreatomagmatic to magmatic eruptions, like those recorded here, are commonplace in basaltic volcanic systems around the world and can easily be achieved by an increase in the magma flux/eruption velocity, depletion of water within the local aquifers during the eruption, destruction or sealing of porosity within the in-situ country rocks during the eruption, or changes in the volatile content of the magma (e.g. Cas and Wright, 1987; Houghton and Schmincke, 1989; Carey et al., 2009; Di Traglia et al., 2009).

5.7.3 General implications

Most kimberlite deposits are found within pipes or craters. These intra-crater settings are different from the extra-crater settings commonly studied in basaltic-rhyolitic volcanic systems, and phreatomagmatic deposits in intra-crater locations are unlikely to contain

tractional base surge bed forms. Hence, for intra-crater kimberlite systems we are left with looking at textural evidence for phreatomagmatic fragmentation, rather than typical phreatomagmatic deposit styles. Characteristic textures resulting from phreatomagmatic fragmentation in kimberlite deposits are expected to be comparable to basaltic-rhyolitic systems in that they are fine grained, poorly sorted, generally country rock fragment-rich, contain variably vesicular pyroclasts and may contain clastic pyroclasts. However, some differences are expected, especially in the morphology and texture of the pyroclasts. These differences result from the very low melt viscosity, as well as the crystal-rich nature of kimberlite magma. In magmatically produced deposits these magma properties result in a lack of formation of vesicular glassy juvenile pyroclasts and bubble wall glass shards. We propose that (variably) vesicular pyroclasts in kimberlite deposits are in fact a result of the rapid quenching by magma-water interaction. In addition, blocky glassy ash particles are unlikely to form given the lack of glass formation in these systems. Lastly, higher abundances of angular broken olivines, indicative of high fragmentation intensities, are expected. Similar textural observations are expected for other low viscosity and/or high crystal content magmas.

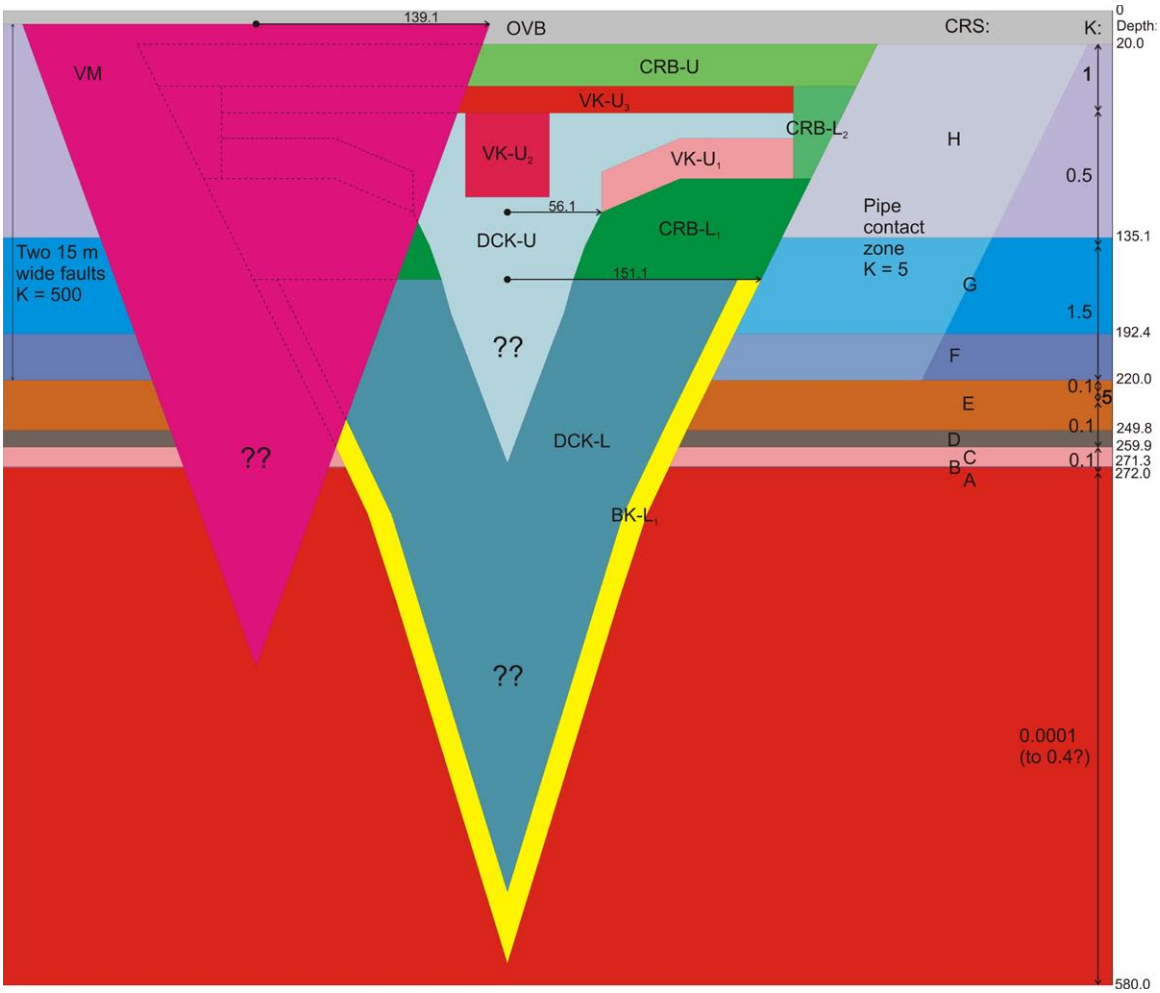

Figure 5.1 Cross section through Victor North showing the local country rock stratigraphy, the Victor Northwest (VNW) and the later crosscutting Victor Main (VM) pipes. The figures hows the schematic internal geology used to calculate kimberlite unit volumes (please refer to Chapter 3, Fig. 3.2 for detailed geological unit representation), the detailed country rock stratigraphy (units *A*-*H*, with depth in meters below the surface), the hydrological properties of the different rock units and the pipe contact zone and two inferred faults (*K* = horizontal hydraulic conductivity in m/day; hydrology after HCI, 2004).

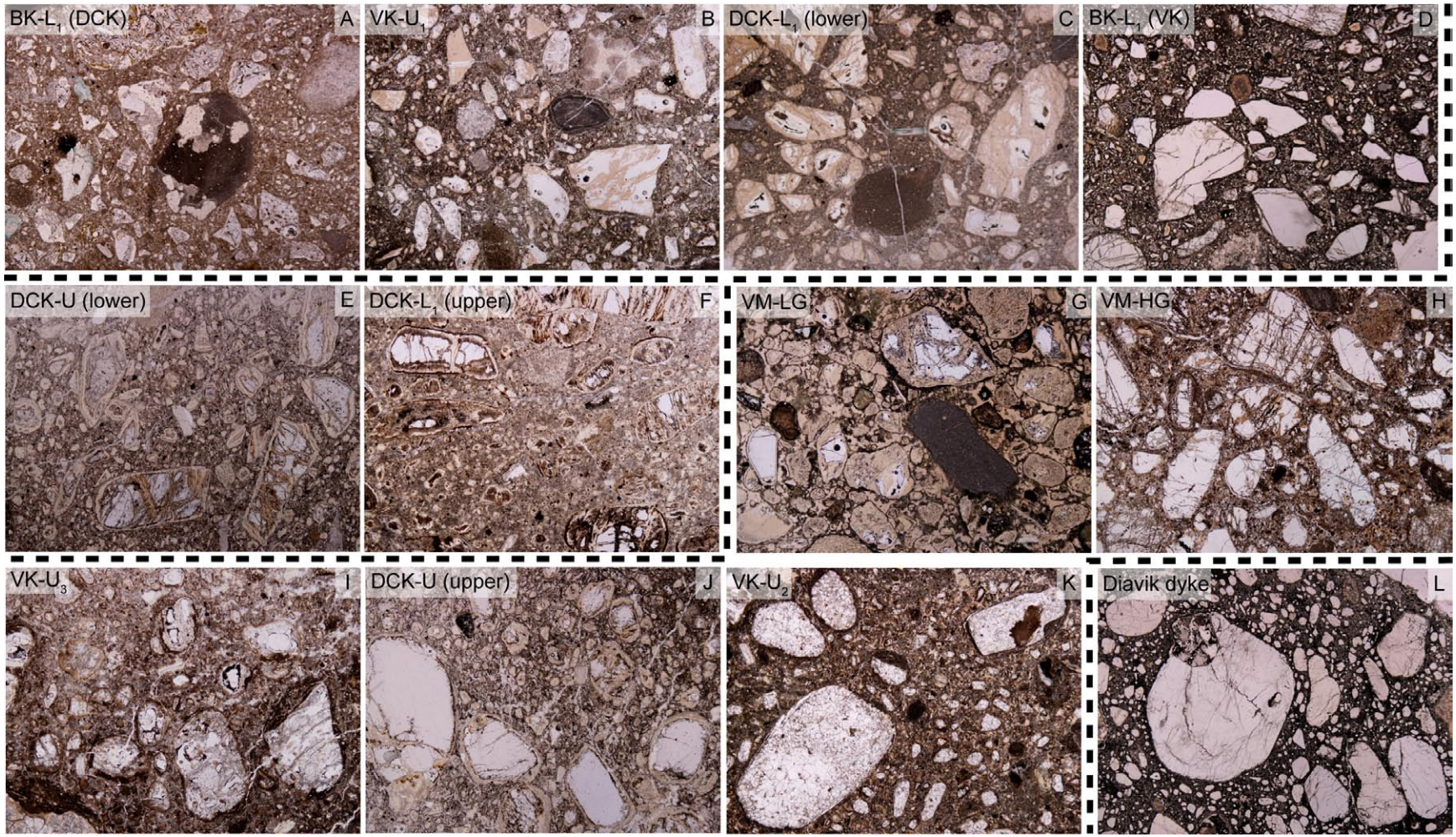

Figure 5.2 Plate with photomicrographs of representative samples of different rock types at Victor North (Fig. 5.1) showing olivine crystal shapes. Note the decreasing proportion of angular broken olivines from top left (A) to bottom right (L). Angular broken olivines are abundant in BK-L_1 (DCK), VK-U_1, DCK-L_1 (lower), and BK-L_1 (VK); moderately abundant in DCK-U (lower) and DCK-L_1 (upper); not very abundant in VM-LG, VM-HG, VK-U_3, DCK-U (upper) and VK-U_2; and absent in a typical sample of intrusive coherent kimberlite from a dyke at the Diavik Diamond Mine, NWT, Canada. FOV = 9 mm.

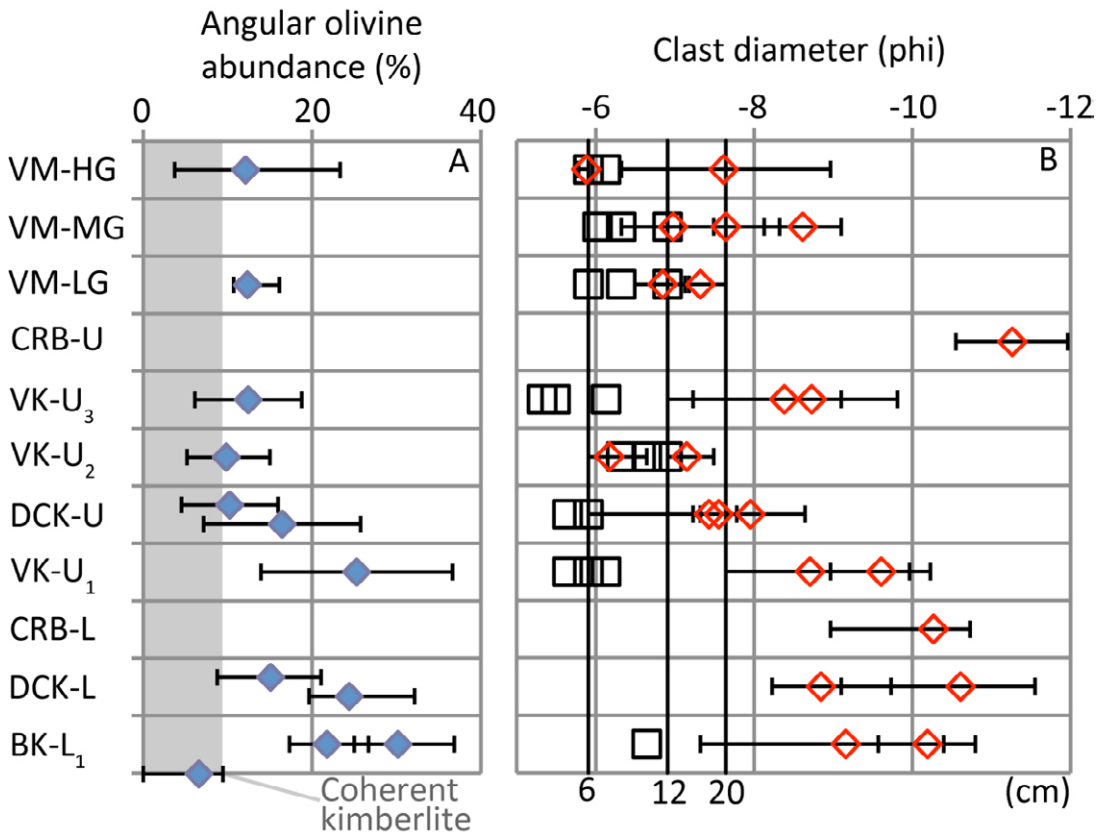

Figure 5.3 Graphs of angular olivine abundance and maximum clast size in all deposits within Victor North. Graph (A) shows the proportion of angular olivine, established by counting the number of olivines with one or more sharp angle (< 80º) out of > 25-50 olivine macrocrysts in one thin section. The first dataset comprises units VK-U_1, DCK-U and VK-U_3 (see Fig. 4.4 for all data), and >25 grains per sample with a total of 550-1500 grains counted for each lithology. The error bars represent 1SD of the data. The second dataset (all other lithologies) comprises >50 counted grains per sample with a total of 150-350 grains counted for each lithology in at least three different samples. Error bars represent the minimum and maximum value for each lithology. For each lithology, the average value is interpreted to represent the proportion of angular broken grains. Counting of two typical macrocrystic intrusive coherent dykes (Snap Lake and Diavik lower A154N pipe, NWT, Canada; see Field et al., 2009 and Moss, 2009 respectively for location), and olivines within a large juvenile pyroclast within VM yield angular broken olivine values from 0-9 %. Graph (B) shows the maximum clast size for each lithology in phi grain size units (where the diameter d [mm] = $2^{-d\,[phi]}$) as measured in drill core. Black squares = two/three largest juvenile pyroclast (JP), granitic (Gr) or kimberlite lithic (KL) clasts within a particular lithology. Red diamonds = average and range in the five largest sedimentary country rock clasts within each unit. For the latter, each point represents data from a different drill hole. Typically, the largest JP/Gr/KL clasts that were sustained by the eruption are in between 6-12 cm, whereas 20 cm was taken as a conservative estimate for the largest country rock clast sustained in the eruption column (see Table 5.1).

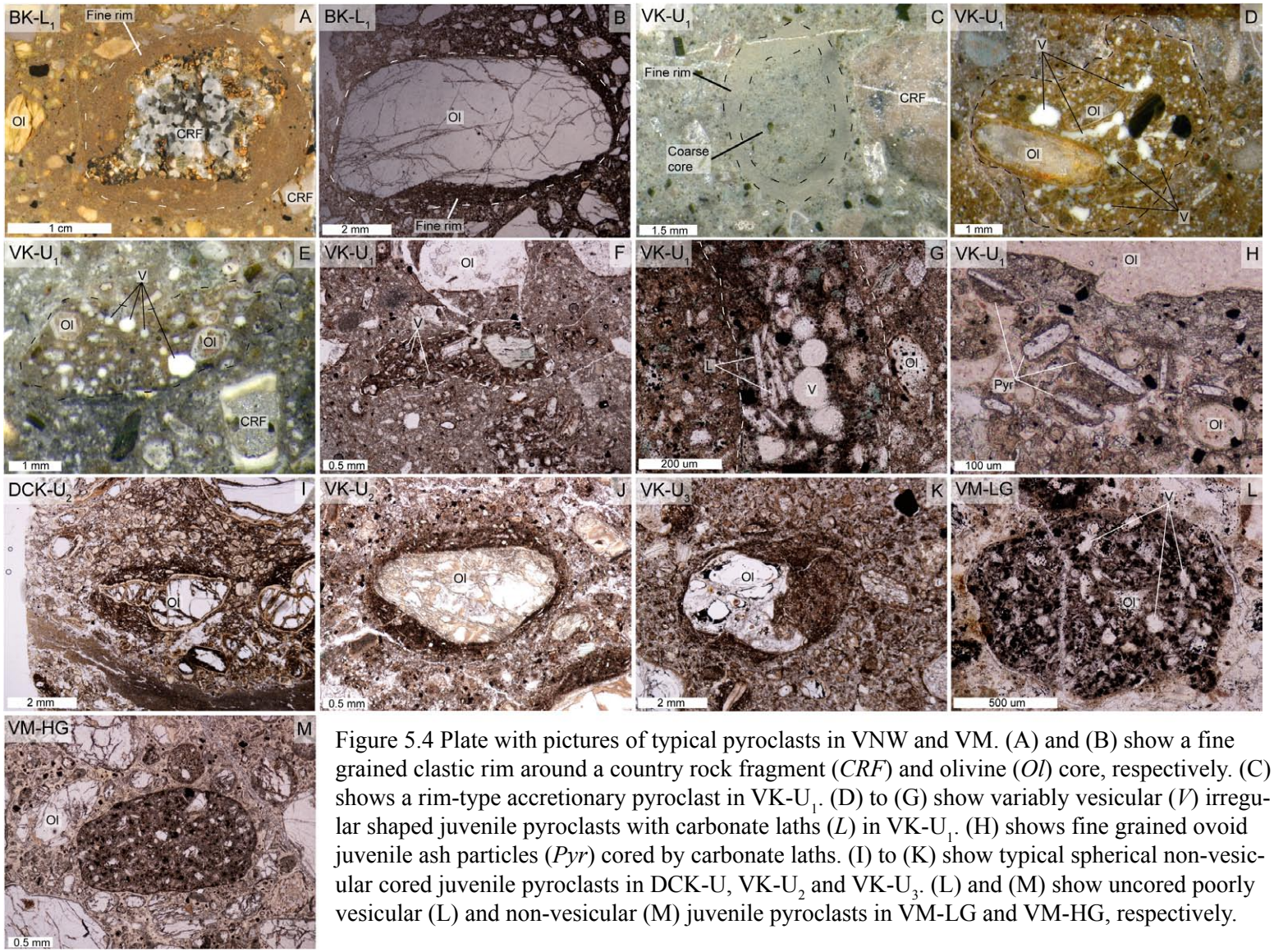

Figure 5.4 Plate with pictures of typical pyroclasts in VNW and VM. (A) and (B) show a fine grained clastic rim around a country rock fragment (*CRF*) and olivine (*Ol*) core, respectively. (C) shows a rim-type accretionary pyroclast in VK-U_1. (D) to (G) show variably vesicular (*V*) irregular shaped juvenile pyroclasts with carbonate laths (*L*) in VK-U_1. (H) shows fine grained ovoid juvenile ash particles (*Pyr*) cored by carbonate laths. (I) to (K) show typical spherical non-vesicular cored juvenile pyroclasts in DCK-U, VK-U_2 and VK-U_3. (L) and (M) show uncored poorly vesicular (L) and non-vesicular (M) juvenile pyroclasts in VM-LG and VM-HG, respectively.

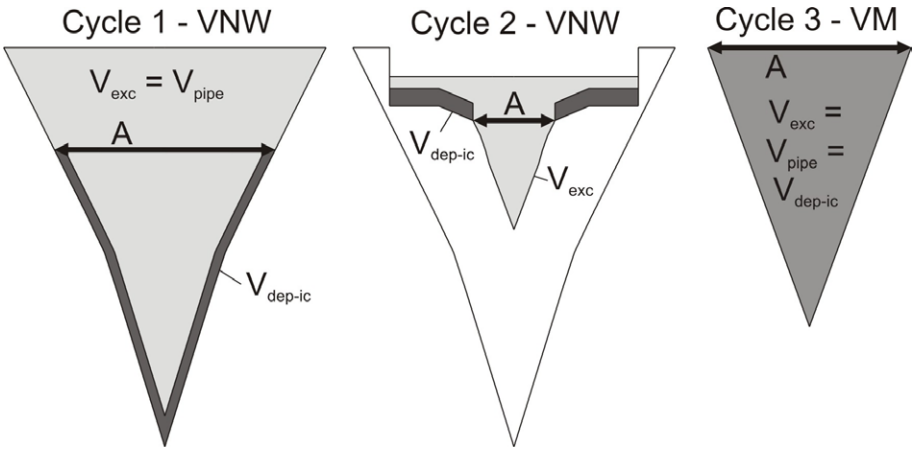

Figure 5.5 Total pipe volume (V_{pipe}), total excavated rock volume (V_{exc}), and intra-crater deposit volume (V_{dep-ic}) for all three crater-excavating eruptions at VNW and VM. Note that the VNW nested crater is only thought to have excavated a partly filled crater; hence we only use the volume up to the 60 mbs level. The tephra flux calculations (Section 5.5.5) use the cross-sectional area (A) indicated with arrows.

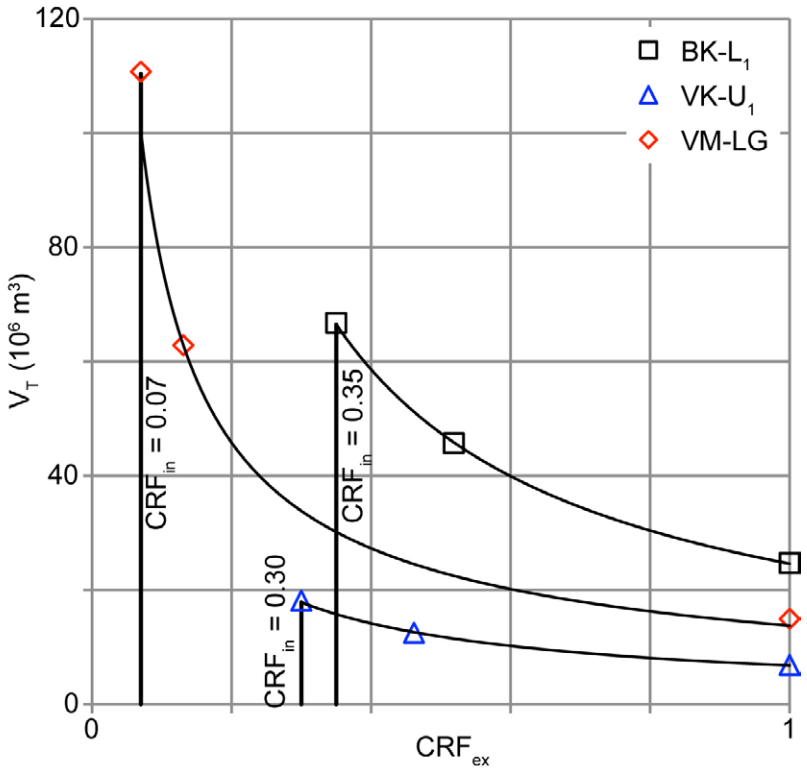

Figure 5.6 Graph showing the reciprocal relationship between the calculated total tephra volume (V_t) and the assumed extra-crater country rock fragment content (CRF_{ex}). Maximum tephra volumes result from similar country rock fragment content in the intra-crater (CRF_{ic}) and extra crater deposits, minimum tephra volumes result from extra crater deposits that consist entirely of country rock fragments (CRF_{ex} = 1). Maximum and average tephra volumes were used for the eruption duration calculations, see text for discussion.

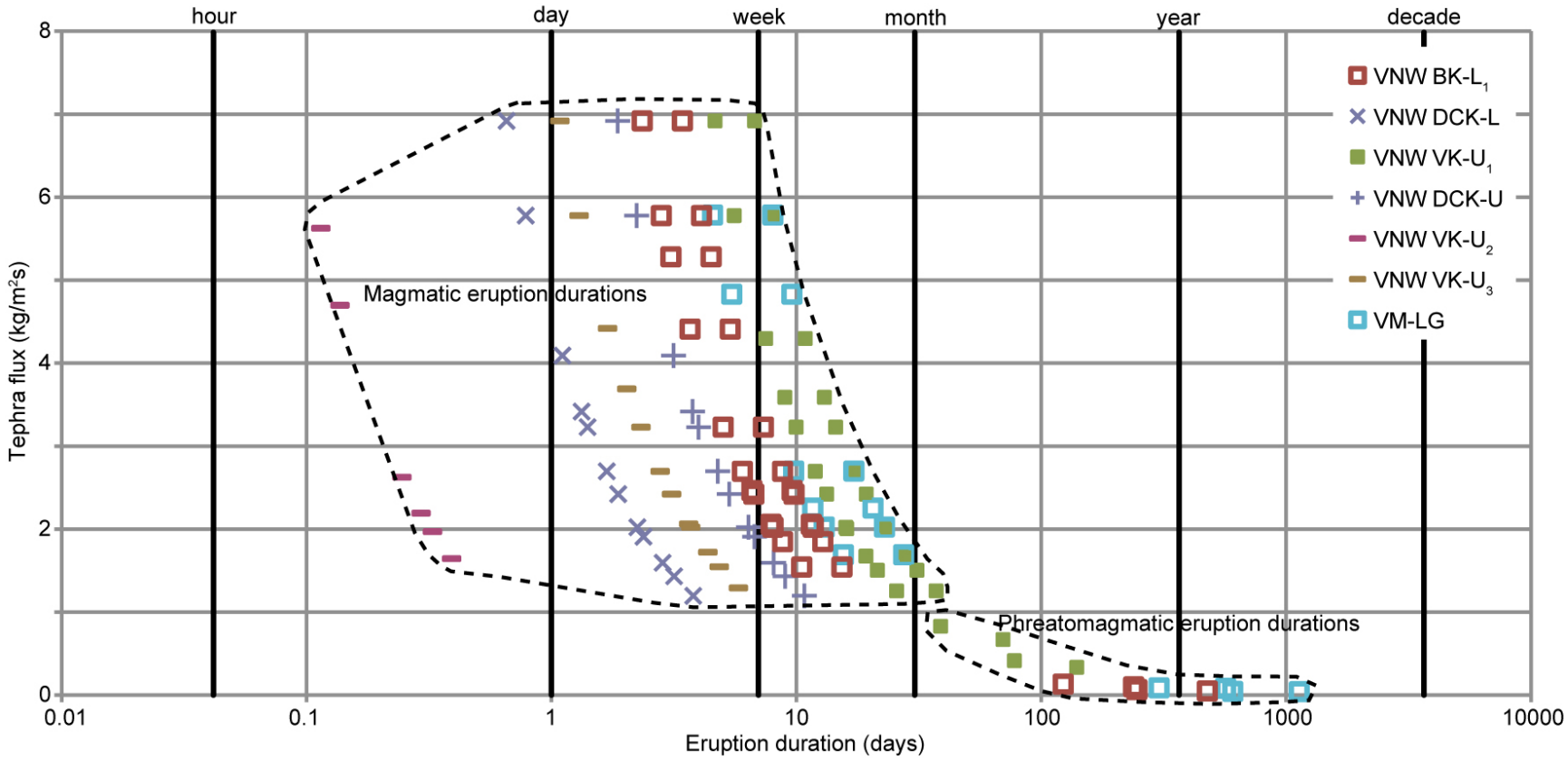

Figure 5.7 Graph of tephra mass flux (F_t) vs. eruption duration (T_e). Each set of calculations plots on the reciprocal relationship between F_t and T_e: F_t [kg/m²s] = M_t [kg]/{86400 · π · (x [m])² · T_e [days]}.

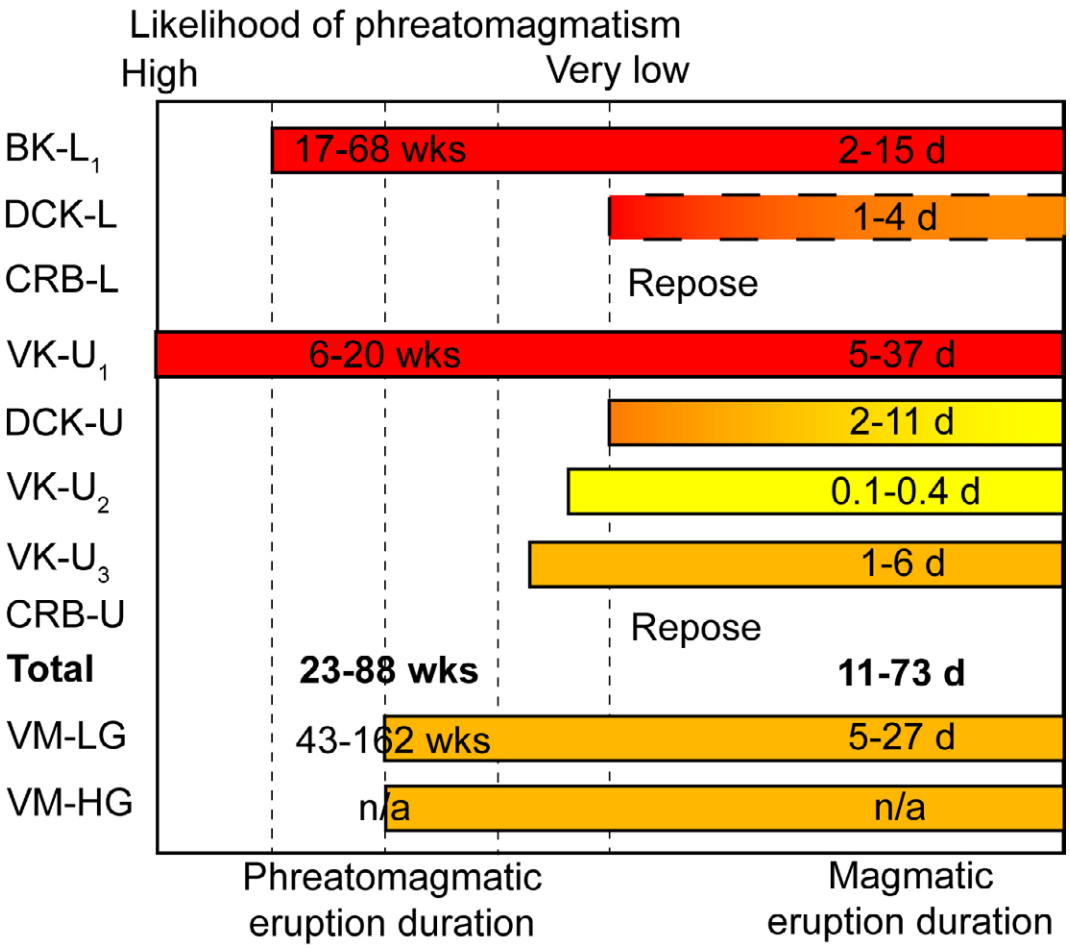

Figure 5.8 Summary of magmatic and phreatomagmatic eruption durations (in days and weeks, respectively), likelihood of phreatomagmatic eruptions based on textural observations and fragmentation intensity of each unit within VNW and VM (red colours = high fragmentation intensity and abundant broken olivine; yellow colours = low fragmentation intensity and minor to no broken olivine).

Table 5.1 Summary of data used for estimating the total tephra and magma volume

Unit	**$V_{dep\text{-}ic}$ (10^6 m^3)**	**CRF_{ic}**	**V_{exc} (10^6 m^3)**	**CRF_{ex}**	**$V_{dep\text{-}ic}/V_t$**	**V_t (10^6 m^3)**		**V_m (10^6 m^3)**	
BK-L_1	2.1	0.4	23.4	0.5	-	45.7		22.4	
				0.4	-	66.7		43.4	
DCK-L	5.7	0.1	-	-	0.5	11.5		10.3	
CRB-L_1	4.5	1.0	-	-	1.0	4.5		0.0	
CRB-L_2	1.5	1.0	-	-	1.0	1.5		0.0	
Total lower	13.9					63.3	84.3	32.7	53.7
VK-U_1	2.1	0.3	5.4	0.5	-	12.5		7.1	
				0.3	-	18.2		12.7	
DCK-U	2.2	0.1	-	-	0.5	4.5		4.1	
VK-U_2	0.1	0.1	-	-	0.5	0.3		0.2	
VK-U_3	1.5	0.3	-	-	0.5	2.9		2.0	
CRB-U	3.6	1.0	-	-	1.0	3.6		0.0	
Total upper	9.5					23.8	29.4	13.5	19.1
Total VNW	23.4					87.0	113.7	46.2	72.8
VM-LG	7.8	0.1	7.8	0.1	-	62.8		55.1	
				0.1	-	110.7		103.0	

Abbreviations used: $V_{dep\text{-}ic}$ = total intra-crater deposit volume, CRF_{ic} = average intra-crater country rock fragment content for each unit, V_{exc} = total excavated rock volume, CRF_{ex} = assumed extra-crater country rock fragment content for each eruptive unit, $V_{dep\text{-}ic}/V_t$ = assumed ratio between intra-crater deposit volume and total tephra volume, V_t = calculated tephra volume, V_m = calculated magma volume

Table 5.2 Summary of magmatic and phreatomagmatic eruption durations (T_e)

Unit	Magmatic eruption											Phreatomagmatic eruption					
	R_c (m) and type				x (m)	m_t (10^3 kg/s)		F_t (kg/m^{2}s)		T_e (days)		m_t (10^3 kg/s)		F_t (kg/m^{2}s)		T_e (days)	
	Min	Type	Max	Type		Min	Max	Min	Max	Min	Max	Min	Max	Min	Max	Min	Max
BK-L_1	0.050	Gr	0.100	Ls	151.1	111	496	1.54	6.92	2.3	10.5	4.7	9.5	0.07	0.13	123	246
	0.050	Gr	0.100	Ls	151.1	111	496	1.54	6.92	3.4	15.4	3.6	7.1	0.05	0.01	238	477
DCK-L	0.030	Gr	0.100	Ls	151.1	86	496	1.20	6.92	0.7	3.8	-	-	-	-	-	-
VK-U_1	0.035	KL	0.100	Ls	56.1	12	69	1.26	6.92	4.7	25.7	4.1	8.2	0.41	0.83	39	78
	0.035	KL	0.100	Ls	56.1	12	69	1.26	6.92	6.8	37.2	3.3	6.6	0.33	0.67	70	140
DCK-U	0.030	Gr	0.100	Ls	56.1	12	69	1.20	6.92	1.9	10.8	-	-	-	-	-	-
VK-U_2	0.060	JP	-	-	56.1	16	56	1.64	5.63	0.1	0.4	-	-	-	-	-	-
VK-U_3	0.035	Gr	0.100	Ls	56.1	13	69	1.29	6.92	1.1	5.8	-	-	-	-	-	-
VM-LG	0.060	Gr	-	-	139.1	103	352	1.69	5.79	4.5	15.6	2.6	5.3	0.04	0.09	303	605
	0.060	Gr	-	-	139.1	103	352	1.69	5.79	8.0	27.4	2.5	5.0	0.04	0.08	566	1131
VM-HG	0.035	JP	0.100	Ls	-	-	-	-	-	-	-	-	-	-	-	-	-

Abbreviations used: R_c = clast radius, x = vent radius (see Fig. 5.1), m_t = tephra mass eruption rate, F_t = tephra mass flux. Clast types: Gr = granite (P_c = 2750 kg/m_3), Ls = limestone (P_c = 2360 kg/m^3), KL = kimberlite lithic, JP = juvenile pyroclast (both P_c = 2600 kg/m^3).

[a] Assumed minimum value; see Fig. 5.3 and Electronic appendix J.

5.8 References

Boxer, G.L., Lorenz, V. and Smith, C.B., 1989. The geology and volcanology of the Argyle (AK1) lamproite diatreme, Western Australia, 4th International Kimberlite Conference. Geological Society of Australia, Perth, Australia, pp. 140-152.

Brand, B., Clarke, A. and Semken, S., 2009. Eruptive conditions and depositional processes of Narbona Pass Maar volcano, Navajo volcanic field, Navajo Nation, New Mexico (USA). Bulletin of Volcanology, 71(1): 49-77.

Buettner, R., Dellino, P. and Zimanowski, B., 1999. Identifying magma-water interaction from the surface features of ash particles. Nature, 401(6754): 688-690.

Carey, R.J., Houghton, B.F. and Thordarson, T., 2009. Abrupt shifts between wet and dry phases of the 1875 eruption of Askja Volcano: Microscopic evidence for macroscopic dynamics. Journal of Volcanology and Geothermal Research, 184(3-4): 256-270.

Cas, R.A.F., Hayman, P., Pittari, A. and Porritt, L., 2008a. Some major problems with existing models and terminology associated with kimberlite pipes from a volcanological perspective, and some suggestions. Journal of Volcanology and Geothermal Research, 174(1-3): 209-225.

Cas, R.A.F., Porritt, L., Pittari, A. and Hayman, P., 2008b. A new approach to kimberlite facies terminology using a revised general approach to the nomenclature of all volcanic rocks and deposits: Descriptive to genetic. Journal of Volcanology and Geothermal Research, 174(1-3): 226-240.

Cas, R.A.F. and Wright, J.V., 1987. Volcanic successions. Chapman & Hall, London, 528 pp.

Clement, C.R., 1982. A comparative study of some major kimberlite pipes in the North Cape and Orange Free State. Ph.D. thesis, University of Cape Town, Cape Town.

Clement, C.R., Skinner, E.M.W. and Scott-Smith, B.H., 1984. Kimberlite redefined. Journal of Geology, 92: 223-228.

Di Traglia, F., Cimarelli, C., de Rita, D. and Gimeno Torrente, D., 2009. Changing eruptive styles in basaltic explosive volcanism: Examples from Croscat complex scoria cone, Garrotxa Volcanic Field (NE Iberian Peninsula). Journal of Volcanology and Geothermal Research, 180(2-4): 89-109.

Dingwell, D.B., 1996. Volcanic dilemma: flow or blow? Science, 273(5278): 1054-1055.

Dingwell, D.B. and Webb, S.L., 1989. Structural relaxation in silicate melts and non-Newtonian melt rheology in geologic processes. Physics and Chemistry of Minerals, 16(5): 508-516.

Field, M. et al., 2009. Variations of olivine abundance and grain size in the Snap Lake kimberlite intrusion, Northwest Territories, Canada: A possible proxy for diamonds. Lithos, 112(Supplement 1): 23-35.

Field, M. and Scott-Smith, B.H., 1999. Contrasting geology and near-surface emplacement of kimberlite pipes in Southern Africa and Canada, Proceedings of the 7th International Kimberlite Conference, Cape Town.

Fisher, R.V. and Schmincke, H.-U., 1984. Pyroclastic rocks. Springer-Verlag, New York, 472 pp.

Geist, D. et al., 2008. The 2005 eruption of Sierra Negra volcano, Galápagos, Ecuador. Bulletin of Volcanology, 70(6): 655-673.

Hayman, P.C., Cas, R.A.F. and Johnson, M., 2009. Characteristics and alteration origins of matrix minerals in volcaniclastic kimberlite of the Muskox pipe (Nunavut, Canada). Lithos, 112(Supplement 1): 473-487.

Houghton, B.F. and Schmincke, H.U., 1989. Rothenberg scoria cone, East Eifel: a complex Strombolian and phreatomagmatic volcano. Bulletin of Volcanology, 52(1): 28-48.

Houghton, B.F. and Wilson, C.J.N., 1989. A vesicularity index for pyroclastic deposits. Bulletin of Volcanology, 51(6): 451-462.

Hydrological Consultants Inc., H., 2004. Dewatering of the Victor diamond project.

Keller, J., 1989. Extrusive carbonatites and their significance. In: K. Bell (Editor), Carbonatites. Genesis and evolution. Undwin Hyman, London, pp. 70-88.

Kienle, J., Kyle, P.R., Self, S., Motyka, R.J. and Lorenz, V., 1980. Ukinrek Maars, Alaska, I. April 1977 eruption sequence, petrology and tectonic setting. Journal of Volcanology and Geothermal Research, 7(1-2): 11-37.

Kong, J.M., Boucher, D.R. and Scott-Smith, B.H., 1999. Exploration and Geology of the Attawapiskat Kimberlites, James Bay Lowland, Northern Ontario, Canada. Proceedings of the 7th International Kimberlite Conference, The J.B. Dawson volume, Cape Town, 452-467 pp.

Kurszlaukis, S., Franz, L. and Lorenz, V., 1998. On the volcanology of the Gibeon Kimberlite Field, Namibia. Journal of Volcanology and Geothermal Research, 84: 257-272.

Kurszlaukis, S. and Lorenz, V., 2008. Formation of "Tuffisitic Kimberlites" by phreatomagmatic processes. Journal of Volcanology and Geothermal Research, 174(1-3): 68-80.

Lefebvre, N. and Kurszlaukis, S., 2008. Contrasting eruption styles of the 147 Kimberlite, Fort a la Corne, Saskatchewan, Canada. Journal of Volcanology and Geothermal Research, 174(1-3): 171-185.

Lorenz, V., 1986. On the growth of maars and diatremes and its relevance to the formation of tuff rings. Bulletin of Volcanology, 48(5): 265-274.

Lorenz, V. and Kurszlaukis, S., 2007. Root zone processes in the phreatomagmatic pipe emplacement model and consequences for the evolution of maar-diatreme volcanoes. Journal of Volcanology and Geothermal Research, 159(1-3): 4-32.

Lorenz, V., Zimanowski, B., Buttner, R. and Kurszlaukis, S., 1999. Formation of kimberlite diatremes by explosive interaction of kimberlite magma with groundwater: field and experimental aspects, Proceedings of the 7th International Kimberlite Conference, Cape Town, pp. 522-528.

Mitchell, R.H., 1986. Kimberlites: Mineralogy, Geochemistry and Petrology. Plenum Press, New York, 442 pp.

Moss, S., Russell, J.K. and Andrews, G.D.M., 2008. Progressive infilling of a kimberlite pipe at Diavik, Northwest Territories, Canada: Insights from volcanic facies architecture, textures, and granulometry. Journal of Volcanology and Geothermal Research, 174(1-3): 103-116.

Moss, S., Russell, J.K., Brett, R.C. and Andrews, G.D.M., 2009. Spatial and temporal evolution of kimberlite magma at A154N, Diavik, Northwest Territories, Canada. Lithos, 112: 541-552.

Moss, S.W., 2009. Volcanology of the A154N kimberlite at Diavik: Implications for eruption dynamics. Ph.D. thesis, University of British Columbia, Vancouver, B.C., Canada.

Newhall, C. and Self, S., 1982. The volcanic explosivity index (VEI) an estimate of explosive magnitude for historical volcanism. Journal of Geophysical Research, 87(C2): 1231-1238.

Norris, A.W., 1993. Hudson Platform - Geology. In: D.F. Stott and J.D. Aitken (Editors), Sedimentary Cover of the Craton in Canada. Geological Survey of Canada, pp. 655-700.

Nowicki, T., Porritt, L., Crawford, B. and Kjarsgaard, B., 2008. Geochemical trends in kimberlites of the Ekati property, Northwest Territories, Canada: Insights on volcanic and resedimentation processes. Journal of Volcanology and Geothermal Research, 174(1-3): 117-127.

Pittari, A. et al., 2008. Eruption processes and facies architecture of the Orion Central kimberlite volcanic complex, Fort ‡ la Corne, Saskatchewan; kimberlite mass flow deposits in a sedimentary basin. Journal of Volcanology and Geothermal Research, 174(1-3): 152-170.

Porritt, L., 2008. The volcanology and sedimentology of the Ekati kimberlites, NWT, Canada, with consideration of the implications for diamond grade. Ph.D. thesis, Monash University, Clayton, Australia.

Porritt, L.A. and Cas, R.A.F., 2009. Reconstruction of a kimberlite eruption, using an integrated volcanological, geochemical and numerical approach: A case study of the Fox Kimberlite, NWT, Canada. Journal of Volcanology and Geothermal Research, 179(3-4): 241-264.

Porritt, L.A., Cas, R.A.F. and Crawford, B.B., 2008. In-vent column collapse as an alternative model for massive volcaniclastic kimberlite emplacement: An example from the Fox kimberlite, Ekati Diamond Mine, NWT, Canada. Journal of Volcanology and Geothermal Research, 174(1-3): 90-102.

Quane, S.L. and Russell, J.K., 2005. Ranking welding intensity in pyroclastic deposits. Bulletin of Volcanology, 67(2): 129-143.

Richter, D.H., Eaton, J.P., Murata, W.A., Ault, A. and Krivoy, H.L., 1970. Chronological narrative of the 1959-60 eruption of Kilauea Volcano, Hawaii. U.S. Geological Survey Professional Paper, 537-E.

Russell, J.K., Gordon, T.M. and Moss, S., 2008. Volatiles in kimberlite: volume relationships and implications for conduit and eruption dynamics. 9th International Kimberlite Conference, Frankfurt, Germany, pp. 3.

Schumacher, R. and Schmincke, H.U., 1991. Internal structure and occurrence of accretionary lapilli - a case study at Laacher See volcano. Bulletin of Volcanology, 53(8): 612-634.

Self, S., Kienle, J. and Huot, J.-P., 1980. Ukinrek Maars, Alaska, II. Deposits and formation of the 1977 craters. Journal of Volcanology and Geothermal Research, 7(1-2): 39-65.

Sheridan, M.F. and Wohletz, K.H., 1981. Hydrovolcanic Explosions: The Systematics of Water-Pyroclast Equilibration. Science, 212(4501): 1387-1389.

Smith, C.B. and Lorenz, V., 1989. Volcanology of the Ellendale lamproite pipes, Western Australia, 4th International Kimberlite Conference. Geological Society of Australia, Perth, pp. 505-519.

Sparks, R.S.J. et al., 2006. Dynamical constraints on kimberlite volcanism. Journal of Volcanology and Geothermal Research, 155(1-2): 18-48.

Sparks, R.S.J., Brown, R.J., Field, M. and Gilbertson, M., 2007. Kimberlite ascent and eruption. Nature, 450(7172): E21-E21.

Suchy, D.R. and Stearn, C.W., 1993. Evidence of a continent-wide fault system on the Attawapiskat River, Hudson Bay Platform, northern Ontario. Canadian Journal of Earth Sciences, 30(10): 1668-1673.

Walker, G. and Croasdale, R., 1971. Characteristics of some basaltic pyroclastics. Bulletin of Volcanology, 35(2): 303-317.

Walker, G.P.L., 1973. Explosive volcanic eruptions — a new classification scheme. International Journal of Earth Sciences, 62(2): 431-446.

Webb, K.J., 2006. Juvenile clasts in kimberlites: Standardizing comprehensive description towards unravelling emplacement models, Kimberlite Emplacement Workshop, Saskatoon, Canada.

Webb, K.J., Scott-Smith, B.H., Paul, J.L. and Hetman, C.M., 2004. Geology of the Victor Kimberlite, Attawapiskat, Northern Ontario, Canada: cross-cutting and nested craters. Lithos, 76(1-4): 29-50.

White, J.D.L., 1991. Maar-diatreme phreatomagmatism at Hopi Buttes, Navajo Nation (Arizona), USA. Bulletin of Volcanology, 53(4): 239-258.

Wilson, L., 1976. Explosive Volcanic Eruptions III. Plinian Eruption Columns. Geophysical Journal of the Royal Astronomical Society, 45: 543-556.

Wilson, L., 1978. Energetics of the Minoan eruption, Second International Scientific Congres, Santorini, Greece.

Wilson, L. and Head III, J.W., 2007. An integrated model of kimberlite ascent and eruption. Nature, 447(7140): 53-57.

Wilson, L. and Head, J.W., III, 1981. Ascent and Eruption of Basaltic Magma on the Earth and Moon. J. Geophys. Res., 86(B4): 2971-3001.

Wilson, L., Parfitt, E.A. and Head, J.W., 1995. Explosive volcanic eruptions VIII. The role of magma recycling in controlling the behaviour of Hawaiian-style lava fountains. Geophysical Journal International, 121(1): 215-225.

Wilson, L., Sparks, R.S.J., Huang, T.C. and Watkins, N.D., 1978. The Control of Volcanic Column Heights by Eruption Energetics and Dynamics. Journal of Geophysical Research, 83(B4): 1829-1836.

Wohletz, K.H., 1986. Explosive magma-water interactions: Thermodynamics, explosion mechanisms, and field studies. Bulletin of Volcanology, 48(5): 245-264.

Wohletz, K.H. and Sheridan, M.F., 1983. Hydrovolcanic explosions; II, Evolution of basaltic tuff rings and tuff cones. Am J Sci, 283(5): 385-413.

Wright, J.V., Smith, A.L. and Self, S., 1980. A working terminology of pyroclastic deposits. Journal of Volcanology and Geothermal Research, 8(2-4): 315-336.

6 SUMMARY AND CONCLUSIONS

In this dissertation I describe the geology of the Victor North kimberlite complex (Northern Ontario, Canada), focussing in particular on volcanic facies analysis, petrology, and economic aspects related to diamond mining. The study uses detailed drill core logging, petrological observations on slabs and thin sections, various analytical techniques and other quantitative methods to derive the emplacement history of the two kimberlite pipes within the Victor North complex.

In this Ph.D. project, I *(1.)* reconstruct the three-dimensional architecture of the volcanic facies within the Victor Northwest kimberlite pipe, *(2.)* interpret the volcanic facies within the Victor North kimberlite pipes, *(3.)* constrain the dynamics and emplacement mechanisms of kimberlite volcanoes, *(4.)* identify the number of magma batches involved in creating the Victor North kimberlite complex and *(5.)* improve our understanding of deep mantle to surface volcanic processes that control the diamond distribution in kimberlite deposits.

6.1 Summary of Chapters 2-5

Chapter 2 discusses the geology of the Victor Main kimberlite pipe. The Victor Main pipe comprises one of the main resources in the Victor mine plan. However, this pipe also contains some low-grade domains of kimberlite that appear to be non-economic. This chapter summarises the petrological and mineral chemical criteria that can be used to differentiate the high- and low-grade kimberlite domains. In addition, oxygen fugacity calculations on groundmass minerals from both domains show similar values. Based on the above observations I conclude that the variation in diamond grade within Victor Main

is most likely caused by differential sampling of mantle material (incl. diamond) by two different magma batches that formed the high- and low-grade domains.

In **Chapter 3**, detailed drill core analyses and petrographic studies are used to reconstruct the intra-crater stratigraphy of the VNW kimberlite. This allows for a detailed reconstruction of the emplacement history of the pipe. I interpret that the VNW pipe was formed by two separate eruption cycles. During the first eruption cycle, the main VNW crater is excavated and partly filled. The second eruption cycle excavates a smaller nested crater within the existing lithified pipe fill. Both eruption cycles can be subdivided into three comparable eruptive stages that produce a similar set of deposits. In both cycles these three stages comprise *(a)* a highly explosive eruption involving crater excavation and deposition of mostly pyroclastic kimberlite, followed by *(b)* lower energy eruptions producing dark and competent kimberlite lithologies and *(c)* final volcanic quiescence resulting in major pipe wall collapse and minor resedimentation by water.

Chapter 4 focuses on a distinctive set of dark and competent kimberlite deposits formed during the second eruption cycle at VNW (cycle 2b). Using a comprehensive volcanological and petrographic analysis of all available drill cores I show that this unit has a fresh well-crystallised coherent groundmass and is extrusive and fragmental in origin. A clastogenic origin is proposed on the basis of deposit morphology, the presence of remnant pyroclasts, angular broken olivines, as well as the gradational nature of contacts with the enveloping pyroclastic units. This study, and a growing number of publications, suggest that spatter-fed crater-filling clastogenic lavas and other extrusive coherent kimberlites (whether or not formed by pyroclastic activity) may be more common than geologists previously thought. The emplacement history and volcanology

of these pipes need to be reconsidered based on the emerging importance of extrusive coherent kimberlite facies.

In **Chapter 5** I provide petrological descriptions of all units within the Victor North kimberlite complex, specifically focusing on textures indicative of eruption and fragmentation mechanisms. There is considerable debate whether kimberlite eruptions are caused by magmatic fragmentation and/or magma-water interaction; this chapter is aimed at addressing this topic by a combination of detailed textural observations and a unique set of eruption dynamics calculations. The textural observations and eruption duration calculations suggest that the crater-excavating eruptions at VNW are either completely phreatomagmatic in nature (cycle 2a), or formed by a combination of magmatic eruptions with possible phreatomagmatism at the end when the magma flux declined (cycle 1a). For both cycles, the phreatomagmatic stage is followed by magmatic lava fountaining eruptions (cycles 1b, 2b). Estimated eruption durations for each cycle ranges from days to months. In contrast, at VM the lack of textural indicators for phreatomagmatism, and the relatively long phreatomagmatic eruption durations of one to several years, suggest that magmatic eruptions are most likely responsible for the formation of these deposits.

6.2 Implications of this study

6.2.1 Implications for mining and exploration

6.2.1.1 Economic viability of Victor Northwest for mining

Given the presence within the open pit mine and proximity of current mining infrastructure, Victor Northwest may be considered a resource in the future. This study provides the first comprehensive reconstruction of the complex volcanic facies

architecture within the Victor Northwest pipe. The geological model for VNW presented here has important economic implications if further evaluation were to be considered. The general implications are summarized below (see Table 6.2 for implications for each individual unit):

- The VNW pipe was formed by at least two different magma batches (Table 6.1), which likely sampled different parts of the mantle, and are likely to contain different diamond populations.
- Each magma batch experienced a range of volcanic processes varying from fragmentation, dilution with country rock fragments, sorting, elutriation, to emplacement and deposition at high temperatures. Each of these processes has had the potential to modify the original diamond population of the magma due to diamond breakage, diluting/concentrating diamonds and diamond dissolution (see Section 6.2.1.3 and Fig. 6.1).

6.2.1.2 Origin and mineralogy of the high- and low-grade kimberlite magmas at Victor Main

The Victor Main pipe comprises one of the main resources in the mine plan, but also includes some low-grade domains that, at the present, appear to be a non-resource. This study confirms that the VM pipe formed from two different magma batches with distinct composition of groundmass spinel, ilmenite and dolomite, as well as distinct abundances of olivine phenocrysts (Table 6.1). In addition, the similar oxygen fugacity results for the two magma batches indicate that differential diamond dissolution (or resorption) during transport cannot be responsible for the grade difference between the high- and low-grade

kimberlite magmas. Thus, the two magmas entrained contrasting amounts of diamond during sampling in the diamond stability field.

6.2.1.3 Processes affecting diamond potential

In this study I have focussed on all processes that can increase or decrease the diamond potential of kimberlite deposits, ranging from diamond sampling in the mantle, to transport towards the surface, and near-surface volcanic emplacement (Fig. 6.1).

6.2.1.3.1 Diamond breakage

Several units within the VNW pipe have a significantly elevated angular broken olivine content, a feature not commonly described for kimberlite deposits. Based on the high abundance of angular broken olivine crystals, I suggest that it is likely that an increased proportion of the diamonds may have become broken as a result of volcanic fragmentation (Table 6.2). The process of the diamond breakage due to volcanic fragmentation has received relatively little attention in the geological literature, but is an important concern during processing of kimberlite ore as well as during reverse circulation large diameter drilling to obtain bulk samples for grade and value estimation (e.g. Fowler et al., 2001). Studies on the physical properties of olivine and diamond show that the pressure required to initiate tensile fracture is about 7.5 times higher for diamond than for olivine (~3.75 GPa in diamond, Field, 1992; 200-800 MPa in olivine, Roedder, 1984; Johnson and Jenkins, 1991; Brett, 2009). Since many impurities and defects are commonly present in both crystal types, I suggest that mainly the energy required to propagate fractures will govern the breakage of these crystals. Experimental studies show that the energy required to create a unit area of new crack surface is only about five times higher in diamond than in olivine (~5.5 J/m^2 for diamond, Field and Friedman, 1981;

Field, 1992; ~1.1 J/m^2 for olivine, Swain and Atkinson, 1978). Given the presence of high abundances of angular broken olivine, and the presence of both diamond and olivine as 'free' crystals within the melt, I expect higher abundances of broken diamonds in these types of deposits. This will negatively impact the value ($/carat), and hence the economic potential, of these type of deposits.

6.2.1.3.2 Dilution, sorting and elutriation

Volcanic processes such as dilution, sorting and elutriation will generally cause the most profound changes to the original diamond population within the magma (Fig. 6.1). Whereas dilution with country rock fragments will simply lower the diamond grade, sorting and elutriation can have a variety of effects on the diamond population. To visualize the effects of all three processes I used a modified crystal-lithic-vitric ternary diagram (Fig. 6.2) commonly used to classify pyroclastic deposits (Fisher and Schmincke, 1984). This plot clearly illustrates the increase in economic potential from the original magma to crystal-rich and lithic-poor pyroclastic kimberlite deposits. It should be noted that, apart from the country rock breccias, the phreatomagmatically formed VK-U_1 has the lowest diamond potential of all units due to the country rock fragment-rich nature, and lack of elutriation of ash sized juvenile melt particles. Unit VK-U_3, which likely formed by a combination of magmatic eruptions and tephra ring collapse, has a higher economic potential due to the loss of juvenile melt. Unit VK-U_2 has an even higher economic potential due to the low country rock fragment content. The deposits in Victor Main have the highest crystal to melt ratio, most likely caused by effective elutriation or winnowing of the ash fraction from the eruption column. Most likely the eruptions at Victor Main were magmatic in origin. Based on the country rock

fragment-rich nature, the lack of melt-loss and the potential of diamond breakage in VK-U_1, I speculate that phreatomagmatic kimberlite deposits that formed in a similar fashion will be significantly less prospective.

6.2.2 Emplacement models for kimberlite deposits

In this dissertation I provide detailed emplacement models for all volcanic facies within the Victor North kimberlite cluster. In this section I will highlight the advances made towards the understanding of pipe-filling coherent rocks (Chapter 4), as well as towards potential phreatomagmatic deposits (Chapter 5). These emplacement models have important implications for both kimberlite exploration, as well as general volcanology (see also Section 6.2.3).

6.2.2.1 Pipe-filling coherent kimberlite

Kimberlite pipes can contain significant proportions of coherent rocks that, until recently, have mostly been interpreted as intrusive coherent (hypabyssal) in origin (e.g. Field and Scott Smith, 1999; Skinner and Marsh, 2004). This study (Chapter 4), and a growing number of publications (Sparks et al., 2006; Nowicki et al., 2008; Brown et al., 2008, 2009; Crawford et al., 2009), suggest that intra-crater extrusive coherent deposits are more common than geologists previously thought.

In this dissertation I discussed possible ways of forming coherent extrusive coherent kimberlite, ranging from effusion, coalescence, agglutination, welding to hot pressing. In this section I have summarized the most important criteria for recognizing these particular facies in Table 6.3. Purely effusive kimberlite lavas are likely to form, but unlikely to be preserved unless formed in an intra-crater environment. Given the low

kimberlite melt viscosity, it is likely that explosive eruptions have produced reconstituted extrusive coherent deposits.

Differences between kimberlite and normal volcanic eruptions include the lack of vesicular pyroclast production and the lack of glass formation during most kimberlite eruptions. A consequence of the absence of glass during kimberlite eruptions is that no archetypal welding can take place. As a result, there will be only two main mechanisms that can cause reconstituted extrusive coherent kimberlite to form. One possibility is that the pyroclasts are (mostly) liquid, and the pyroclasts are able to coalesce back together upon deposition. Alternatively, the pyroclasts will crystallise with cooling and the formation of consolidated deposits is only possible via a process referred to as hot pressing (Chapter 4). Depending on the explosivity and pyroclast crystallinity the deposits will range from purely effusive, to clastogenic, to hot pressed extrusive coherent kimberlite deposits (Table 6.3).

Typical features of effusive, clastogenic and hot pressed extrusive coherent kimberlite deposits are summarized in Table 6.3. The main difference between kimberlite and basaltic clastogenic lavas is the lack of stretched vesicular remnant pyroclast outlines in the former deposit. In addition, hot pressed extrusive coherent kimberlite deposits will be fairly comparable to welded deposits in normal basaltic to rhyolitic volcanic rocks. However, the extremely equant crystal and pyroclast shapes, absence of intra-clast porosity (vesicular pyroclasts), and resultant lower volumetric strain in these kimberlite deposits will significantly decrease the visibility of the compaction and pore space reduction that accompany hot pressing. Hot pressed deposits will most likely create a non-uniform matrix, poorly to well-crystallised groundmass, show remnant pore-space

and a possible ‘welding’ gradient due to vertical changes in the overburden pressure and/or post-depositional cooling rate (Table 6.3).

Based on the evidence presented here, kimberlite and other similar magma types are likely to produce reconstituted extrusive coherent facies, especially within intra-crater settings. Any dark, dense, competent, massive, featureless and coherent-looking unit within a pipe and with a pipe-filling geometry should be suspected to have formed via these processes. The emplacement history and volcanology of these occurrences need to be reconsidered based on the emerging importance of this particular facies.

6.2.2.2 Phreatomagmatic deposits

My work also provides general guidelines for recognizing intra-crater pyroclastic kimberlite deposits formed as a result of phreatomagmatism (Chapter 5). Typical characteristics of these facies, and the differences to magmatically produced pyroclastic deposits, are summarized in Table 6.4.

There are several complicating factors when identifying possible intra-crater phreatomagmatic kimberlite deposits. Most importantly, the intra-crater setting will prevent the formation of archetypical tractional base surge bed forms that are often the prime indication for phreatomagmatic activity. Given the lack of indications for phreatomagmatism based on the deposit style, we are left with looking at textures caused by phreatomagmatic fragmentation. Characteristic textures resulting from phreatomagmatic fragmentation in kimberlite deposits are expected to be comparable to basaltic-rhyolitic systems in that they are fine grained, poorly sorted, generally country rock fragment-rich, contain variably vesicular pyroclasts and may contain clastic pyroclasts. However, some features are expected to be different, especially the

morphology and texture of the pyroclasts. These differences result from the very low melt viscosity, as well as the crystal-rich nature of kimberlite magma. In magmatically produced deposits these magma properties result in a lack of formation of glass, vesicular juvenile pyroclasts and bubble wall shards. We propose that (variably) vesicular and irregular shaped pyroclasts in kimberlite deposits are most likely a result of the rapid quenching by magma-water interaction. Higher abundances of angular broken olivines, indicative of high fragmentation intensities, are expected.

In addition, I suggest that in most magmatic kimberlite eruptions the melt is efficiently stripped from the crystals and elutriated within the eruption column, leading to melt-poor deposits (Fig. 6.2). In contrast, most intra-crater kimberlite phreatomagmatic eruptions are likely to retain their fine-grained grain size fraction, which can easily be observed by looking at their juvenile melt or opaque mineral content (Fig. 6.2).

6.2.2.3 General kimberlite emplacement models are oversimplified

The distinction of kimberlite pipes into three classes, presumed to be influenced primarily by the local country rock and/or magma volatile content (Field and Scott Smith, 1999; Skinner and Marsh, 2004; see summary in Chapter 1), is oversimplified. The research presented here, as well as numerous publications (e.g. Berryman et al., 2004; Nowicki et al., 2004; Kjarsgaard et al., 2006; Porritt et al., 2006; Sparks et al., 2006; Brown et al., 2008; Cas et al., 2008a, b; Lefebvre and Kurszlaukis, 2008; Moss et al., 2008; Nowicki et al., 2008; Pittari et al., 2008; Porritt et al., 2008; Brown et al., 2009; Crawford et al., 2009; Gernon et al., 2009; Moss, 2009; Porritt and Cas, 2009) show that an extremely wide variety of volcanic processes can excavate a pipe, and a multitude of volcanic and

sedimentary processes can fill the pipe, even in areas with similar country rock and/or for pipes filled with a similar magma type.

6.2.3 Implications for general volcanology

No kimberlite eruption has ever been observed, and apart from one possible Quaternary kimberlitic volcano at Igwisi Hills (Reid et al., 1975; Dawson, 1994; see Chapter 4, Section 4.5.3.1) the youngest kimberlite occurrences are Middle to Early Eocene in age (Creaser et al., 2004; Heaman et al., 2004; Batumike et al., 2008). The lack of witnessed eruptions, general lack of recent deposits, and resultant limitation to study the non-eroded intra-pipe remains of kimberlite volcanoes severely complicates the reconstruction of eruption dynamics and mechanisms. Volcanology is largely based on observations of modern extra-crater basaltic to rhyolitic volcanic deposits that formed by eruption of relatively silica-rich, relatively viscous and crystal-poor magma. The physical properties of the latter melts contrast to inferred kimberlite magma properties, which likely have much lower SiO_2 contents, lower melt viscosities, higher abundance of potential volatile compounds such as CO_3^{2-} and OH^- and high crystal content (see Chapter 1; Section 1.1.1). Until the last decade, kimberlite economic geology research has largely been decoupled from mainstream geology and volcanology, resulting in separate terminology (e.g. Field and Scott Smith, 1999; see discussion by Cas et al., 2008a) and some unique emplacement models (Clement, 1982; Field and Scott Smith, 1999; Skinner and Marsh, 2004). In this contribution I demonstrate that despite the generally more extreme range of physical properties of kimberlite melt, kimberlites erupt in a similar fashion as more common basaltic-rhyolitic volcanoes.

In this dissertation I show that low energy lava fountaining filled most of the VNW pipe. In addition, in one of the eruptive cycles, I ascribe the change from highly explosive crater-excavating eruptions to low energy lava fountaining to varying degrees of magma-water interaction. Both phreatomagmatic and lava fountaining eruptions, as well as the transition between them, are extremely common for basaltic volcanic systems (e.g. Houghton and Schmincke, 1989), and illustrate the comparable nature of kimberlite and basaltic-rhyolitic volcanism. In addition, this study shows that a large variety of volcanic processes can create and fill a kimberlite pipe. From this study, and the literature it is clear that these processes can range from:

- Highly explosive phreatomagmatic maar-type eruptions (Chapter 5)
- Low energy magmatic lava fountaining creating clastogenic lavas as well as non-coalesced pyroclastic deposits (Chapters 4, 5)
- Explosive magmatic eruptions capable of forming high eruption columns (10-35 km, Sparks et al., 1997; Sparks et al., 2006; 4-11 km using tephra production rates provided by Porritt et al., 2009 and calculations by Wilson et al., 1978) that create massive intra-vent column collapse deposits as well as extra-vent pyroclastic flows (Sparks et al., 2006; Cas et al., 2008b; Moss et al., 2008; Porritt, 2008; Porritt et al., 2008; Gernon et al., 2009; Moss, 2009; Porritt and Cas, 2009)

6.3 Limitations of this study

The most important limitations of this study are listed below.

- Working with drill core. Larger scale structures such as bedding, grading and contact relationships are more difficult to reconstruct in drill core. In addition, the total

sample volume is fairly small relative to the total pipe volume studied. However, drill core allows for almost continuous exposure and making excellent observations at the macro- to microscale. Models will likely prove to be oversimplified when open-pit exposures will be available for more detailed study.

- Limited practical applications of methods used to discriminate the high- and low-grade domains in the Victor Main kimberlite pipe. Despite significant additional study, I did not find any reliable macroscale characteristics that can be used to differentiate the two units in the open pit during mining.
- The inability to check the diamond grade predictions against real data. This study provides implications for macro diamond content within the Victor North kimberlite pipes. However, for most of these occurrences detailed knowledge on the macro diamond grade (carats/tonne), value ($/carat), morphology (angularity, resorption), stone number (stones/tonne) or stone size distribution is either not known or confidential in nature.
- Restriction of the volcanological analysis to only one kimberlite complex. The general implications for the eruption of kimberlite are based on detailed study of only one kimberlite occurrence. While other researchers have described deposits with comparable textures, this does not necessarily imply a similar origin as proposed here. Further study needs to confirm if rock types such as extrusive coherent kimberlite are indeed as common as suggested.

6.4 Directions for further study

Based on my Ph.D. research, I would like to suggest the following new directions of study:

A.) Study the typical HK-TK transition zone in Southern African type pipes in light of the possibility that the transition is caused by varying degrees of reconstitution (e.g. coalescence, agglutination, welding or hot pressing). No one has looked at this particular facies from this point of view, despite a number of studies on other pipe-filling coherent kimberlite deposits, and suggestions that this transition might in fact be welded in origin (Russell and Moss, 2006; Sparks et al., 2006).

B.) Constrain various physical properties of kimberlite melt at eruption conditions such as viscosity, glass transition temperature, etc. using synthetic kimberlite melts. Numerous estimates on kimberlite melt composition are available (see Chapter 1, Section 1.1.1). The main problem will be to decide on the volatile content of the melt, as well as to perform actual experiments on such volatile-rich melts. In addition to constraining the physical properties of the melt and establish the cooling rates needed to form glass, I would like to observe the crystallisation sequence in these melts upon cooling.

C.) Study the effect of temperature and pyroclast crystallinity on coalescence and hot pressing of pyroclasts in laboratory experiments. One way of achieving this would be to first create synthetic (basaltic or kimberlitic) melts with varying crystallinity (i.e. completely glassy to completely crystalline) by slow cooling. For each melt the lowest temperature of the sample before quenching should be recorded. Subsequently, the different samples should be cut into artificial clasts, and tightly packed clasts should be brought back to their respective lowest pre-quenching temperature. Different samples

with the same crystallinity should be kept at the specified temperature for different time periods and subsequently quenched. Resulting samples should be observed texturally, and measured for the change in porosity ($\varphi_{ratio} = \varphi_{new}/\varphi_{original}$). I predict that the non-crystalline and poorly crystalline particles will simply coalesce back into a liquid with complete loss of original intra-clast porosity ($\varphi_{ratio} = 0$). The more crystalline particles will only show minor flow of particles, some loss of intra-clast porosity, and the clasts will fuse together at the point contacts. At high crystallinities the particles will only fuse together at the point contacts and show very minor change in porosity. At the lowest temperatures, the completely crystalline particles will simply remain unchanged ($\varphi_{ratio} \approx 1$). The experiments are expected to show the change from completely coalesced rocks to completely non-coalesced pyroclasts, where additional time should show the effects of hot pressing on compaction of (partly) crystalline material. Additional studies could investigate the effect of adding load to the tightly packed clasts, observe the rate of deformation and determine the bulk viscosity.

D.) Perform analogue experiments using low viscosity liquids. These experiments could be used to determine the influence of adding particles ('crystals') on the effective viscosity of the suspension. In addition, gas bubble migration speeds could be used to better constrain the timescales at which gas bubbles can migrate out of juvenile pyroclasts during eruptions. Finally, by ejecting a low viscosity liquid plus crystals out of a vertical tube (at varying eruption velocities) I would like to observe the influence of velocity on the degree of separation of melt and crystals during the eruption, the constituents, morphology and sphericity of the pyroclasts in the eruption column, and (if possible) the size distribution of pyroclasts within the eruption column. It should be

possible to capture most of these attributes with a high-speed camera. Given the lack of experimental data on kimberlites, these data would provide important constraints on the eruption dynamics of kimberlite volcanoes.

E.) Quantify particle size distributions and opaque mineral abundance in a diverse number of kimberlite deposits and pipes to constrain eruption dynamics and deposition processes. For this I would use representative samples from a large number of well-studied kimberlite pipes, focussing on macrocrystic kimberlite dykes, a variety of pyroclastic deposits, including a number of pipe-filling coherent and suspected phreatomagmatic deposits. Quantifying particle size distributions could be done using image analysis methods at the slab, thin section an/or scanning electron microscope scale. In addition, the abundance of individual components could be quantified using whole rock analysis. The amount of olivine breakage could perhaps be linked to the total energy release during kimberlite eruptions by using the increase in surface area of these crystals upon breaking (cf. Kueppers et al., 2006).

F.) Open pit mapping of the low- to high-grade transition zone in the Victor Main pipe to try and differentiate the two grade zones. In Chapter 2 I have described an increase in country rock fragment content around the change from the low- to high-grade zone (Electronic appendix F). These observations were made in drill core, but such megascopic observations should be easier to make in the open pit.

G.) Compare intra-crater kimberlite deposits to well-exposed intra-crater deposits of related rocks (lamproites, carbonatites, melilitites, etc.) and basaltic-rhyolitic systems, focussing on changes in deposit morphology, pyroclast and other textures as a result of

variation in magma viscosity, magma crystal content as well as differences in fragmentation mechanisms (i.e. magmatic vs. phreatomagmatic).

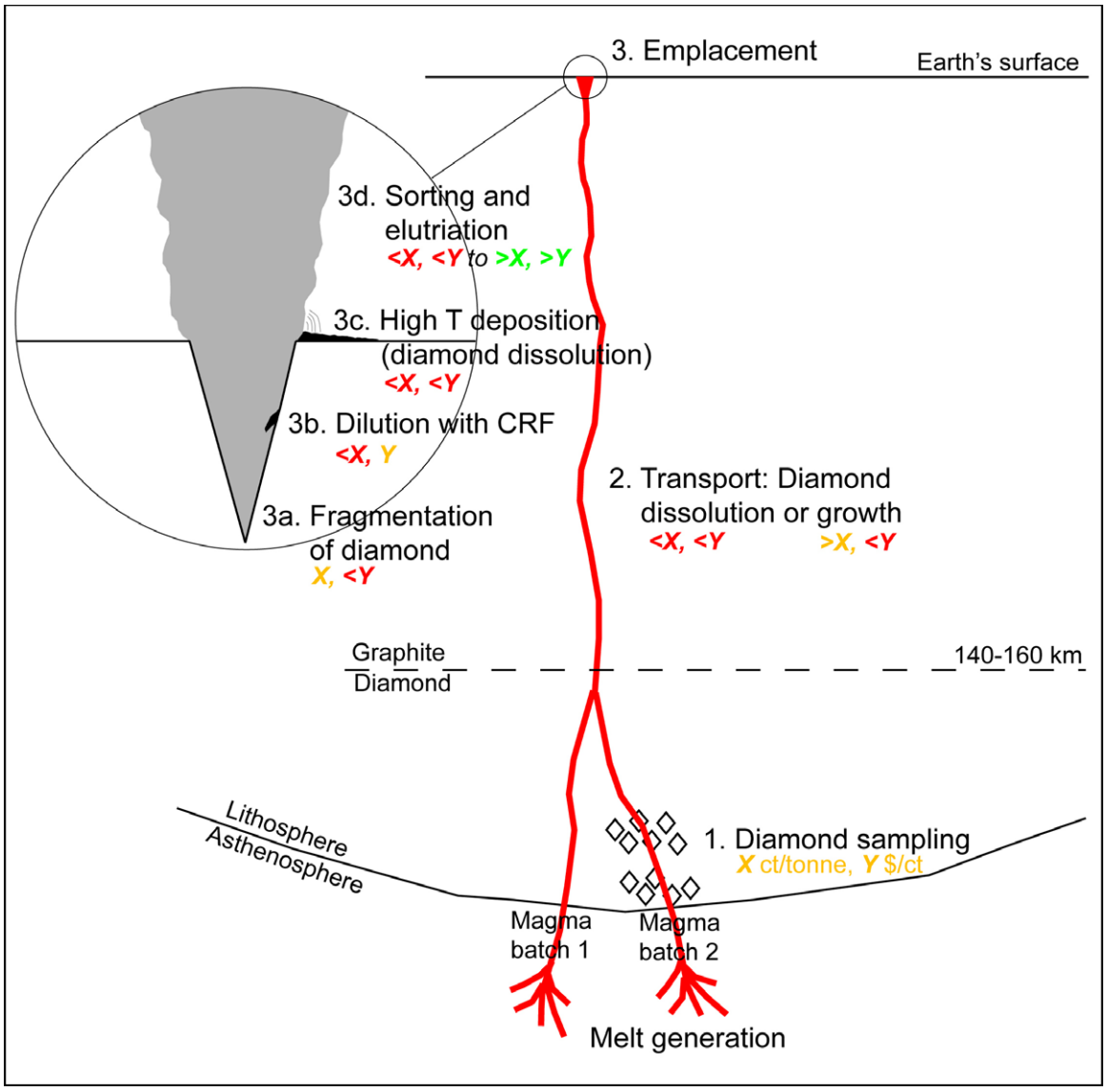

Figure 6.1 Schematic summary of processes affecting the diamond potential of primary pyroclastic kimberlite deposits. The figure shows the change in the diamond grade (*X* carats/tonne) and value (*Y* $/carat), as well as potential economic influences (positive = green, neutral = yellow, negative = red) for each process. These processes range from diamond sampling in the mantle (determines the characteristics of the diamond population), magma transport, and final emplacement. For simplicity I have ignored volcano-sedimentary and sedimentary processes subsequent to emplacement.

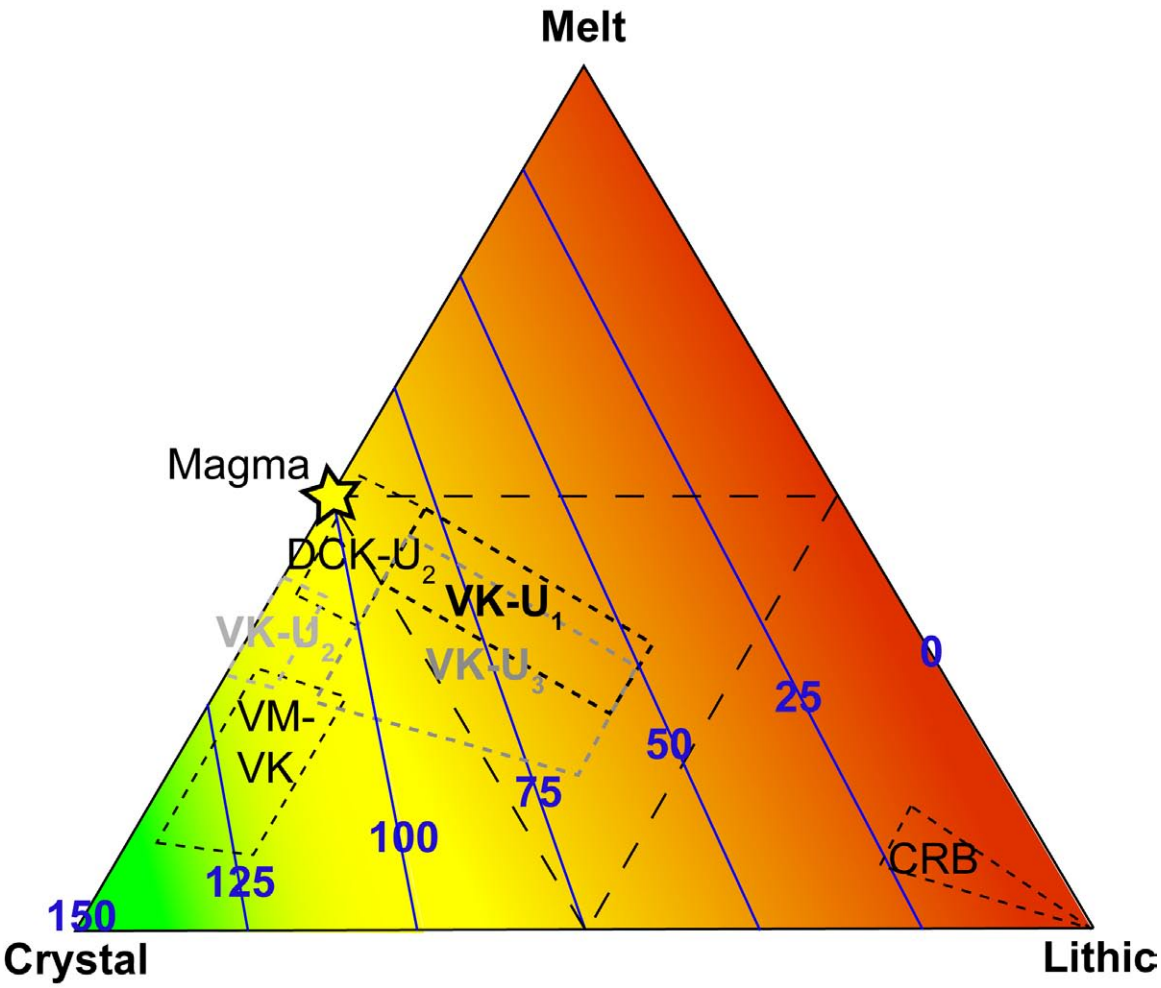

Figure 6.2 Ternary diagram with the theoretical effect of dilution, sorting and elutriation processes on the macro diamond grade (blue lines and numbers, in carats/m^3) relative to the original magma. I chose an arbitrary 100 ct/m^3 diamond grade for the magma (yellow star and yellow coloured field). Increasing the country rock fragment content and/or melt fraction reduces the theoretical diamond grade to 0 ct/m^3 (red field), whereas increasing the crystal fraction increases the diamond grade to 150 ct/m^3 (green field). The latter value was calculated assuming ~25% intra-clast porosity. Approximate locations of a selection of lithologies within Victor North are shown for reference, and are based on rough visual estimates on the presence of melt, crystals and lithic clasts. The proportion of melt was estimated by assessing the fraction of opaque minerals present in thin section relative to the original magma.

Table 6.1 Characteristics of the four magma batches emplaced at Victor North

Magma batch	**Pipe, location**	**Juvenile groundmass mineralogy** [1-3]	**Juvenile groundmass chemistry** [1]	**Olivine macrocryst content** [1-4]	**Mantle indicator mineral content** [1,3,6]	**Mantle indicator mineral chemistry** [7]	**Macrodiamond population** [1-5,7]
1	VNW lower	Ol, Carb L, Spl, Mtc, Pv ± Phl L ± MX Carb ± CX Srp	n/o	Macrocrystic (fresh to altered)	Comparable to magma batch 2	Comparable to magma batch 2, but Ilm have lower TiO_2 content	Limited to no sampling done
2	VNW upper	Ol, Carb L, Spl, Mtc, Pv ± Phl L ± MX Carb ± CX Srp	n/o	Macrocrystic (fresh to altered)	2-3 grains/40 cm2 slab, Grt = Ilm >> Cr-Di	Comparable to magma batch 1, but some non-kimberlitic Ilm might be present, and the kimberlitic Ilm have higher TiO_2 content	Limited sampling done
3	VM outer	Abundant Ol, Carb L, Spl ± Phl L ± MX Carb ± CX Srp ± *Ilm ± Rt (all Carb: Dol>Cal)*	Lower Mg# for Chr cores, Ilm, Dol L; similar oxygen fugacity as magma batch 4	Macrocrystic (generally altered)	Comparable to magma batch 4	Could be similar to magma batch 4. Ilm have higher TiO_2 content than both magma batches in VNW.	Low-grade
4	VM central	Few Ol, Carb L, Spl ± Phl L ± MX Carb ± CX Srp ± *Ilm ± Rt (all Carb: Dol>Cal)*	Higher Mg# for Chr cores, Ilm, Dol L; similar oxygen fugacity as magma batch 3	Macrocrystic (generally fresh)	~28 grains/40 cm2 slab, Cr-Di = Ilm > Grt	Could be similar to magma batch 3. Ilm have higher TiO_2 content than both magma batches in VNW.	High-grade, high value

Mineral abbreviations after Kretz (1983); Carb = carbonate, Cr-Di = Crome-diopside, Mg# = magnesium number, L = lath, MX = microcrystalline, CX = cryptocrystalline, minerals in italic identified using SEM/EMP, n/o = not observed. Sources: [1] Chapter 2, [2] Chapter 3, [3] Chapter 4, [4] Chapter 5, [5] Webb et al. (2004), [6] Electronic appendix N, [7] De Beers Canada Inc., confidential data

Table 6.2 Parameters affecting the diamond potential of volcanic units within the Victor NW kimberlite pipe

Magma batch	Eruption cycle	Eruption stage	Unit	Approximate range in dilution (vol.%)	Considerations for resource evaluation
M1	C1	Sa	BK-L_1	10-45	Possible Dia breakage, poorly constrained stratigraphy
		Sb	DCK-L_1, -L_2	3-20, rarely 25-30 and some 100	Possible Dia breakage at lower levels, possible Dia resorption, poorly constrained stratigraphy
			BK-L_2	10-100	Poorly constrained stratigraphy
		Sc	CRB-L_1	75-100	Poorly constrained stratigraphy
			RVK-L	25-50	Poorly constrained stratigraphy
			CRB-L_2	~100	Poorly constrained stratigraphy
M2	C2	Sa	VK-U_1	15-40, locally up to 100	Possible Dia breakage
		Sb	DCK-U_1	~10	Possible Dia breakage, possible Dia resorption
			DCK-U_2	2-10	Possible Dia resorption
			VK-U_2	~6	Small volume
			VK-U_3	10-40, locally up to 100	-
		Sc	RVK-U	~8	-
			CRB-U	~100	-

Abbreviations used: Dia = Diamond

Table 6.3 Characteristic features of extrusive coherent kimberite facies

Feature	Effusive	Coalescence	Hot pressing
Juvenile pyroclast state during deposition	None present	Liquid	Crystallized
Juvenile pyroclast outlines	None present	Rare-moderately abundant	Rare-abundant
Groundmass	Uniform, well-crystallized	Uniform, well-crystallized	Non-uniform, poorly to well-crystallized
Remnant (intra-clast) pore space	None	None	Possible-likely
Broken olivines	None	Possible	Possible
Fabric	Possible linear flow fabric	Possible linear flow fabric	Weak planar compaction fabric, possible rheomorphic linear flow fabric
Patchy grain size variations/bedding	Minor-none	Possible	Likely
Contacts with primary pyroclastic deposits	Sharp, except for possible fused bases	Gradational over short distance due to high emplacement temperature	Gradational over larger distance, possible welding gradient due to vertical changes in overbuden pressure an/or post-depositional cooling rate

Table 6.4 Characteristic features of phreatomagmatic vs. magmatic pyroclastic kimberite facies

Phreatomagmatic	Magmatic
Generally country rock fragment-rich	Country rock fragment-poor to -rich
Heterolithic small country rock fragments	Mono- to heterolithic variably sized country rock fragments
Fine grained, poorly sorted	Variable, but generally not as much fine grained particles, and better sorted
Broken olivines	Minor to no broken olivines
Possible clastic pyroclasts (ash-armoured clasts, accretionary pyroclasts, etc.)	No significant proportions of clastic pyroclasts
Variably vesicular, irregularly shaped, juvenile pyroclasts	Non-vesicular spherical juvenile pyroclasts
Likely opaque-rich matrix, suggesting a lack of loss of ash-sized components	Generally opaque-poor matrix, but can vary

6.5 References

Batumike, J.M. et al., 2008. LAM-ICPMS U-Pb dating of kimberlitic perovskite: Eocene-Oligocene kimberlites from the Kundelungu Plateau, D.R. Congo. Earth and Planetary Science Letters, 267(3-4): 609-619.

Berryman, A.K., Scott-Smith, B.H. and Jellicoe, B.C., 2004. Geology and diamond distribution of the 140/141 kimberlite, Fort a la Corne, central Saskatchewan, Canada. Lithos, 76(1-4): 99-114.

Brett, R.C., 2009. Kimberlitic olivine. Unpublished M.Sc. thesis. University of British Columbia, Vancouver, B.C., Canada, 86 pp.

Brown, R., Tait, M., Field, M. and Sparks, R., 2009. Geology of a complex kimberlite pipe (K2 pipe, Venetia Mine, South Africa): insights into conduit processes during explosive ultrabasic eruptions. Bulletin of Volcanology, 71(1): 95-112.

Brown, R.J., Buse, B., Sparks, R.S.J. and Field, M., 2008. On the Welding of Pyroclasts from Very Low-Viscosity Magmas: Examples from Kimberlite Volcanoes. The Journal of Geology, 116(4): 354-374.

Cas, R., Porritt, L., Pittari, A. and Hayman, P., 2008. A new approach to kimberlite facies terminology using a revised general approach to the nomenclature of all volcanic rocks and deposits: Descriptive to genetic. Journal of Volcanology and Geothermal Research, 174(1-3): 226-240.

Cas, R.A.F., Hayman, P., Pittari, A. and Porritt, L., 2008. Some major problems with existing models and terminology associated with kimberlite pipes from a volcanological perspective, and some suggestions. Journal of Volcanology and Geothermal Research, 174(1-3): 209-225.

Clement, C.R., 1982. A comparative study of some major kimberlite pipes in the North Cape and Orange Free State. Unpublished Ph.D. thesis. University of Cape Town, Cape Town.

Crawford, B., Hetman, C., Nowicki, T., Baumgartner, M. and Harrison, S., 2009. The geology and emplacement history of the Pigeon kimberlite, EKATI Diamond Mine, Northwest Territories, Canada. Lithos, 112(Supplement 1): 501-512.

Creaser, R.A., Grutter, H., Carlson, J. and Crawford, B., 2004. Macrocrystal phlogopite Rb-Sr dates for the Ekati property kimberlites, Slave Province, Canada: evidence for multiple intrusive episodes in the Paleocene and Eocene. Lithos, 76(1-4): 399-414.

Field, J.E., 1992. Strength, fracture and erosion properties of diamond. In: J.E. Field (Editor), The properties of natural and synthetic diamond. Academic Press, London, pp. 473-513.

Field, J.E. and Freeman, C.J., 1981. Strength and fracture properties of diamond. Philosophical Magazine A, 43(3): 595 - 618.

Field, M. and Scott-Smith, B.H., 1999. Contrasting geology and near-surface emplacement of kimberlite pipes in Southern Africa and Canada, Proceedings of the 7th International Kimberlite Conference, Cape Town.

Fisher, R.V. and Schmincke, H.-U., 1984. Pyroclastic rocks. Springer-Verlag, New York, 472 pp.

Fowler, J.A., Grutter, H.S., Kong, J.M. and Wood, B.D., 2001. Diamond Exploration in Northern Ontario with Reference to the Victor Kimberlite, Near Attawapiskat. Exploration and Mining Geology, 10(1-2): 67-75.

Gernon, T.M. et al., 2009. Pyroclastic flow deposits from a kimberlite eruption: The Orapa South Crater, Botswana. Lithos, 112(Supplement 1): 566-578.

Heaman, L.M., Kjarsgaard, B.A. and Creaser, R.A., 2004. The temporal evolution of North American kimberlites. Lithos, 76: 377-397.

Houghton, B.F. and Schmincke, H.U., 1989. Rothenberg scoria cone, East Eifel: a complex Strombolian and phreatomagmatic volcano. Bulletin of Volcanology, 52(1): 28-48.

Johnson, E.L. and Jenkins, D.M., 1991. Synthetic H2O-CO2 fluid inclusions in spontaneously nucleated forsterite, enstatite, and diopside hosts: The method and applications. Geochimica et Cosmochimica Acta, 55(4): 1031-1040.

Kjarsgaard, B.A. et al., 2006. Volcanic stratigraphy, eruptive sequences and emplacement of the 140/141 kimberlite, Fort a la Corne field, Saskatchewan, Kimberlite Emplacement Workshop, Saskatoon.

Kueppers, U., Scheu, B., Spieler, O. and Dingwell, D.B., 2006. Fragmentation efficiency of explosive volcanic eruptions: A study of experimentally generated pyroclasts. Journal of Volcanology and Geothermal Research, 153(1-2): 125-135.

Lefebvre, N. and Kurszlaukis, S., 2008. Contrasting eruption styles of the 147 Kimberlite, Fort a la Corne, Saskatchewan, Canada. Journal of Volcanology and Geothermal Research, 174(1-3): 171-185.

Moss, S., Russell, J.K. and Andrews, G.D.M., 2008. Progressive infilling of a kimberlite pipe at Diavik, Northwest Territories, Canada: Insights from volcanic facies architecture, textures, and granulometry. Journal of Volcanology and Geothermal Research, 174(1-3): 103-116.

Moss, S.W., 2009. Volcanology of the A154N kimberlite at Diavik: Implications for eruption dynamics. Unpublished Ph.D. thesis. University of British Columbia, Vancouver, B.C., Canada.

Nowicki, T. et al., 2004. The geology of kimberlite pipes of the Ekati property, Northwest Territories, Canada. Lithos, 76: 1-27.

Nowicki, T., Porritt, L., Crawford, B. and Kjarsgaard, B., 2008. Geochemical trends in kimberlites of the Ekati property, Northwest Territories, Canada: Insights on volcanic and resedimentation processes. Journal of Volcanology and Geothermal Research, 174(1-3): 117-127.

Pittari, A. et al., 2008. Eruption processes and facies architecture of the Orion Central kimberlite volcanic complex, Fort a la Corne, Saskatchewan; kimberlite mass flow deposits in a sedimentary basin. Journal of Volcanology and Geothermal Research, 174(1-3): 152-170.

Porritt, L., 2008. The volcanology and sedimentology of the Ekati kimberlites, NWT, Canada, with consideration of the implications for diamond grade. Unpublished Ph.D. thesis. Monash University, Clayton, Australia.

Porritt, L.A. and Cas, R.A.F., 2009. Reconstruction of a kimberlite eruption, using an integrated volcanological, geochemical and numerical approach: A case study of the Fox Kimberlite, NWT, Canada. Journal of Volcanology and Geothermal Research, 179(3-4): 241-264.

Porritt, L.A., Cas, R.A.F. and Crawford, B.B., 2006. The origin and implications of the TK-like infill of the Fox kimberlite, Ekati Diamond Mine, NWT, Canada, Kimberlite Emplacement Workshop, Saskatoon, Canada.

Roedder, E., 1984. Fluid Inclusions. Reviews in Mineralogy. Mineralogical Society of America.

Russell, J.K. and Moss, S.W., 2006. Volatiles and kimberlite eruption: insights from Diavik, Kimberlite emplacement workshop, Saskatoon, Canada.

Skinner, E.M.W. and Marsh, J.S., 2004. Distinct kimberlite pipe classes with contrasting eruption processes. Lithos, 76: 183-200.

Sparks, R.S.J. et al., 2006. Dynamical constraints on kimberlite volcanism. Journal of Volcanology and Geothermal Research, 155(1-2): 18-48.

Sparks, R.S.J. et al., 1997. Volcanic plumes. John Wiley & Sons, 574 pp.

Swain, M.V. and Atkinson, B.K., 1978. Fracture surface energy of olivine. Pure and Applied Geophysics, 116(4): 866-872.

Wilson, L., Sparks, R.S.J., Huang, T.C. and Watkins, N.D., 1978. The Control of Volcanic Column Heights by Eruption Energetics and Dynamics. Journal of Geophysical Research, 83(B4): 1829-1836.

LIST OF ELECTRONIC APPENDICES

A. Graphic summary of all drill cores intersecting VNW (pdf)

B. Tabulated summary of all drill core logs (pdf)

C. Geographic coordinates and down hole surveys of all drill cores (pdf)

D. Sample lists (pdf)

E. Detailed graphic logs for Victor Northwest (pdf)

F. Detailed graphic logs for Victor Main (pdf)

G. Electron microprobe data on oxides, carbonates, phogopites and apatites within Victor Main (xls)

H. Data on olivine alteration within the upper stratigraphy of VNW (pdf)

I. Data on angular olivine content within Victor North (xls)

J. Maximum clast sizes within Victor North (pdf)

K. Reconstructed pipe and unit volumes for Victor North (pdf)

L. Eruption duration calculations at Victor North (xls)

M. Image analysis methodologies and results for Victor North (pdf)

N. Data on mantle indictor mineral abundance at Victor North (xls)